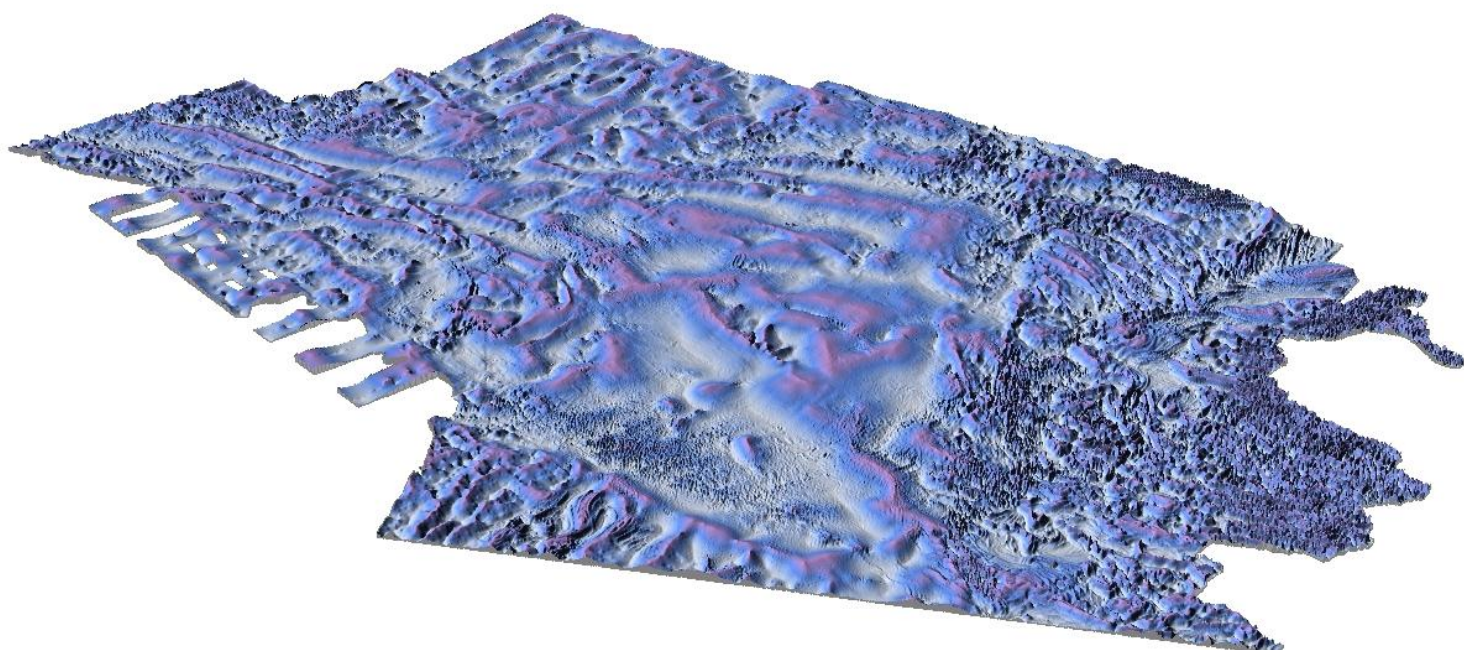


BArents Sea Aeromagnetic Remapping 2009

– BASAR-09

Acquisition and processing report and preliminary interpretation of the SW Barents Sea

M. Brønner, L. Gernigon, Ch. Pascal, J. Koziel
and Laura Marello



NGU Report 2010.056

Barents Sea Aeromagnetic Remapping 2009

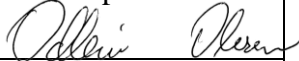
BASAR-09

Acquisition and processing report and
preliminary interpretation of the
SW Barents Sea

Geological Survey of Norway (NGU)
 N-7441 Trondheim, Norway
 Tel.: 47 73 90 40 00
 Telefax 47 73 92 16 20



REPORT

Report no: 2010.056		ISSN 0800-3416	Grading: Confidential to November 2015	
Title: Barents Sea Aeromagnetic Remapping BASAR-09 – Acquisition and processing report and preliminary interpretation of the SW Barents Sea				
Authors: Marco Brønner, Laurent Gernigon, Christophe Pascal, Janusz Koziel and Laura Marello		Clients: Det norske oljeselskap, ENI Norge, Norwegian Petroleum Directorate, Statoil and Norges geologiske undersøkelse		
Map-sheet name (M=1:250.000)		Map-sheet no. and -name (M=1:50.000)		
Deposit name and grid-reference:		Number of pages. 210	Price (NOK).	
		Map enclosures. X		
Fieldwork carried out: May- October 2009	Date of report: 18.11.2010	Project no.: 330600	Person responsible: 	
Summary: <p>A high-sensitivity aeromagnetic survey, BASAR-09, was carried out in an area of 106,300 km² in the Norwegian Barents Sea. Data processing comprised spike-removal and data editing, systematic corrections, and statistical and micro-levelling. Processing and interpretation of the new dataset included a compilation and merger of the surveys in the entire Norwegian Barents Sea. Several potential field maps were produced from the survey area. Examples of various filtering applied to the magnetic field have been illustrated. A depth-to-magnetic source was calculated, applying Euler deconvolution techniques.</p> <p>Structural interpretation of the updated aeromagnetic compilation of the southern Norwegian Barents Sea and 2D modelling along four regional seismic lines was carried out in conjunction with the existing gravity data. An existing regional 3D model of the entire Barents Sea was clipped to the Norwegian Barents Sea and refined, updated and readjusted employing the new magnetic data. The new and reprocessed magnetic data represent an important and beneficial improvement to the Norwegian shelf magnetic map, reflecting the regional basement settings with a significantly greater accuracy and providing new insights into the interaction of the various basins and basement highs within the survey area and the complex development of the southern Barents Sea. High-frequency anomalies from shallower structures were utilised to obtain a comprehensive overview of the distribution of dykes and salt diapirism in the area and were helpful in linking and identifying geological structures offshore by onshore-offshore correlations. Grav/Mag 2D and 3D modelling gave additional information on depth-to-basement, deeper crustal setting and the crustal thickness. A 2D heat flow modelling along one of the interpreted seismic lines gave additional constraints for the different basement units.</p>				
Keywords. Geofysikk		Berggrunnsgeologi	Magnetometri	
Kontinentalsokkel		Varmestrøm	Fagrapport	

CONTENTS

Contents	5
1 INTRODUCTION	8
1.1 Aeromagnetic data and exploration	8
1.2 Objective: BArents Sea Aeromagnetic Remapping 2009 (BASAR-09)	10
2 Geological frameWork	13
2.1 Introduction.....	13
2.2 Troms and Finnmark Geology.....	13
2.2.1 Troms.....	14
2.2.2 Finnmark.....	16
2.3 Geodynamic and geological background of the Barents Sea	21
3 SURVEY CHARACTERISTICS and ACQUISITION	27
3.1 Survey area and equipment.....	27
3.2 Personnel.....	29
3.3 Equipment and technical specification	30
3.4 Acquisition.....	30
3.5 Magnetic conditions.....	31
3.6 Gridding, map production, projection and archive CD	35
4 DATA PROCESSING AND PROFILE LEVELLING.....	36
4.1 Preliminary noise filtering and basic corrections	36
4.1.1 Noise filtering	36
4.1.2 Systematic lag corrections	36
4.1.3 International Geomagnetic Reference Field (IGRF correction)	36
4.2 Levelling and micro-levelling of the magnetic profiles	38
4.2.1 Diurnal variation and use of base-magnetometer readings.....	38
4.2.2 Statistical levelling.....	40
4.2.3 Micro-levelling	42
5 FINAL MERGER AND COMPARISON WITH PREVIOUS COMPILATION	45
5.1 Merger of the BASAR-09 grid with the former regional grid.....	45
5.2 Comparison with the previous compilation.....	48
6 OTHER DATASETS	49
6.1 Bathymetry	49
6.2 Gravity	49
6.3 Seismic data.....	49
7 CONVENTIONAL FILTERING TECHNIQUES	51
7.1 Wavelength filtering, RTP and derivatives	51
7.2 Reduction to the pole (RTP)	52
7.3 Wavelength and continuation filtering	54
8 ENHANCEMENT OF TREND USING STRUCTURAL FILTERS	57
8.1 Derivative filters	57
8.1.1 Vertical derivatives.....	57
8.1.2 The horizontal derivatives	60

8.1.3	Analytic signal	60
8.1.4	Tilt derivative (TDR).....	62
9	ESTIMATION OF MAGNETIC DEPTHS.....	65
9.1	Implications	65
9.2	Euler deconvolution.....	65
9.3	Interpretation of the structural indices	66
9.4	Located 3D Euler method.....	68
9.5	Werner deconvolution	73
10	INTERPRETATION	74
10.1	Main regional trends and potential field interpretation	74
10.1.1	Loppa High (LH)	82
10.1.2	Stappen High (SH).....	83
10.1.3	The Hammerfest Basin	84
10.1.4	Bjørnøya Basin	85
10.1.5	Tromsø Basin.....	86
10.1.6	The Bjarmeland Platform	86
10.1.7	The Nordkapp Basin and surrounding margins	92
10.1.8	The Ottar Basin.....	95
10.1.9	The Finnmark Platform - Kola Kanin Monocline	96
10.1.10	Onshore-offshore relationships.....	99
11	2D MODELLING ALONG SPECIFIC TRANSECTS.....	104
11.1	Potential field modelling: methods and assumptions	107
11.1.1	Gravity and magnetic modelling	107
11.1.2	Forward modelling.....	107
11.1.3	Magnetic modelling	111
11.1.4	Quantitative approach: Werner and Euler deconvolution	114
11.2	Implementation and modelling results.....	115
11.2.1	Transect 1: Section NBR07-232948.....	115
11.2.2	Transect 2: Section 7355-94	128
11.3	Transect 3: Section BV12-86.....	132
11.3.1	Transect 3: Section BV3-86.....	138
11.4	Implication of the modeling, ongoing understanding & models to test	142
11.4.1	Crustal structure and implications for the stretching model.....	142
11.4.2	Deep structures, sutures and modelling results: still open questions.....	145
11.5	Conclusions – Limitations - Perspectives.....	147
12	3D modelling	149
12.1	Introduction.....	149
12.2	Modelling Concept	149
12.3	Data.....	151
12.3.1	Petrophysical data.....	152
12.3.2	Geometric constraints from seismics.....	153
12.3.3	Model parameters	155

12.4	Modelling.....	156
12.4.1	Model correlation.....	156
12.4.2	Modelling results	159
12.4.3	Depth to top basement	166
12.4.4	Depth to the crust-mantle boundary (Moho)	169
12.5	Conclusions	170
13	2D THERMAL MODELLING	172
13.1	Introduction.....	172
13.2	Modelling approach	172
13.3	Results	174
13.4	Conclusions	177
14	CONCLUSIONs AND PERSPECTIVES	178
14.1	Main results	178
14.2	Proposition for further work	179
15	ACKNOWLEDGEMENTS.....	180
16	REFERENCES	181
17	LIST OF FIGURES and Tables:.....	202
18	APPENDIX 1 CD content	209
18.1	Folders	209
18.1.1	Report	209
18.1.2	Presentations	209
18.1.3	Data.....	209
18.1.4	Figures & Maps	210

1 INTRODUCTION

Laurent Gernigon & Marco Brönnert

Like several countries (e.g. Australia, Canada, Finland, Sweden, U.S), Norway was one of the first to support a vigorous government programme to develop a countrywide, modern, high-resolution, aeromagnetic database. This programme includes continuous data acquisition, and the merging and re-processing of data from individual surveys. In this context, the Geological Survey of Norway (NGU) plays a crucial role in maintaining and continuously updating this national database. NGU's most recent aeromagnetic acquisitions proved the need for modern data in order to validate the first-order geophysical and geological features of the Norwegian continental shelf and contiguous oceanic domain. Comparing vintage and modern aeromagnetic surveys is like comparing 2D seismic lines from the 1970s with the most advanced 3D surveys of today and everybody usually agrees that the modern data provide much more detail and significantly improve our geological knowledge. Consequently, NGU has launched a series of remapping projects of the Norwegian continental shelf and adjacent oceanic basins with funding provided by the petroleum industry and governmental institutions. The need for a new generation of high-quality data has now become a reality for both academia and industry.

1.1 Aeromagnetic data and exploration

The delineation of gravity and magnetic anomalies should normally be the first geophysical method to be applied to a new basin or region under evaluation or re-evaluation. In frontier and under-explored areas, where seismic data are sparse or non-existent, aeromagnetic acquisition still remains the cheapest and easiest way to obtain and/or refine a picture of the structural setting of the study area. Aeromagnetic data can also be useful for the strategic planning of new seismic and electromagnetic acquisitions and help to define potential prospects. Large aeromagnetic surveys can be carried out efficiently and safely almost everywhere, in a short period of time and at a reasonable cost.

Also, when integrated with seismic and gravity interpretations, modern aeromagnetic information can reduce the risk of making faulty geological interpretations. Both gravity and magnetic data are independent of seismic data, both physically and from the technical measurement point of view. A joint interpretation that combines seismic and potential field data thus produces a synergy that helps to significantly improve and validate the geological and structural interpretation of potential prospects.

Modern aeromagnetic data are usually applied as a relevant complement for basin and geodynamic interpretation in Norway. If the seismic coverage is poor, it can be jointly combined with gravity data to confirm and/or estimate the lateral extent of basement features,

lava flows, magmatic intrusions, salt structures or sand channels that may be observed in the sparse seismic sections (Fig. 1.1). High-resolution aeromagnetic surveys also represent relatively inexpensive tools for the 3D mapping of faults and fracture systems propagating through hydrocarbon-bearing sedimentary successions.

A variety of modern techniques to process, display and model the magnetic anomalies are offered for basin analysis. Several magnetic techniques can support the basin analysis and permit geoscientists: 1) to identify and delineate in depth mafic intrusions and volcanic rocks, 2) to quantify and evaluate the top of the magnetic basement and infer the location of the thickest sedimentary section, 3) to detect subtle, intra-sedimentary, ‘micro-magnetic’ anomalies, and 4) to evaluate, to some extent, the temperature of the crust (Curie temperature).

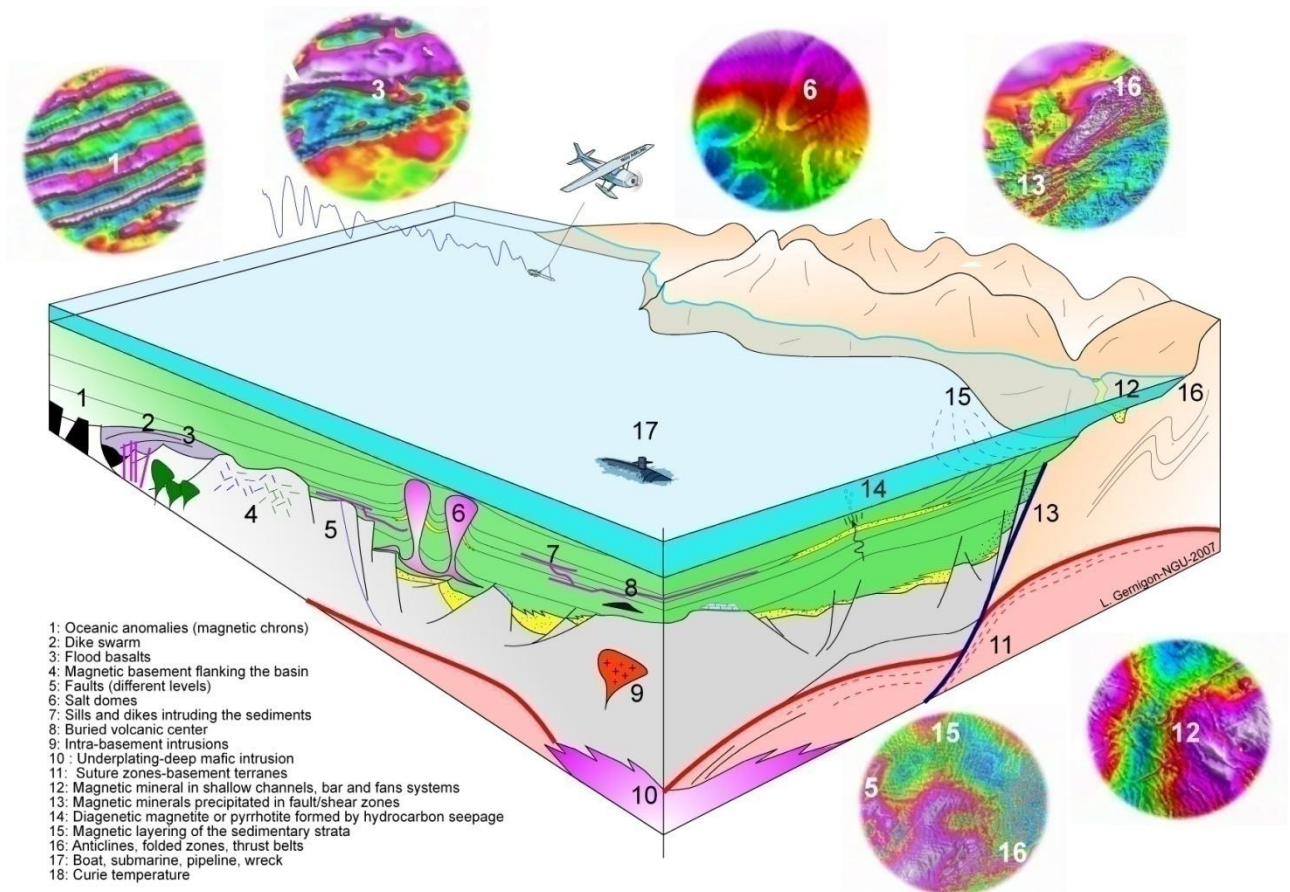


Figure 1.1 3D cartoon and examples of the application of modern NGU aeromagnetic surveys to basin or geodynamic studies. The cartoon illustrates structures and geological units that can cause observable magnetic responses (Gernigon et al. 2007a).

1.2 Objective: BArents Sea Aeromagnetic Remapping 2009 (BASAR-09)

As part of the NGU mapping programme, a high-resolution aeromagnetic survey was acquired in the Norwegian Barents Sea in 2009 (BASAR-09). NGU initiated the BASAR-09 project as a follow-up of the successful Barents Sea Aeromagnetic Surveys BAS-06 and BASAR-08. The survey closes a gap that existed in the state-of-the-art aeromagnetic data in the southern Barents Sea in between the HRAMS-97/98 and BASAR-08 campaigns and replaces the existing sparse and poor-quality data.

Figure 1.2 shows the location of the new survey area and an outline of the previous magnetic acquisition in the study area. A substantial part of the survey area was covered with aeromagnetic data in the 1980s during the TAMS-84, BAMS-85 and BSA-87 surveys. In the southwestern part the last acquisition was carried out 40 years ago and was flown with a limited number of tie-lines, which were insufficient to consider and correct diurnal variations adequately. In the meantime, modern and more accurate magnetometers, navigation systems and recent advances in processing techniques have allowed us to seriously improve the quality of aeromagnetic mapping (Luyendyk 1997). Modern magnetometers, as used for the

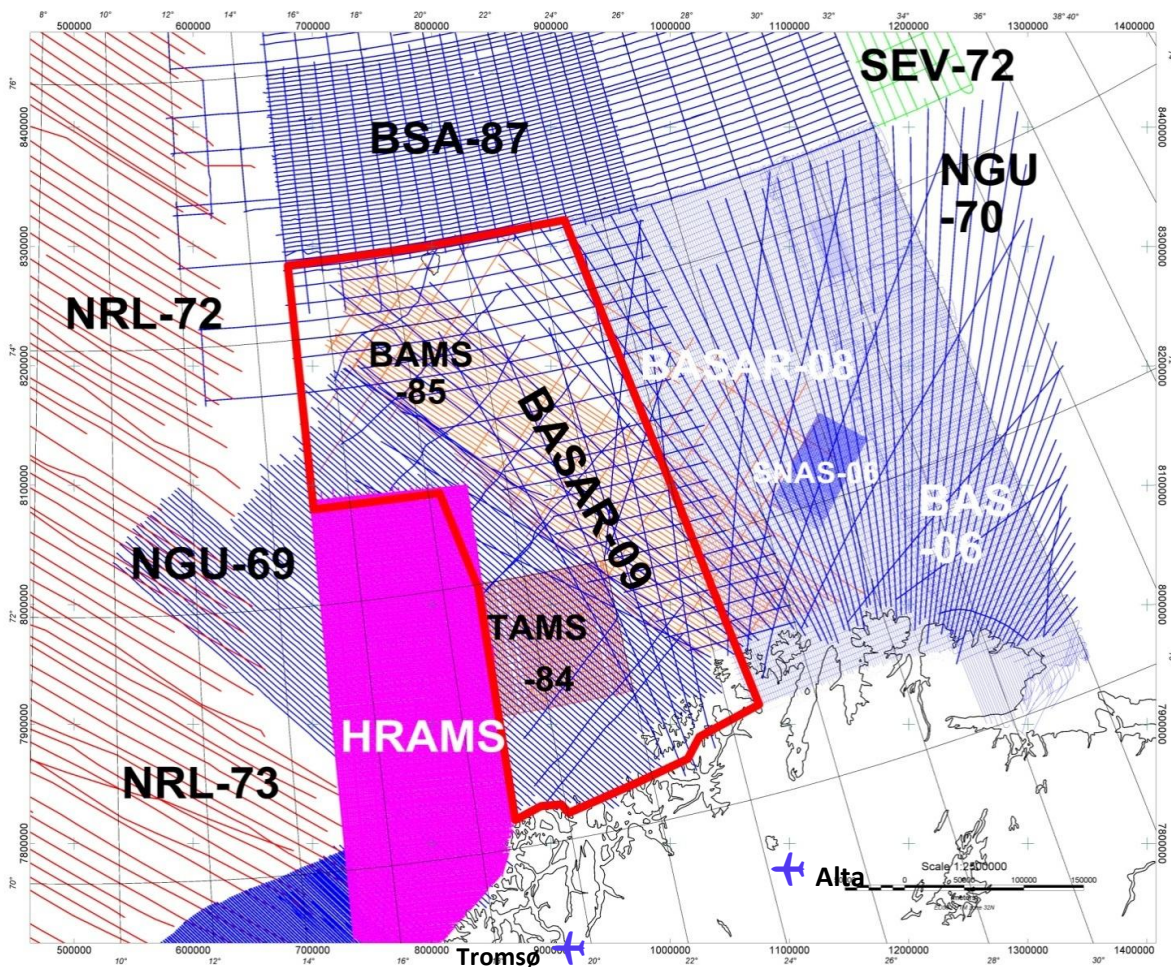


Figure 1.2 Geographic location of the BASAR-09 survey area and outline of the previous aeromagnetic surveys in and surrounding the Barents Sea (Olesen et al. 2006, 2010, Gernigon et al. 2007b). Alta and Tromsø airports were used during the survey acquisition.

BASAR-09 survey, provide new total field measurements of high sensitivity, with virtually no drift and to all intents and purposes can be regarded as giving a reliable reading with typical noise envelopes of ± 0.1 nT.

Advances in data acquisition techniques (more sensitive magnetometers, full release of modern Global Positioning Systems, pre-planned drape surveys, etc.), as well as data processing and displaying procedures (such as micro-levelling and advanced gridding techniques), and have also significantly improved data quality and resolution, providing levels of detail that are compatible with those derived from seismic recording, well logging and surface geological mapping. Being aware of such major geophysical improvements, the primary objectives of the BASAR-09 project were multiple:

- 1) To provide a better and more reliable magnetic coverage of the study area.
- 2) To refine the interpreted tectonic and geodynamic settings of the Barents Sea, which are far from being well understood.
- 3) To interpret the tectonic framework, basement structure and lithology.
- 4) To correlate and combine these results with the known geology of the study area as an aid in the identification of new structural features.

The interpretation involves the application of improved processing techniques and cultural source removal from the total magnetic field. In order to enhance the signatures of the basement structures and lithological units, a number of processed images and interpretations have been produced during this project.

In the first part of this report we describe the acquisition, processing, levelling and map production of the BASAR-09. Filtering techniques and data enhancement methods are described, leading subsequently to an integrated study of the survey area in 2D and 3D and a discussion of the most interesting features revealed by this new dataset.

The second main part focuses on the geophysical and geological interpretation of the new survey, including also gravity and available and released seismic lines, kindly provided by the Norwegian Petroleum Directorate (NPD). This leads to a preliminary interpretation of the survey area and opens discussions on onshore-offshore relationships and the development of the Barents Sea.

The BASAR-09 acquisition was co-funded by the Norwegian Petroleum Directorate, Statoil, Det norske oljeselskap and Eni Norge. The final compilation will certainly be welcomed by most researchers and explorationists working within the fields of geodynamics and geophysics and should provide a step further in our geodynamic knowledge of the Nordic seas.

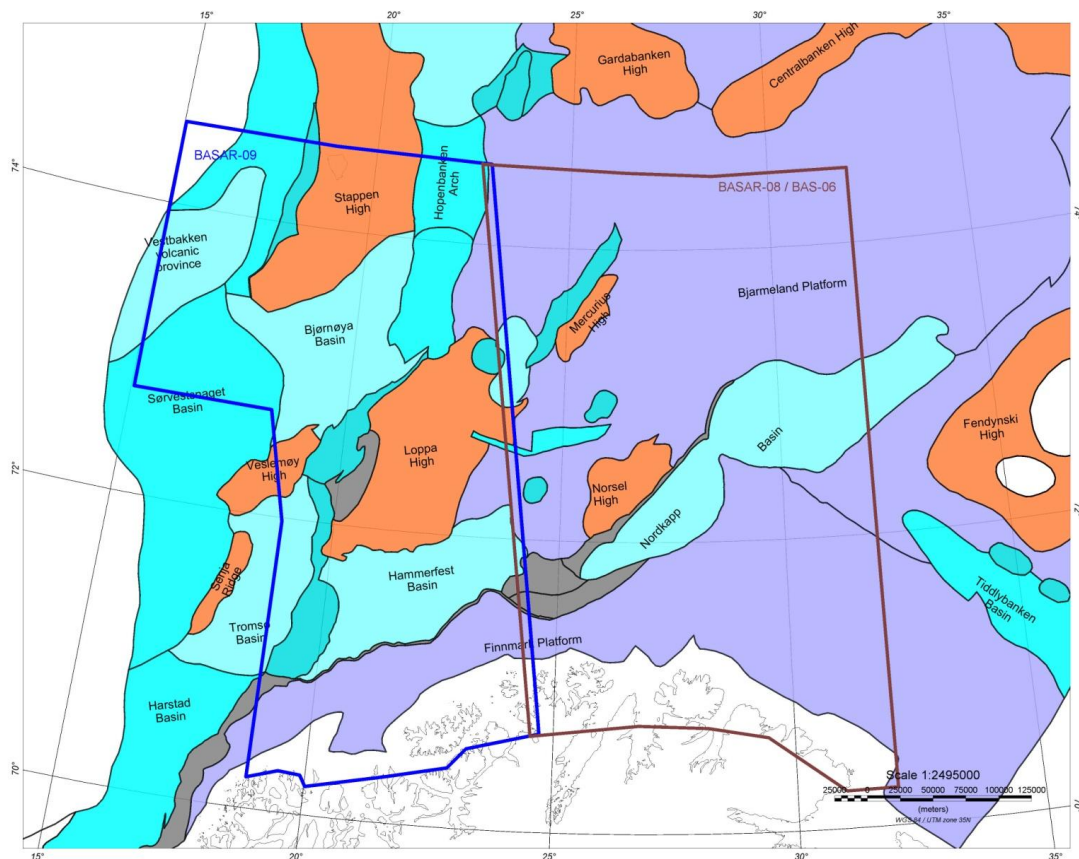


Figure 1.3 Location of the BASAR-09 survey area (and outline of BAS-06 and BASAR-08). The main structural elements of the western Barents Sea are from NPD (Gabrielsen et al. 1990).

2 GEOLOGICAL FRAMEWORK

Marco Brønner & Laurent Gernigon (with contributions from David Roberts)

2.1 Introduction

Because of a longstanding dispute between Russia and Norway about an area in the Barents Sea northeast of Varanger -a settlement for which was finally reached earlier this year- the remapping of the southern Norwegian Barents Sea is not yet completed. With the BASAR-09 survey and the BASAR-08, BAS-06 and HRAMS-97/98 data, however, we provide a high-resolution, state-of-the-art aeromagnetic compilation from the Norwegian coast up to 74°N latitude, which covers the major structural units in the area such as the major basins of Nordkapp, Hammerfest, Tromsø and Bjørnøya. The new grid covers the Norsel High, Loppa High and the southern part of the Stappen High as well as the Veslemøy High and most of the Vestbakken volcanic province and large parts of the Finnmark and Bjarmeland platforms. All the new surveys extend towards the coastline of Troms and Finnmark and cover the islands of Sørøya, Rolfsøya and Magerøya, which allow us to link onshore and offshore structures visible from the magnetic field. The magnetic patterns are directly linked to the geological evolution and tectonic history of the area and we therefore here provide a short summary of the tectonostratigraphic evolution of the study area in order to set the scene for the structural interpretation of the new magnetic data and modelling results. For further information and references about the geodynamic and paleogeographic framework of the Barents Sea we refer particularly to Gabrielsen *et al.* (1990, 1992), Johansen *et al.* (1993), Doré (1995), Gudlaugsson *et al.* (1998), Larssen *et al.* (2005), Worsley (2006) and Barrère *et al.* (2009).

The Barents Sea consists of complex structural elements with platform areas, basement highs and sedimentary basins (Figs. 1.3 and 2.1). It has been affected by a long and complicated tectonic development involving deformation of the entire crust, with major continental collisions and orogenesis followed by a complex rifting history that ultimately led to continental breakup in Cenozoic time (Gudlaugsson *et al.* 1998, Faleide *et al.* 1993).

The western Barents Sea region (Fig. 1.3) covers a large part of the Norwegian continental shelf and there is still a considerable lack of knowledge and understanding of the geology and petroleum potential of this province. Previous and ongoing exploration in this region suggests that it has the potential to become a world-class petroleum province. Exploration in this vast region will benefit greatly from an improved knowledge of the tectonic and crustal development of its complex regional structures.

2.2 Troms and Finnmark Geology

The geology of mainland Troms and Finnmark, northern Norway, is dominated by Precambrian basement and Caledonian nappes (Andresen 1980; Sigmond *et al.* 1984, Zwaan

1995). A variety of gneisses, supracrustals and intrusive rocks of Archaean and Palaeoproterozoic age in the Precambrian basement are draped by thrust sheets comprising rocks of mostly Neoproterozoic to Silurian age that were emplaced during the protracted Caledonian orogeny.

The Scandinavian Caledonides as a whole have been divided tectonostratigraphically into major Lower, Middle, Upper and Uppermost Allochthons as well as a thin, underlying Autochthon and Parautochthon (Roberts & Gee 1985). All these units, perhaps with the exception of the Uppermost Allochthon, are represented in Finnmark, whereas Troms is dominated by the Middle and Upper Allochthon to the east (Zwaan & Roberts, 1978, Roberts & Gee, 1985) and the Uppermost Allochthon in the southwest (Andréasson *et al.*, 2003). The Lower and Middle Allochthons are considered to consist of shelf and continental rise units deposited along the Baltoscandian margin, which faced the Iapetus Ocean in Early Palaeozoic time (Stephens & Gee 1985, Siedlecka 1987, Roberts 2003). The Upper and Uppermost Allochthons comprise, respectively, oceanic complexes and exotic continental margin units of Laurentian origin.

2.2.1 Troms

The westernmost part of Troms is characterised by a number of coastal islands where Archaean to Palaeoproterozoic gneisses and intrusive bodies are exposed in the West Troms Basement Complex. This comprises crustal blocks of migmatites, granitoid rocks and supracrustal belts which were metamorphosed and deformed to variable grades and degrees during the Svecofennian orogeny (Armitage & Bergh 2005). An overview of the geology is summarised in Zwaan *et al.* (1998) and Corfu *et al.* (2003). The West Troms Basement Complex (WTBC) extends over the islands of Senja, Kvaløya and Ringvassøya. Gneisses in northern Senja and Kvaløya occur as megablocks and blocks divided by narrow, approximately NW-SE striking ductile shear zones, which also comprise part of the Senja Shear Belt (Tveten & Zwaan 1993).

The geology of Kvaløya is dominated by the Ersfjord Granite and Neoproterozoic tonalitic gneisses of the Kattfjord Complex in the north and by the Bakkefjord Diorite and Gråtind Migmatite in the south which are separated by N-S striking metasupracrustal rocks (Zwaan *et al.* 1998, Corfu *et al.* 2003). The dominant strike of the foliation on Kvaløya is N-S, but locally the main foliation is rotated into a NW-SE to E-W strike, reflecting a later phase of deformation (Armitage & Bergh, 2005). Later emplacement of the Ersfjord Granite (at 1792 Ma, Corfu *et al.* 2003) was associated with migmatitisation and this was succeeded by the intrusion of granitoid pegmatite dykes (Binns 1985). These granitoid dykes also transect common mafic dykes in the Bakkefjord Diorite.

On Ringvassøya supracrustal sequences of intermediate to mafic metavolcanic and terrigenous metasedimentary rocks of assumed Palaeoproterozoic age overlie Neoproterozoic

tonalitic gneisses (Ringvassøya Greenstone Belt), which represent the major unit in the northern part of the WTBC (Zwaan, 1995, Kullerud, *et al.* 2006a, Bergh *et al.* 2007). Mafic dykes that cross-cut both the gneisses and the Ringvassøy Greenstone Belt were emplaced at c. 2400 Ma (Kullerud *et al.* 2006b). These dykes correlate broadly with a global Palaeoproterozoic magmatic event that formed extensive bimodal intrusive and extrusive suites in most Archaean cratons, including the northeastern Fennoscandian Shield (Zozulya *et al.* 2009).

The island of Vanna is dominated by c. 2.86 Ga tonalitic gneisses, with local cross-cutting 2.4 Ga mafic dykes (Bergh *et al.* 2007). Along the southern and western coasts of the island, however, these rocks are unconformably overlain by metasedimentary rocks of the Vanna Group which are intruded by c. 2.22 Ga dioritic and gabbroic sills (Bergh *et al.* 2007). The WTBC is separated from the Caledonian thrust complex to the east by a combination of a basal, low-angle, Caledonian thrust fault and Palaeozoic-Mesozoic normal faults (e.g. Zwaan 1995, Olesen *et al.* 1997), later interpreted as an extensional detachment (Ramberg *et al.* 2008, Ch.7). It is generally believed that the WTBC represents a westward extension of similar rocks occurring in the Fennoscandian Shield in the northern Sweden and Finland, but the remarkably weak Caledonian overprint of the rocks of the WTBC has led some workers to suggest that the complex is in a parautochthonous to allochthonous position (e.g. Brueckner 1971, Dallmeyer 1992, Motuza 1998).

Whilst the lowermost nappes are well represented in Finnmark, they are only sparingly present in Troms and northern Nordland where, instead, the Middle, Upper and Uppermost Allochthons are predominant. The Kalak Nappe Complex of the Middle Allochthon occurs widely over large areas in innermost north Troms. It comprises five, separate nappes or thrust sheets, each dominated by arkosic metasandstones and some with slices of older gneissic basement rocks at their base (Zwaan 1988). The Čorrovárri Nappe is the uppermost tectonostratigraphic unit of the Kalak Nappe Complex and consists mainly of a Neoproterozoic metasedimentary succession cut by mafic dykes dated to c. 580 Ma (Zwaan & van Roermund 1990). This nappe is truncated by the overlying Váddás Nappe of the Reisa Nappe Complex, which is part of the Upper Allochthon. The rocks of the Kalak Nappe Complex were metamorphosed in highest greenschist-facies, locally up to amphibolite facies, during the Late Silurian-Early Devonian, Scandian orogeny (Lindahl *et al.* 2005).

The Reisa Nappe Complex consists of four, regionally extensive nappes, the Váddás, Tamokdalen, Kåfjord and Nordmannvik Nappes, each containing a lower shallow-marine succession of schists, conglomerates and calcite marbles which pass upwards into deeper-marine turbidites with sporadic mafic lava flows and gabbro bodies (Lindahl *et al.* 2005). Mafic dykes occur widely throughout the succession. In one area, a marble member contains fossils of latest Ordovician-Early Silurian age (Binns & Gayer 1980). Metamorphic grade is

generally in amphibolite facies, but granulite-facies conditions prevail locally in the highest thrust sheet, the Nordmannvik Nappe.

The Uppermost Allochthon occurs extensively in west and southwest Troms. In northern areas it was initially termed the Tromsø Nappe Complex (Andresen *et al.* 1985), but was later extended and subdivided into three separate nappes, the Lyngsfjell, Nakkedal and Tromsø Nappes (Krogh *et al.* 1990, Zwaan *et al.* 1998). The basal Lyngsfjell Nappe contains the Early/Mid Ordovician, ophiolitic Lyngen Magmatic Complex (Furnes & Pedersen 1995), which is overlain unconformably by the locally fossiliferous, Late Ordovician-Early Silurian, Balsfjord Supergroup (Binns & Matthews 1981, Bergh & Andresen 1985). In southwestern Troms, there is different subdivision of the Uppermost Allochthon with 4 or 5 separate nappes (Steltenpohl *et al.* 1990, Melezhik *et al.* 2003), all dominated by diverse schists and calcite or dolomite marbles but with slices of ophiolite, equivalent to the Lyngsfjell Nappe, at the base. Chemostratigraphical studies on the marbles have revealed a variety of ages in different thrust sheets ranging from Early Cryogenian to Silurian (Melezhik *et al.* 2003, 2007). A review of the geology of the Uppermost Allochthon is given in Roberts *et al.* (2007).

2.2.2 Finnmark

The geology of the northern Finnmark region is characterised mainly by Mesoproterozoic to Early Palaeozoic sedimentary successions. With the exception of rocks on the island of Magerøya, these successions are generally inferred to have been deposited along the northern and northwestern margin of the Fennoscandian Shield and later folded and thrust during the Caledonian orogeny (Fig. 2.1).

The Upper Allochthon in Finnmark is represented solely by the Magerøy Nappe. This is an exotic, Iapetan element which has recently been interpreted to have Laurentian affinities (Corfu *et al.* 2006). This may imply that the Magerøy Nappe could form a part of the Uppermost Allochthon, rather than the Upper Allochthon, but this question does not concern us directly here.

The Caledonian tectonostratigraphy in Finnmark (Ramsay *et al.* 1985, Rice *et al.* 1989a, Siedlecka & Roberts 1996) above the level of the Paraautochthon is divided into four major nappe units (Fig. 2.1), in ascending structural order: (1) the Gaissa Nappe Complex, (2) Laksefjord Nappe Complex, (3) Kalak Nappe Complex and (4) Magerøy Nappe. The Gaissa Nappe Complex is a part of the Lower Allochthon and comprises low-grade, Neoproterozoic to Early Ordovician sedimentary rocks. The Laksefjord Nappe Complex, which includes a basal thrust sheet of Precambrian crystalline basement rocks (Rice 2001), constitutes the lowermost unit of the Middle Allochthon in the Laksefjorden area. The metasediments in the Laksefjord Nappe Complex are considered to be of Neoproterozoic age (Sundvoll & Roberts 2003). The Kalak Nappe Complex constitutes the main part of the Middle Allochthon

(Roberts 1985, Rice & Frank 2003) and consists largely of Meso- to Neoproterozoic metasedimentary rocks with slices of older basement rocks in the BASAR-09 and BASAR-08 survey areas. The nappe complex consists of at least 25 thrust sheets group into 7-8 nappes (e.g. Gayer *et al.* 1985, 1987, Ramsay *et al.* 1985). Sørøya and the coastal area just south of the island which marks the border to the survey area BASAR-09 form part of the Sørøy-Seiland Nappe. Sørøya is dominated by a dissected metasedimentary succession of Cryogenian to Early Silurian age (Kirkland *et al.* 2005, Slagstad *et al.* 2006), part of which is intruded by gabbros, diorites and carbonatites of the Seiland Igneous Province (Roberts 1973, Robins 1996). U-Pb isotopic dating has shown that the voluminous magmatic rocks of the Seiland Igneous Province, which reaches down to depths of 7-8 km (Olesen *et al.* 1990) were intruded in Vendian (Ediacaram) time at 570-560 Ma (Roberts *et al.* 2006, 2010).

The Magerøy Nappe comprises metasedimentary rocks of Early Silurian age that are intruded by a Silurian, mafic-ultramafic, plutonic complex, the Honningsvåg Igneous Suite (Robins 1998, Roberts *et al.* 2003, Corfu *et al.* 2006). On Magerøya, there are also a few mafic dykes of Carboniferous age, dated to c. 337 Ma (Lippard & Prestvik 1997, Roberts *et al.* 2003). The dykes occur in several different places on the island and generally lie parallel to NW-SE-trending extensional faults. Accordingly, the dykes and faults have been interpreted as associated with the Late Palaeozoic extension and rifting in the Barents Sea (Roberts *et al.* 1991, Lippard & Prestvik 1997).

East of Tanafjorden, in the northwestern part of the Varanger Peninsula, mid greenschist-facies, turbiditic metasedimentary rocks of the Berlevåg Formation (Levell & Roberts 1977) occur within the Tanahorn Nappe, which is generally considered to form the lowest part of the Kalak Nappe Complex on this peninsula (Levell & Roberts 1977, Rice & Frank 2003, Roberts 2009). The base of the Tanahorn Nappe is a steep, NW-dipping, thrust fault that separates the Berlevåg Formation from what has been termed the Barents Sea Caledonides (Gayer *et al.* 1987), part of the Lower Allochthon, coinciding with a drop in metamorphic grade from mid greenschist-facies to epizone (Rice *et al.* 1989b). Below the basal Tanahorn thrust fault, the rocks of the Lower Allochthon comprise the Løkviksfjellet Group, a 5.8 km-thick, terrigenous sandstone sequence of assumed Vendian age that unconformably overlies turbidites and deltaic rocks of the 9 km-thick, Riphean to Lower Vendian, Barents Sea Group (Siedlecka & Siedlecki 1971, Siedlecka 1987, Gernigon *et al.* 2007b).

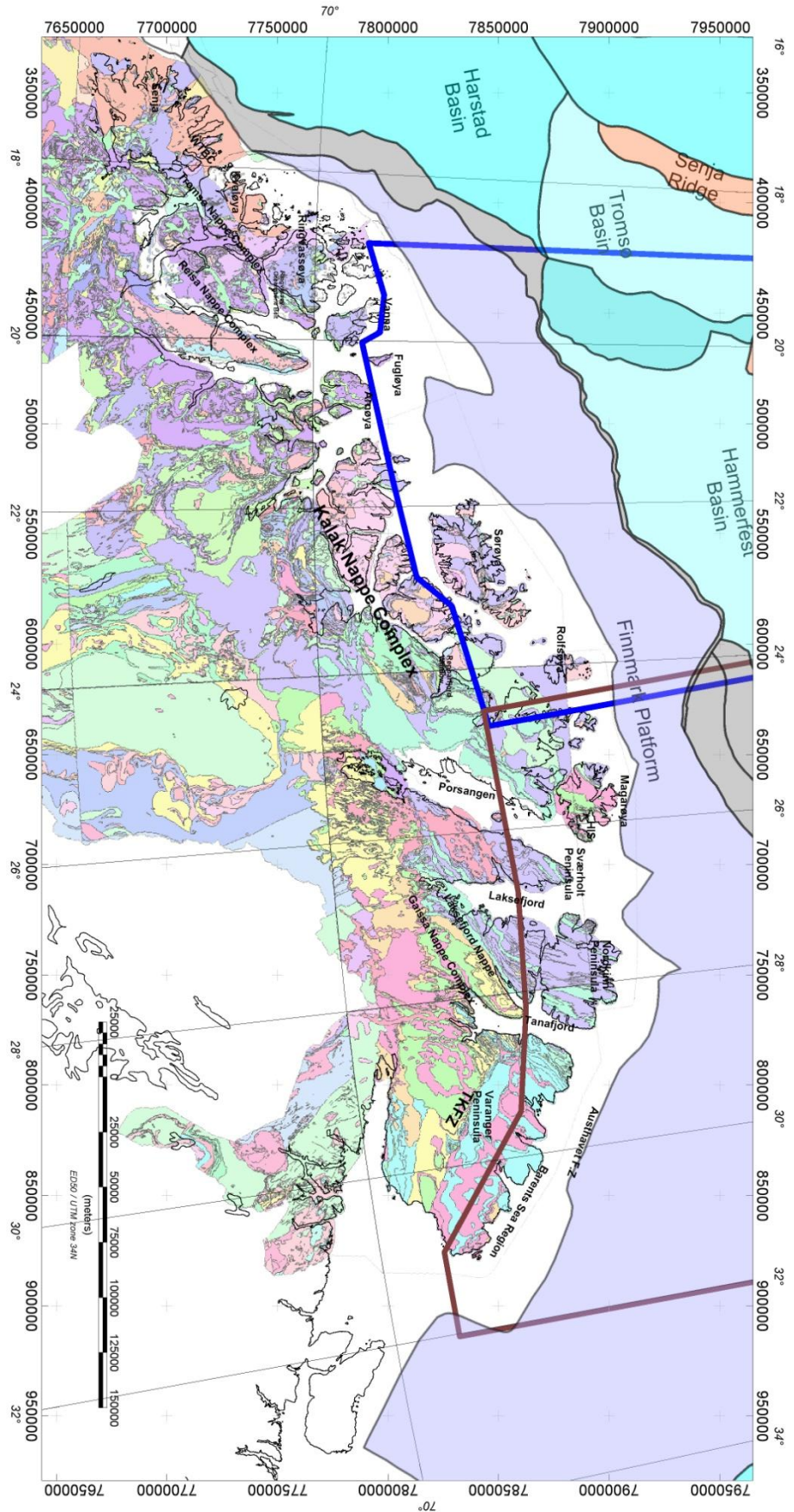


Figure 2.1 Fimmærk and Troms geology from a 1:500,000 map (Siedlecka & Roberts 1996) and several 1:250,000 maps (Roberts 1973, Zwaan 1988, Grogan & Zwaan 1997, Zwaan et al. 1998). The main structural elements of the southern Fimmærk Platform are shown with survey outlines (blue - BASAR-09, brown - BASAR08/BAS-06) and locations of the geological sections in this report (black) (Gabrielsen et al. 1990).

The Varanger Peninsula is divided into two regions separated by the major, c. NW-SE-trending, Trollfjorden-Komagelva Fault Zone (TKFZ), which marks a clear metamorphic and structural boundary (Siedlecka & Roberts 1992). The Barents Sea Region (BSR) lies to the north of the TKFZ and the Tanafjorden-Varangerfjorden Region (TVR) represents the southern part of the peninsula. The TVR consists of up to 3.8 km of Late Riphean (Cryogenian) to Early Cambrian successions lying unconformably upon the Neoproterozoic basement complex of the Fennoscandian Shield (Siedlecka & Roberts 1992).

The regional significance, structure and evolution of the TKFZ has been discussed in several publications (e.g., Siedlecka 1975, Rice *et al.* 1989a, Siedlecka & Roberts 1992, Karpuz *et al.* 1993a, b, 1995, Herrevold *et al.* 2009). The fault zone is almost parallel to the axis of the Kola-Kanin Monocline, offshore Kola Peninsula, NW Russia, and extends southeastwards onto the Rybachi and Sredni peninsulas along in Russia (Roberts 1995). A northwestern extension of the TKFZ into the Southwest Barents Sea has also been proposed by Gabrielsen & Færseth (1989).

Previous, integrated, remote sensing and aeromagnetic studies of the Varanger Peninsula have indicated that major, penetrative, NW-SE, NNW-SSE to NNE-SSW and NE-SW lineaments were inherited from the Archaean to Palaeoproterozoic crystalline basement features (Karpuz *et al.* 1993a, b, 1995). The NW-SE-trending lineament zones are particularly prominent and significant in both remote sensing and potential field datasets and, by comparison with the structural history of Kola Peninsula, probably represent the oldest weakness zones in this part of the Fennoscandian Shield (Karpuz *et al.* 1995). Structural investigations have suggested that many of these lineaments have been reactivated at several stages in their history from Archaean to Mesozoic time (Siedlecka & Roberts 1992, Karpuz *et al.* 1993b, 1995).

The metasedimentary succession of the Barents Sea Group was deposited in a basin bounded to the south by a precursor fault to the TKFZ. During most of the Neoproterozoic this structure was a major, extensional, border fault separating a platformal domain to the southwest from a basin deepening to the northeast (Siedlecka 1985, Siedlecka & Roberts 1992). In Vendian time, during the Timanian orogeny, basinal inversion along the fault led to SW-directed thrusting. Subsequently, dextral strike-slip deformation occurred along the TKFZ during the Caledonian orogeny, in Early Ordovician time (Rice & Frank 2003), with later dip-slip or oblique-slip movements in the Late Palaeozoic and Mesozoic (Lippard & Roberts 1987). Several estimates of the amount of Caledonian, dextral strike-slip displacement along the TKFZ have been proposed, but an offset of just 50-100 km seems to be most reasonable (Rice 1994). Jensen & Sørensen (1992) also considered a post-Caledonian dextral movement along the TKFZ of less than 5 km associated with a Late Palaeozoic rifting phase in the southwestern Barents Sea.

From east to west, the BSR shows a complex structural setting influenced by both the Timanian and the Caledonian orogenies. To the east, the low-grade rocks of the Barents Sea Group in the Vardø district show a fold axial trend and associated, steep cleavage oriented between NW-SE and NNW-SSE near the eastern coastline, swinging gradually towards c. N-S farther to the west (Karpuz *et al.* 1993a,b, Roberts 1996). In earlier interpretations a Scandian (Silurian) age was assumed for the NNW-SSE structural grain in this part of the BSR, the folds arising either through buffering in front of a rigid basement block (Roberts 1972) or as tip-folds that developed by late-Caledonian back-thrusting (Rice *et al.* 1989a). Comparative field studies on the Rybachi Peninsula just 50 km to the southeast in Russia provided convincing evidence that the main folds and cleavage in the eastern part of the BSR formed during the Vendian-age Timanian orogeny.

This inferred Timanian structural grain in the eastern BSR, however, is interrupted by cross-folds and a weak cleavage of ENE-WSW to NE-SW trend, interpreted by Roberts (1996) to be Caledonian in age and most likely Ordovician (Rice & Frank 2003, Herrevold *et al.* 2009). Only one attempt at dating the older penetrative cleavage in this area has been made, providing an imprecise Rb-Sr whole-rock isochron date of 520 ± 47 Ma (Taylor & Pickering 1981). Recalculations of these analytical data have tended to favour an older, Vendian age (B. Sundvoll, pers. comm., in Roberts & Olovyanishnikov 2004).

In western Varanger Peninsula the principal structures are of Caledonian age (Roberts 1972, Karpuz *et al.* 1995) and have been isotopically dated to Early to Mid Ordovician time (Rice & Frank 2003). In the BSR there is a general decrease in intensity of deformation from northwest to southeast. Structural features are mostly NE-SW to ENE-WSW trending and represent SE-verging folds and thrusts. In the footwall of the Tanahorn Nappe, the Lower Allochthon is represented by the Rákkočearru thrust sheet (Roberts 2009). Similar structures occur southwest of the TKFZ in the western TVR, in the Gaissa Nappe Complex (Rice *et al.* 1989a, Siedlecka & Roberts 1996), where there are also indications of possible Finnmarkian, low-grade metamorphism (Sundvoll & Roberts 2003), here of post-Early Tremadoc age.

In the central parts of the BSR, there is a zone of transition where the Caledonian structures appear to die out eastwards against, but also overprint, the Timanian folds (Herrevold *et al.* 2009). However, a basal thrust sheet of the Lower Allochthon appears to enter the sea in Syltefjorden (D. Roberts, pers. comm. 2007). Earlier, the precise age of the Caledonian deformation in the BSR was not well constrained, but in a ^{40}Ar - ^{39}Ar study Rice & Frank (2003) have shown that the pervasive cleavage in the Tanahorn Nappe and subjacent rocks is of Early to Mid Ordovician age. This was also the time of the major, dextral strike-slip movement along the TKFZ.

A feature of the northwestern and central parts of the BSR is that metadolerite dykes are profuse and locally attain swarm proportions (Roberts 1972), but no maps showing all the dykes have so far been published. Most of the mafic dykes are of Vendian age and thus pre-

date the Caledonian folding (Rice *et al.* 2004), but there is also a later set of more sporadic dolerite dykes of Late Devonian age (Guise & Roberts 2002) which relate to a phase of rifting recorded in NW Russia and the southern Barents Sea.

The Nordkinn Peninsula, west of Tanafjorden, lies within the onshore area covered by the BASAR-08 survey. There, the upper greenschist-facies succession forms part of the Kalak Nappe Complex and consists of diverse metasandstones and phyllites with garnet appearing as an index mineral in the western areas (Roberts & Andersen 1985). The arkosic sandstone formations on Nordkinn are invariably cross-bedded and locally enriched in heavy-mineral layers. Palaeocurrent data indicate that the source areas for the detritus were situated to the south and southeast (Roberts 2007).

2.3 Geodynamic and geological background of the Barents Sea

The tectonic and 'basement' history of the Barents Sea is strongly influenced by the Palaeoproterozoic (Karelian) orogeny, which established the stable Russian-European platform adjacent to the Archaean Fennoscandian Shield (Alsgaard 1993, Gee *et al.* 2008). Subsequently, a latest Neoproterozoic Timanian orogeny (previously called Baikalian) developed as a fold-and-thrust belt in the eastern part of the Barents Sea region during Ediacaran (Vendian) time. The Timanide orogen resulted from the accretion and assemblage of diverse magmatosedimentary terranes including intra-oceanic subduction systems, islands arcs and isolated micro-blocks, as the paleocontinent Arctida collided with Baltica (Kuznetsov *et al.* 2010). The main NW-SE Timanian orogenic trends are exemplified by the Kanin-Timan Ridge and the Kola-Kanin Monocline southwest of the Timan-Pechora and Barents provinces (Roberts & Siedlecka 2002, Gee & Pease 2004). In the Timan-Kanin-Pechora region, major NW-SE structural trends also reflect the reactivation of known Palaeoproterozoic and older lineaments during the Meso- to Neoproterozoic (Mid to Late Riphean) crustal extension which characterised the Timanian margin of proto-Baltica. Field evidence of Timanian deformation in Russia, as described in detail later in this report, is also documented in the eastern part of the Varanger Peninsula (Roberts 1995, 1996, Roberts & Olovyanishnikov 2004, Herrevold *et al.* 2009) as noted earlier.

The geology of the West Barents Sea province (Fig. 1.3 & 11.1) was mostly controlled by major post-Caledonian rifting phases as well as later episodes of rifting leading to continental breakup along the northwestern margin of the Eurasian plate (Smelror *et al.* 2009).

The tectonic and basement history of the Barents Sea is quite complex and locally still debatable, but the main outlines are relatively well established up to the time of the Late Palaeoproterozoic (Karelian) orogeny, setting the stable Russian-European platform adjacent to the Archaean Fennoscandian Shield (Alsgaard 1993, Gee *et al.* 2008). Subsequently, the Late Neoproterozoic Timanide Orogen developed as a fold-and-thrust belt in the eastern part of the Barents Sea region during Vendian (Ediacarian) time (Gee and Pease 2004, Roberts

and Olovyanishnikov 2004), the suture between Arctida and Baltica extending northwestwards across the southern Barents Sea (Kuznetsov *et al.* 2010).

In the West Barents Sea area, the basement history largely corresponds with that of the Scandinavian Caledonides and its subjacent Precambrian crystalline complexes. The Caledonian Orogeny culminated approximately 400 million years ago, and resulted in a consolidation of the Laurentian and Baltican plates into the Laurasian continent and a closure of the Iapetus Ocean, a major seaway that occupied a position more or less similar to the modern Northeast Atlantic Ocean (Torsvik and Cocks 2005). The Caledonian Orogeny is traditionally regarded onshore Norway as originating from two major tectonic phases: 1) the early Finnmarkian phase (Late Cambrian to Early Ordovician) and 2) the later Scandian phase (Mid-Silurian-Devonian) (Rice and Frank 2003, Roberts 2003). Recent isotopic dating, however, has revealed some ambiguities in the timing of the early Caledonian tectonic phase which, in some thrust sheets, could be older and Neoproterozoic in age (Corfu *et al.* 2006).

In Norway the Caledonides extend over a distance of nearly 2000 km and, as noted earlier, are widely exposed in northwest Finnmark and Troms close to our study area (Fig. 2.1). The Caledonian Orogen is also well documented on Svalbard, where generally N-S-striking Caledonian bedrock is exposed along most of the northern and western coasts of Spitsbergen (Gee & Tebenkov 2004). Caledonian structural imprints can be seen in the N-S structural grain of the western Barents Sea margin and Svalbard, and the NE-SW grain of the southwestern Barents Sea and Finnmark. Old inherited structures usually appear to be the first order crustal parameters that control the rift or basin architecture in the West Barents Sea area. This is clearly highlighted by potential field data (Figs. 10.6), which are in turn influenced by the basement configuration at in the western Barents Sea scale.

The Late Palaeozoic and Mesozoic tectonic history of the Barents Sea was mostly dominated by extensional tectonics which followed the collapse of the Caledonian and Uralian orogenic belts. Rift episodes have been documented in the Early-Middle Devonian, Carboniferous, Permian, Triassic and Late Jurassic-Early Cretaceous (Johansen *et al.* 1993). These events created the major rift basins on the Barents Shelf. Regional extension dominated the western Barents Sea area during the Carboniferous. This episode is part of the long-lived Palaeozoic-Mesozoic, pre-opening, rifting episodes that led to the development of the North Atlantic Ocean. On seismic data, the rift structures are locally recognised below the extensive Upper Carboniferous to Lower Permian carbonate platform deposits which cover larger parts of the Barents shelf (Rønnevik & Jacobsen 1984, Gabrielsen *et al.* 1990, Johansen *et al.* 1993, Larssen *et al.* 2005). In the Late Palaeozoic, thick successions of evaporites accumulated locally in the different graben systems developed in the southwestern parts of the shelf (i.e. the Ottar, Tromsø, Bjørnøya and Nordkapp basins).

During the Early to Late Permian transition, regional seaways developed around Baltica and the western shelf margins, and progressively opened a connection between the Boreal Realm,

the central European Zechstein Basin and the proto-North Atlantic rift system (Brekke *et al.* 2001, Worsley 2008, Smelror *et al.* 2009). On the central and western Barents shelf, the emergent Uralide Orogen and the connection with the Tethys Ocean led to a drastic change in depositional regime from warm-water platform carbonates to deeper cold-water fine clastics and silica-rich spiculites due to reorganisation of the ocean currents (Bugge *et al.* 1995, Bugge *et al.* 2002, Larssen *et al.* 2005).

A major Early Triassic rift episode has also been described from the Barents Sea, and is also recognised in many parts of the Arctic and North Atlantic regions. Mid-Late Triassic times was generally characterised by post-rift thermal subsidence in the North Atlantic and Arctic basins. In the Western Barents Sea, the Lower to Middle Triassic succession comprises T-R cycles of marine, deltaic and continental clastics, and a number of discrete minor tectonic events can be recognised. To the west of the Hammerfest Basin, a latest Permian to Early Triassic rifting event is assumed to have occurred, which may have continued until late Anisian to early Ladinian time. During that period, salt movements in the Bjørnøya Basin (BB) are interpreted to have begun in early Scythian time and continued into later Triassic time in the Nordkapp Basin (Gabrielsen *et al.* 1992, Koyi *et al.* 1993, Nilsen *et al.* 1995). In Svalbard itself, minor faulting activity occurred during the Triassic period. Lower to Middle Triassic strata reflect repeated deltaic progradation from a westerly Laurentian source, which decreased in importance through time. Triassic tectonism in the Bjørnøya and Stappen High (SH) area most likely comprised repeated uplifts. This interpretation is supported by a slight angular unconformity between the Triassic strata and underlying Upper Permian carbonates and the fact that the succession is highly discontinuous.

From Mid to Late Triassic time, a significant change occurred in the paleogeography of the Barents shelf area. This change coincides with the initiation of a progressive uplift of the northern, eastern and southern Barents Sea regions. The evidence for this event includes a significant westward thickening of the Carnian strata (Smelror *et al.*, 2009). This thickening is interpreted as representing a clastic influx from the Fennoscandian Shield and possibly also from a westerly Laurentian source. By late Carnian time, much of the western Barents Shelf, including the Hammerfest Basin, was covered by widespread alluvial plains in coastal and shelf-break settings.

Renewed tectonic activity was apparent towards the end of Late Triassic time in both the North Atlantic and the Arctic regions, continuing into earliest Jurassic time. In the Canadian and Alaskan Arctic, uplift and erosion are apparent, but on Svalbard and the Barents Shelf evidence for fault activity, presumably linked with extension in the North Atlantic region to the south, seems to be more significant. Simultaneously with these North Atlantic and western Arctic events, compression and uplift, generated by the Uralian Orogeny still controlled the sedimentation in the Eastern Barents and Timan-Pechora areas. By Late Triassic, uplift and erosion in the eastern Barents Sea-Kara Sea region led to extensive westward coastal progradation and development of continental and coastal-plain

environments over major parts of the Barents Sea area, whilst marine environments were restricted to the westernmost parts.

In the western Barents Sea, the northern progradation of the Mid Jurassic to Early Cretaceous Atlantic rifting affected particularly the western margin of the Barents Shelf and triggered the development of a marine connection across the Barents Shelf. In the northern areas, tectonic activity appears to be related to extension in the Amerasia Basin, a precursor to the Arctic Ocean opening. Major transgressions in the early Late Jurassic and by the very end of the Jurassic period flooded the entire Barents Shelf, and shallow-shelf to deep-marine sedimentation prevailed over large areas. During the Early Cretaceous, the northern Barents Sea area was subsequently uplifted and large volumes of sediments were shed from the uplifted continental areas in the northeast into deeply subsiding basins in the west. This Early Cretaceous uplift was associated with a major volcanic event which occurred on Franz Joseph Land, Kong Karls Land and adjacent offshore areas (Grogan *et al.* 1998). This Cretaceous magmatic event possibly coincides with the onset of sill intrusion activity in the southern Barents Sea which again suggests a widespread and major phase of volcanic activity in the Barents Sea and Arctic regions. This tectono-magmatic event along the northern rim relates to the onset of break-up prior to the opening of the Arctic Ocean.

Along the southwestern Barents Shelf, successive rifting episodes during the Cretaceous led to rapid subsidence and the development of major deep sag basins such as Harstad, Tromsø, Bjørnøya and Sørvestsnaget basins. These events represent the northern extension of similar phases recorded along the Mid-Norwegian margin. Evidence of Aptian rifting is found in several places on the shelf and a major Cretaceous thinning of the crust affected the Bjørnøya and Sørvestsnaget Basins. Uplift continued towards the north, and by Late Cretaceous time large parts of the Barents Shelf were uplifted. The Late Cretaceous to Paleocene period between Norway and Greenland was progressively taken up by strike-slip movements and deformation within the De Geer Zone leading to the formation of pull-apart basins in the westernmost parts of the Barents Sea, south and west of the SH area.

The Paleocene-Eocene transition marks the continental breakup of the North Atlantic margin and opening of the Norwegian-Greenland Sea at around 55-54 Ma. This event is also characterised by a major volcanic event as witnessed by massive volcanic traps and the formation of volcanic rifted margins which have been identified from the Irish margin up to the Lofoten and NE Greenland shelves. Toward the north, the breakup development along the western Barents Sea sheared margin was younger, locally magmatic (e.g. Vestbakken volcanic province) and rather complex (Faleide *et al.* 1988).

Prior to the opening of the Norwegian-Greenland Sea, a transpressive event developed between Svalbard and the northern Barents Shelf margin. Crustal shortening was concomitant with major extension between Norway and Greenland and is estimated to have been around 30 km (NGU, Batlas). Progressively, the continental strike-slip system, active from the

Paleocene to the Eocene, was subsequently followed by a passive sheared margin development, leading to breakup from Early Oligocene time. Since Oligocene times, separation of the Barents Shelf and Greenland/North America has continued, leading to the opening of the Fram Strait and establishing a North Atlantic-Arctic marine connection in the Miocene.

Lower Tertiary deposits are virtually absent on the eastern and central Barents shelf but marine slope to basinal successions are preserved along the western margin. In the Vestbakken volcanic province there is evidence of breakup-related sill intrusions. A significant magmatic event, which affected the northern part of the Barents Sea, is also recognised in Early Cretaceous time and was most likely part of a Large Igneous Province linking Greenland, Svalbard, Franz-Joseph Land and adjacent shelf areas before the continental break-up and ocean basin formation occurred (Grogan *et al.* 1998, Maher 2001).

During the Pliocene-Pleistocene, the entire Barents Shelf was also eroded and large volumes of glacial and glaciomarine sediments were shed towards the shelf margin where they accumulated as up to 3 km-thick wedges of shelf-margin, basin slope and deeper marine origin (Bjørnøya and Storfjorden fans).

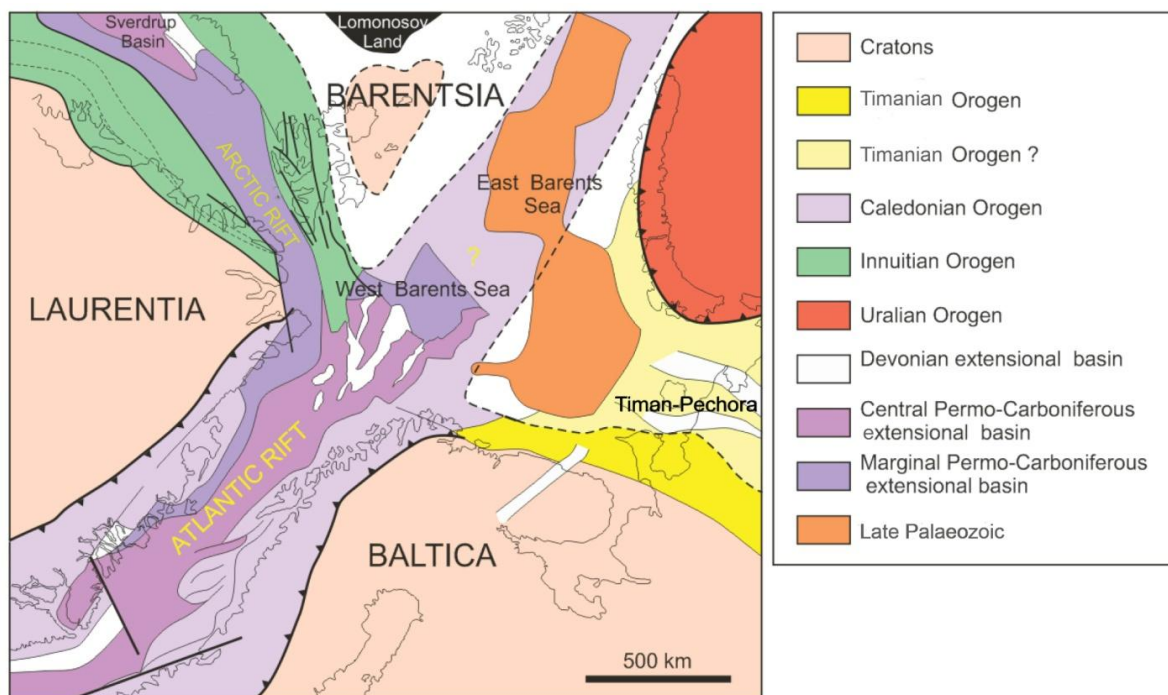


Figure 2.2 Regional palaeotectonics and main orogens and rift zones of the Barents Sea area. Reconstruction at end-Permian time (modified after Gudlaugsson *et al.* 1998).

The eastern side of the Barentsian Caledonides is flanked by the remnants of the Late Neoproterozoic Timanian fold belt, recognised in the Timan-Pechora and Novaya Zemlya regions (Gudlaugsson *et al.* 1998, Roberts & Siedlecka 2002). In southern Novaya Zemlya,

there is evidence that the Timanian orogeny extended up into the Cambrian period (Pease & Scott 2009). The eastern part of the Barents Sea was subsequently affected by a younger collision phase between the Laurasian continent and western Siberia, which culminated in latest Permian to earliest Triassic time. The Urals mountain chain and its northern extension, Novaya Zemlya, mark the suture zone of this closure, which appears to be younger in the latter region.

3 SURVEY CHARACTERISTICS AND ACQUISITION

Marco Brönnner & Janusz Koziel

3.1 Survey area and equipment

The survey area is approximately 486 km long and c. 185 km wide in the south and c. 262 km wide in the north. It covers the area between the HRAMS-97/98 and the BASAR-08 surveys and has an overlap with both of about 4 km to guarantee a proper coupling (Fig. 1.2). The acquisition was carried out during the period 14 May – 14 October 2009. A total of 83 flight-days were necessary to cover the proposed area. For the data acquisition a caesium magnetometer was installed in a so-called ‘bird’ and towed at a sufficient distance from the aeroplane (70 m) to render the plane's magnetic effects negligible (Fig. 3.1).



Figure 3.1 Piper Chieftain from Fly Taxi Nord with the towed Scintrex Caesium Vapour MEP 410 high-sensitivity magnetometer (still in the docking cradle).

The airborne magnetic survey was conducted with constant flight-line orientations, which were adapted from the BASAR-08 survey. In-lines were running almost N-S (c. -5.85° off geogr. N) with perpendicular E-W-oriented tie-lines (Fig. 3.2). Line spacing was equivalent

to the BASAR-08 acquisition and was set to 2 km x 5 km to achieve a good control of diurnal variations of the magnetic field during the data processing.

The entire system was run by the pilots; no additional NGU personnel was required on board to save costs and time. The data were stored on an USB memory stick and sent to NGU by email subsequent to each flight, where it was instantly quality controlled and pre-processed. Before and during flights, NGU staff were permanently controlling the magnetic diurnals through the web page of the Tromsø Geophysical Observatory (<http://flux.phys.uit.no/geomag.html>) and could redirect or abort the flight at any time using a satellite telephone when required.

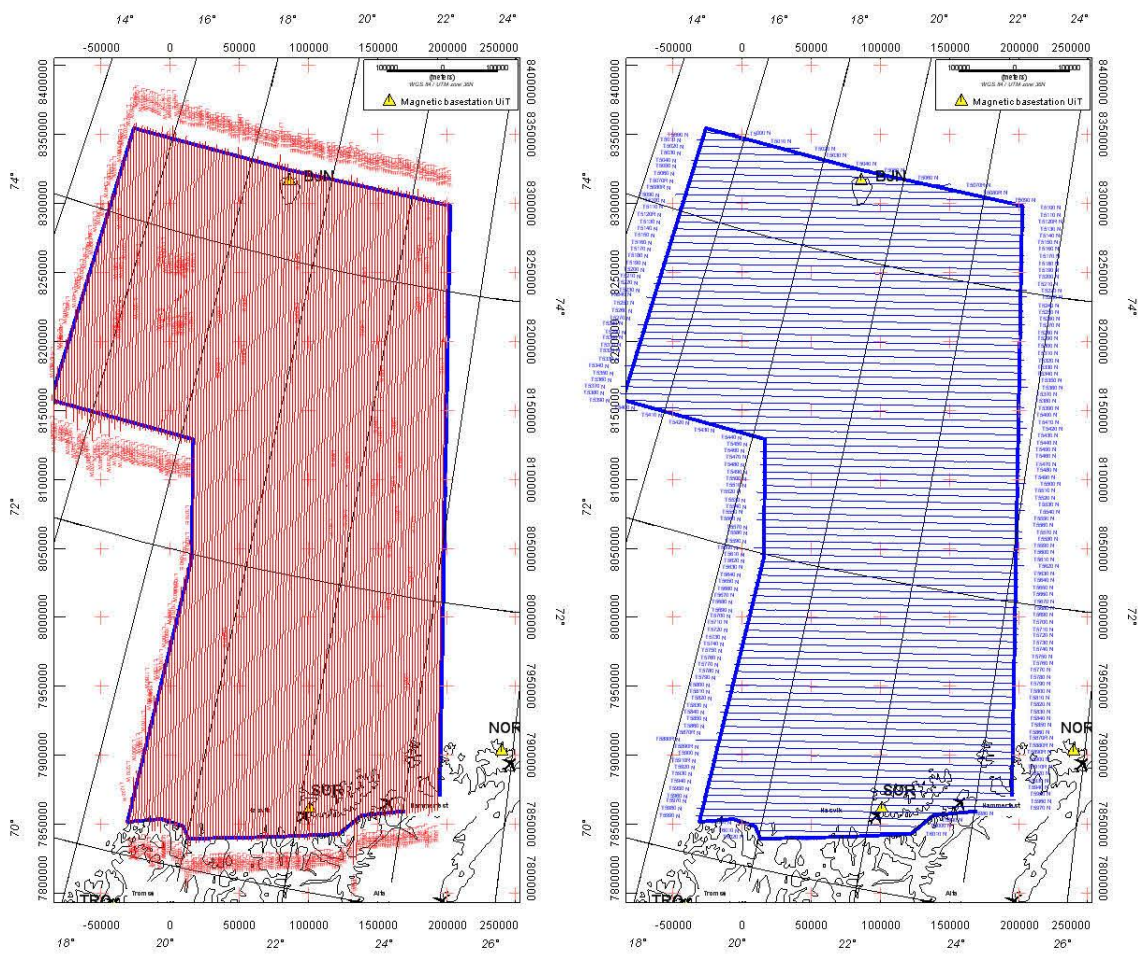


Figure 3.2 Flight pattern (red lines and blue tie-lines) of the BASAR-09 survey.

Table 3.1 defines the coordinates of the original survey area.

Longitude	Latitude	xUTM 36, WGS84	y UTM 36, WGS84
22.57.05	74.33.06	202537	8298792
24.39.46	70.48.13	194894	7876512
24.42.29	70.40.35	194603	7862213
23.13.21	70.33.05	138035	7856559
22.51.27	70.24.42	122042	7843415

21.39.19	70.19.16	75788	7841373
20.01.20	70.11.49	12554	7840049
19.53.42	70.16.10	9575	7848988
19.26.45	70.16.56	-6673	7854102
18.49.39	70.12.48	-31209	7851872
18.51.07	71.58.35	15449	8043524
18.16.29	72.43.20	16297	8129217
15.04.00	72.43.23	-86364	8158063
15.02.19	74.33.41	-26125	8354902
18.57.36	74.33.57	86526	8324283

Table 3.1 Coordinates of the BASAR-09 survey area.

The following summary provides the essence of the survey programme:

Base of operation	Alta and Tromsø airports
Traverse line spacing and trend	2 km, north – south (5.85° cw from N)
Tie line spacing and trend	5 km, east – west
Flying height /sensor altitude	~300 m/230 m.
Speed	~225 km/h
Total line kilometres (in contract)	73,650
Total line kilometres (acquired)	~77,000
Total flight-days	83
Data recorded	Magnetic field intensity, radar altitude and GPS positioning data

Table 3.2 Main characteristics of the BASAR-09 survey.

3.2 Personnel

Participants from NGU:

Project leader:	Odleiv Olesen
Senior engineer:	Janusz Koziel (leader of field operations)
Engineer:	Thomas Møller
Engineer:	Tore Vattekar
Geophysicist:	Marco Brønner

Participants from Fly Taxi Nord:

Captain:	Ronny Thorbjørnsen
Captain:	Ole Thorbjørnsen
Co-pilot:	Andreas Drevvatnet
Co-pilot:	Gard Pettersen

3.3 Equipment and technical specification

The following equipment was used in the survey:

- Aircraft: Piper Chieftain PA31 (registration. LN-ABZ) with long-range fuel tanks from Fly Taxi Nord in Tromsø (Fig. 3.1).
- Navigation: An Ashtech G12, 12 channel GPS receiver combined with a Trimble Navbeacon DGPS correctional receiver (SATREF) with a flight guidance system from Seatex ASA was used for real time differential navigation. The navigation accuracy was better than ± 5 m throughout the survey.
- Altimeter: A KING KRA 405 radar altimeter is an integrated instrument of the aircraft and the data were both recorded and shown on the pilot's display. The altimeter has an accuracy of 0.25% with a resolution of 1 foot (0.3048 m) (Fig. 3.3).
- Magnetometer: A Scintrex Caesium Vapour MEP 410 high-sensitivity magnetometer with a CS-2 sensor was employed in the data acquisition. The noise envelope of the onboard magnetometer was 0.1 nT. Most of the data fell within the limits of ± 0.04 nT.
- Data logging: NGU data logger was used to record the different datasets from the survey.

3.4 Acquisition

The whole area was covered with both tie-lines and traverse lines (Fig. 3.2). The total survey area covered was c. 106,300 km² and consisted of 21,250 km tie-lines and 53,000 km ordinary profiles. The aircraft altitude in the offshore area was 300 m a.s.l. on average (1000 feet) (Fig. 3.3). The magnetic sensor was towed approximately 70 m below and behind the aircraft, giving a sensor altitude of about 230 ± 10 m. For the onshore areas, flight clearance was naturally greater due to topography and poor weather conditions. The flying speed was 225 km/h and magnetic data were sampled at a rate of 5 Hz, giving a spatial sampling interval of 11-14 m along the lines.

The acquisition was planned and carried out within c. 24 weeks from May to October 2009.

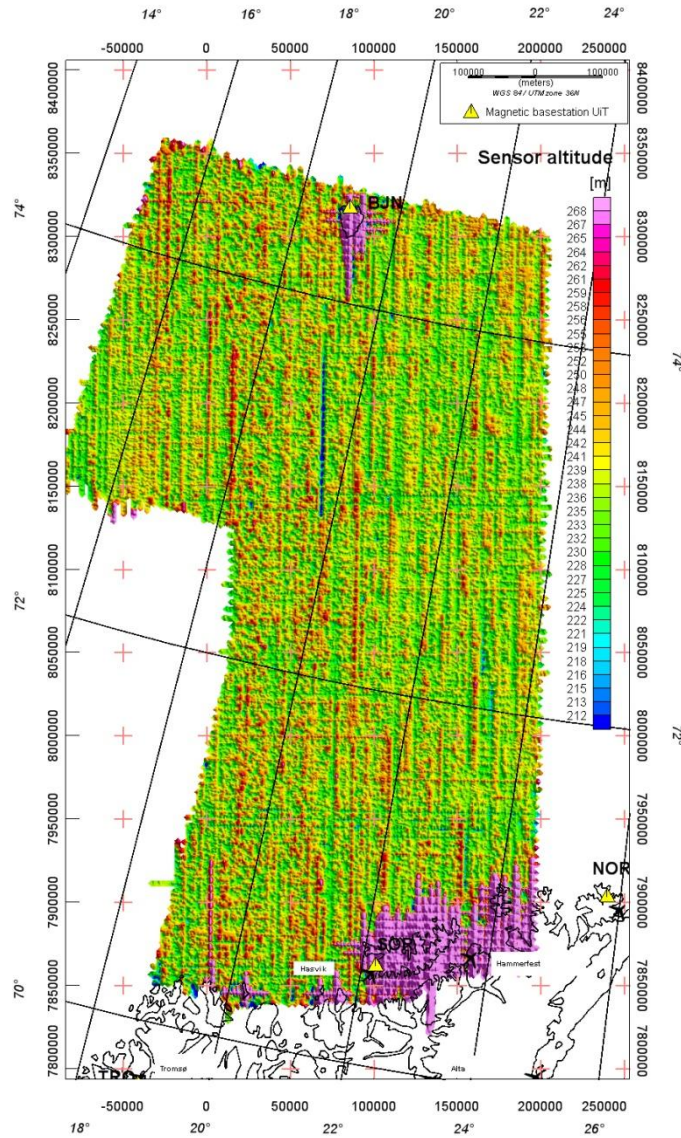


Figure 3.3 Sensor altitude (plane radar altitude – 70 m). In the offshore regions the sensor height was in a range of approximately 220 -250 m. Over onshore Finnmark the ground clearance was generally higher on account of the steep coastal topography and changing weather conditions.

3.5 Magnetic conditions

The most complex problem during magnetic acquisition is probably the diurnal variation of the Earth's magnetic field influenced by solar storms, which are particularly active at high latitudes (i.e. aurora borealis). This usually causes tie-lines and regular survey lines to have different readings at the same geographical point (crossover point). Such misfits can produce artefacts during interpolation and consequently, erroneous interpretations if no suitable corrections have been applied.

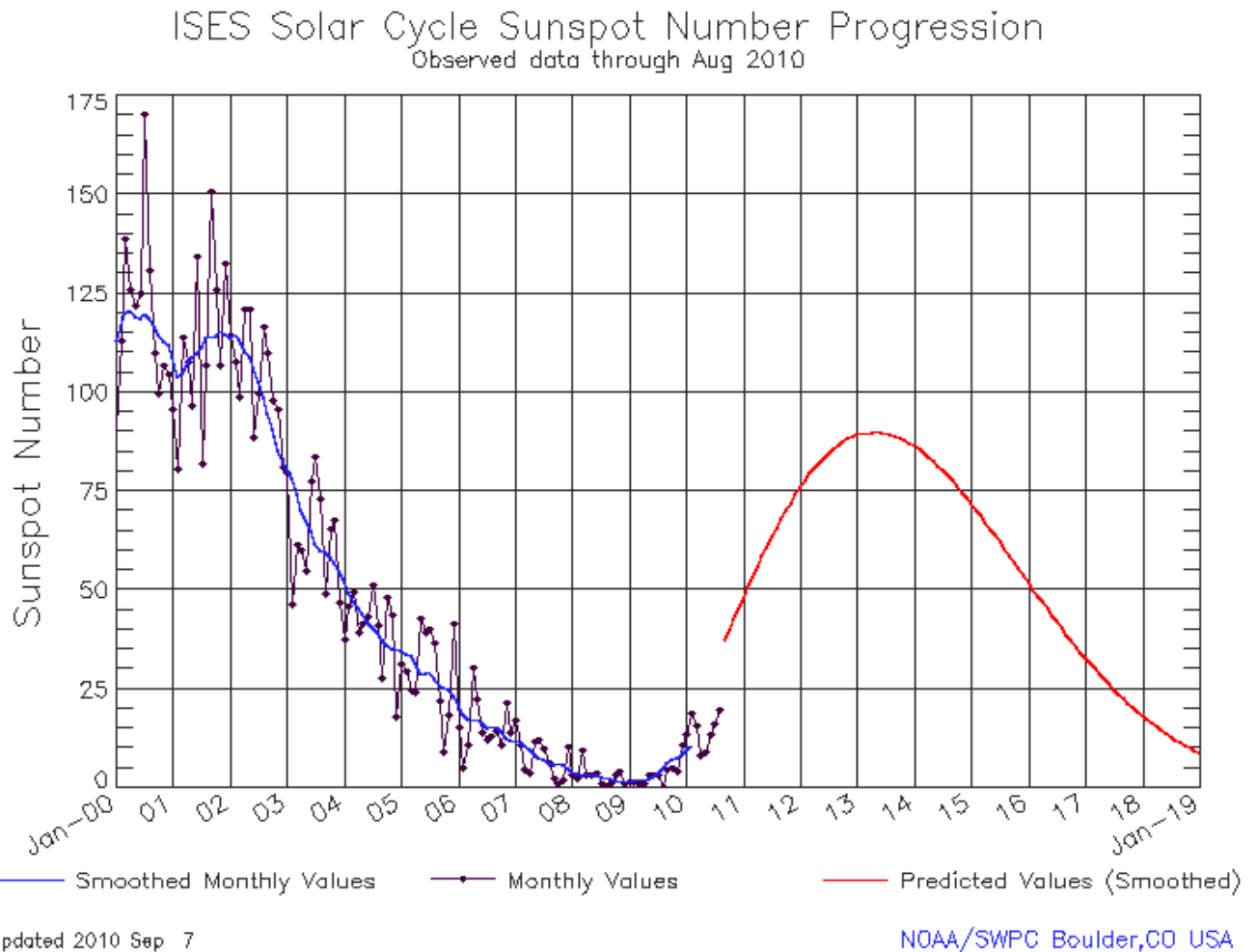


Figure 3.4 Observations and prediction models of sunspot numbers from the US National Oceanic and Atmospheric Administration (NOAA)(<http://www.swpc.noaa.gov/SolarCycle>). Monthly averages (updated monthly) of the sunspot numbers show that the number of sunspots visible on the sun waxes and wanes with an approximate 11-year mega cycle. The BASAR-09 survey was carried out during a period of extremely low solar activity, which presented excellent conditions for the aeromagnetic acquisition.

If the survey is located close to a base station site, the lines can be directly corrected for diurnal variation. However, most of the offshore acquisition extends far away from land stations and is then liable to experience different diurnal variations. Efficient statistical algorithms and filtering are usually required to solve this issue and to ‘level’ in an acceptable way all the magnetic profiles (see Chapter 4). The sunspot cycles strongly influence the geomagnetic field and diurnals. The BASAR-09 was acquired during a relatively quiet period. Solar cycle predictions suggest that 2009 was in a minimum of sunspot activity (Figs. 3.4, 3.5), thus providing relatively good magnetic conditions at the time of acquisition. Nevertheless, due to the high latitude of the survey area, magnetic data can be locally strongly influenced by variations in the Earth's magnetic field. Therefore, we applied several steps of quality control to minimize the amount of data affected by these variations:

- The daily flight-plan was made under consideration of the recorded Earth’s magnetic field variations from base-stations in the area, e.g. Tromsø, Bjørnøya and Sørøya (Recordings in real-time provided by the University of Tromsø: <http://flux.phys.uit.no/>).
- Data QC of every flight-day was carried out using base-mag data from these three stations to classify the data quality and to plan possible repeat flights (Tab. 3.3).
- Tie-line levelling was carried out in conjunction with the recorded variations in the Earth's magnetic field.

The diurnals for all flights are included in the database file delivered on the BASAR-09 archive CD. These plots ease the quality control of the acquired profiles. The data were classified into two quality groups according to the magnetic diurnals:

Class	Criteria	Profile length
1	< 10 nT/10 min. Linear	74,300 km
2	10 – 30 nT/10 min. Linear	2,700 km
Total		77,000 km

Table 3.3 Results from data QC and the re-fly programme of BASAR-09.

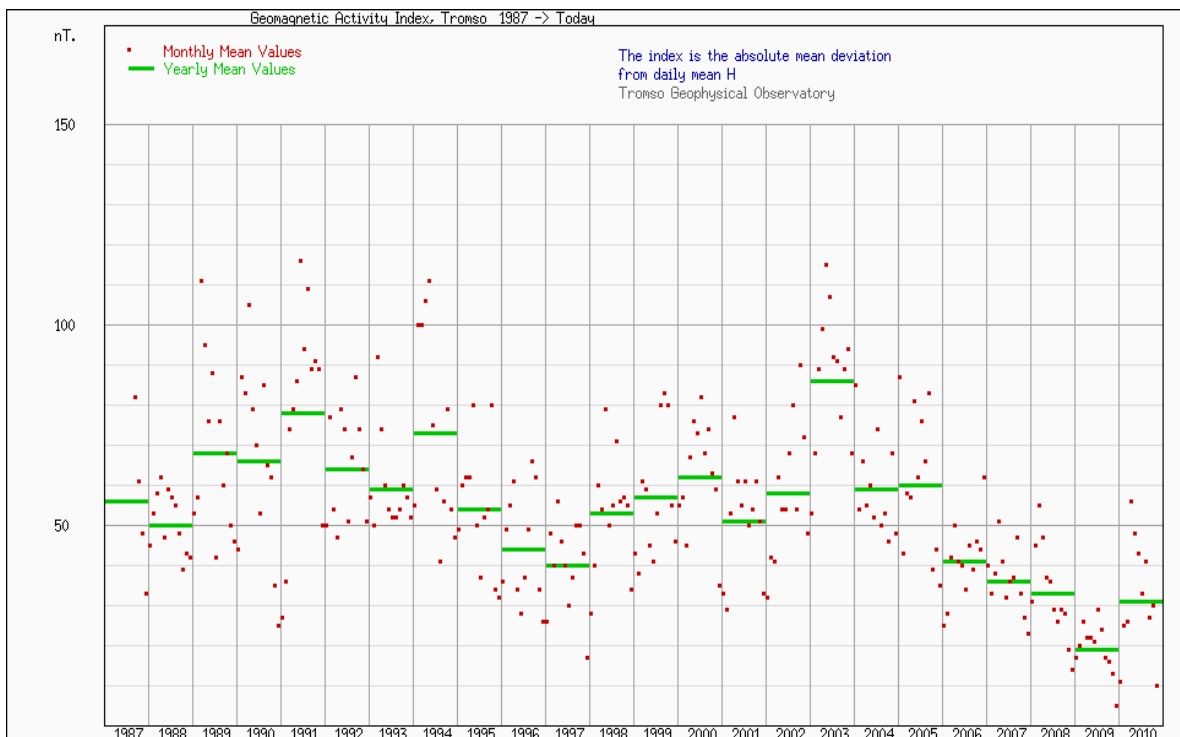


Figure 3.5 Diagram of the monthly mean values of the horizontal intensity of the geomagnetic field (H) observed at the Tromsø Observatory from 1987 to 2010. This graph illustrates the good correlation between the periodic and semi-periodic evolution of the field and sunspot activity. A similar variation between the polynomial average of H and its running average illustrates the average good magnetic conditions for aeromagnetic surveying during the period May-October 2009. Geomagnetic data derive from Tromsø Geophysical Observatory (<http://www.tgo.uit.no/aix>).

A total of c. 2700 line km was of intermediate quality (Fig. 3.6) and reflight at the end of the acquisition. During the levelling process, all remaining effects from the background magnetic field variations were further removed or reduced to a minimum.

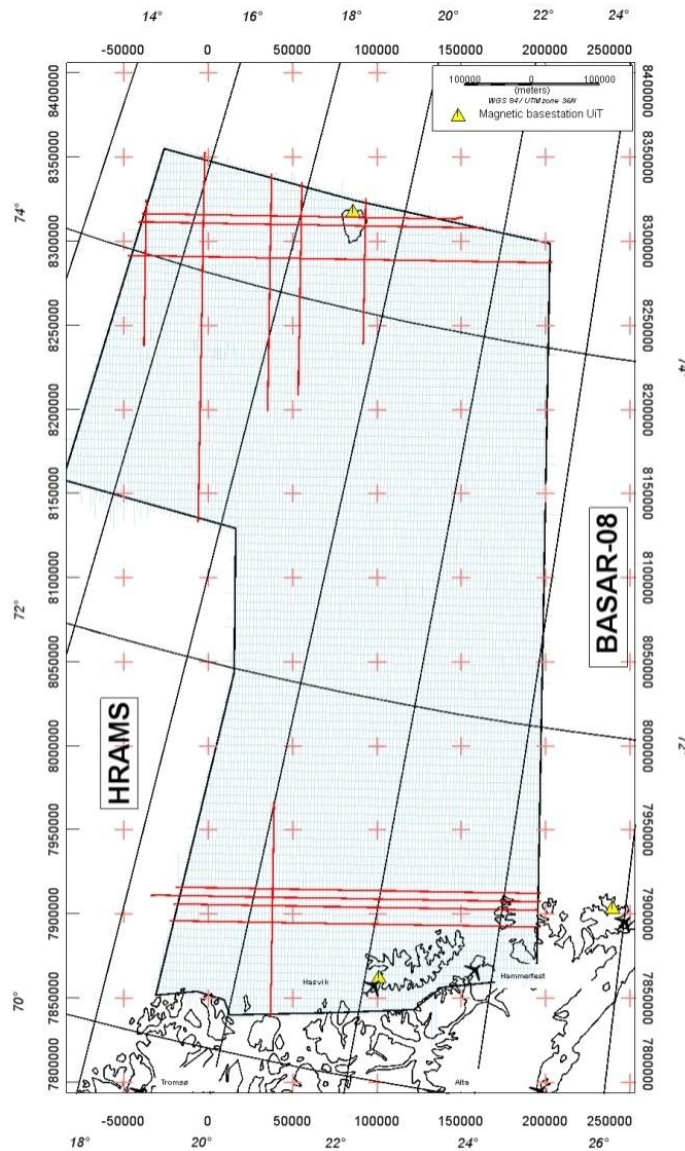


Figure 3.6 Profiles with locally intermediate quality due to strong diurnal variations (i.e. diurnal variation between 10 and 30 nT per 10 minutes) were evaluated for reflaying. The total length of intermediate-quality data is 2700 km (i.e. 3.5 % of the total survey). The red lines mark the profiles which were decided to be reflown.

To estimate the influence of the magnetic signature of the aeroplane, a magnetic heading test (clover-leaf test) was carried out in October 2006 in the Hammerfest region for the SNAS-06 and BAS-06 projects. The magnetic signature of the aeroplane also includes 1) its permanent magnetisation induced by its motion through the Earth's magnetic field, 2) a component due to the flow of electric current within the plane, and 3) the orientation of the magnetic sensor inside the bird. The permanent magnetisation of the plane varies as the plane changes its

orientation, thus leading to heading errors. The maximum difference of magnetometer readings in the four different directions as it turned out from this test was small: 1.2 nT. We decided not to carry out another new clover-leaf test in 2009 and considered the effect as negligible.

3.6 Gridding, map production, projection and archive CD

The Oasis montaj software (Geosoft 2004) was used throughout for the map production. This software package has become a standard for many potential field experts in the mineral and petroleum industry. All databases and grids in Geosoft format are provided on the BASAR-09 archive CD. The grids are usually presented with a shaded relief technique (illumination from the northeast) and a non-linear colour scale. Gridding was performed using the bi-directional gridding technique with a grid cell size of 400 x 400 m ($1/5$ of the inline profile distance). Bi-directional interpolation produces a smooth grid while attempting to honour the data as closely as possible. The interpolation is especially better adapted to elongated, very narrow and high-amplitude anomalies which are not parallel to the profiles (e.g. onshore-offshore Sørøya and close to the shoreline). Presentation of the maps with the shaded relief technique enhances lineaments that trend oblique to the illumination direction. Colour scale and colour distribution for the datasets have been computed using a histogram equalisation technique. These maps have been produced in the Universal Transverse Mercator projection (UTM zone 36) using the WGS 84 datum. However, for the regional interpretation we used the UTM 35 projection.

On the CD we provide an Oasis montaj Viewer and its tutorial for companies that do not use Oasis montaj specifically. The Oasis montaj Viewer is a free and easy-to-use software that allows anyone to view, share and print published Geosoft grid (.grd) and database (.gdb) files. The viewer can also be used to convert grids and images to a variety of supported data formats, including AutoCAD, ArcView, ER Mapper, TIF and many more. The free software can also be shared and downloaded from

<http://www.geosoft.com/pinfo/Oasismontaj/free/montajviewer.asp>.

For specific questions on special needs, please do not hesitate to contact NGU (either Marco.Bronner@ngu.no or Odleiv.Olesen@ngu.no).

4 DATA PROCESSING AND PROFILE LEVELLING

Marco Brönnner

RAW-magnetic data (Fig. 4.1) cannot be used directly for gridding and require a number of processing steps before the production of the final aeromagnetic grid and the map of the total magnetic intensity (TMI) for interpretation use. Noise filtering and statistical levelling processing were carried out using the professional Oasis montaj software (Geosoft 2005b). Micro levelling was performed using the MAGMAP FFT package from Oasis montaj (Geosoft 2005a). The raw data have been processed using standard procedures and methodologies used in many other geological surveys (Luyendyk 1997). The various processing steps and standard procedures are outlined below.

4.1 Preliminary noise filtering and basic corrections

4.1.1 Noise filtering

High-frequency noise is usually created as the aeroplane is manoeuvring. After acquisition, initial raw data were imported directly into an Oasis montaj database and subsequently interpolated to a regular grid of 400 x 400 m cells, to check the quality of lines and tie-lines (Fig. 4.1). Spikes due to minor noise and artefacts were first removed by non-linear (Naudy) filtering and subsequently smoothed with a light low-pass filter (10 fiducials=500 m) in order to keep the signal intact.

4.1.2 Systematic lag corrections

A systematic lag correction for the BASAR-09 data was tested but not applied as it did not affect the data quality.

The TMI RAW data reflect the recorded magnetic field, including the Earth's geomagnetic main field and all disturbances. The data are dominated by the Earth's geomagnetic field, observable by the increasing magnetics to the northeast.

4.1.3 International Geomagnetic Reference Field (IGRF correction)

As part of the processing, the total magnetic intensity (TMI) field is computed from the recorded magnetic field after subtraction of the International Geomagnetic Reference Field (IGRF) model (Fig. 4.2). The IGRF is a mathematical representation of the undisturbed Earth's geomagnetic field. The change of the IGRF field in the BASAR-09 survey area is about +57 nT per year, on average.

The International Geomagnetic Reference Field for 2009 (IGRF-2009) was calculated using the Oasis montaj IGRF tool (Geosoft 2005b). The result of this subtraction isolates the component of the magnetic total field, which is dominated by the magnetic effects from the underlying crustal rocks.

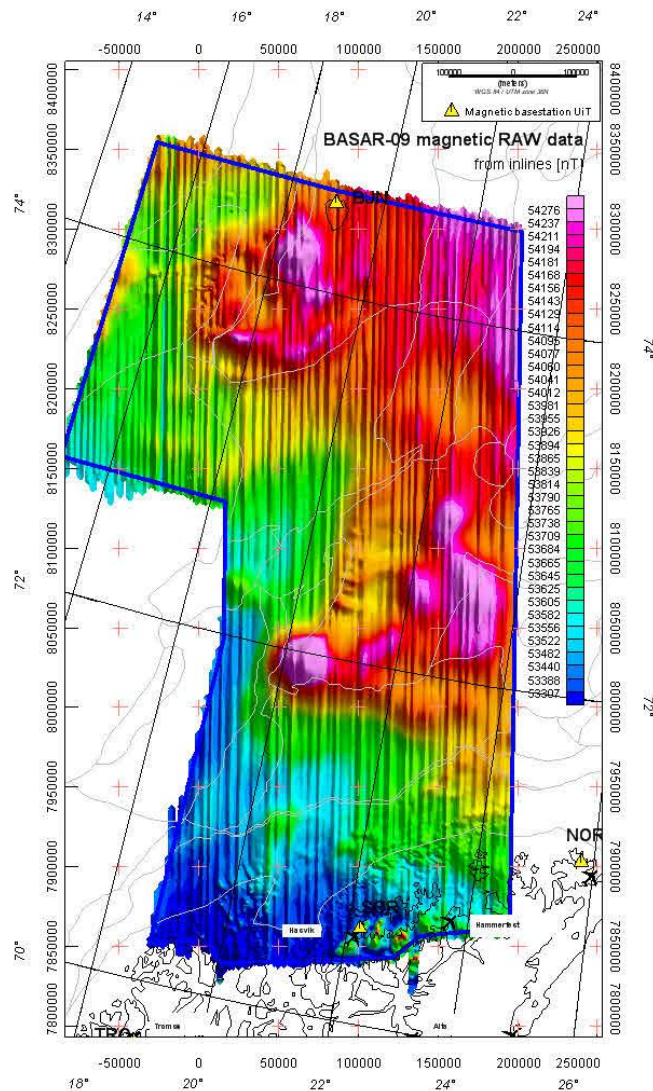


Figure 4.1 BASAR-09 TMI RAW magnetic profile data (without levelling) gridded by means of the minimum curvature algorithm (grid cell size at 400 x 400 m). Note that the artefacts are mostly parallel to the line profiles due to diurnals. Projection UTM 36, WGS 84.

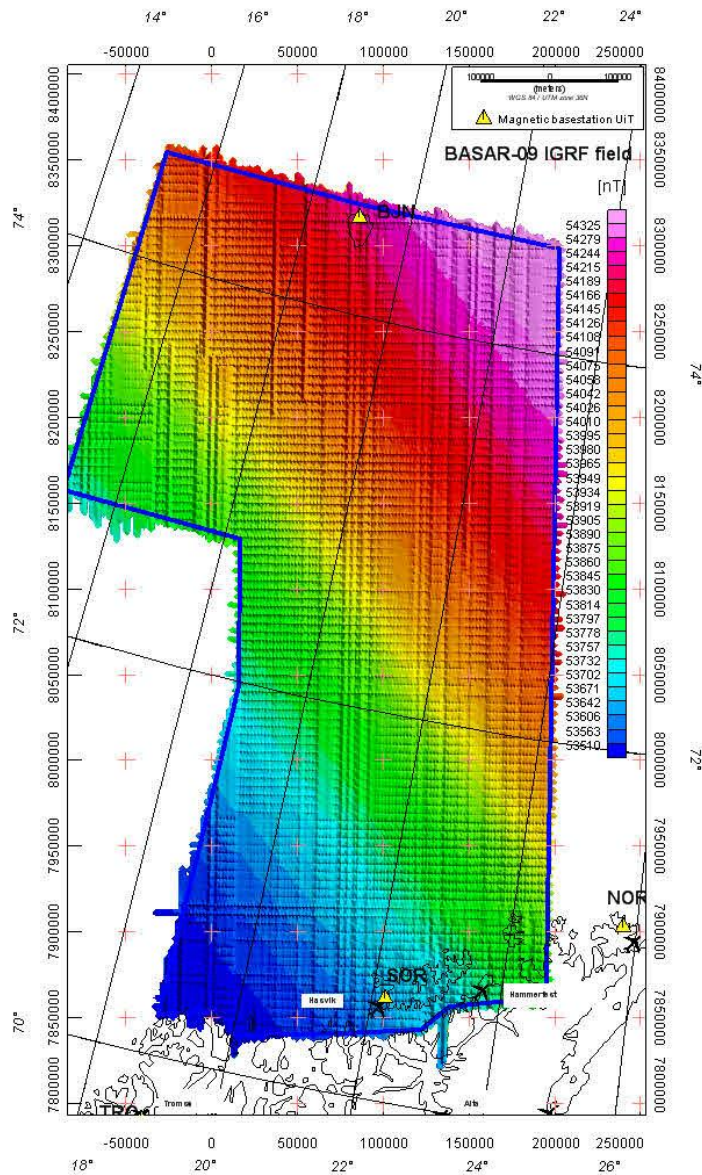


Figure 4.2 The IGRF-2009 (formally 2005) model within the BASAR-09 survey area.

4.2 Levelling and micro-levelling of the magnetic profiles

4.2.1 Diurnal variation and use of base-magnetometer readings

As shown in figures 4.1 and 4.3, a variety of external, time-varying, field factors usually influences and causes errors during aeromagnetic acquisition. This includes time variation in the magnetic field, ground clearance variation, altitude variation, magnetic effects of seawater swells and diurnal effects. These factors are usually sufficient to explain the errors at crossover points between lines and tie-lines. The most complex and significant problem is probably the diurnal variation of the Earth's magnetic field influenced by the solar wind (Fig.

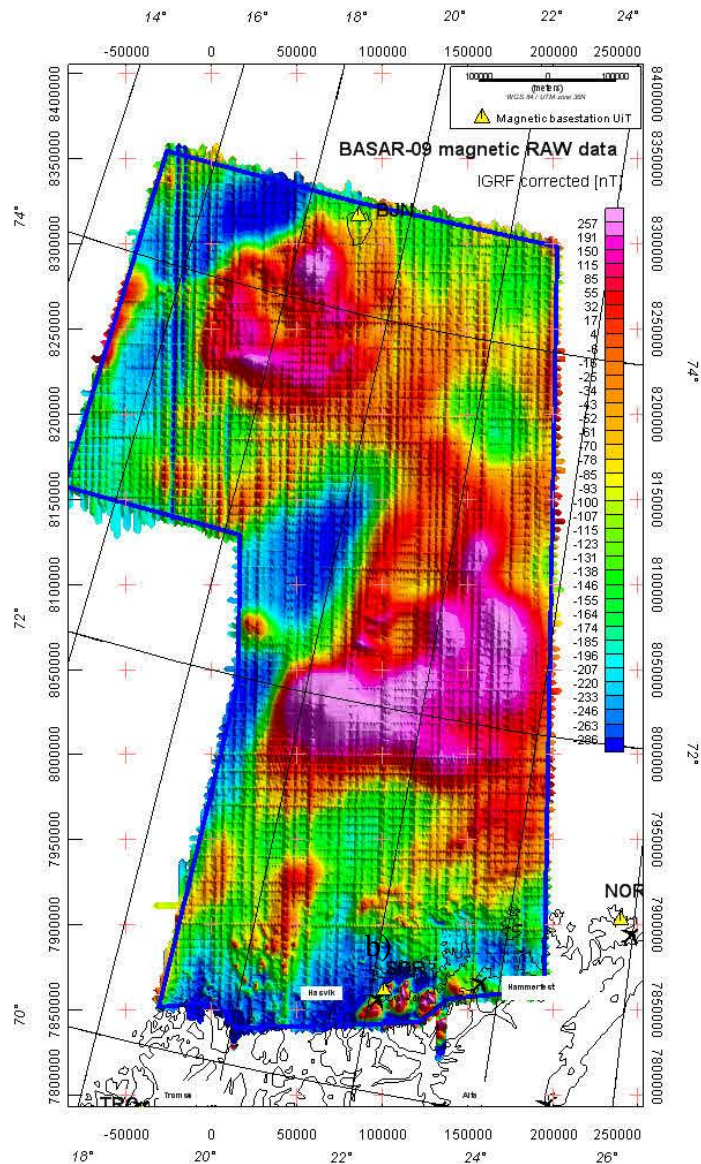


Figure 4.3 BASAR-09 IGRF-corrected total magnetic field of the TMI RAW data.

2.6). At polar latitudes, the most famous and spectacular expression of these diurnal effects is the aurora borealis, known to be caused by the collision of charged particles (e.g. electrons) in the magnetosphere with atoms in the Earth's upper atmosphere. Diurnal variations in the magnetic field can cause tie-lines and regular survey lines to have different readings at the intersections. Even if they are small, these long-wavelength effects can be visually distracting, particularly on image-enhanced displays. Such misfits can produce artefacts during interpolation and, consequently, erroneous interpretation if no suitable corrections have been applied.

The most important reason for this is the time shift in the Earth's magnetic field variations between the large survey area and the onshore base station. There is normally a spatial difference in amplitude and frequency of these diurnals. However, for the BASAR-09 survey,

two base magnetometer stations of the Tromsø Geophysical Observatory were situated within the survey area: Bjørnøya in the north and Sørøya in the south. During statistical levelling the tie-line data and base-magnetometer records of the closest station were tested for a noticeable diurnal effect, and lines with an obvious correlation were tentatively corrected by subtracting a 20 km low-pass filtered signal of the corresponding base-magnetometer records.

	Tie-line number
Bjørnøya base-magnetometer corrected	5000 – 5340, 5470 -5490
Sørøya base-magnetometer corrected	5690 - 6020
No correlation with base-magnetometer records	5350 -5460, 5500 - 5680

Table 4.1 Overview of tie-line corrections with lowpass filtered records from base-magnetometers in Sørøya and Bjørnøya. If no correlation was found, only statistical levelling was applied.

This technique was beneficial to the data quality for tie-lines in the northern and southern parts of the survey area, but did not work for some tie-lines in the north and in the central part of the area, where the time-dependence of the field variations was too large (Tab. 4.1). Here, only statistical levelling was applied.

4.2.2 Statistical levelling

The purpose of levelling is to minimise the residual differences in a coherent way by proportioning them between lines and tie lines. Proper levelling or micro-levelling algorithms usually require close and proper line spacing, and the quality of the final result is generally a function of this crucial parameter. The large line spacing of previous surveys did not allow proper levelling, and interpolation of raw data produced erroneous or factitious anomalies.

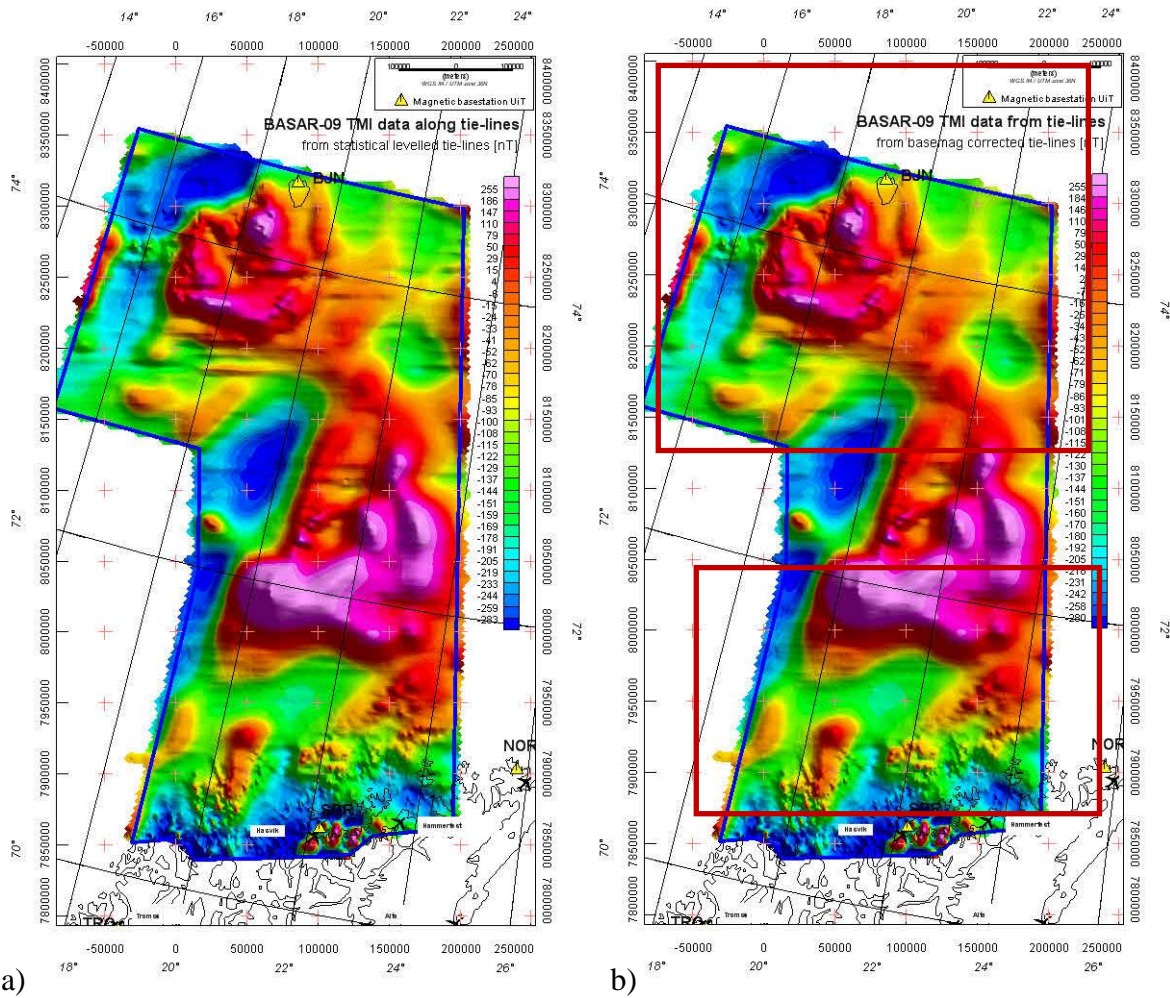


Figure 4.4 a) Statistical tie levelling of the magnetic profiles and b) additional basemag corrected tie-lines (Sørøya (red rectangular) and Bjørnøya (green) basestation corrected). Gridding of the tie profiles used the minimum curvature algorithm (grid resolution: 400 x 400 m).

For this project, levelling was undertaken using a standard statistical levelling method of the tie-lines and survey lines, provided as part of the Geosoft Oasis montaj package (Geosoft 2005a). The new aeromagnetic survey was processed using a statistical levelling method by which the discrepancies between the readings at each crossover point were reduced by systematically proportioning them between the tie and line profiles. ‘Suspicious’ crossover differences (outliers) were first removed manually before levelling and full-levelling of the tie-lines and line profiles. After the described base-magnetometer correction for almost all tie-lines, a first-order (linear) trend removal was applied during the tie-line levelling, but for a few lines in the central part of the survey an additional tension spline (b-spline) correction was necessary after several preliminary tests. Line levelling was carried out using only first order detrending (Fig. 4.5). Extreme mis-tie values (outliers) were checked and removed again manually before calculating the next full-levelling correction, until convergence was achieved.

The final result has to be considered as the best compromise between the removal of levelling errors and anomaly preservation.

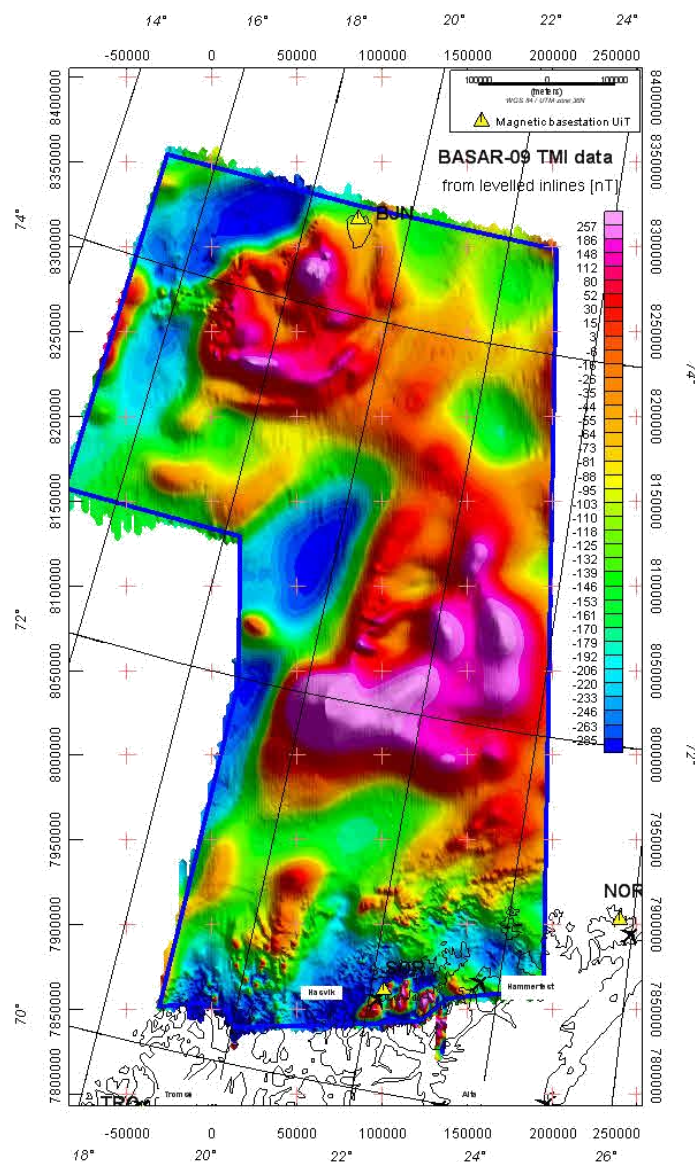
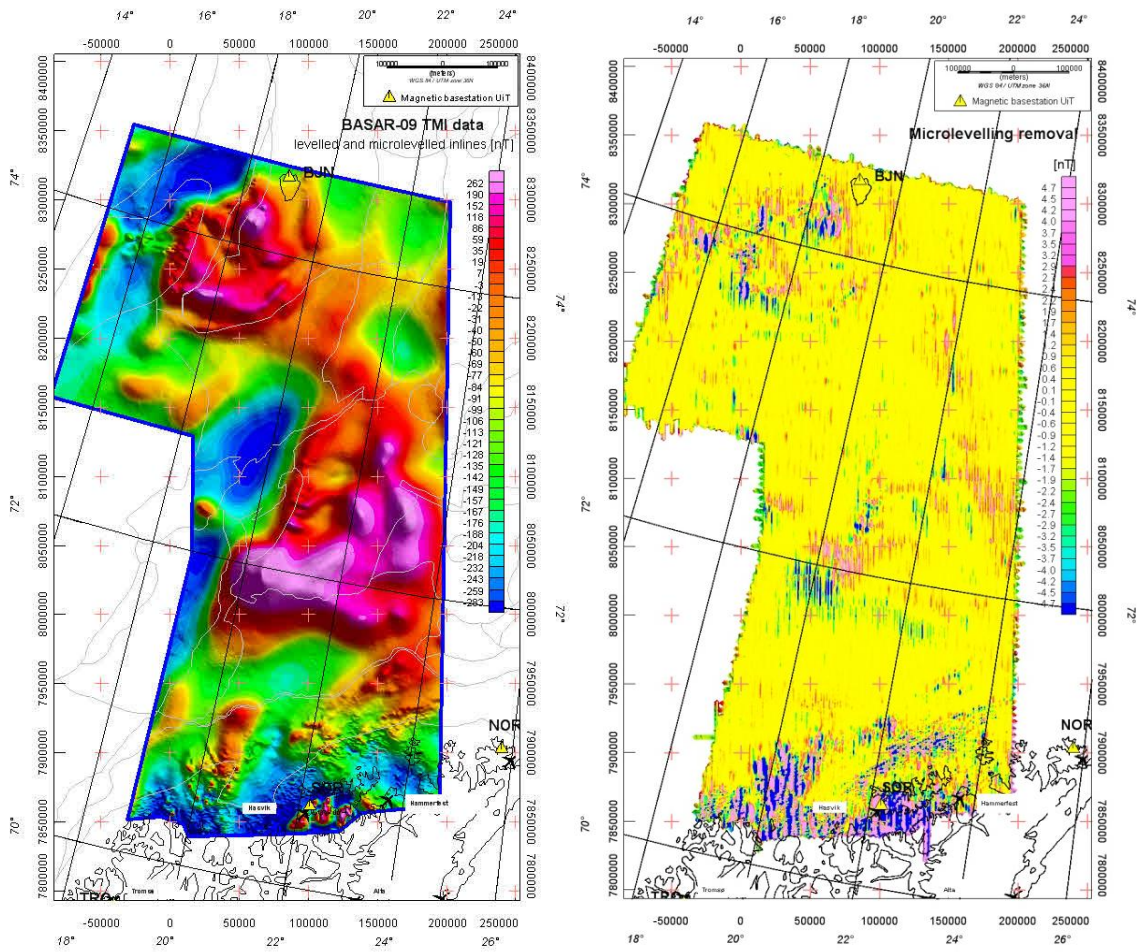


Figure 4.5 Full levelling of the magnetic data. Gridding of the profiles used the minimum curvature algorithm (grid resolution: 400 x 400 m).

4.2.3 Micro-levelling

We performed micro-levelling to remove minor ('micro') levelling errors still remaining along parts of some profiles after the statistical levelling. To improve the levelling, the Geosoft micro-levelling approach using the PGW GX system of the available MAGMAP processing package (Geosoft 2005a) was used. It proved to be better adapted to preserve geological information for this specific case where the remaining levelling errors are irregularly distributed. The PGW GX system applies a decorrugation process in the frequency domain to isolate the levelling corrections before applying them to the original data (Figs. 4.4a and b). The BASAR-09 data have been decorrugated to reduce line-to-line

levelling errors, which are visible as linear magnetic features parallel to the flight lines (Fig. 4.5). Decorrugation is simply a frequency domain procedure based on a directional cosine filter. This filter retains anomalies, from gridded data, in the flight line direction only. First, a Butterworth high-pass filter is set to four times the line spacing to pass wavelengths on the order of two to four line separations. Such a process results from a line-to-line levelling error. In a second step, a directional cosine filter is set to pass wavelengths only in the direction of the lines. Afterwards, a line-based filter was used to separate the high-frequency geological signal from the longer wavelength levelling errors.

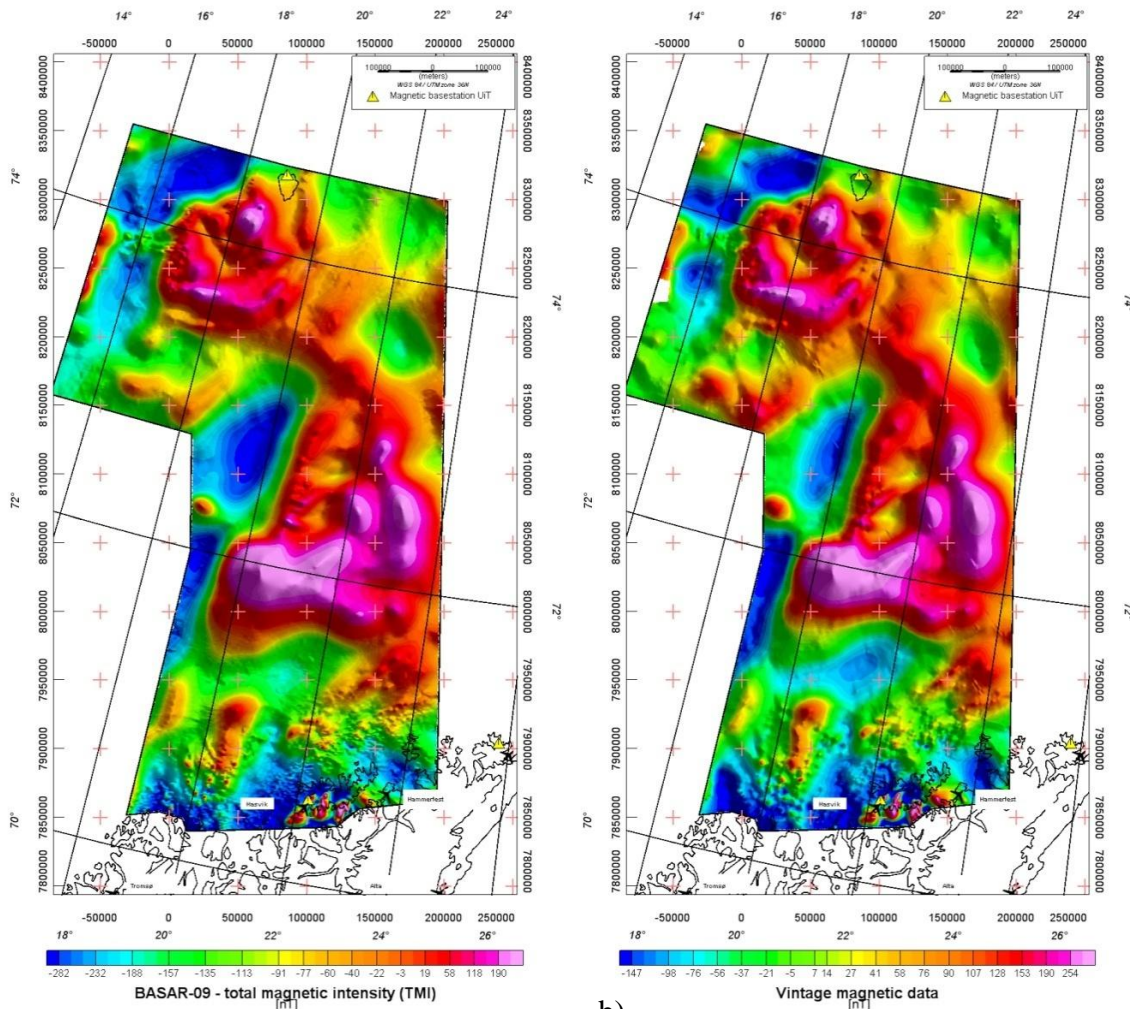


a)

b)

Figure 4.6 a) TMI field after micro-levelling and b) magnetic residual after micro-levelling by decorrugation and subtraction of the total field obtained by statistical levelling (400 x 400 m grid cell spacing).

A Naudy, non-linear, low-pass filter was finally applied to clean the levelling error channel. The micro-levelling result was obtained by subtraction of the magnetic residual levelling grid (Fig. 4.6b) from the original dataset (Fig. 4.4a). The subtracted field is mostly rather small in a range of appr. ± 2 nT. Only locally and in the onshore regions, where the amplitudes are much higher, were larger values subtracted from the original field.



a)

b)

Figure 4.7 a) BASAR-09 total magnetic field from both tie-lines and in-lines after micro-levelling. Results from the FFT decorrugation technique of Geosoft. The 400 x 400 m grid was produced using the minimum curvature gridding algorithm. b) Vintage NGU-69, NGU-70 and BAMS-85 data (Olesen et al. 2010).

5 FINAL MERGER AND COMPARISON WITH PREVIOUS COMPILATION

Marco Brönnner

5.1 Merger of the BASAR-09 grid with the former regional grid

With the completion of covering the entire southern Norwegian Barents Sea with new and state-of-the-art aeromagnetic data, we assembled a new compilation by merging every single survey together from scratch. For merging we used the INTREPID software GridMerge, which allows merging multiple grids in a selected order, considering the quality and resolution of the various surveys. The BASAR-09 grid has been merged with the pre-existing surveys of the Norwegian Barents Sea and mainland Norway:

- BASAR-09
- BASAR-08
- BAS-06
- HRAMS 97/98
- SPA-88
- BSA-87
- NGU-70
- NGU-69
- Norway mainland

The grid-merge of data with different quality can locally decrease the resolution of high-quality datasets (in particular in the overlapping areas). For local interpretation and modelling, we consequently recommend using the original BASAR-09 grid. The compilation grid can only be provided to the partners that also purchased the vintage NGU magnetic datasets, which were used for this compilation.

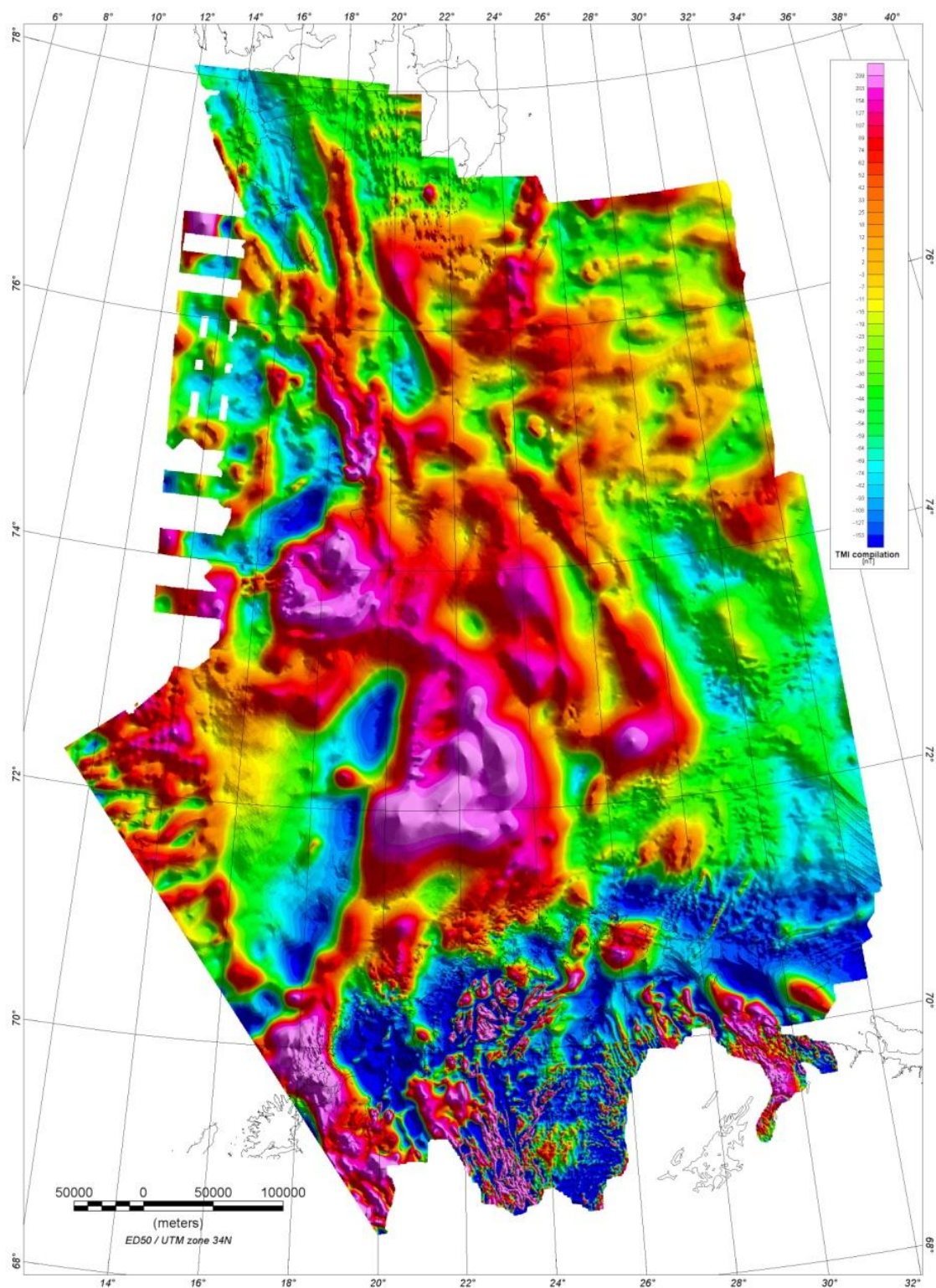


Figure 5.1 Updated regional compilation with BASAR-09 and previous BASAR-08, BAS-06, HRAMS-97/98, BSA-87 SPA-88, NGU-69 and -70 and mainland data (Åm 1975, Skilbrei et al. 1990, Skilbrei 1991, 1992, 1993, Olesen et al. 2006, 2010, Brønner et al. 2009).

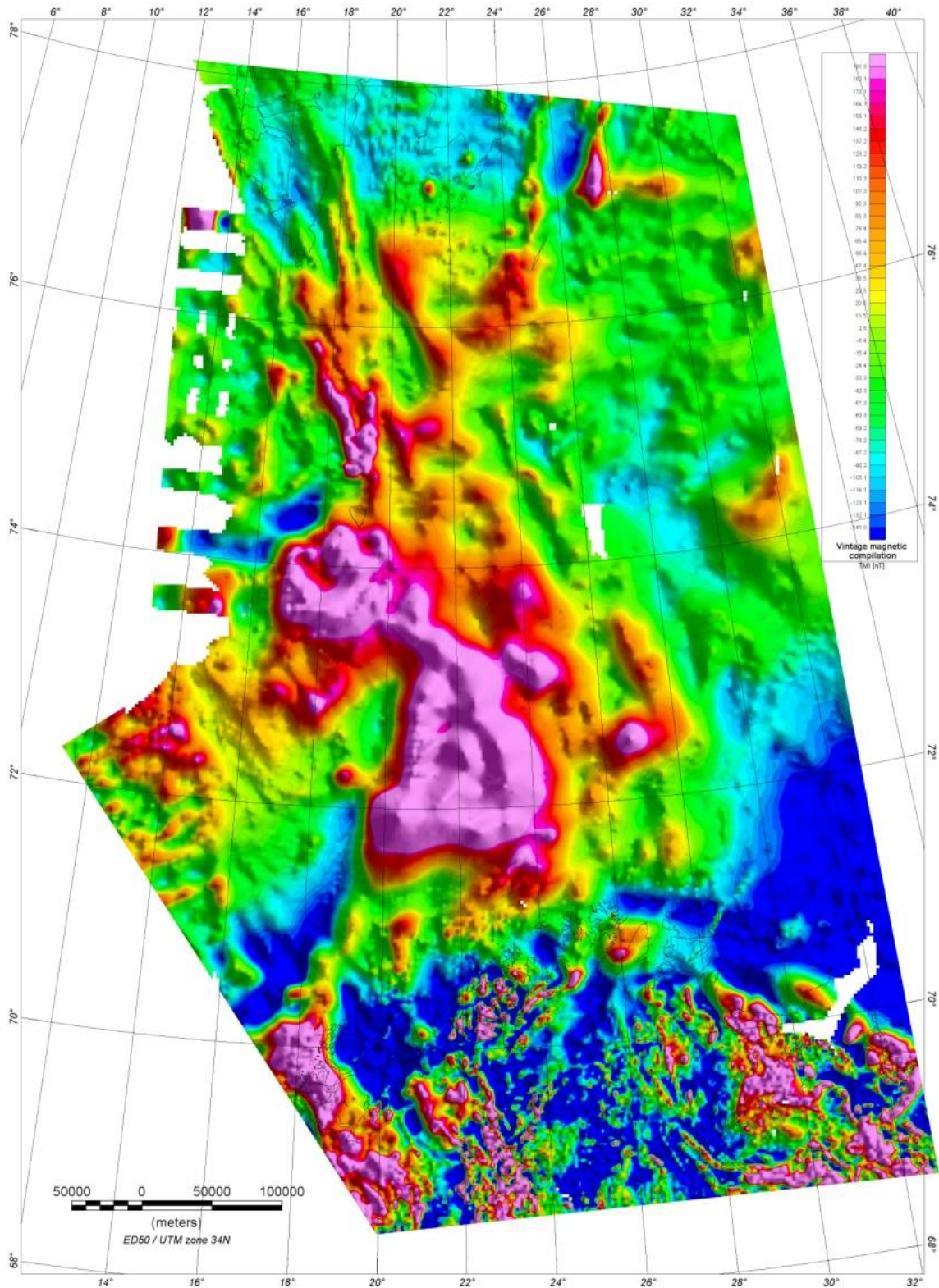


Figure 5.2 Regional compilation using vintage NGU data (Åm 1975, Skilbrei et al. 1990, Skilbrei, 1991, 1992, 1993, Olesen et al. 2006, 2010).

5.2 Comparison with the previous compilation

A comparison between the new compilation, including the most recent surveys HRAMS-97, BAS-06, BASAR-08 and BASAR-09 and the vintage dataset reveals a significant improvement in data quality and resolution (Figs. 4.7a, b, 5.1 and 5.2). Some principal anomalies, such as the Stappen, Loppa, Norsel and Mercurius highs and the Western Varanger Graben, remain similar but in the new dataset additional small-amplitude features are revealed and the principal structures appear much more differentiated and more coherent. The extension of the basins appears sharper and the signature of the shallow salt structures, especially in the Nordkapp Basin but also in the Tromsø and Hammerfest basins, is much more coherent. The HRAMS-97/98 data with only 1000 m line spacing map the western flank of the Tromsø Basin and the Senja Ridge remarkably well and show a lot of shallow, probably intrasedimentary structures. In the BASAR-09 and BASAR-08 area, and even more so in the BAS-06 area, various magnetic lows and some smaller magnetic highs are much more pronounced than in the vintage datasets.

For the Stappen and Loppa highs the new dataset shows much more details and an improved image of the existing features. For example a magnetic lineament east of Bjørnøya runs continuously into the Stappen High, while the connection between the Stappen and Loppa highs appears narrower. North of this connection, two NNE-SSW-striking lineaments can be observed from the new data, which are likely to correlate with the Leirdjupet Fault Complex previously observed on seismics. The longish, tail-like, magnetic high running north-northwest from the Norsel High appears to be narrower and more continuous and isolated from the adjacent areas than before. Just to the east, a distinct magnetic low runs almost parallel to this structure continuously into the central Nordkapp Basin. Moreover, the previously undifferentiated magnetic high south of the southern Nordkapp Basin shows lineament features and a possible trisection. Furthermore, the new datasets also reveal lineaments passing through and around the Tromsø, Hammerfest and Nordkapp basins and on the Finnmark Platform along the northern Norwegian coast, which are likely to be fault- and/or dyke-related. Some of these lineaments were already mapped from other datasets like reflection seismics or gravity, and here the new magnetic data can be helpful to complete or refine the picture of their geometry. Other structures are completely new, as e.g. a lineament trending WSW-ENE and crossing almost the entire BASAR-08 survey area and into the BASAR-09 area.

The acquisition of the new data during the last four years also, and in particular wanted, to close the gap between offshore and onshore observations to allow a combined interpretation and correlation of the onshore geology of Finnmark and Troms with the offshore regions on the Finnmark Platform and beyond. A number of additional linear features, which can be linked with structures observed onshore could be followed into offshore regions and were thus allowing a better onshore-offshore correlation and provide a better basis for the interpretation of particular features.

6 OTHER DATASETS

Marco Brønner

6.1 Bathymetry

The bathymetric grid used in the present study is a NGU compilation and gridding of several ship-track bathymetric profiles available along the study area (Olesen *et al.* 2010). All the profiles have been levelled using the moving median filtering method (Mauring *et al.* 2002, Mauring & Kihle 2006).

6.2 Gravity

The gravity grid was compiled from gravity stations on mainland Norway with the addition of marine gravity data from the Geological Survey of Norway, the Norwegian Mapping Authority, the Norwegian Petroleum Directorate, and Norwegian and foreign universities and commercial companies (Olesen *et al.* 2010). The compiled Free-air dataset has been interpolated to a square grid of 2 km x 2 km using the minimum curvature method (Geosoft 2005a). The simple Bouguer correction at sea (Mathisen 1976) was carried out using the bathymetry data and a density of 2670 kg/m³. The International Standardization Net 1971 (I.G.S.N. 71) and the Gravity Formula 1980 for normal gravity have been used to level the surveys (Fig. 6.1).

6.3 Seismic data

Seismic reflection profiles provided by the Norwegian Petroleum Directorate were combined with gravity and magnetic data for interpretation and modelling. The seismic data were only available in two-way travel times. For the potential field modelling, a depth conversion was necessary and carried out by NGU using EasyDepthTM from Beicip-Franlab (Beicip-Franlab 2002). The resulting depth models were directly imported into the GM-SYS package and used for potential field modelling.

The interpretation of four regional transects, expanding the original survey area, has been realised during this work. We used key horizons presented in the previously published reports and papers and also used well information provided by NPD to constrain the geological model. A detailed description of the depth conversion and potential field modelling is presented in chapter 11.

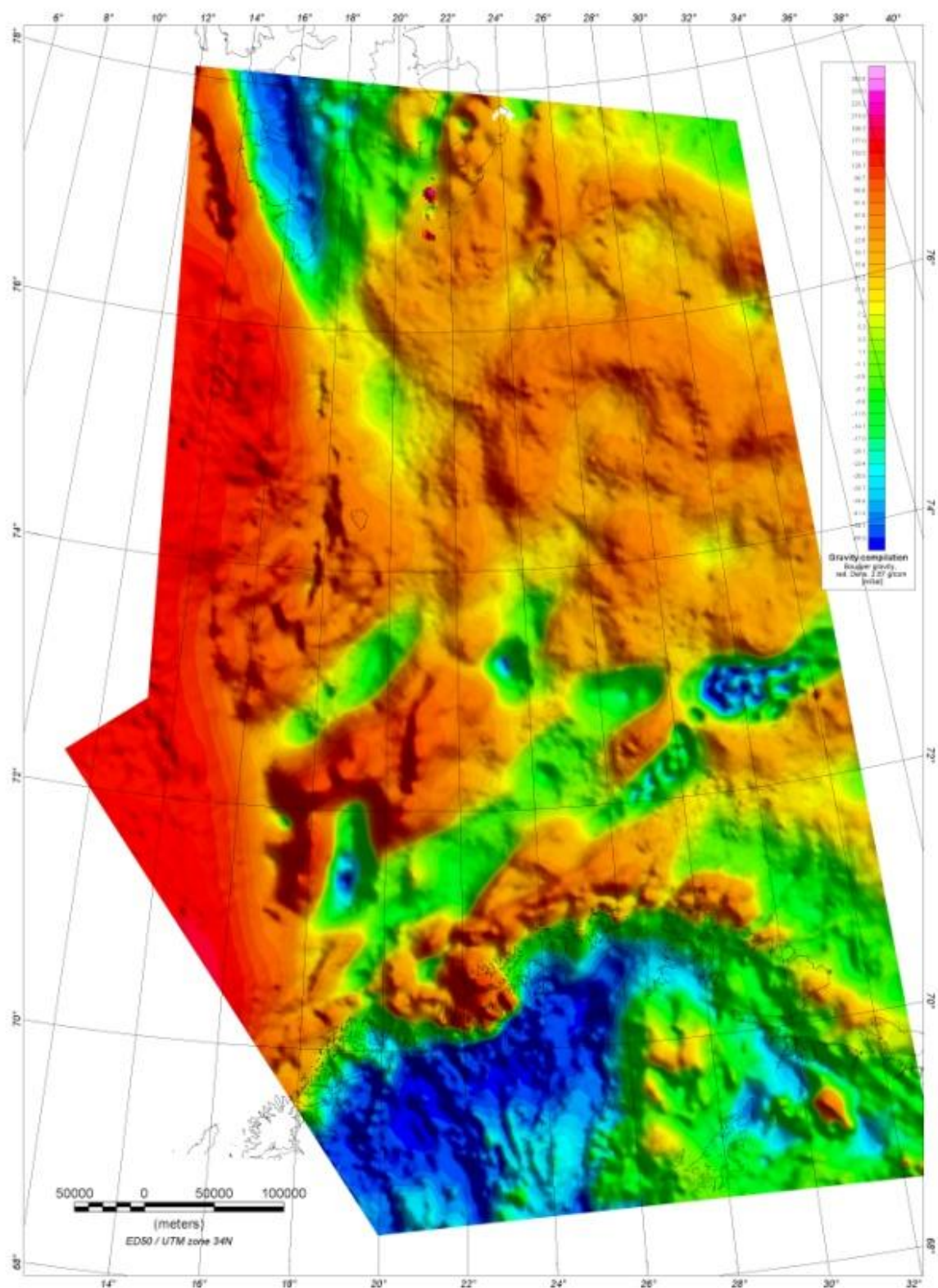


Figure 6.1 Bouguer gravity of the southern Barents Sea (reduction density 2.67 g/cm³).

7 CONVENTIONAL FILTERING TECHNIQUES

Marco Brønner

Affirmed development of the interpretation theory is usually associated with many case studies of successful application of seismic methods combined with filtered gravity and magnetic data in solving problems in exploration and structural geology. During the interpretation of the BASAR-09 survey, potential field techniques have been used intensively as complementary tools for the interpretation of the survey area. It was also a good way to test the validity of other geophysical models and was extremely beneficial for the seismic interpretation. Relevant filtering has been carried out in order to enhance the main structural changes and linear features observed within the BASAR-09 study area.

The aim of this section is to briefly present and discuss the different processing techniques used to enhance and model the magnetic data across the BASAR-09 survey area. Specific and preliminary interpretations based on these grids will be presented in another part of the present report (Chapters 10, 11 and 12).

7.1 Wavelength filtering, RTP and derivatives

Magnetic (and gravity) anomalies whose wavelengths are long relative to the dimensions of the geological objectives of a particular investigation are called regional anomalies. Because shallow geological features can have large lateral dimensions, one has to be careful, but regional anomalies are usually considered to reflect the effects of relatively deep features. Anomalies whose wavelengths are similar to the dimensions of the geological objectives of a particular investigation are called local anomalies. In the processing of magnetic data, it is beneficial to separate the regional and local anomalies prior to interpretation. Magnetic anomalies observed within the BASAR-09 survey area show the superposition of various sources, reflecting the regional field, noise and lateral magnetic variations within the crust and upper mantle (e.g. Blakely 1995). Measured gravity anomalies, therefore, represent a combination of wavelengths associated with the spatially distributed sources.

During the BASAR-09 project, a number of transformation methods were used after data levelling in order to enhance the main structural and magnetic features. These techniques, used to separate regional from local gravity anomalies, take many forms and can all be considered as filtering in a general sense (Blakely 1995). Many of these techniques are the same as those employed in enhancing traditional remote sensing imagery, seismic data or processing digital elevation data (Milligan 1998, Mari *et al.* 2001).

Filters have been applied to the BASAR-09 gridded anomalies which enable us to isolate, interpret and/or enhance the wavelengths of greatest interest, therefore facilitating geological interpretations (e.g. Blakely 1995). The magnetic (and/or gravity) gridded datasets can be transformed from the space domain into the spectral domain and vice-versa using the Fast

Fourier Transform (FFT). Transformation of the gridded data into the frequency domain is completed by application of a discrete 2D Fourier transform (DFT) (Bhattacharya 1966; Blakely 1995).

For spectral analysis we used the Geosoft MAGMAP Discrete Fourier Transform algorithm (Geosoft 2005c), which applies the method of Bhattacharyya (1966). The DFT algorithm works fast by exploiting symmetries that are present for images of certain dimensions. The algorithm implemented by Geosoft in Oasis montaj is explicitly the Winograd DFT (Winograd 1978, Geosoft 2005c). This FFT transformation requires that the image fills an entire rectangle, a condition not met by the BASAR-09. Therefore, any survey gaps or irregular edges will also need to be filled with synthetic data. The edge matching and the gap filling were achieved using the maximum entropy algorithm (Burg 1975).

7.2 Reduction to the pole (RTP)

The magnetic data were reduced to the pole to properly register and locate the magnetic anomalies spatially above the magnetic bodies within the crust. The RTP is a process involving a phase transformation of the magnetic anomaly, within the Fourier domain. The measured total field anomaly is transformed into the vertical component of the field (Arkani-Hamed 1988, Blakely 1995). The assumption, following this transformation, is that the magnetic anomalies had been magnetised vertically at the pole and that the anomalies are observed from the pole. Key assumptions are that the magnetisation of the source is entirely due to induced magnetisation. Therefore, the phase of the anomaly is transformed into simpler symmetrical shapes that are assumed to lie directly over the magnetic sources (Blakely 1995).

This assumption is essential for future mapping and analysis of the magnetic anomalies because it is assumed, when applying edge enhancement, that the causative field is vertical. Consequently, some workers agree that the RTP correction should be carefully considered. Moreover, it is assumed that both the magnetic field and the magnetisation of the crust have constant directions within the study area (Arkani-Hamed 2007). The RTP filtering is also limited for large surveys because each RTP equation does not consider the synchronous variation of both inclination and declination. Each transformation only considers one value for inclinations and declinations. Even if only minor changes can be observed in the BASAR-09 at the Barents Sea latitude, the process is usually recommended for the application of magnetic data, and makes magnetic maps more reliable for geological interpretation by removing some of the inherent complexity (Blakely 1995).

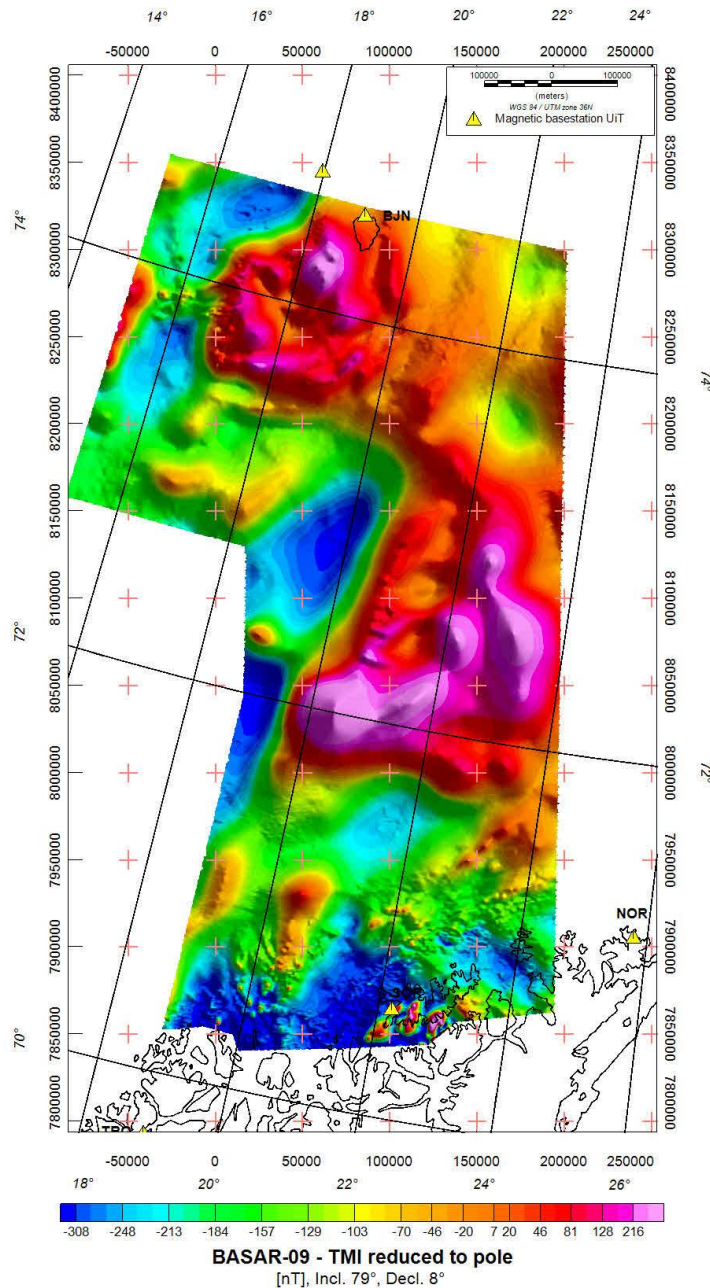


Figure 7.1 Gridded anomaly map of the total magnetic field reduced to the pole (Incl: 79°; Decl: 8°). The RTP transformation was carried out using a 2D-FFT filtering along the microlevelled grid (400 x 400 m). The RTP correction transforms the anomaly into the one that would be observed with vertical magnetisation and with a vertical Earth's field, i.e. the anomaly that would be observed if the sources were located at the Earth's magnetic north pole. As a result, reduction to the pole removes asymmetries caused by the non-vertical inducing field and places the anomalies more directly over their causative bodies, thus facilitating the interpretation of the magnetic dataset. For the Barents Sea latitude these changes are relatively small.

For BASAR-09 the RTP correction was carried out using an average value for inclination and declination within the study area, derived from the IGRF model (Fig. 7.1). The corrections of the survey are rather small due to the high latitude.

7.3 Wavelength and continuation filtering

Wavelength filters are a common tool in helping to distinguish and to delineate shallow crustal features of shorter wavelengths from the regional field and support a more accurate interpretation of sedimentary rock tectonics and basement structures.

The regional anomalies can be estimated employing a variety of analytical techniques, including high-pass and low-pass filters (Fig. 7.2). The magnetic data were most useful for determining the presence, trends and depth of intrusions, faults and basement structures. High-pass filtering of the data at 30 km was used to highlight fault structures, salt diapirs and lineaments, which are most likely related to basement variations and/or intruded material in the upper basement and overlying sedimentary strata (Fig. 7.2a). Figure 7.2b shows the corresponding 30 km low-pass filtered dataset, which represents predominant basement variations, as well as faults with a more regional impact.

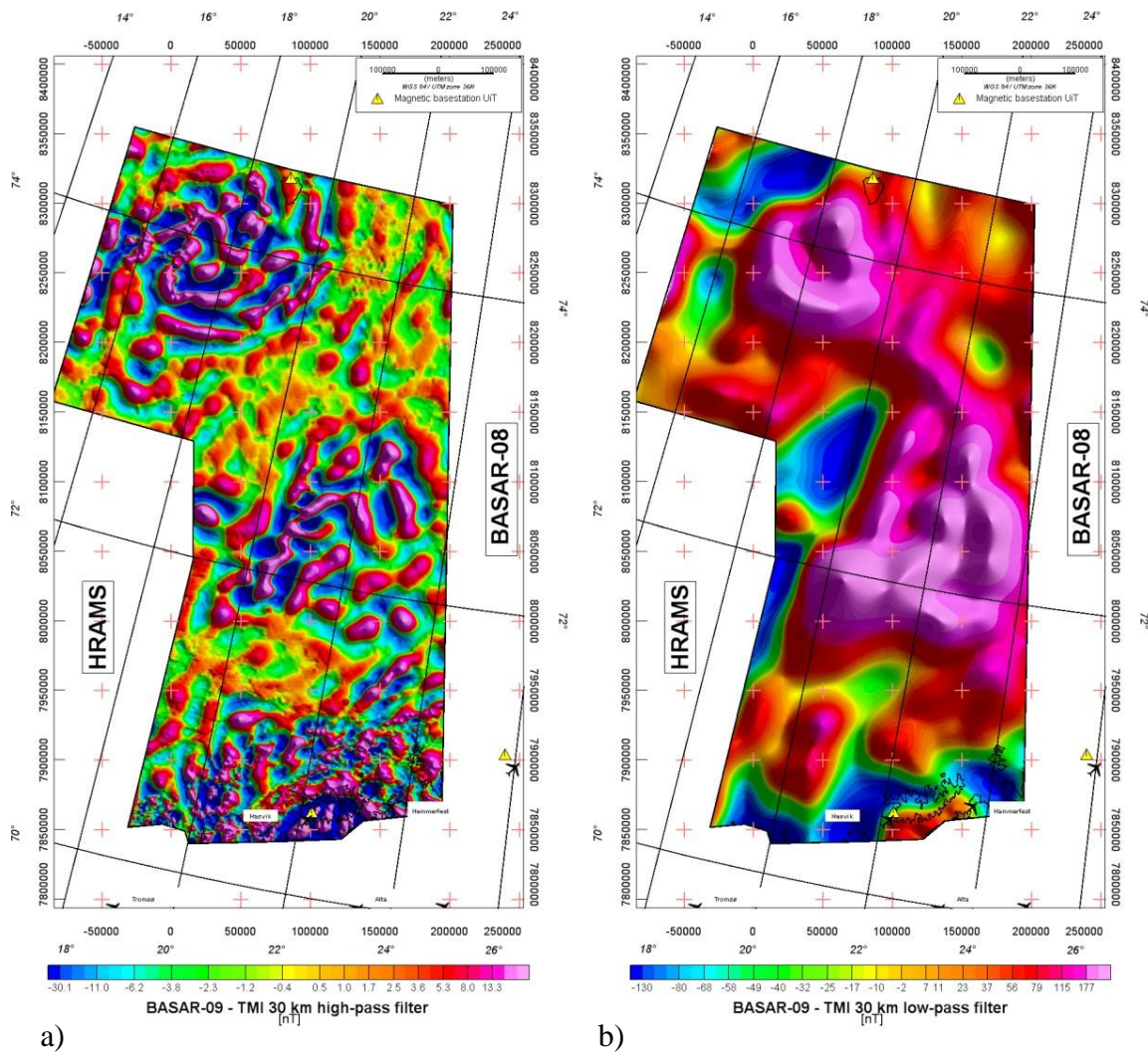
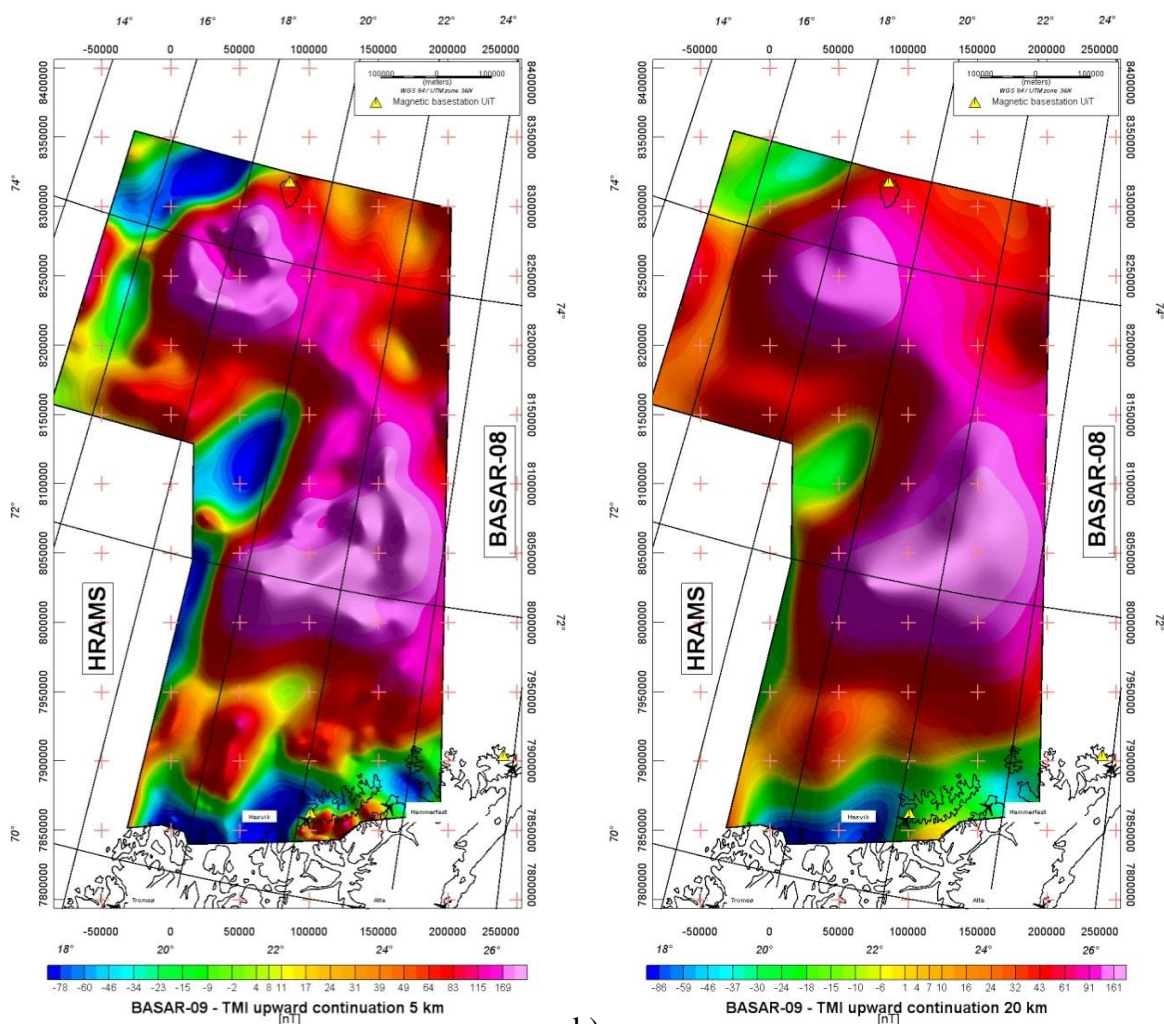


Figure 7.2 a) High-pass filtering (30 km) of the magnetic total field. This filter underlines the distribution of the short wavelengths. B) Low-pass filtered data (30 km) showing the corresponding residual field. Grid cell size is 400 x 400 m.

Upward continuation is a low-pass filtering process simulating the result of the survey as if it had been carried out at a higher elevation (Fig. 7.3). This process is based on the physical fact that the further the observation is from the body causing the anomaly, the broader is the anomaly. The technique provides an excellent integrated view of the deeper magnetic settings undistorted by the local, high-amplitude and high-gradient anomalies of the magnetic sources in the shallow portion of the subsurface.

Upward continuations to 5 and 20 km have been used to provide indications about the main magnetic and tectonic units in the area. From the 5 km upward continuation map (Fig. 7.3a) the predominant role of the Stappen and Loppa highs is underlined, as can also seen in the low-pass filtered data (Fig. 7.2b).



a) b)
 Figure 7.3 Upward continuations of the magnetic total field to a) 5 km and b) 20 km, respectively. Upward continuation uses wavelength filtering to simulate the appearance of potential-field maps as if the data had been recorded at a higher altitude. Large-scale regional anomalies and the main crustal patterns are revealed by this process.

On the 20 km upward continuation filter (Fig. 7.3b), however, the narrow connecting magnetic high between the Loppa and Stappen highs, here referred to as the 'catwalk', is still pronounced and thus must be seen as a very deep and regional structure, similar to the two basement highs.

8 ENHANCEMENT OF TREND USING STRUCTURAL FILTERS

Marco Brönnner

The purposes of this chapter are 1) to show the benefit of derivative and normalised filters in investigation of the structural setting in the survey area; 2) to evaluate the images produced by several enhancement techniques for lineament mapping; and 3) to prepare structural and depth to magnetic basement estimation maps (lineament) based on magnetic data interpretation. Some newly discovered lineaments and features might subsequently be used as a reference for future geological mapping, interpretation or re-interpretation.

8.1 Derivative filters

Derivatives of the magnetic total field and its analytical signal have been computed within this study to enhance short-wavelength features and the main lineations. Computation of the three orthogonal derivatives, (x, y, z) within potential field modelling is considered as a universally applicable and basic processing step (Thurston & Brown 1994, Blakely 1995, Nabighian *et al.* 2005).

8.1.1 Vertical derivatives

Vertical derivatives (VDR) were used to enhance localised near-surface sources and trends, and to improve source resolution, assuming high-quality data (Figs. 8.1 and 8.2).

Transformation of potential field data into a derivative map enhances edges or contacts by placing anomaly maxima at the point of the maximum horizontal gradient identified within the x- and y-orientations of the grid. The key assumptions made when transforming gravity and magnetic field data into the three orthogonal derivatives are that: (1) the potential field measured at the surface is the vertical component of the field (for gravity); (2) the lithological contacts giving rise to the anomalies are abrupt, near-vertical and isolated from other sources. The first assumption is essentially true for gravity and for magnetic data reduced to the pole (Blakely 1995). In reality, however, geological contacts are rarely vertical, and density and magnetisation can vary in all directions in a geological unit. Computation of the first vertical derivative (FVD) has been referred to as a pre-processing step, particularly before the interpretation of the Euler and analytical signals (see Chapter 9).

The FVD does, however, help to map and interpret magnetic lineaments and structural elements as it highlights the edges of lateral changes in the observed magnetic field. From the FVD (Fig. 8.1) the high-amplitude lineaments in the south, for example, are better pronounced as well as the volcanic intrusions in the Vestbakken volcanic province (VVP).

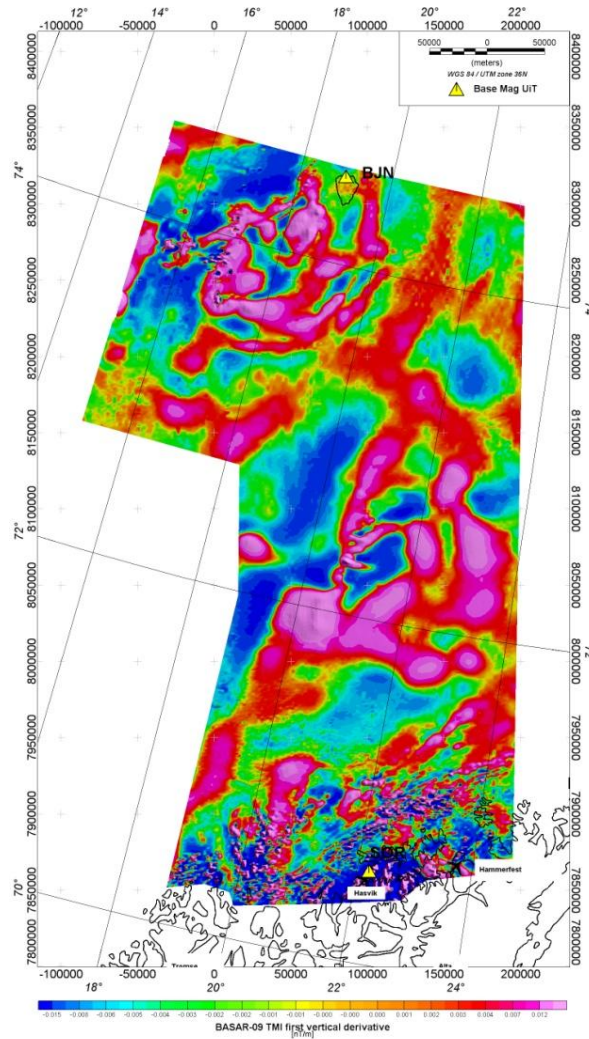


Figure 8.1 First vertical derivative obtained by convolution along the magnetic total field, reduced to the pole and gridded with a cell size of 400 m using minimum curvature. The vertical derivative of an anomaly is related to the depth and geometry of the causative body. The gradient operator attenuates broad, more regional anomalies and enhances local, more subtle, magnetic responses and, as such, is sensitive to shallow magnetic source bodies and contacts.

The rounded shape structure of the Stappen High appears much more differentiated, which allows a more accurate interpretation. The catwalk appears to be subordinate in the FVD, which points to a deep-seated structure at the base of the Björnøya Basin.

Computation of the second vertical derivative (SVD) (Fig. 8.2) as described by Blakely (1995) can be unstable. The second vertical derivative, or rate of change of the fall-off rate of an anomaly, may be considered equivalent to a residualisation of the data and is a common tool delineating source bodies. To stabilize the calculation and to suppress high-frequency noise and emphasizing contact features of various wavelengths, different low-pass filters were applied during the calculation. Figure 8.2 shows the SVD of the TMI data low-pass filtered with 2 km (a) and 5 km (b). Figure 8.2a is significantly affected by high-frequency noise due to the line character of the

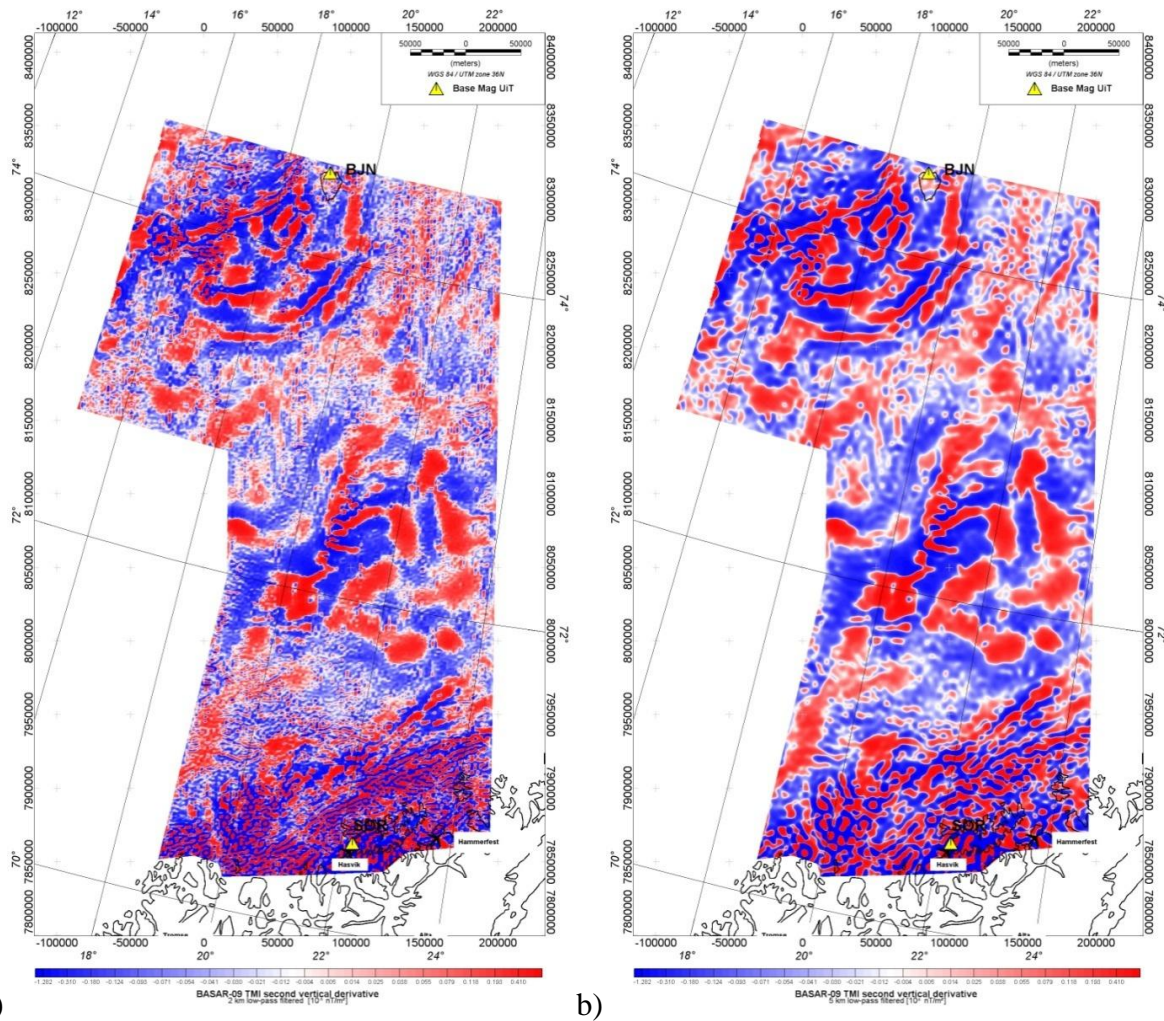


Figure 8.2 Second vertical derivative (SVD) obtained by convolution along the magnetic total field reduced to the pole. The data were low-pass filtered with a) 2 km and b) 5 km cut-off to suppress high-frequency noise and to highlight contact features of different wavelengths.

data acquisition, but nevertheless it emphasises the different magnetisations of the shallower sources such as quite a few lineaments in the onshore-offshore region.

From the SVD, the southern flank of the Hammerfest Basin and the eastern flank of the Tromsø Basin are well defined, as well as the northwestern and eastern boundary of the Bjørnøya Basin. The predominant NE-SW trend of the magnetics on the Finnmark Platform is noticeable, whilst crosscutting NW-SE-striking lineaments are emphasised. Furthermore the SVD reveals different magnetic characteristics of the Stappen and Loppa highs. Whereas the Stappen High shows rather concentric magnetic anomalies, the magnetic signature of the Loppa High is much more irregular, which might point to different evolutions of these basement highs. Applying different low-pass filters can also provide hints of the development of different structures with depth.

8.1.2 The horizontal derivatives

The horizontal derivatives (HDR) can be used to predict the locations of major basement structures or sedimentary rock tectonics, igneous bodies and changes in basement grain (Grauch & Cordell 1987, Gunn 1997).

Similar to the way the first directional derivative defines the slope at any point on the surface, the terrain slope filter has been applied to calculate the slope at any grid node of the BASAR-09, the so-called horizontal gradient magnitude (HGM) (Fig 8.3). Grid files of the terrain slope can produce contour maps that show isolines of constant steepest magnetic slope. For any particular point on the surface, the HGM is based on the direction of steepest descent or ascent of the magnetic field at that point. This means that across the surface, the gradient direction can change. This operation is similar to the way the first directional derivative filter defines the slope at any point on the surface, but is more powerful as it automatically defines the gradient direction at each point on the map.

The HGM aided in defining the location of linear features which, in turn, are related to the trends of the lineaments in the area. It produces maximum ridges over edges of magnetic basement blocks and faults or other magnetic bodies.

8.1.3 Analytic signal

The analytic signal combines calculated first derivatives in the x, y and z directions. The technique creates peaks over the edges of wide magnetic bodies and the centres of small bodies. The concept of the analytic signal applied to magnetic anomalies was developed in two dimensions by Nabighian (1972) based on a concept initially proposed by the Frenchman Ville in 1948.

A common theme of the normalised derivatives is the concept of mapping angles (or functions of angles) derived from the gradients of the magnetic intensity.

The resulting shape of the analytic signal is expected to be centred above the magnetic body (Fig. 8.4). This has the effect of transforming the shape of the magnetic anomaly from any magnetic inclination to one, positive, body-centred anomaly, at least in 2D (Nabighian 1972).

The main advantage of the total gradient over the HGM is its lack of dependence on dip and magnetisation direction, at least in 2D. When interpreting the analytic signal it is assumed that the causative sources are simple near-vertical or step-like geological structures (Roest *et al.* 1992, Roest & Pilkington 1993). Therefore, the 2D analytic signal has significant advantages over the simple derivatives and this application was utilised to map changes in

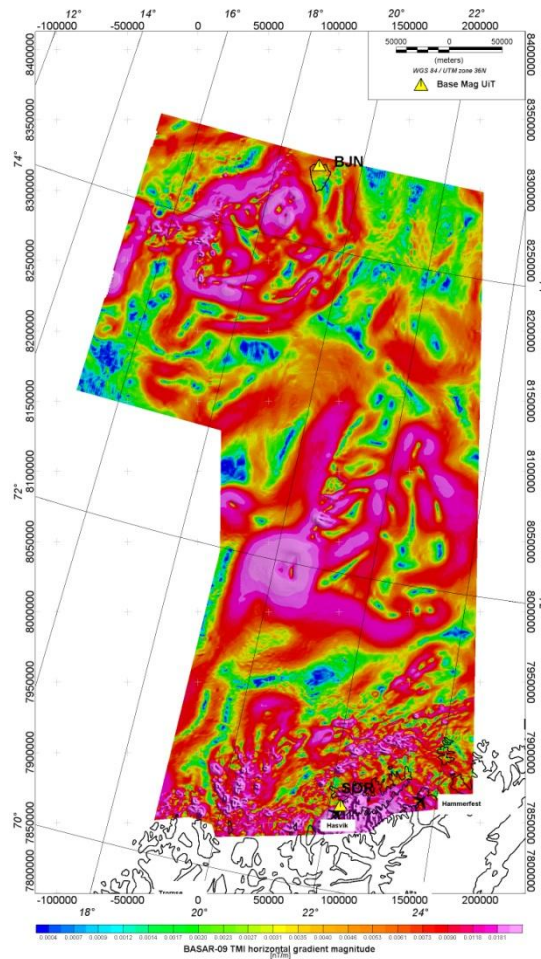


Figure 8.3 Horizontal gradient magnitude (HGM) of the BASAR-09 dataset, reduced to the pole. After the reduction-to-pole correction, a magnetic body is spatially more directly associated with the related magnetic response. The horizontal gradient magnitude of the anomaly slope is then located near or over the body edge; i.e., the horizontal gradient operator, in map form, produces maximum ridges over edges of magnetic basement blocks and faults or other magnetic bodies. In addition, the horizontal gradient highlights linear and round-shaped features, related to magnetic contacts, in the dataset.

basement structure, fabric and trends. Synthetic modelling has proved that the maxima of the analytic signal are located over the edges of anomalous sources (Roest *et al.* 1992). This simplification of the potential field, however, results in the compromise whereby during computation the sign of the original gravity and magnetic field is lost. Therefore, it cannot be determined whether the analytic signal anomaly represents a positive or a negative density or magnetic susceptibility contrast compared to its surroundings.

For large-scale magnetic surveys like the BASAR-09 or for shallower depths of causative bodies, the analytic signal method provides a useful and fast way of delineating magnetic boundaries in the subsurface (Fig. 8.4).

The analytic signal has been utilised widely for the mapping of structures and for determining the depths of sources (Pilkington *et al.* 2000, Florio *et al.* 2006).

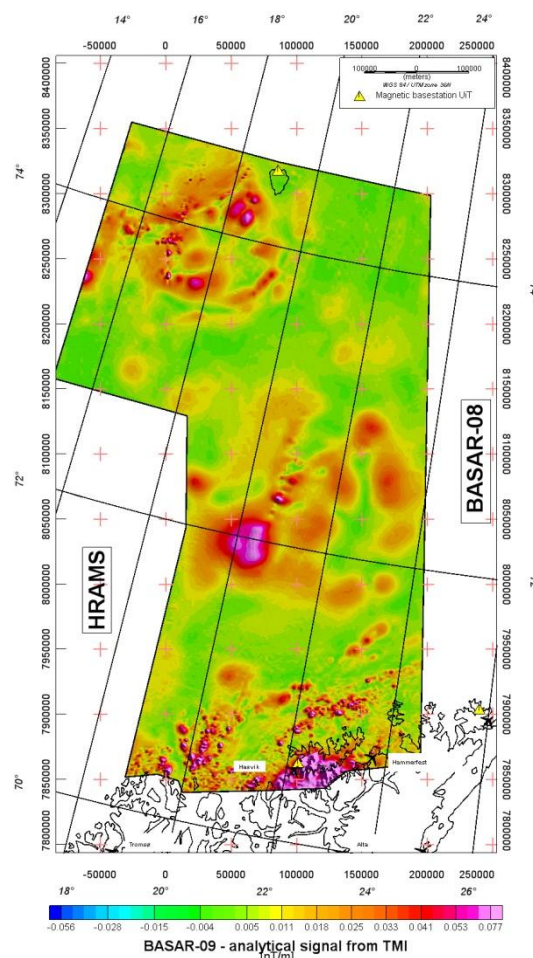


Figure 8.4 Analytic signal of the magnetic total field grid, reduced to the pole (400 x 400 m cell size, normalised colour distribution).

8.1.4 Tilt derivative (TDR)

The tilt derivative filter (TDR) is another powerful and normalised derivative tool for shape and edge detection (Figs. 8.5). The result is strongly peaked along the maxima of the horizontal gradient. It gives a much sharper definition of the magnetic contacts than the horizontal gradient map.

For the BASAR-09 interpretation, this filter is particularly useful in identifying dykes or dyke swarms in the Barents Sea and onshore in the Troms-Finnmark area, lineaments of shallow origins. The tilt derivative confirms the predominant NE-SW strike of the lineaments offshore mainland Norway. In addition, some cross-cutting NW-SE trending features are observed. The major basins Hammerfest, Tromsø and Bjørnøya are expressed by extended magnetic lows and salt diapirism is locally visible in the Tromsø and Bjørnøya basins, while the Svalis Dome is also easily detectable.

The short-wavelength anomalies within the Vestbakken volcanic province are discernable by scattered structures, but also by two NE-SW-striking, non-continuous lineaments west of Bjørnøya. In the western corner of the survey area, randomly scattered anomalies might indicate the presence of sills within the sedimentary succession.

In the southern part of the survey area, a few NW-SE-striking lineaments are visible south of the Hammerfest Basin, indicating thrusts or dykes, and show a similar trend to that observed onshore Finnmark from the BASAR-08 project (Brønner *et al.* 2009).

The TDR is defined in terms of the ratio between the first vertical derivative of the potential field and its total horizontal gradient of the field (Miller & Singh 1994, Verduzco *et al.* 2004, Cooper & Cowan 2006).

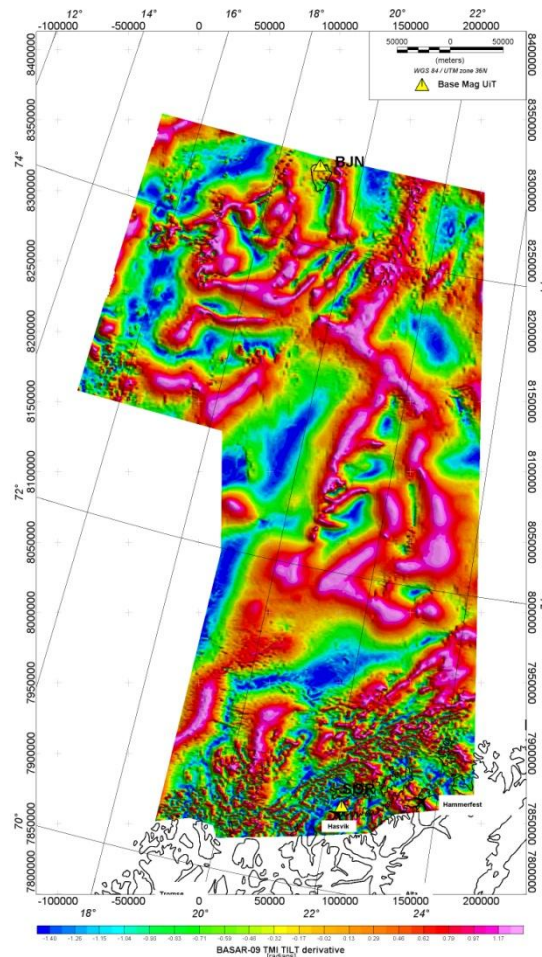


Figure 8.5 Tilt derivative of the magnetic total field. The tilt derivative (TDR) is an alternative method for deriving the maximum gradient anomalies associated with magnetic contacts.

The TDR is restricted to values in the range $+\pi/2 > \text{Tilt} > -\pi/2$, and can be considered as an expression of the vertical derivative normalised by the total horizontal derivative. This measure has the property of being positive over a source and negative elsewhere (Fig. 8.5).

The tilt filter technique tends to enhance mapping of the subtle magnetic anomalies and maximises the geometrical contrast of the internal basin structure (partly constrained by seismics). The tilt angle was compared with other edge detection methods such as the horizontal gradient, the second vertical derivative and the analytic signal, and has been found to have the added advantage of responding well to both shallow and deep sources within the BASAR-09 area. Combined with the 30 km high-pass wavelength filter, results were particularly useful for the structural interpretation of the BASAR-09 dataset.

9 ESTIMATION OF MAGNETIC DEPTHS

Marco Brönnner

9.1 Implications

Depth to magnetic source calculation is a challenging and important task in magnetic interpretation. A complete and quantitative interpretation of potential field data aims at estimating information about the depth, dimension and contrast of the relevant geological units. Magnetic depth estimates are often a reasonable approximation to depth to the magnetic basement (i.e., metamorphic, igneous, oceanic), and the crystalline basement depth (or alternatively, the sedimentary thickness) is a primary exploration risk parameter. Furthermore, estimating basement depths are directly applicable to thermo-kinematical modelling and thermal maturity applications (e.g., heat-flow estimation, source-rock burial depth, distribution and volume).

It is noticeable, however, that such an interpretation of depth to basement suffers from an inherent ambiguity. As a matter of fact, it is not possible to obtain all three types of information simultaneously without other a priori information (e.g., the geological context or seismic data). These methods usually work for simplified source geometries (dimensions) and are most of the time independent of the susceptibility contrast. The depths estimated by some methods can be used as the final, quantitative solution in some ideal situations (i.e., where the anomaly is well isolated and the noise is insignificant or removed).

In this chapter, we present the results obtained using the 3D-located Euler deconvolution of the magnetic total field.

9.2 Euler deconvolution

The Euler method uses Euler's homogeneity equation to construct a system of linear equations, and then determines, through a least-squares inversion for one window, the (vertical and horizontal) position of a single source for a given source geometry (Reid *et al.* 1990). Euler deconvolution was first presented by Thompson (1982) for profile data and by Reid *et al.* (1990) for gridded data.

The method requires the use of the calculated horizontal and vertical derivatives of the magnetic field. Thompson (1982) called the fall-off rate (i.e., the negative of the degree of homogeneity) the structural index (N). Synthetic tests (Silva & Barbosa 2003, Keating & Pilkington 2004, Stavrev & Reid 2007) indicate (1) that the Euler method can locate the outline and depth of a variety of simple geometrical shapes; and 2) that the structural indices will cluster and determine the best structural interpretation. Although detailed as vertical

contacts, faults with a large throw may be best displayed with a structural index of zero (Table 8.1).

Euler's homogeneity equation is valid for bodies of arbitrary shape, characterised by these indices. In practice, the Euler method assumes idealised structures such as contacts, thin sheets (dykes), vertical or horizontal cylinders and a 3D sphere. In this section of the report we therefore briefly describes the theory, advantages and limitations behind the technique and presents its applications for the BASAR-09 survey.

Structural Index	Magnetic field	Gravity field
0	contact	sill/dyke/step
0.5	thick step	ribbon
1	sill/dyke	pipe
2	pipe	sphere
3	sphere	

Table 9.1 Summary of the structural indices for simple geometric models from magnetic or gravity anomalies (Reid et al. 1990, Marson & Klingele 1993, Bainbridge et al. 2002).

Euler 3D deconvolution is a semi-automated technique enabling rapid qualitative interpretation and depth estimation of source depths from large gridded gravity and magnetic datasets (Reid *et al.* 1990, Barbosa *et al.* 2000, Pilkington *et al.* 2000, Hsu 2002, Mushayandebvu *et al.* 2004, Florio *et al.* 2006). The technique has considerable advantages. 1) It can operate on large datasets extremely quickly; 2) provide a qualitative interpretation of geological structures; 3) provide depth estimates for the sources of the anomalies; 4) magnetic data do not need to be reduced to the pole (Reid *et al.* 1990); and 5) it is also insensitive to magnetic inclination, declination and remanence since these become part of the constant in the anomaly function of a given model.

9.3 Interpretation of the structural indices

Careful consideration of the distribution and clustering of Euler solutions is, however, required to discriminate which solution best represents the causative source at depth within the crust. Although in theory, interpretation of the Euler solutions requires no prior geological knowledge, Reid *et al.* (1990) acknowledged that this can be significantly beneficial. Reid *et al.* (1990) claimed that the choice of structural index remains the prime limitation of the traditional Euler technique. This and other limitations arise as a product of some of the simplifying assumptions of the technique, which assume that the source is (1)

equivalent to a simplified geometrical feature, (2) spatially homogeneous, (3) independent of neighbouring magnetic sources and (4) has a heterogeneous magnetisation or density.

In the BASAR-09 survey, as in the entire Barents Sea, most of the geological structures are most likely arbitrarily shaped sources, and are therefore not simply modelled or defined by the structural index. The fact that the sources may not be internally or spatially homogeneous (i.e. the magnetisation and shape of the source change with depth or along strike), or the source-to-observation distance increases (thus, the anomaly shape changes with depth) or other sources impinge on each other's spatial positions, are inherent sources of scatter (Reid *et al.* 1990, Keating & Pilkington 2004). Consequently, it is necessary to examine a number of structural indices to compare results and clustering of solutions for several individual features. Alternatively, in such situations, geological constraints from external data sources would be beneficial to the interpretation of the BASAR-09 dataset in the future.

Complexities also arise with respect to the depth of burial of the source. Ravat (1996) noted that there was a strong inter-dependency between the choice of the structural index and the distance of the source-to-observation, and that with increased distance the results were biased towards the higher structural indices, explained by the exponential decay of a source anomaly with depth. It can be predicted that with increasing depth the attenuation rate of the anomaly is less; deeper sources may therefore only be represented by higher values (Ravat 1996). The relationships between the source type and the observation level are considerably altered following upward continuation of the observation level, thus increasing the possibility of mis-identification of the true structural index (Ravat 1996).

For this report we decided to apply Euler deconvolution to the recompiled new magnetic grid of the western Barents Sea to obtain a better and comprehensive overview of the depth-to-basement features we can get from the Euler deconvolution. We found some correlation with the main trends, which were independent of the SI. Lineaments associated with faults and mafic intrusions revealed both shallow and deep Euler solutions, which could give indications of the angle of dip, depth and the geotectonic impact of the different structures. Contacts with salt diapirs yielded a magnetic anomaly marking the outline of the salt structures and produced Euler solutions of rather shallow depth. Some major features, which are likely to be related to basement structures, produced a stable distribution of Euler solutions. A final comparison with seven wells, where basement was penetrated at depth, shows similar or greater depths from the Euler deconvolution with $SI=0.5$.

A detailed presentation of the results is given in Chapter 9.4.

9.4 Located 3D Euler method

Euler deconvolution usually assumes a ‘moving window’ technique (Reid *et al.* 1990). This standard technique produces a mathematical solution for each position of the window, estimating the unknowns after each sequential movement. The minimum and maximum depths that can be resolved are related to the grid cell size and the window size selected, highlighting the importance of the quality of the dataset and the nature of the investigations.

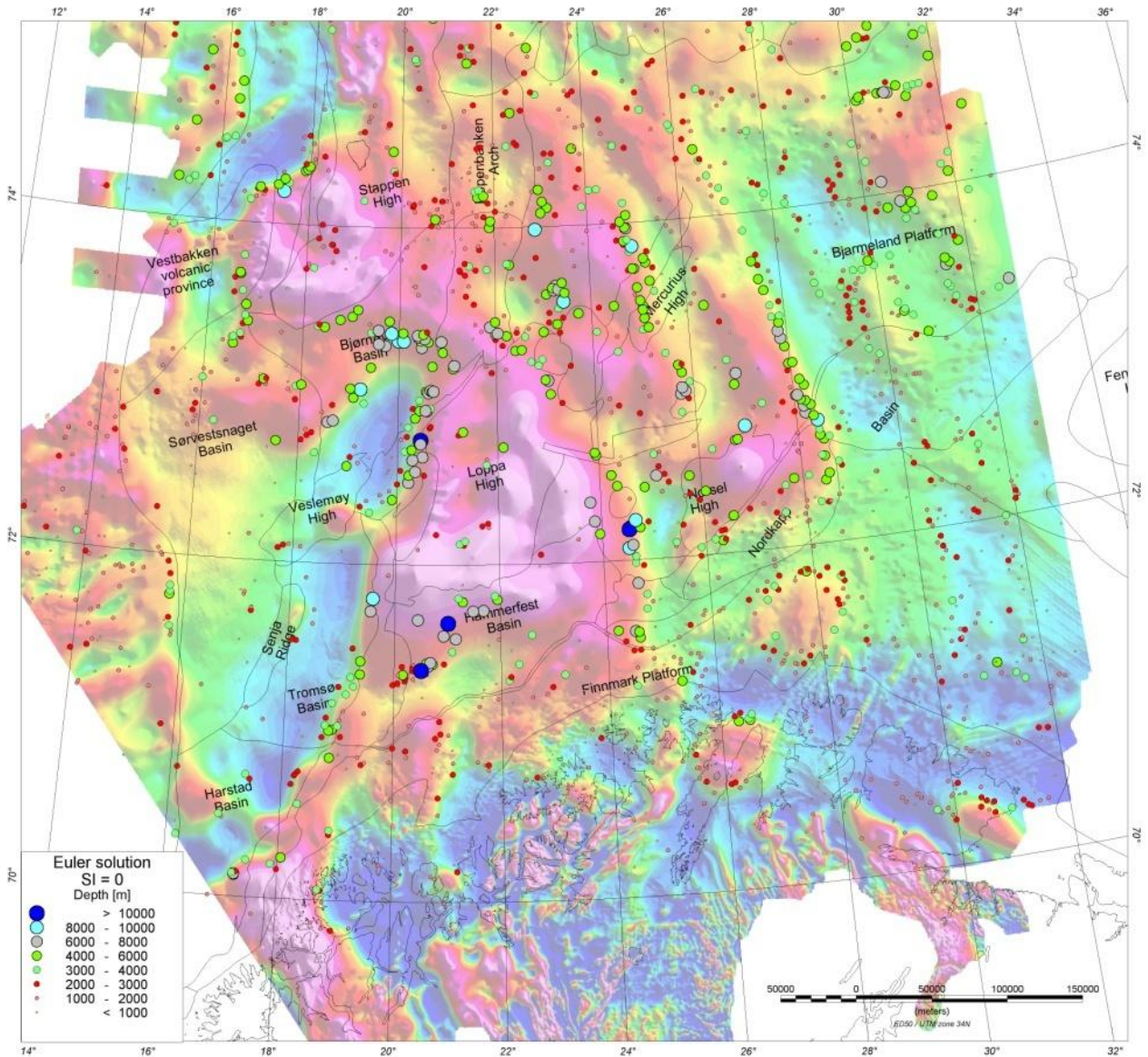


Figure 9.1 Result from the located Euler deconvolution data. Solutions derived by using a structural index of 0.

For this report, we preferred the ‘Located 3D Euler method’, which is a modified version of the standard Euler deconvolution (Bainbridge *et al.* 2002). The located 3D Euler method refines the standard method by first running a peak-finding routine (Blakely & Simpson

1986), which locates peaks and estimates an appropriate window size before the deconvolution. This method produces far fewer solutions because only a small subset of the grid will be at the centre of peaks in the dataset. Combined with discrimination techniques, we can obtain more reliable Euler solutions. Peak detection was automatically obtained using the Blakely grid peak-picking algorithm of Blakely & Simpson (1986).

A pre-processing of the dataset used the analytic signal as the primary grid for Euler deconvolution. However, such procedures may increase the ratio of noise to signal within the grid; therefore, such pre-processing is limited by the initial quality of the dataset, because noise will contribute to the scattering of solutions. In the present project, we tried different upward continuations to remove some remaining noise within the magnetic compilation. We finally dispensed with this smoothing for two reasons:

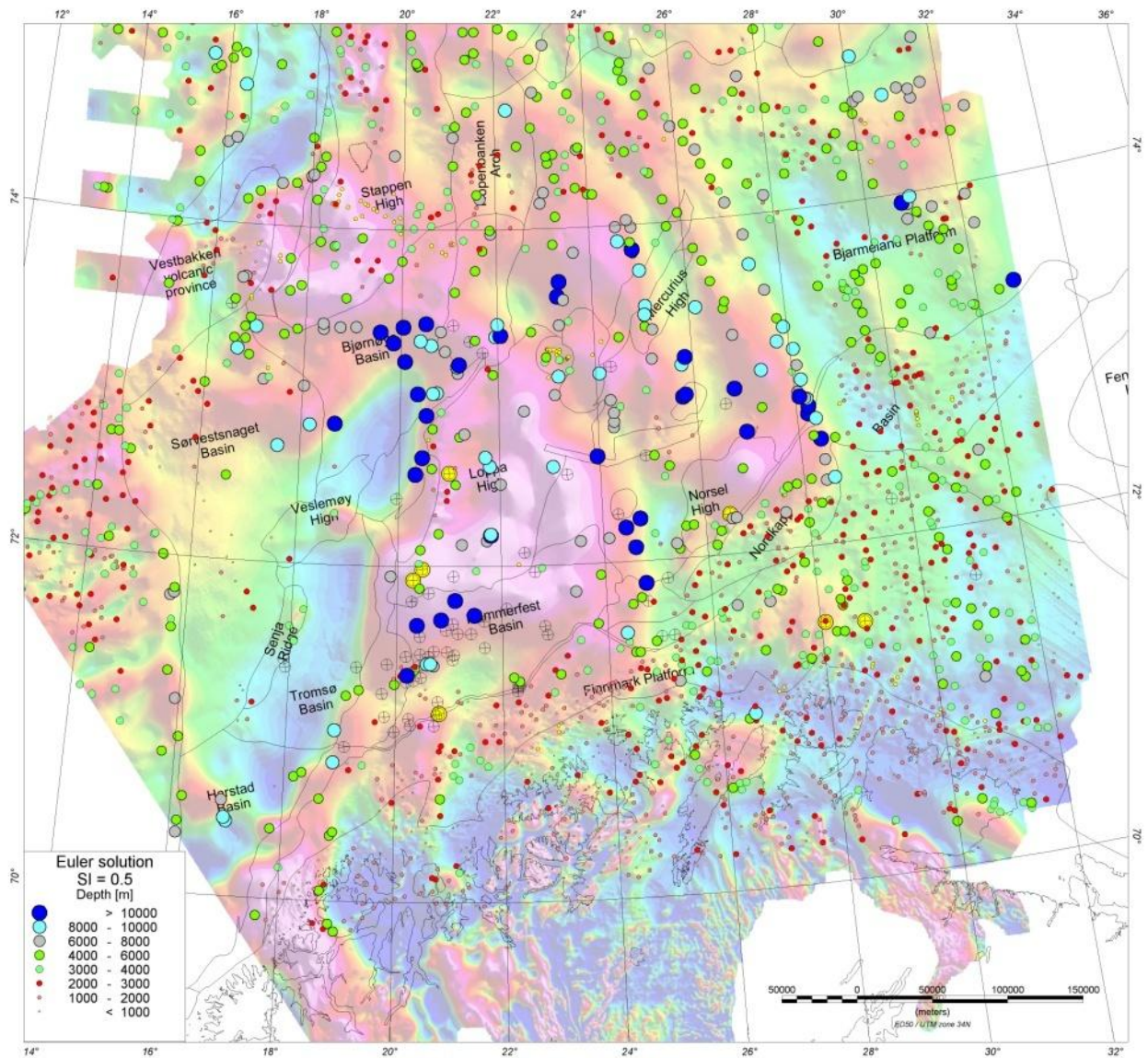


Figure 9.2 Result from the located Euler deconvolution data. Solutions derived by using a structural index of 0.5

- 1) this could have significant consequences for the determination of the source-to-window ratio and would complicate the depth interpretation of the deconvolution (Ravat *et al.* 2002), and 2) the new magnetic dataset shows quite a number of interesting high-frequency and low-amplitude anomalies which would be suppressed by upward continuation. Instead we decided to clip the results and eliminate depth solutions shallower than 500 m, which suppress at least some of the noise.

During the present study, a series of maps, encompassing the different structural indices, was required to accurately assess the different geological structures present within a study area, particularly within complex regions. Best results have been obtained using the located Euler solution using indices of 0, 0.5 and 1, and are displayed in figures 9.1, 9.2 & 9.3.

Figure 9.1 shows located Euler solutions using the structural index 0, which is supposed to reflect 'infinite steps' and highlights geological contacts. Apart from some sparsely distributed irregular locations, the Euler solutions for this index are concentrated at the edges of the major magnetic highs Stappen, Loppa and Norsel, where the NNW-SSE-striking tail of the Norsel High marks an important basement structure in the eastern part of the study area (see also BASAR-08 report). The depth solutions are predominantly rather shallow at depths of c. 2000 – 6000 metres and probably reflect mostly intra-sedimentary thrusting, nappe structures or contacts between sedimentary strata and uplifted basement blocks. The few deeper solutions appear rather arbitrarily distributed and are not sufficient for a detailed interpretation. Although the fact that a number of deep solutions are concentrated at the western flank of the Loppa High and around the magnetic minimum at the southern part of the Bjørnøya Basin is interesting, and points to an extremely deep basin with probably a very thin and/or low-magnetic basement underneath.

In calculating Euler solutions for the structural indices $SI=0.5$ and $SI=1$ (Figs. 9.2 and 9.3), which are more adapted to discover 'thick steps' and 'sheet edges', the picture becomes more complex as Euler solutions for more of the shallower features are calculated. Nevertheless, apart from some scattered noise-related solutions, most of the depth estimations can be correlated with geological structures and reveal some interesting insights into the geological setting.

The $SI=1$ reflects anomaly characteristics caused by dykes and 'sheet edges'. Accordingly the Euler deconvolution finds a number of solutions of rather shallow origin, most likely associated with intra-sedimentary faults. The deepest solutions are again situated in the vicinity of the three major magnetic highs, but much deeper than before and most likely do not reflect the top of the basement but rather the regional impact of the deep-seated faults at the rims of these basement blocks. A correlation with solutions at or close to the wells, which were drilled into basement, confirms that the solutions are generally too deep.

Concerning the correlation between basement wells and depth solutions from Euler

deconvolution, the index $SI=0.5$ produced the best matches. Nevertheless, especially on the Finnmark and Bjarmeland platforms, the calculated solutions are mostly associated with faults, whereas in the Nordkapp Basin shallow salt diapirs cause most of the magnetic anomalies and Euler solutions accordingly. However, as seen previously, the deepest solutions picture the edges of the major magnetic highs, which again underlines the regional impact of these contacts or faults in the study area.

The actual depth and characteristics of these solutions and the possible interaction of different basement lithologies was investigated during modelling along selected 2D (Ch. 11) profiles and in 3D Ch. 11).

In general, the Norsel, Stappen and Loppa highs appear as kinds of compact blocks with predominantly deep Euler solutions. Shallower features are rare here or magnetically invisible, and underline a different feature of these structures in comparison with areas on the platforms or within the basins. For these areas, the deeper Euler solutions likely mark the principal geotectonic units as seen from figure 9.1, possibly related to basement structures, but a multiplicity of magnetic features is obviously of a shallower and intra-sedimentary origin. For the Nordkapp Basin, for example, solutions along the outline of the salt diapirs are prominent and probably conceal a proper depth-to-basement calculation by using the Euler deconvolution. A number of lineaments with NW-SE and NE-SW trends are situated in the southern part of the magnetic grid, onshore Norway, offshore on the Finnmark Platform and within the Nordkapp and Tromsø basins. Euler solutions for these structures are of rather shallow depths of maximum 4,000 m, and are definitely of intra-sedimentary origin. Some of them can be correlated with onshore features such as faults and dykes or high-magnetic sedimentary rocks. Depth solutions show intermediate depths of c. 5,000-10,000 m on top of the Stappen and Loppa highs and along the edge of the Sørvestsnaget, Tromsø and Bjørnøya basins. Major lineaments which were previously interpreted in the context of an eastward propagation of the Caledonian nappes show similar depth solutions, with some maximum solutions of ~15,000 m north of the Norsel High.

Well name	Depth-to-drilled-basement	Structure drilled
7226/11-1	c. 5140 m	Norsel High
7128/4-1	c. 2500 m	Finnmark Platform
7128/6-1	c. 2530 m	Finnmark Platform
7220/6-1	c. 1480 m	Loppa High
7120/2-1	c. 3470 m	Loppa High
7120/1-1 R2	c. 3947 m	Loppa High
7120/12-2	c. 4660 m	Finnmark Platform

Table 9.2 Wells, with drilled basement, were use to constrain the Euler deconvolution results.

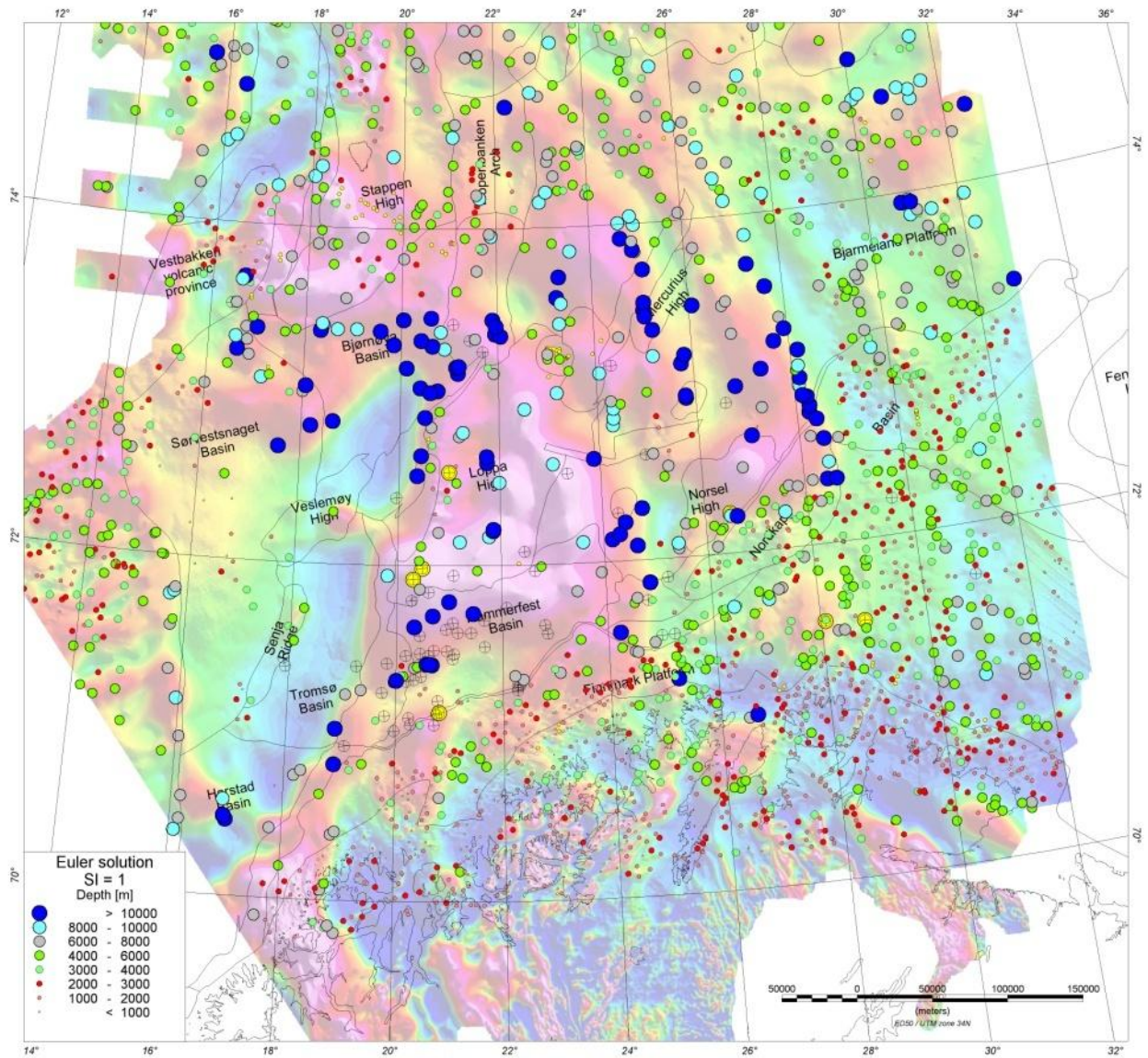


Figure 9.3 Result from the located Euler deconvolution data. Solutions derived by using a structural index of 1.

To estimate the reliability of the method, the depth-to-basement results from Euler deconvolution were compared with observed basement depths from well logs and depth-converted seismics, and we could achieve similar results from Euler deconvolution and a SI=0.5. Basement was reached in seven wells, which are listed in the table below:

Along the provided four seismic lines, additional correlations with basement depth could be made. Some Euler solutions could also be linked to the presence of sills within the sedimentary successions (see Chapter 11 for more details). Nevertheless, we consider the study area to be not so perfectly adapted for the Euler techniques. Thick piles of sediment (5-10 km or more) and probably a small magnetic sediment-basement contrast over wide areas of the survey blur the magnetic signature from the basement and reduce the applicability of

the Euler deconvolution in terms of a depth-to-magnetic basement calculation. Here, modelling rather than Euler techniques is definitely the method of choice to obtain a better hand on the depth-to-basement.

9.5 Werner deconvolution

The Werner deconvolution method (Werner 1953, Gunn 1997) was applied to the new magnetic dataset along the four seismic lines to support the modelling and interpretation in 2D. It has been used to estimate and/or underline the potential depth of magnetic sources along these specific transects (see Chapter 11). The basic assumption of the Werner deconvolution is that all magnetic anomalies are the result of the presence of either a sequence of dykes or edge interfaces. The strike lengths and depths of the source bodies are also assumed to be infinite, whereas the width of each body is assumed to be either: (1) finite, representing a dyke; or (2) approaching zero, such that it represents an interface between two bodies of differing magnetic susceptibility. The robustness of the technique is such that no reduction to the pole is required, and it works effectively with both induced and remnant magnetisations. The results were compared with the Euler solutions computed in the previous part of the chapter.

Werner (1953) recognised that analysing magnetic anomalies could be complicated because of the superposition from adjacent anomalies and the effect of noise (e.g. diurnal variations, non-two-dimensionality and induced versus remnant magnetism). For this reason, the Werner deconvolution algorithm uses simple models for the sources and a quadratic form for the source/noise interference to determine the magnetisation properties of the causative bodies. To reduce the noise we applied first an upward continuation filter to smooth the magnetic data. If the deconvolution is successful in defining a 'real' source, then depth estimates should define either the edges of the causative body or the depth range of an interface or the upper boundary of an intrusion.

10 INTERPRETATION

Marco Brønner

10.1 Main regional trends and potential field interpretation

With the new aeromagnetic dataset of the southern Norwegian Barents Sea and the integration with gravity data (Figs. 10.1, 10.2 and 10.3), a number of structural elements could be observed and utilised for a detailed and more accurate interpretation than had been possible from the previous dataset. The high quality and resolution of the new aeromagnetic compilation allow new insights into the main regional trends and basement settings of the study area.

Both magnetic and gravity measurements are usually sensitive to variations in the structure and composition of the crystalline basement. The comparison of main magnetic and gravity anomalies is used to discover the distribution of different basement types and basement faulting, which gives a direct indication of the geological development of the area (Fig. 10.3). Most of the bodies within the basement have distinctive magnetic signatures, characterised by their anomaly magnitudes, heterogeneity and magnetic fabric. By calibrating noticeable features from gravity and/or magnetic maps with known onshore geology, these structures can be linked directly together and thus support a more detailed and reliable interpretation.

The main boundaries that delineate units of the first structural order within a basin can generally be identified from correlating aeromagnetic and gravity maps. Major basement domains are expected to have pronounced expressions in both aeromagnetic and gravity data. Figure 9.5 illustrates the correlation between gravity and magnetic highs and lows. However, as discussed before (Gernigon *et al.* 2007, Brønner *et al.* 2009) for the southern Barents Sea, such a correlation cannot be found for all the principal anomalies. The Norsel High and the NNW-SSE-striking magnetic high M-BH2 (Fig. 10.3) have rather good counterparts in both the magnetic and the gravity maps. Also, the Kola-Kanin Monocline and at least the central Nordkapp Basin show extended magnetic and gravity lows. Furthermore, the Loppa and Stappen highs produce both pronounced gravity and magnetic highs, and the Tromsø Basin and the central part of the Bjørnøya Basin show extended lows in gravity and magnetics. On the other hand, for most of the area the correlation is poor and appears to be accidental. One possible explanation, as pointed out earlier, can be that we have a less well developed magnetic sediment-basement contrast, but a c. 5-10 km thick succession of sedimentary rocks could also blur basement signatures in the magnetic data. For the gravity map, thick piles of sediments can cause similar high densities in the sedimentary successions as in the basement due to high compaction, which can conceal the real extension of deep sedimentary basins such as the Sørvestsnaget and Ottar basins.

A comparison of the gravity and magnetic data leads to an enhanced interpretation of the regional geological setting in the study area. The Bouguer gravity highlights the locations and

extensions of sedimentary basins such as the Nordkapp, Tromsø, Bjørnøya and Maud basins, and assists in explaining several linear features and structural changes observed in the magnetic data. Furthermore, where one has correlation of positive anomalies, the opposite conclusion based on our assumption of a blurred magnetic basement signature, this can imply the presence of uplifted and possibly rotated basement blocks on the Norsel, Loppa and Stappen highs and the magnetic high M-BH5 (Fig. 10.3). A correlation of magnetic and gravity lows as we observe for the Tromsø and Bjørnøya basins, definitely points to deep sedimentary basins, in extreme cases possibly combined with crustal thinning and a regional tectonic impact.

Another interesting and noteworthy feature is that the magnetic signature can often be associated with both deep and shallow structures, as suggested by the combination of seismic observations with the potential field data (Figs. 11.5, 11.6 and 11.8). Since the earliest basement configuration is probably a first-order factor for subsequent fault reactivation and subsidence patterns, it appears that several magnetic domains are associated with more than one structural level.

Previous studies have shown that subcropping, tilted, sedimentary strata or folded sedimentary units have generally low magnetic susceptibilities but might also generate measurable magnetic anomalies (Gibson & Millegan 1998). Faults, carbonate units or other irregularities in the sedimentary strata do influence mainly the short-wavelength magnetic signature and can be distinguished from basement structures by appropriate filter techniques. In our approach we extracted and interpreted such small-wavelength attributes by mostly using the tilt derivative (TDR) (Verduzco *et al.* 2004) and a 30 km high-pass filter.

The various magnetic and gravity attribute maps interpreted in this report (Figs. 10.1, 10.2 and 10.5) describe the features and patterns of the basement blocks relative to their surroundings. The structural pattern of the basement as revealed from magnetic interpretations combined with gravity was characterised by a hierarchy of structural elements involving 1) large structural zones, 2) tectonic domains and 3) sub-domains and internal magnetic lineaments (Figs. 10.6, 10.7 and 10.8). For each domain there are also additional extended features that overprint some of these structures and are potentially related to the deposition of basin sediments, salt tectonics and dyke intrusions.

The western part of the magnetic compilation is clearly dominated by the Stappen and Loppa highs, which are connected by the 'catwalk', a narrow but deep-seated NW-SE-striking anomaly (Figs. 7.2b, 7.3b and 10.5a), cross-cutting the northern part of the Bjørnøya Basin (Fig. 10.1). The two highs are surrounded by major basins, of which the Tromsø and the Bjørnøya basins are well expressed and form – together with the Harstad Basin in the south – a rather continuous NNE-SSW striking magnetic low, which abruptly stops at the catwalk anomaly. Advanced filter-techniques reveal for this area various 2nd- and 3rd- order trends

(Figs. 10.6a & b), which are limited to the basins and the platforms, whilst for the basement highs no trend could be observed (Figs. 10.5a, b). 1st-order lineaments are barely visible.

The western Finnmark Platform is clearly dominated by NE-SW-striking Caledonian lineaments, locally cross-cut by NW-SE-trending dyke-related features. The Sørvestsnaget Basin and the southern part of the Tromsø Basin show mainly NW-SE striking lineaments, almost parallel to the continent-ocean transition zone (COT), whilst the Hammerfest Basin shows weak signs of an E-W trend in structural features, bending towards NE-SW in the southwestern part of the basin. In the Bjørnøya Basin, lineaments are only visible sporadically. At this point it is worthwhile mentioning the resolution difference between the BASAR-09 survey, flown with 2 km line spacing, and the HRAMS-97/98 survey, which was flown with 1 km line spacing. Regarding resolution and interpretation of shallow intrasedimentary features, a denser line spacing is obviously beneficial. For the Stappen and Loppa highs, however, no prevailing trends could be observed. The Stappen High shows circular, almost concentric shaped structures at its principal anomaly southwest of Bjørnøya in the magnetic tilt derivative and filtered data. The Loppa High, however, shows rather irregular structures with a predominant magnetic high at its southwestern edge (Figs. 8.3, 8.4 and 10.7a). Interestingly the shapes of the two basement highs are still visible in the HGM and analytical signal, which confirms them to be compact and deep crustal blocks. The shallower parts of the highs, however, are obviously deeply fractured and most likely have a rather rugose surface (Figs. 10.7a & b). For the Loppa High, the compact rounded anomaly, noticeable from the HGM and the irregular-shaped magnetic signature in the HGM, might indicate a different basement composition, e.g. alternating low- and high-magnetic basement of different ages on top of the block. As an interesting fact in this regard, we notice that the Loppa High Graben (as interpreted by Gabrielsen *et al.* 1990) is obviously not visible in the magnetic data at all. A possible reason could be that it is embedded in a low-magnetic basement sheet.

East of the Loppa High Caledonian trends clearly dominate the basement architecture especially on the Finnmark Platform and locally on the Bjarmeland Platform, but farther east and especially in the southeast, Timanian trends are more and more noticeable and are most likely to have influenced the rift and basin configuration particularly in the central Nordkapp Basin. Old inherited structures usually appear to be the first-order crustal parameters that control the rift or basin architecture (e.g. Doré *et al.* 1997, Roberts & Lippard 2005). Caledonian influences are usually recognised by the N-S structural grain of the western Barents margin and Svalbard, and the NE-SW grain of the southwestern Barents Sea and Finnmark (e.g. Doré 1991, 1995, Fichler *et al.* 1997, Roberts & Lippard 2005).

The new magnetic data confirm this general interpretation, showing these trends quite clearly (Fig. 10.5). Prominent, almost N-S-trending and eastward-bended, 1st-order lineaments are interpreted as different settings or stages in what is most likely a Caledonian basement and reveal a clear tripartite division of the area: Westernmost Barents Sea, and the Bjarmeland

and Finnmark platforms. The westernmost Barents Sea is almost devoid of first-order lineaments. A couple of parallel major faults are observed north of Bjørnøya, striking NW-SE and fading out at the Hoppenbanken Arch. Another possible 1st-order lineament is the 'catwalk'. Although the origin of this anomaly is not quite obvious from the structural interpretation, a relationship with the Stappen and Loppa highs is likely and the anomaly should consequently be considered as a part of the basement highs. It is debatable if the dominance of the Stappen and Loppa highs in the magnetic signal conceals 1st-order structural elements within the basement. Possible lineaments are definitely observed at the eastern edge of the Loppa High, but they are rather short and probably related to some local faults. In the favour of this idea would be the absence of the Loppa Graben in the magnetic data, which is observed from seismics. In this case, a clearly higher-magnetic basement dominates over possible magnetic lineaments from a shallower low-magnetic basement and thus makes it transparent in the magnetic map. Consequently, this leads to the conclusion that there is a different basement type for both the Stappen and the Loppa highs in comparison to the surroundings. Alternatively, one could assume a completely different evolution for the area west of the Loppa High, decoupled from the Finnmark Platform. Extensive rifting and large and deep basins around the two basement highs may well have obliterated the old inherited crustal structures.

The eastern part of the area is bisected by a distinct fault complex between the Norsel High and the Nordkapp Basin. The penultimate identified curved lineament to the east on the Finnmark Platform can even be linked directly to the base of the Middle Allochthon (Tanahorn Nappe) on northwestern Varanger Peninsula. WNW-ESE-striking, high-amplitude magnetic lineaments, however, cross-cut and superpose signatures from deeper origins and complicate the tracing of more of these N-S lineaments across the Austhavet Fault Zone. Nevertheless, the strike of the geological units on the Nordkinn and Sværholt peninsulas is clearly parallel to the lineaments observed and interpreted offshore.

From a comparison with the Bouguer gravity (Figs. 10.6 and 10.8a), we notice a connection between the distribution of the basins in the area and the disruption of the N-S-trending lineaments. Not only in the Nordkapp Basin but also in the Ottar Basin and potentially in the Maud Basin there are similar disturbances of the basement signatures, which are in line with the seismically proven, post-Caledonian, rifting structures and basin development in the Barents Sea (e.g. Faleide *et al.* 1993, Breivik *et al.* 1995, Gudlaugsson *et al.* 1998).

Two systems of principal and probably deep faults can be observed from the new magnetic dataset (Fig. 10.6a). The first one is north of the Nordkapp Basin striking NW-SE, and located at the northern flank and within the Ottar Basin. The fault to the south of the basin separates the Swaen Graben from the Norvarg Dome and runs into the Norsel High to the southwest. It is located at the southern edge of a gravity minimum (G-BL3) (Fig. 10.3), and with regard to the Ottar Basin configuration defined by Gudlaugsson (1994) and Breivik *et*

al. (1995) it might possibly coincide with the edge of an intra-basin high but not with the actual boundary of the basin.

Two lineaments are observed at the northern rim of the Ottar Basin (Fig. 10.6b), and might link to two major rifting structures and a gently dipping basin flank. There is weak evidence for a south-westward continuation of the southerly located lineament into the central Nordkapp Basin which, in fact, partly coincides with an intra-basin fault observed on seismics. The second system coincides with the mapped fault complex south of the Nordkapp Basin (Måsøy and Thor Iversen fault complexes). The main feature of this complex is a distinct linear structure that is obvious from the 30 km high-pass filtering and strikes NE-SW (Figs. 10.6b, 10.7b). This lineament can be observed all the way from south of the central Nordkapp Basin south-westwards almost to the coast where its clear signature defuses into in a swarm of parallel lineaments. The structure is disturbed by a NNW-SSE-oriented, dextral strike-slip fault in the central part of the fault zone just south of the narrow part of the Nordkapp Basin, and provides evidence of an additional NNW-SSE stress component in the eastern part of the survey area. The western part of this same lineament transects the southern Nordkapp Basin and probably marks the northern flank of the Måsøy Fault Complex, whereas to the east the width of the fault complex is less well defined. Here, there are no additional sharp linear features to be seen except for the lineament and the coinciding Thor Iversen Fault Complex. The N-S-trending curved characteristics of the magnetic data fade out towards the lineament instead of ending abruptly as they do further west. This, however, might indicate that it is either a less distinct fault system or a superposition of magnetic signatures from other origins in this particular area.

Together with the distribution of the basins (Fig. 10.6b) and the correlations with the Bouguer gravity (Fig. 10.2a), the first-order lineaments already provide new insights into the basement structure and different basement domains in the southern Norwegian Barents Sea.

In addition, we have mapped second-order structures using TILT derivatives and high-pass frequency filtering. Such features are likely to be of shallower origin, deriving from somewhere within the sedimentary succession, and in fact there are a number of obvious similarities between the existing BCU map (Gabrielsen *et al.* 1990) and observable features from the high-pass filtering (Figs. 10.6b and 10.7b). We used the new magnetic dataset to supplement the existing BCU map, even though the origin is not compulsively the BCU, but intrasedimentary. A comprehensive overview of the observable short-wavelength lineaments can be interpreted and directly linked with diverse structures within the sedimentary successions. The resulting map expresses the different structural developments of the Bjarmeland and Finnmark platforms with opposed strike orientations, a feature probably deriving from the time of the initial rifting phase in the Late Palaeozoic. Nevertheless, both platforms also show some lineaments orientated along the principal trend of the other platform which gradually decrease from west to east on the Finnmark Platform and from east

to west on the Bjarmeland Platform. A detailed description and interpretation for each area is presented below.

Whilst the observed structures on the platforms are probably associated with reactivation along Early Palaeozoic and Precambrian basement structures, the lineaments within the Nordkapp and Hammerfest basins are different and rather reflect the different rifting phases in Mesozoic and Ceneozoic times. We should point out that the salt signature in the Nordkapp Basin made it difficult to establish a clear differentiation between salt-related features and faults. Nevertheless, based on the mapped lineaments, there is strong evidence that the southern and central parts of the Nordkapp Basin show different structural developments.

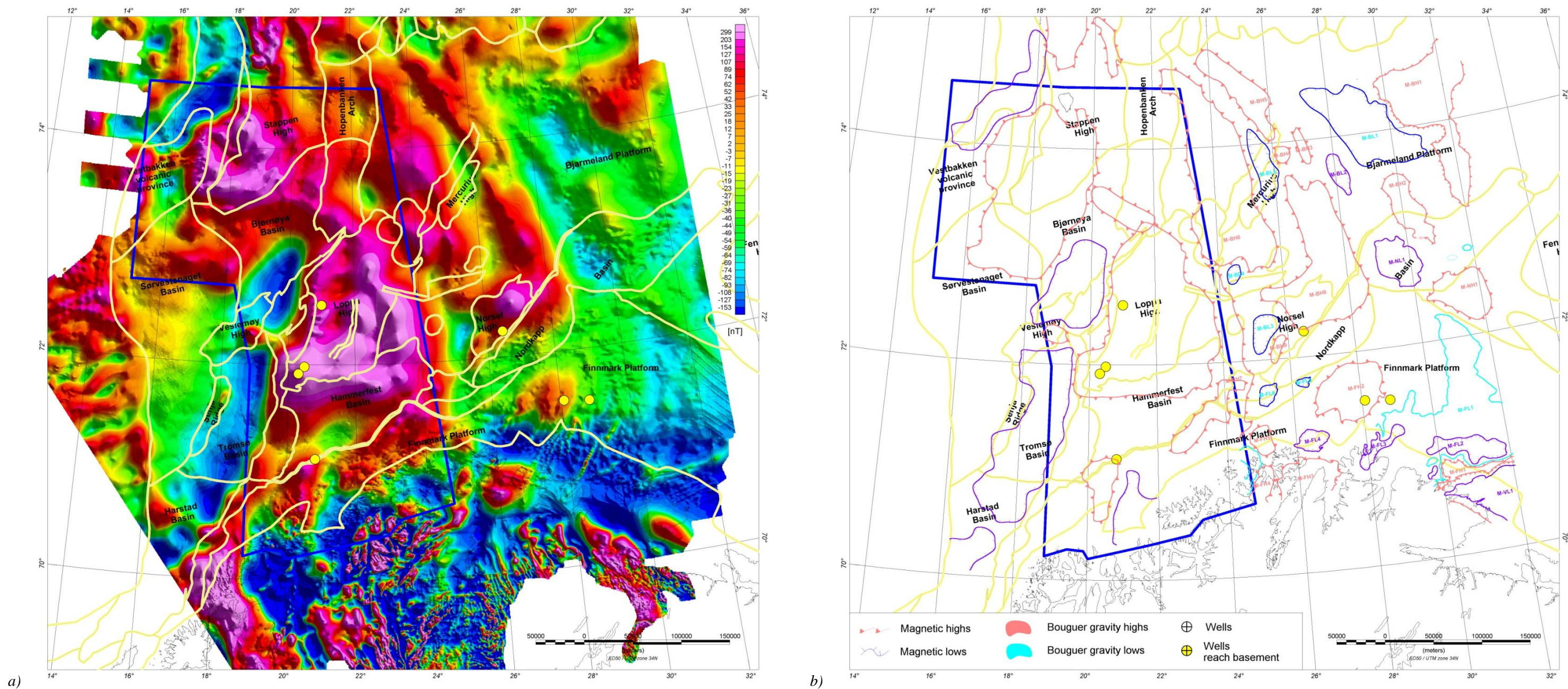
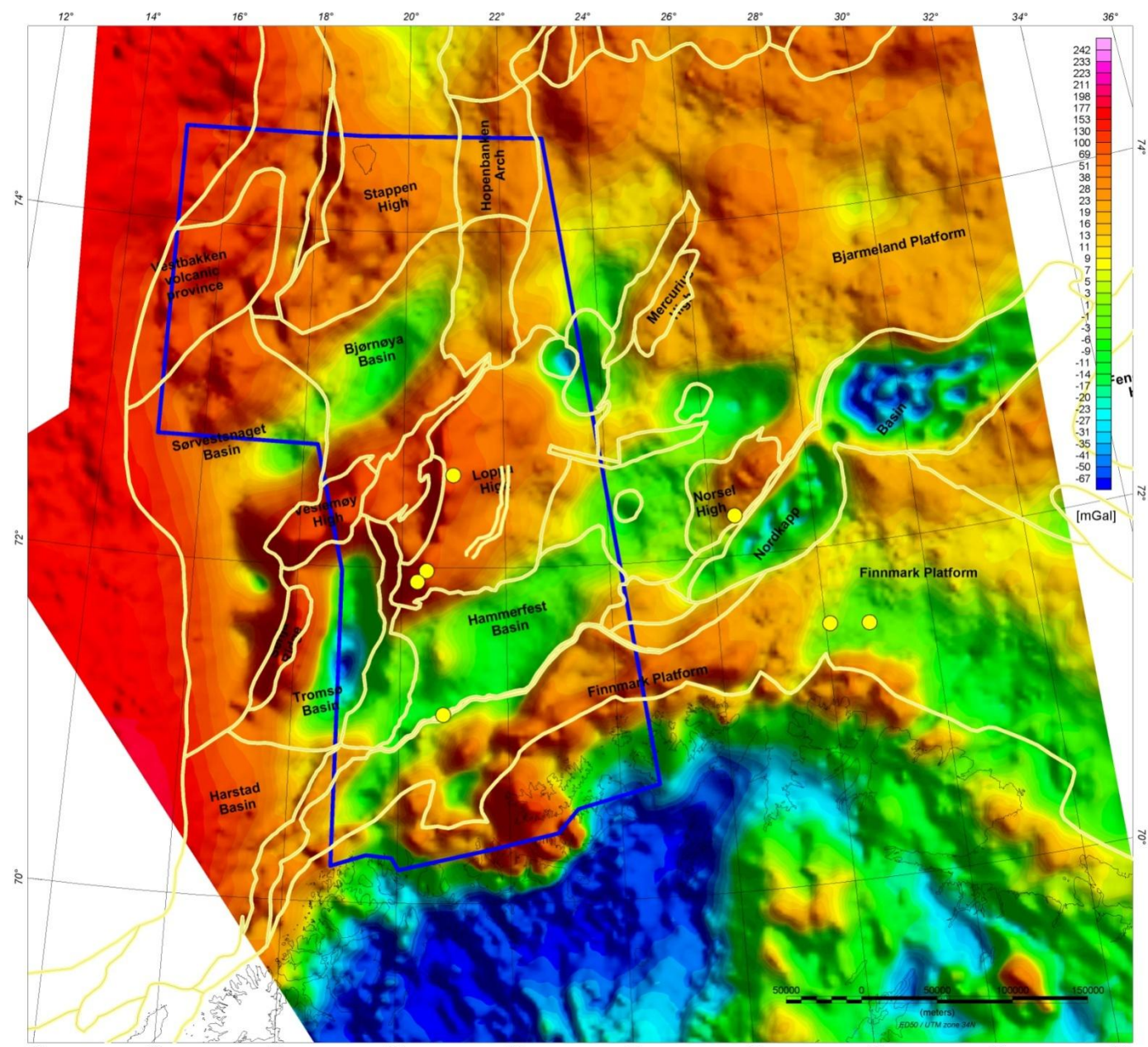
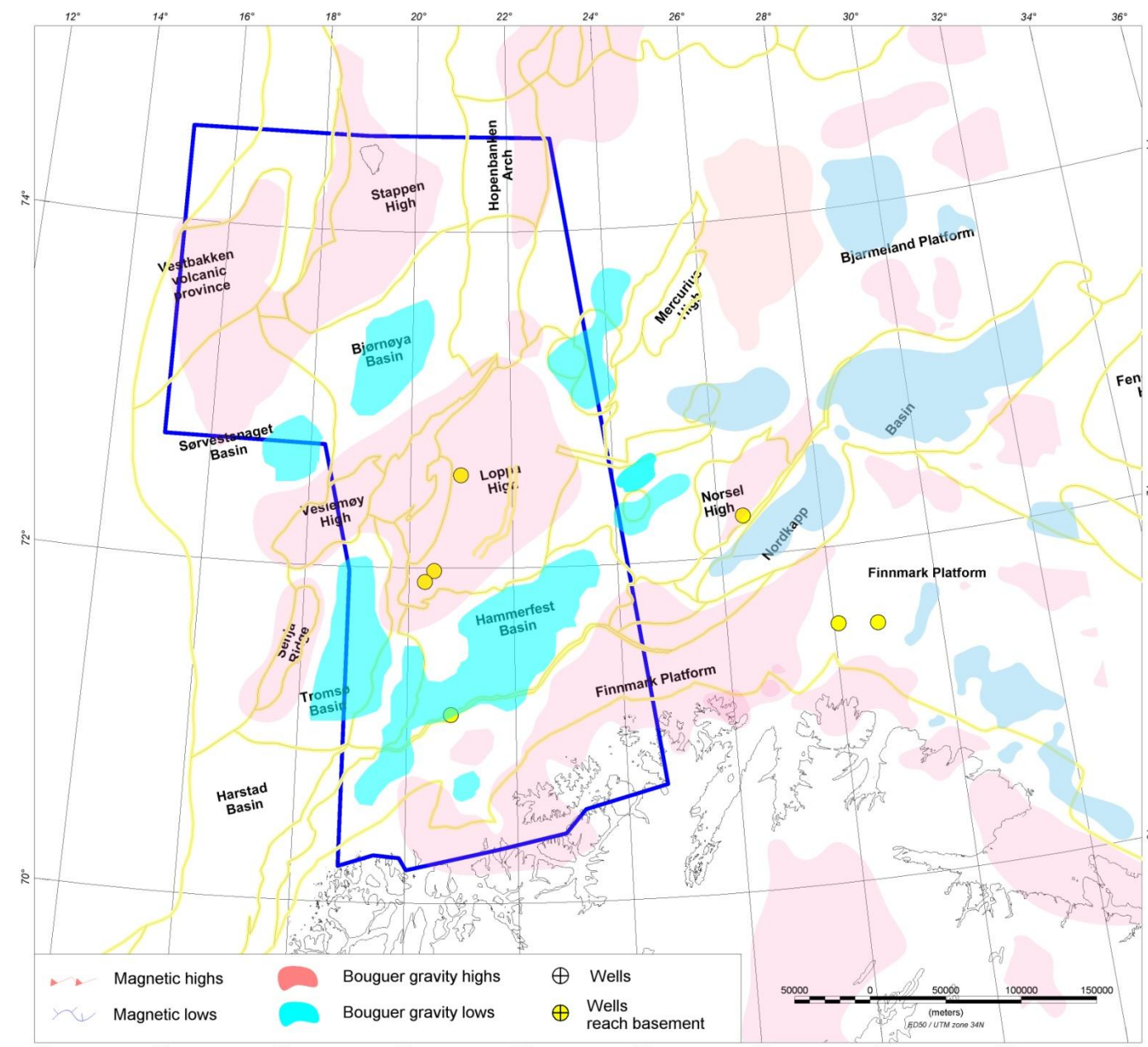


Figure 10.1 a) Magnetic total field (left) and b) outline of the main anomalies (right). Black and yellow lines underline the main structural features of the area (Gabrielsen et al. 1990).



a)



b)

Figure 10.2 a) Bouguer map and b) interpretation of the main anomaly highs and lows. Black and yellow lines underline the main structural features of the area (Gabrielsen et al. 1990).

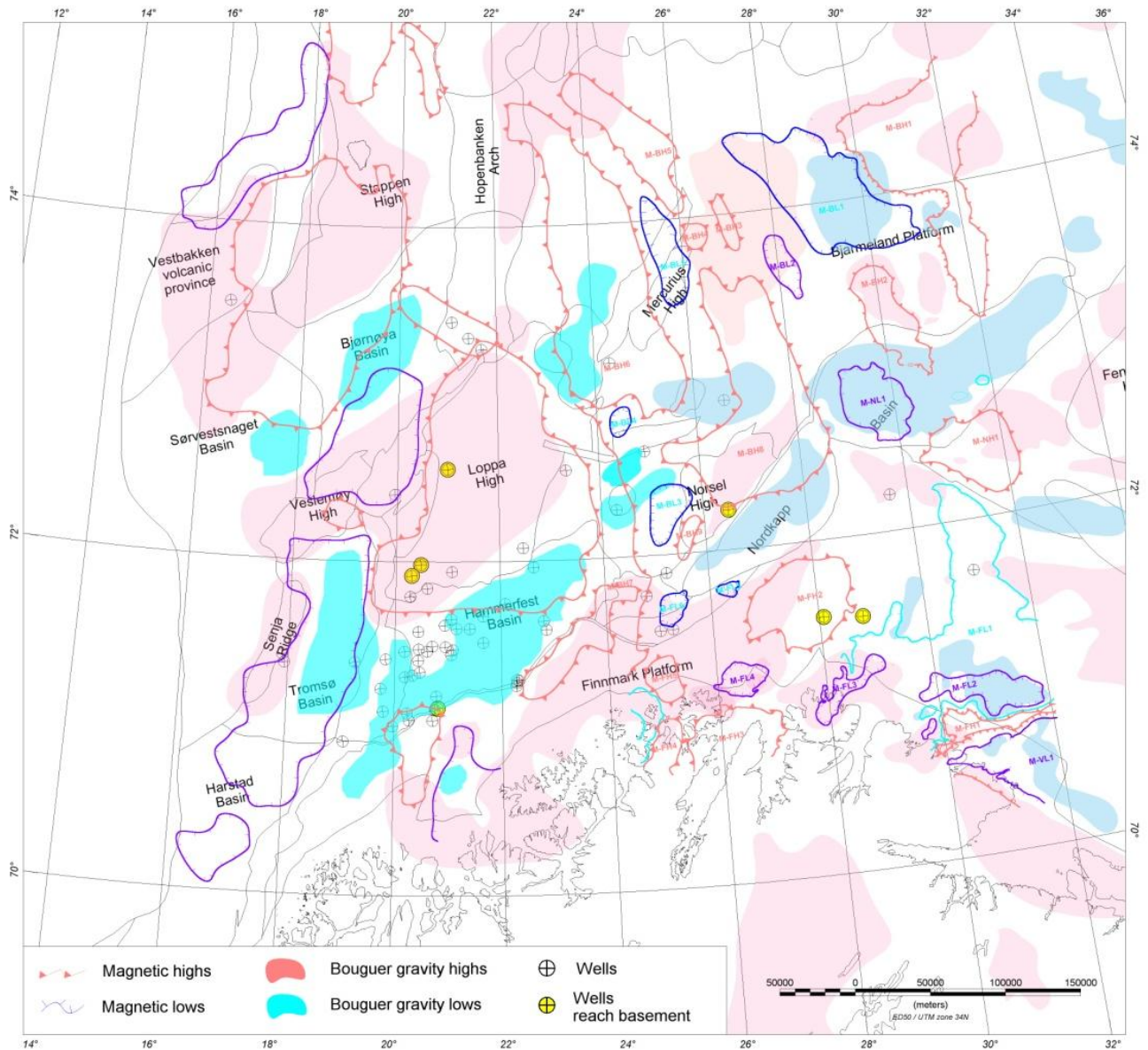


Figure 10.3 Interpretation of the main anomaly highs and lows from Bouguer (filled) and TMI (outlines) maps. Black and yellow lines underline the main structural features of the area (Gabrielsen *et al.* 1990). Grey lines represent the faults mapped at base Cretaceous level (Gabrielsen *et al.* 1990).

10.1.1 Loppa High (LH)

Various stages of uplift and erosion since Devonian time have resulted in a rather complex structure of the Loppa High. The LH, as defined now, has most likely been in its high position since Late Jurassic to Early Cretaceous time (Gabrielsen *et al.* 1990).

From gravity and magnetic maps the LH is well expressed on both, which indicates a crustal-scale basement block of higher magnetisation. Together with the Stappen High it is a predominant feature in the Barents Sea and at the boundary to an obvious structural change in the basement characteristics of the southern Barents Sea. Basement was drilled in three wells (Tab. 9.1) at c. 1480 m in the central part and c. 3500 m and c. 3900 m in the south of the LH.

According to the gravity and magnetic data the two southern wells show diabase and amphibolite as the main basement rock with both high densities of more than c. 2760 kg/m³ and up to c. 0.034 SI in susceptibility (Slagstad *et al.* 2008). No further information is available for the well from the central area. A TILT derivative multiscale edge detection (Lahti & Karinen 2010) was carried out to determine the tilt of the LH (Fig. 10.8b), which showed the block to be seated fairly vertically in the crust. No predominant rotation is indicated. Nevertheless, the signature of this unit from the gravity and magnetic data is rather different (Fig. 10.3). The magnetic data show a southeastward extension into the Hammerfest Basin, whilst the gravity data indicate that the LH expands westwards and into the Veslemøy High. A simple explanation for this difference is hard to find. One could speculate if the origin for this discrepancy is either situated in the shallow basement due to, e.g., volcanic intrusions or if it is due to the presence of high-magnetic lower-density bodies in the deeper crust.

10.1.2 Stappen High (SH)

The Stappen High is situated to the northwest of the LH and has apparently undergone a similar, complex, tectonic evolution, marked by different episodes of uplift and erosion. Very little is known about the basement structure of the SH, although Bjørnøya is generally considered as an exposed window in the economic basement of the SH (Braathen *et al.* 1999, Worsley *et al.* 2001).

The main magnetic anomaly of the SH is expressed as a noticeable round magnetic high, slightly displaced to the west relative to the structural outline of the SH as interpreted by Gabrielsen *et al.* (1990), and reaching into the Vestbakken volcanic province (Fig. 10.1). Upstream to the south, another magnetic anomaly is noticeable which is in good correlation with the gravity data (Fig. 10.2) and is possibly an extension of the SH. Comparison of both the gravity and the magnetic data (Fig. 10.3), however, shows a rather good correlation. The TILT derivative multiscale edge detection (Fig. 10.9b) indicates a tilt and rotation to the north-northwest for both anomalies. Direct methods like FVD or HGM (Figs. 8.1 & 8.3) reveal an almost concentric arrangement of the magnetic anomalies, which most likely reflects the surface structure of the SH basement block. Euler solutions for the SH are also irregularly distributed and of rather shallow depth (4 - 7 km, Fig. 9.2), supporting this assumption. Such a ring-shaped structure in crystalline rocks is well known from weathered basalt but has to our knowledge never been observed at this scale. However, the Richat Structure in Mauritania (Matton *et al.* 2005) probably represents the closest analogue known so far. It remains questionable as to what has caused this rather regular structure, but due to the similarity with the LH and the reported repeated phase of uplift and exhumation, the magnetic anomalies from advanced filtering are likely to reflect the surface morphology of the two highs, which are much more jagged than e.g. the Norsel High (Fig. 10.7a). The absence of any indications of major faults and thrusts in the area underline the compact structure of the SH.

10.1.3 The Hammerfest Basin

The Hammerfest Basin is a relatively shallow Mesozoic basin, 50-75 km wide and located between the Finnmark Platform and the LH (Berglund *et al.* 1986). The structure of the basin is mostly dominated by extension of features and shows a clear graben-type form. An episode of strike-slip deformation has been suggested in Late Jurassic-Early Cretaceous time (Gabrielsen and Færseth 1989). The basin is separated from the Finnmark Platform to the south-southwest by the Troms-Finnmark Fault Complex and borders the LH along the Asterias Fault Complex to the north. The Asterias Fault Complex has an east-west trend, and is a zone of normal faulting and local transpression which dies out into the eastern flexure as it begins to head in a north-northeast direction. The western limitation of the Hammerfest Basin is defined by the southern segment of the Ringvassøy-Loppa Fault Complex and its eastern border is marked by a progressive flexure towards the Bjarmeland Platform (Gabrielsen *et al.* 1990). The Hammerfest Basin includes both deep-seated, high-angle faults along the basin margin and a normal fault detached in the Permian-Carboniferous strata. As earlier suggested by Gabrielsen and Færseth (1989), the extension of the Trollfjord-Komagelva Fault Zone trends could explain the subdivision of the Hammerfest Basin. The central fault system is composed of different segments with E-W, ENE-WSW and WNW-ESE-trending faults that formed the Hammerfest Basin fault system named (informally) by Gabrielsen (1984).

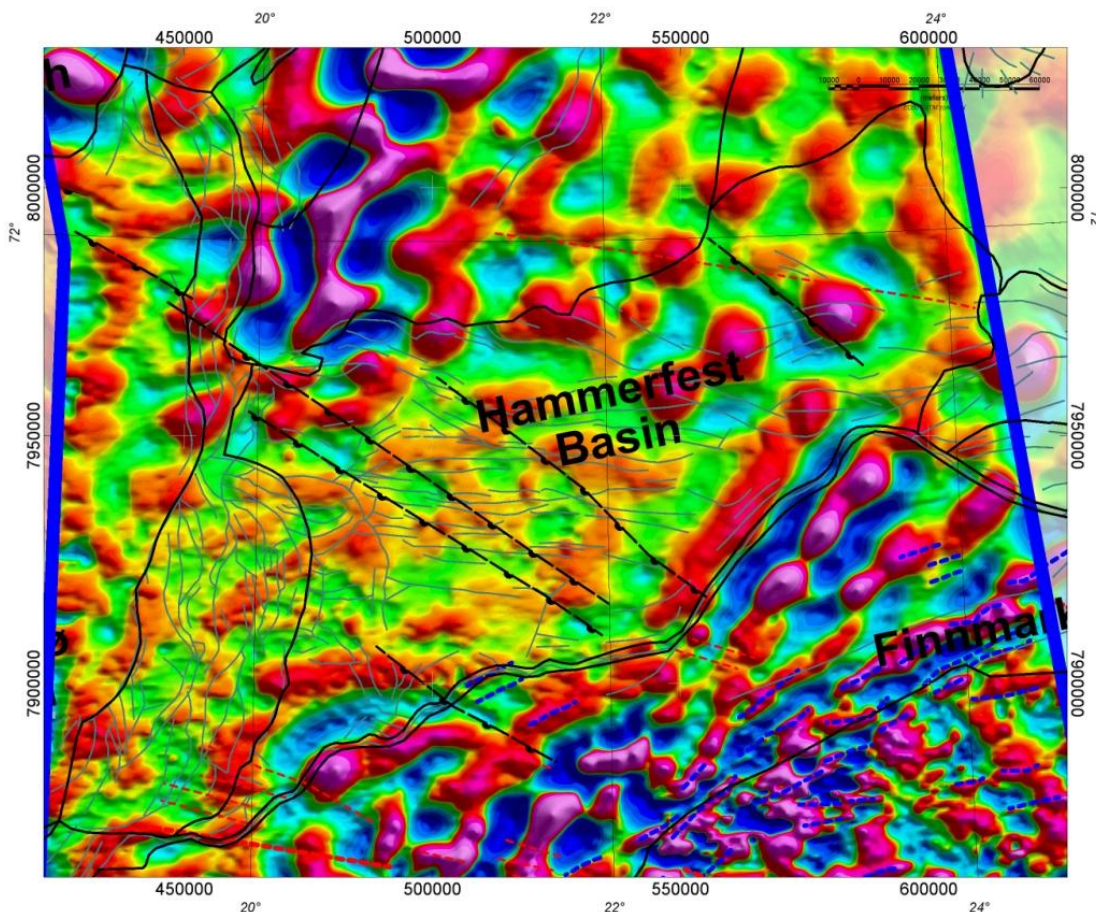


Figure 10.4 Structural interpretation of the Hammerfest Basin and 20 km high-pass filtering of the TMI data.

The origin of the Hammerfest Basin can be traced back to a period of inferred post-Caledonian orogenic collapse (Gudlaugsson *et al.* 1998), and it has been affected by extension in the Carboniferous (Berglund *et al.* 1986) and from Triassic to Early Jurassic time. The basin was probably a distinct depocenter already in late Scythian time (Gabrielsen *et al.* 1990). The main rifting episode was initiated in the Mid Jurassic and continued during a period of major tectonic subsidence into the Early Cretaceous.

From the magnetic data the Hammerfest Basin is relatively inconspicuous; the northeastern part is inferred by the high-magnetic LH basement, whilst it is noticeable as an intermediate gravity low on the Bouguer gravity map. Structural elements are of small amplitude and occur at shallow depths (Fig. 10.4). A NW-SE-striking fault system can be observed in the central and eastern parts of the basin, but the dominant trend of lineaments is E-W to ENE-WSW, which is in good agreement with the observations from seismics (Gabrielsen 1984, Gabrielsen *et al.* 1990).

10.1.4 Bjørnøya Basin

Formed between the LH and the SH, the Bjørnøya Basin is a large and deep basin. The Bjørnøya Basin is limited to the west by the Bjørnøyrenna Fault Complex and to the northeast by the Leirdjupet Fault Complex that marks the boundary between the deep Bjørnøya Basin itself and the shallower Fingerdjupet Subbasin.

The basin developed mainly in Early Cretaceous but is also considered to contain a thick Late Permian section (Gabrielsen *et al.* 1990). Structural lineaments are uncommon, striking NE-SW. Salt diapirism has been interpreted by Faleide *et al.* (1984), whereas Rønnevik & Jakobsen (1984) could not find any indication for the mobilisation of salt. However, unlike in the Nordkapp Basin, salt structures are not that obvious from the magnetics, but in the gravity map at least one salt structure is noticeable as a small minimum north-northeast of the Veslemøy High. The correlation of gravity and magnetic data for the Bjørnøya Basin is rather poor and does not reflect the outline of the basin observed on seismics (Gabrielsen *et al.* 1990). While the basin shows a NE-SW-striking, lens-shaped, gravity minimum, the minimum in the magnetic data is an oval N-S-oriented anomaly parallel to the basin axis and extends into the Veslemøy High and the Sørvestsnaget Basin and across the Bjørnøyrenna Fault Complex. It appears as the northern extension of a large and elongated magnetic minimum, observable from the Harstad Basin through the Tromsø Basin into the Bjørnøya Basin, only truncated by a magnetic high caused by an intrusional structure at the Veslemøy High (Mjelde *et al.* 2002). Low-pass filtering and upward continuations (Figs. 7.2b & 7.3a & b) suggest that the structure is a regional and extended basement low. The contradiction between the magnetics and gravity (Fig. 10.3) could be an expression of significant crustal thinning and a deep-seated basement. Different degrees of compaction within the sediments, faulting along the southeastern margin and thus a different sedimentary succession occurring along the Veslemøy High –

Bjørnøyrenna Fault Complex would have led to higher densities in the southern part of the basin.

The so-called 'catwalk' cuts the northern part of the basin, and was previously identified as a very deep and regional structure (Fig. 7.3b), associated either with a basement ridge or a very deep-seated and steep thrust of crustal scale and with a regional impact. However, the basin does seem to be shallower in the north (Fig. 10.1a).

10.1.5 Tromsø Basin

The Tromsø Basin is located south of the Bjørnøya Basin and the Veslemøy High. It is bordered by the Senja Ridge to the west and the Ringvassøy-Loppa Fault Complex to the east. Observed lineaments from the magnetic data (Fig. 10.5) are of rather shallow origin and are mostly observed in the central, western and southern parts of the basin, which is to some extent due to the higher resolution of the HRAMS-97/98 data, flown with a denser line spacing (1 km). The strike of the lineaments is mainly NNW-SSE, which is the same trend as in the Sørvestsnaget Basin and most likely reflects the effect of the sheared margin. Other, rounded structures are observed and are salt-related. Thick Cretaceous sediments dominate the sedimentary infill of the basin and might conceal NE-SW-striking Late Devonian to Early Carboniferous structural elements, which are prominent to the east of the basin (Gabrielsen *et al.* 1990). Gabrielsen *et al.* (1990) found indications that the Bjørnøya and Tromsø basins were united during the Early to Mid Mesozoic, but in contrast to the Bjørnøya Basin both gravity and magnetics indicate lows for the basin, which are in very good correlation (Fig. 10.3). The development of the basin was most likely more homogeneous, at least since the Late Mesozoic if Gabrielsen *et al.* (1990) are correct. Subsidence and compactions were not disturbed by faulting. Therefore, the magnetic data show much better the related development of the three basins Harstad, Tromsø and Bjørnøya, and the opening along their NNE-SSW striking axis.

10.1.6 The Bjarmeland Platform

The Bjarmeland Platform includes the extensive platform areas east of the Loppa High and north of the Nordkapp Basin. The platform was established in the Permian but subsequent uplift and erosion tilted the Palaeozoic and Mesozoic sequences southwards, with unconsolidated Quaternary sediments overlying successively older rocks towards the north. Five exploration wells have been drilled on the Bjarmeland Platform, exclusively in the southern part. Two of the wells were drilled into the transitional area between the platform and the Nordkapp and Hammerfest basins. Both wells (7226/11-1 and 7124/3-1) reached the Upper Palaeozoic succession, and in the former case demonstrated a mid-Carboniferous onlap of the basement (Larsen *et al.* 2005).

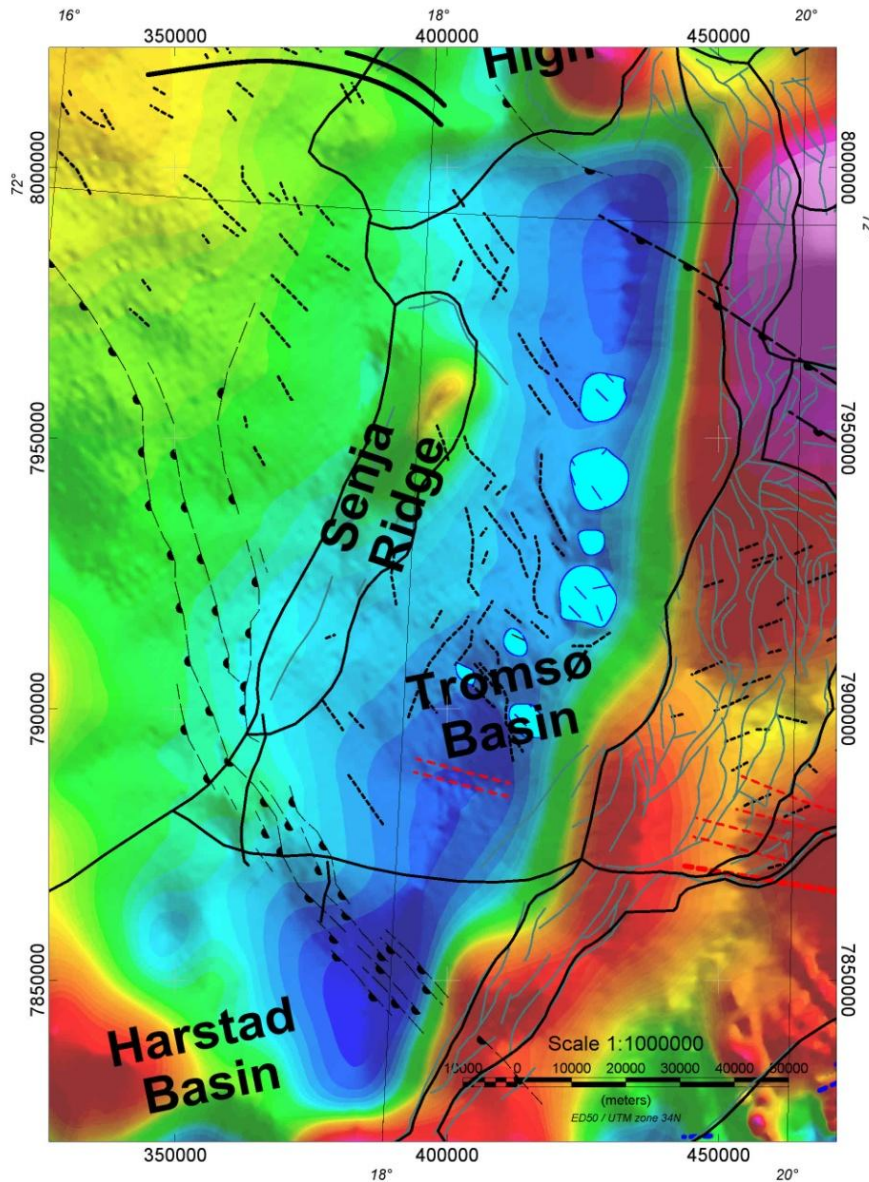


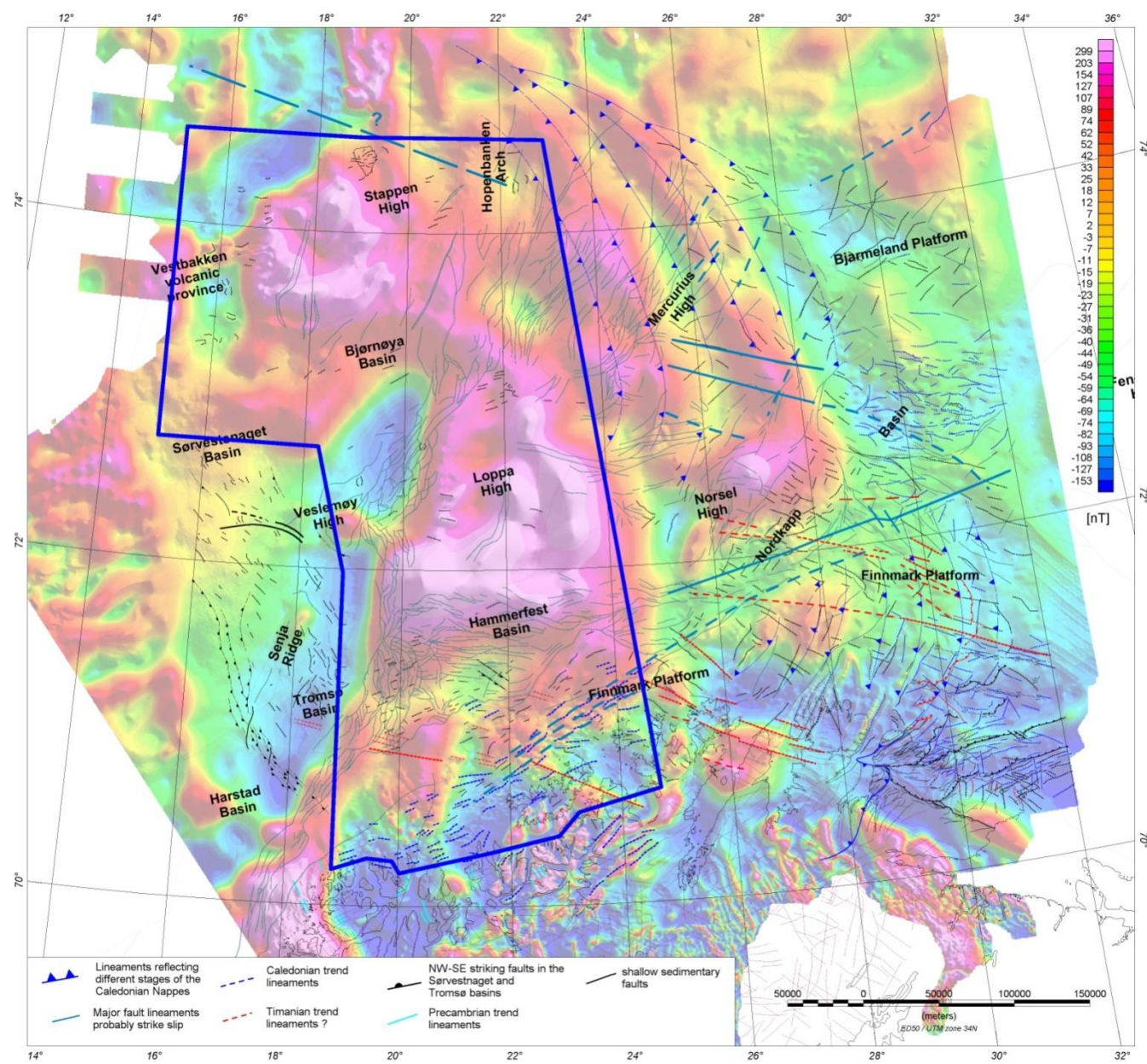
Figure 10.5 Structural interpretation of the Tromsø Basin with the TMI data.

The central part of the Bjarmeland Platform is dominated by the magnetic high centred on the Norsel High (Fig.10.1b) and its NNW-SSE-trending tail-like structure (M-BH8) that extends all the way to the north of the survey area with extended magnetic lows to the west and east (M-BL2 and M-BL5). A marked magnetic high (M-BH6, M-BH7) appears in the westernmost part of the platform with smaller but noticeably round magnetic minima southwards between the Norsel High and the easternmost extension of the Loppa High (M-BL3 and M-BL4). The area to the east is characterised by regional NNW-SSE-striking (M-BH2 and M-BH1) anomaly highs. The structures reflect the predominantly Caledonian character of the basement of the Bjarmeland Platform. Nevertheless, a noticeable change in the amplitude is visible east of the Norsel High and M-BH8, and deep Euler solutions indicate that a major structural change is probably present in the basement at this location. The magnetic data to the east appear smoother with smaller anomalies and gentler slopes. Filtered magnetic data reveal the absence of the

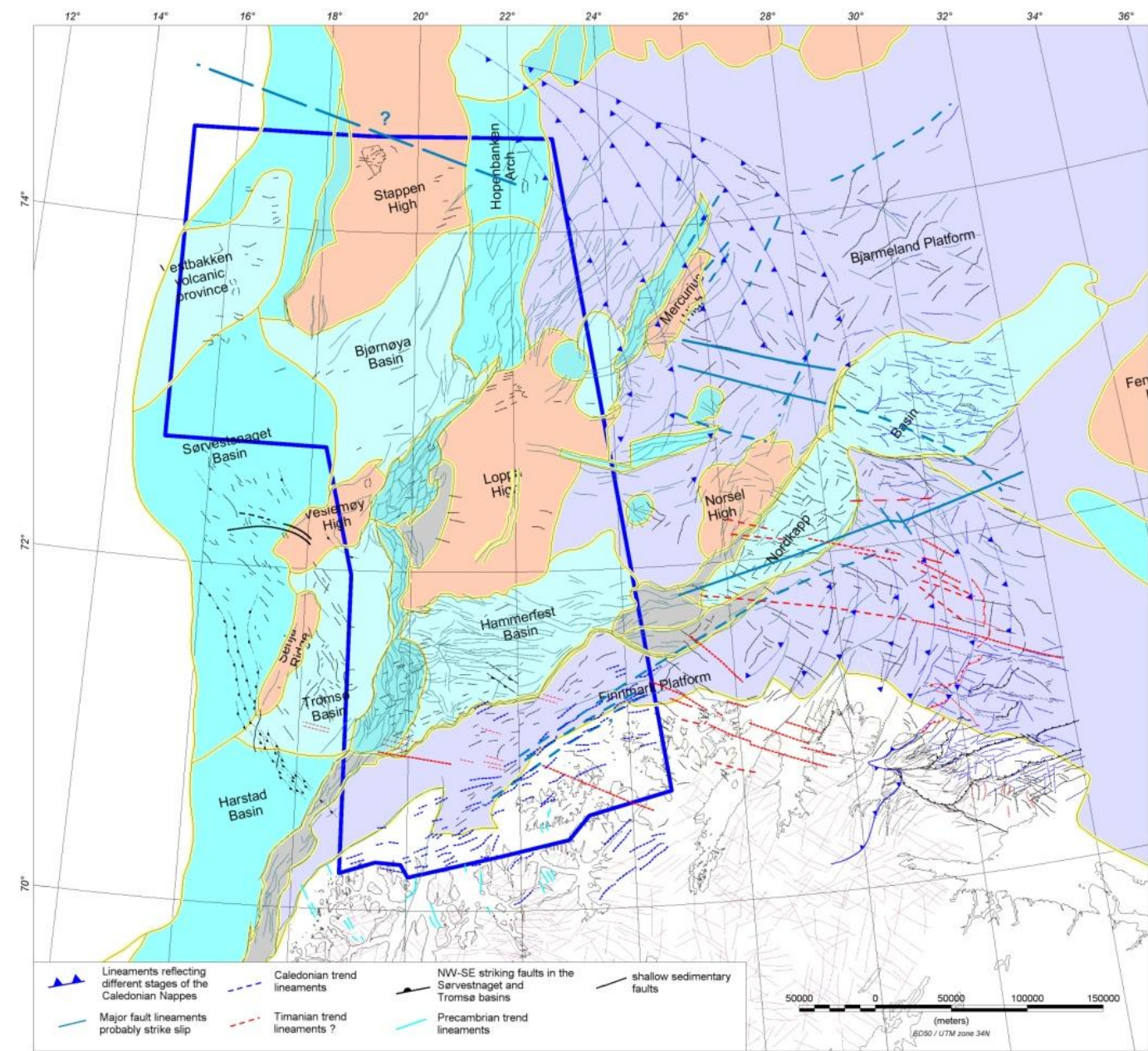
characteristic N-S-oriented and curved lineaments in this part of the platform. From wavelength filtering and derivatives, the magnetic field shows mainly second-order, NE-SW-oriented lineaments, which are prominent in the western Bjarmeland Platform and are of Caledonian origin. To the east, the NE-SW trend progressively interferes with the NW-SE-striking features (Figs. 10.6b). These latter magnetic patterns could be inherited from the Timanian structural grain or even date back to Archaean time, as recognised mainly along the Kola-Kanin Monocline structure, and probably extend as far as to the Timan-Pechora Basin on the Russian side. The NW-SE regional and crustal trends are particularly prominent in the area of the Finnmark Platform but are also seen on the Bjarmeland Platform and have probably been reactivated during the different Late Palaeozoic and Mesozoic rifting events.

The Norsel High and the broad NNW-SSE positive anomaly (M-BH2) are prominent magnetic highs on the platform and coincide with gravity highs. This correlation usually reflects old tectonic features most likely associated with basement units. Indeed, M-BH2 could fit with high-amplitude seismic reflections observed on the northern flank of the Nordkapp Basin, but the seismic imaging is still too poor to pursue this idea at the present stage. As NE-SW seismic lines were not available to us during any of the BAS and BASAR projects, we could not execute an accurate structural investigation. For the Norsel High, the basement was drilled at c. 5150 m, showing what was interpreted to be a 'Pre-Devonian Basement'. Basement rock samples from the Finnmark Platform generally show a rather low magnetisation for the inferred Caledonian basement, which raises the question as to whether the two highs in the survey area represent basement blocks of Precambrian age or at least a partial Precambrian basement in an uplifted position. Precambrian basement usually shows higher magnetisation and could therefore explain the high amplitude of the magnetic anomalies. Modelling during the BASAR-08 project (Brønner *et al.* 2009) revealed, however, a more complex picture involving intruded and highly magnetic mafic rocks at a shallow depth. This would appear to better explain the gravity and magnetic observations, and in particular the significantly different shape of the Norsel High anomaly on both datasets.

Due to the asymmetric and deep and steep basin characteristics of the Nordkapp Basin one could also consider either deep-crustal thrusting or intruded high-magnetic, serpentinised mantle material, or both, to explain the different shapes of the gravity and magnetic anomalies. This hypothesis has not yet been tested.

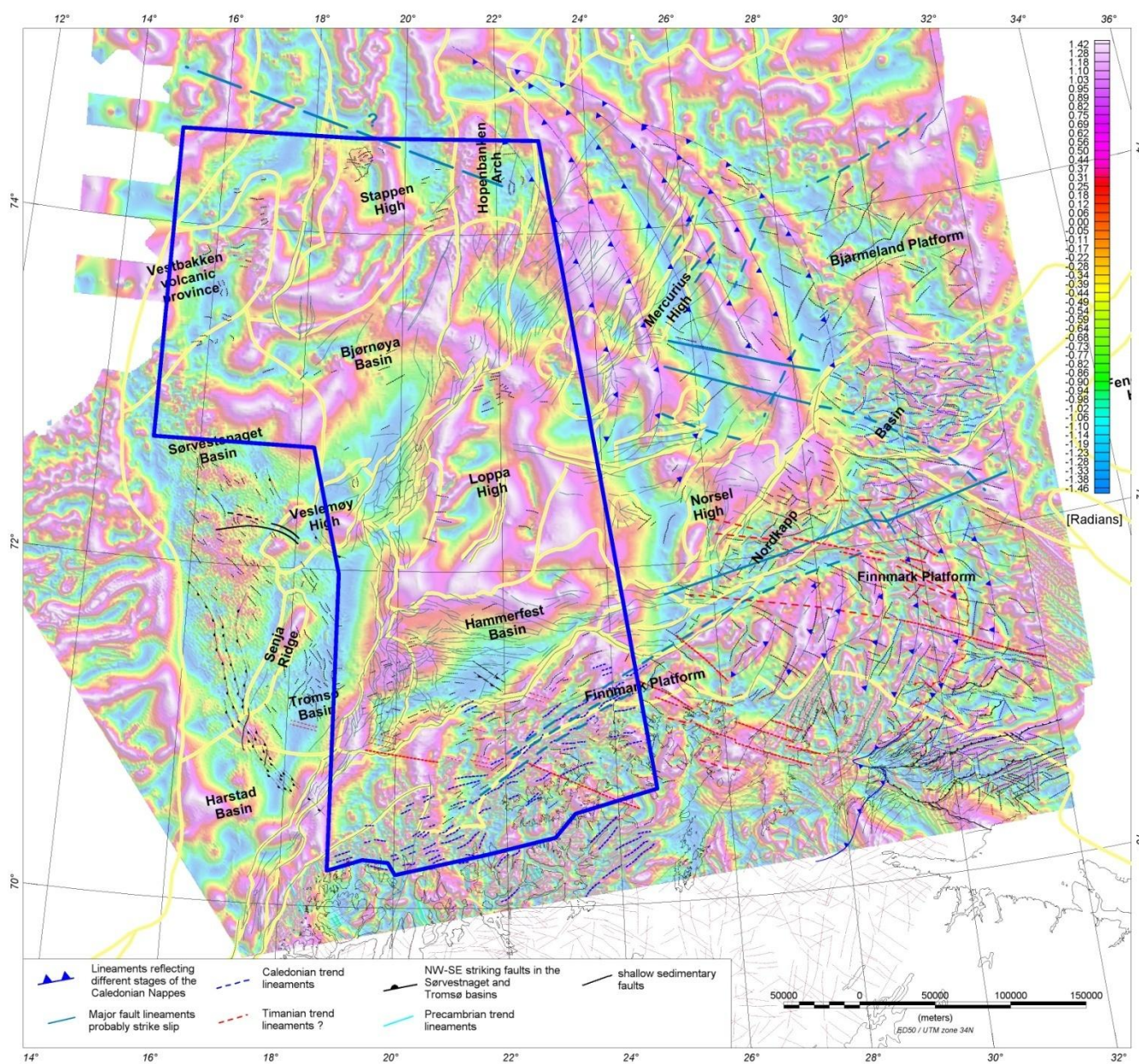


a)

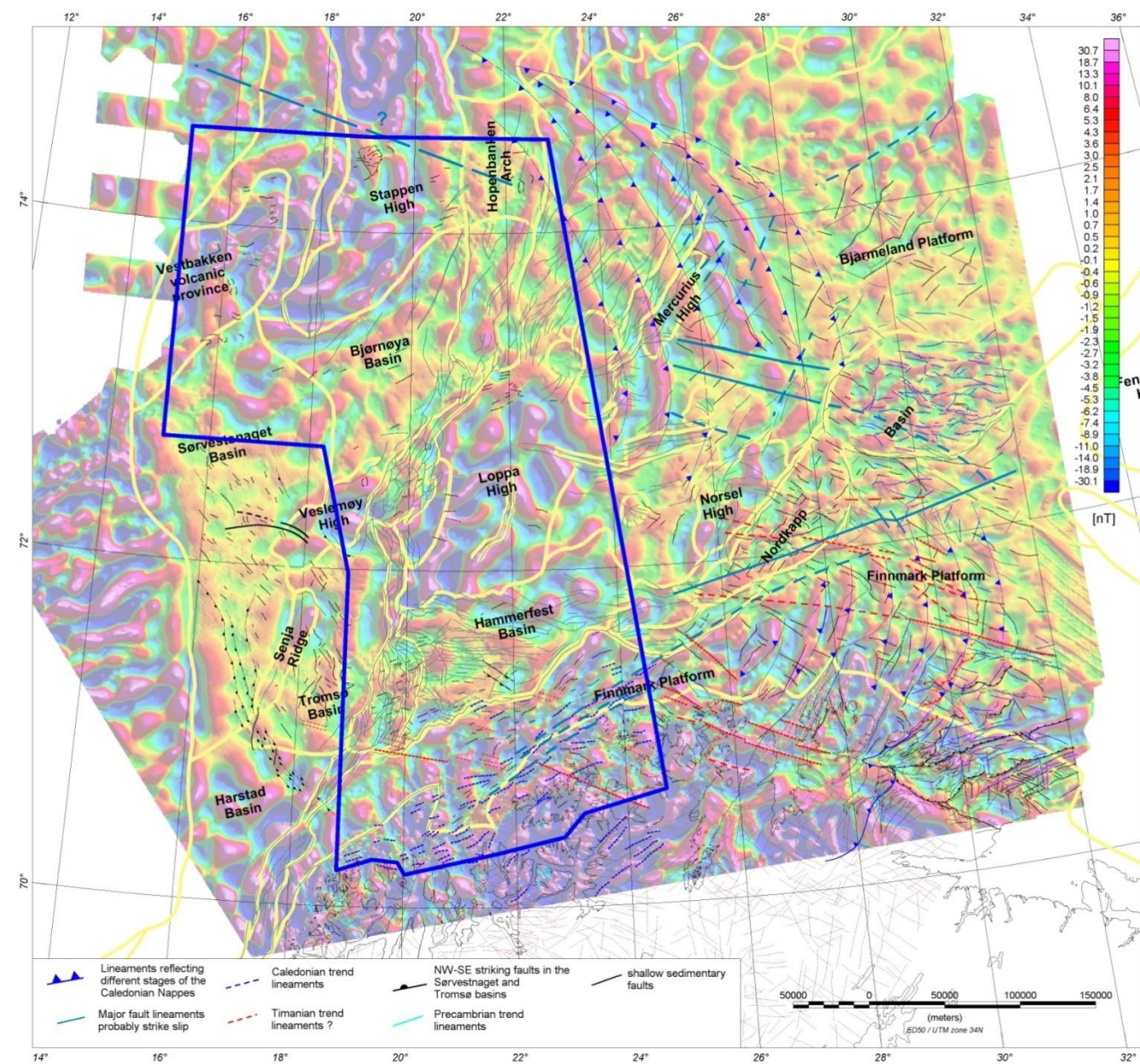


b)

Figure 10.6 a) TMI grid with complete structural interpretation, b) Structural elements with complete structural interpretation. Blue curved lines are observed lineaments from the magnetic map and are most likely associated with Caledonian nappes, dark blue lines are major faults. Red lines show fault-related lineaments probably associated with high-magnetic material such as dykes (see text). Black and yellow lines underline the main structural features of the area (Gabrielsen et al. 1990). Grey lines represent the faults mapped at base Cretaceous level (Gabrielsen et al. 1990), black and blue dotted lines represent second-order lineaments with a more shallow origin, based on magnetic interpretation.

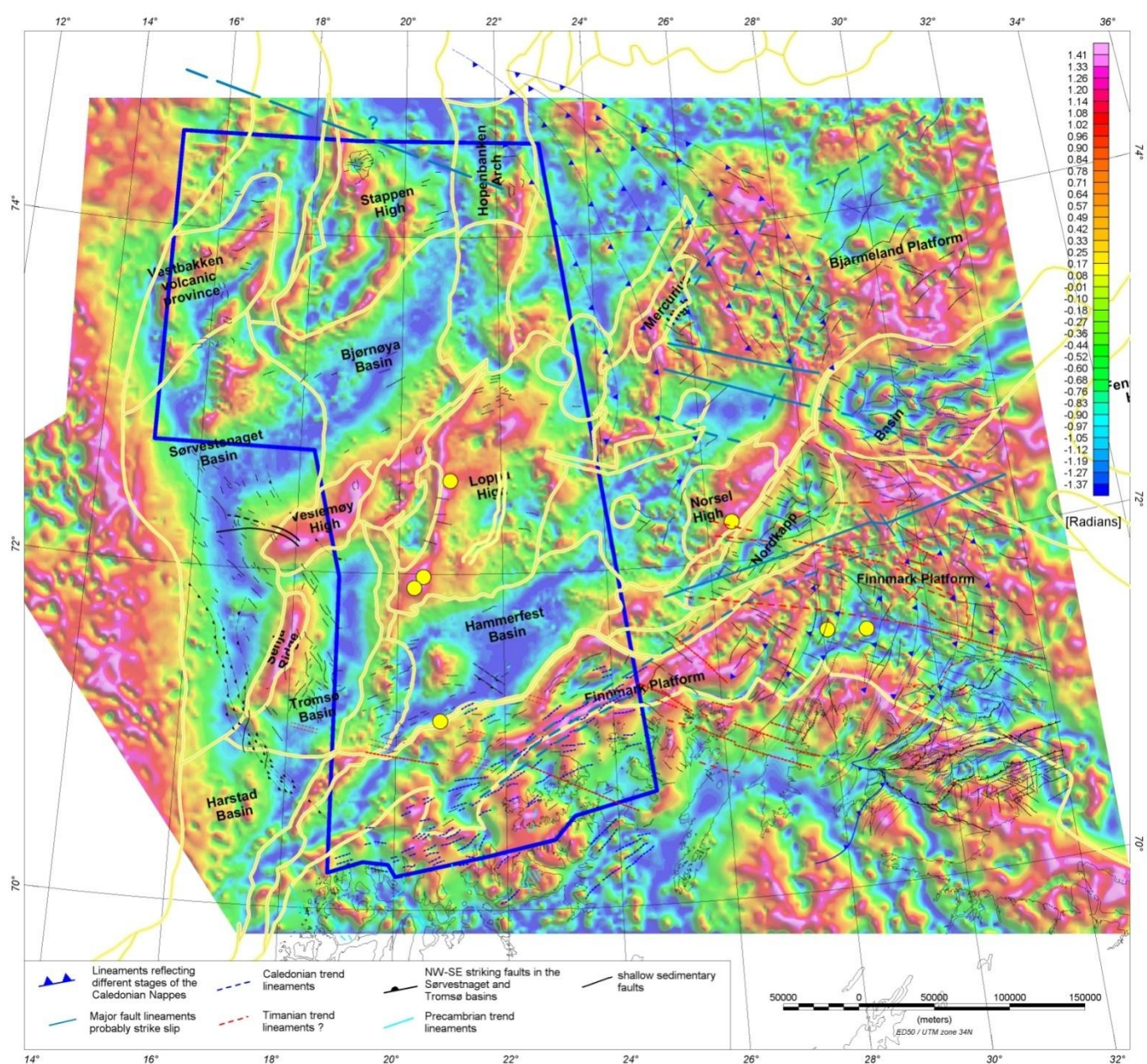


a)

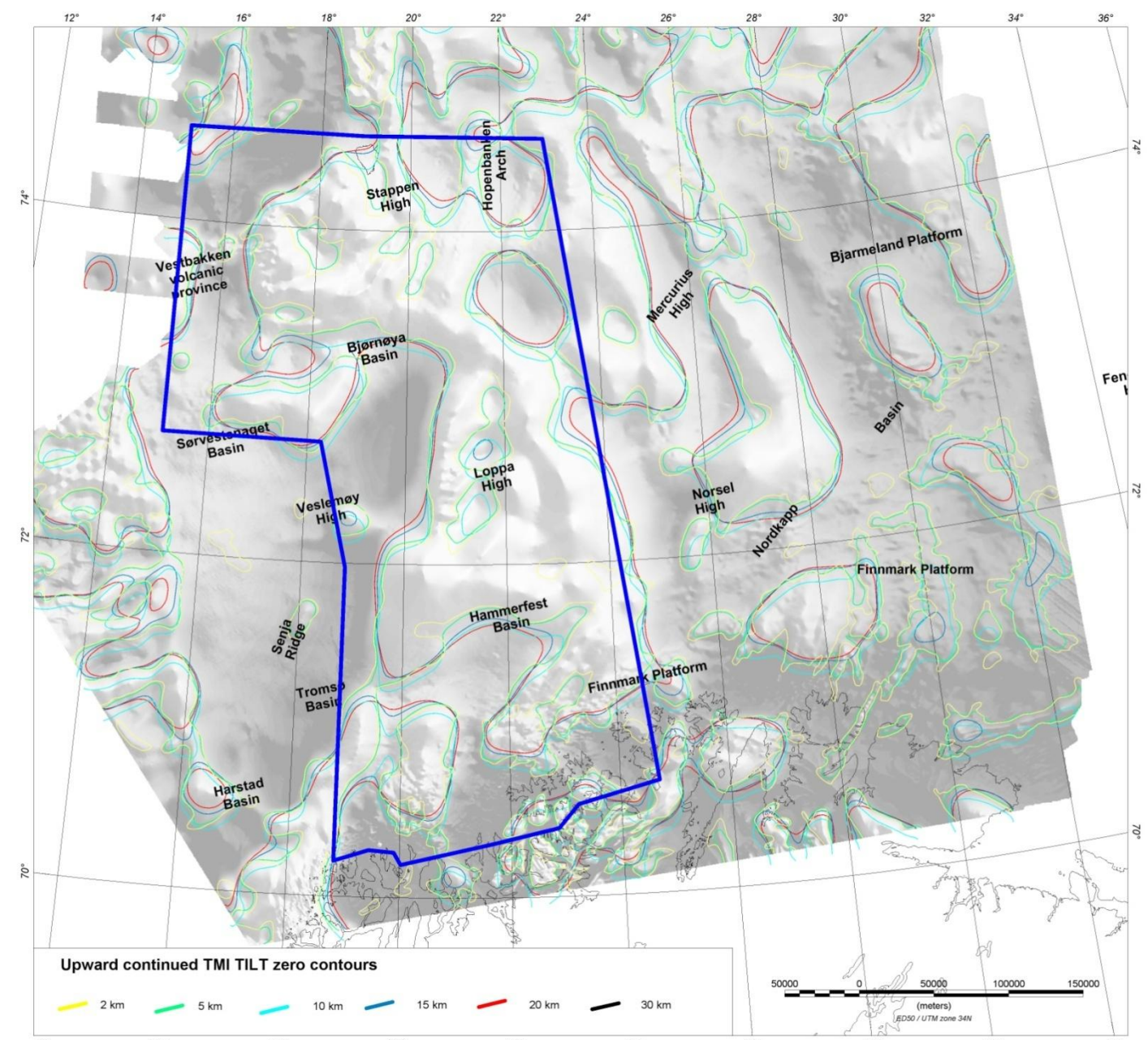


b)

Figure 10.7 a) TILT derivative from TMI grid with principal possibly intruded faults, b) 30 km high-pass filter from TMI with complete structural interpretation and c) the complete structural interpretation. Blue curved lines are observed lineaments from the magnetic map and are most likely associated with Caledonian nappes, dark blue lines are major faults. Red lines show fault-related lineaments probably associated with high-magnetic material such as dykes (see text). Black and yellow lines underline the main structural features of the area (Gabrielsen et al. 1990). Grey lines represent the faults mapped at base Cretaceous level (Gabrielsen et al. 1990), black and blue dashed lines represent second-order lineaments with a more shallow origin based on magnetic interpretation.



a)



b)

Figure 10.8 a) 30 km high-pass filtering of the Bouguer gravity with complete structural interpretation from the new magnetic data b) TILT derivative multiscale edge detection to (Lahti & Karinen 2010) determine the tilt of the main magnetic basement highs. Blue curved lines are observed lineaments from the magnetic map and are most likely associated with Caledonian nappes, dark blue lines represent major faults. Red lines show fault-related lineaments probably associated with high-magnetic material such as dykes (see text). Black and yellow lines underline the main structural features of the area (Gabrielsen et al. 1990). Grey lines represent the faults mapped at base Cretaceous level (Gabrielsen et al. 1990), black (BASAR-08) and blue (BAS-06) dashed lines represent second-order lineaments with a more shallow origin, based on magnetic interpretation.

10.1.7 The Nordkapp Basin and surrounding margins

Both the SNAS-06 and the BAS-06 surveys have already provided a new, reliable and almost complete magnetic coverage of the Nordkapp Basin. With the reprocessed and merged dataset from BAS-06 and BASAR-08, a comprehensive overview of the magnetic settings in the Nordkapp Basin can now be presented, covering the entire Nordkapp Basin except for the northern end, which was located in a Norwegian-Russian disputed area until April 2010.

A comparison of the old and new magnetic data reveals a number of new details such as salt structures and fault systems (Fig. 10.9). Furthermore, the outline and the shape of the anomalies in the basin give new and important evidence for the depth-to-basement structure, and the presence of possible sub-basins and intra-basin highs, which results in a more accurate and sophisticated interpretation of the Nordkapp Basin and its overall development. New trends are now observed from the magnetic surveys and suggest a more complex crustal and basin architecture for the Nordkapp Basin, which is clearly divided into sub-magnetic segments.

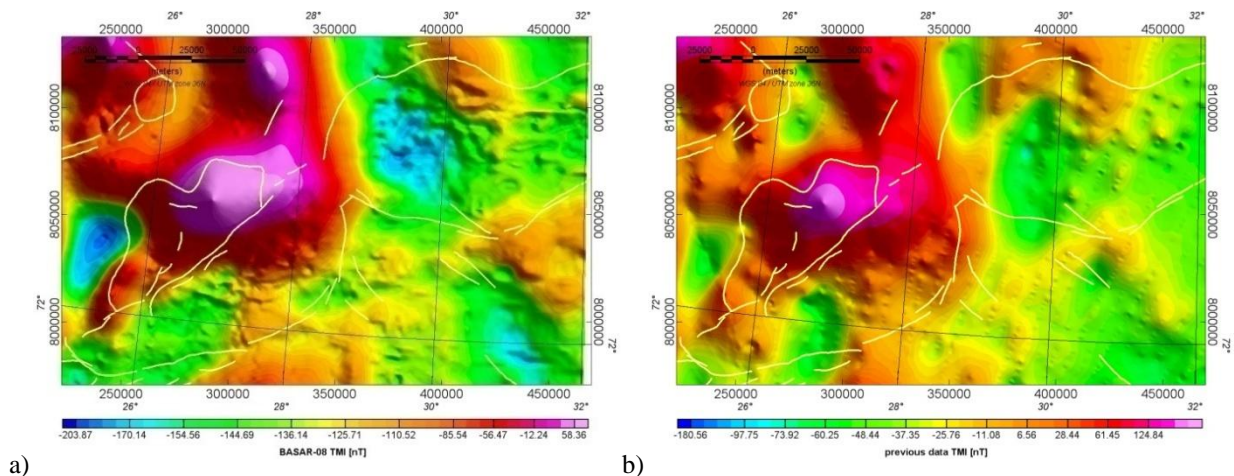


Figure 10.9 Comparison between (a) the new and (b) the vintage magnetic data for the Nordkapp Basin. The BASAR-08 data (left) have a significantly higher resolution, showing various features such as salt structures and faults in much more detail.

The Nordkapp Basin is a fault-controlled graben located along the NE-SW-trending rift system that extends eastwards from the Hammerfest Basin to the disputed area between Russia and Norway (Gabrielsen *et al.* 1990, Nilsen *et al.* 1995). The basin was initiated during Late Palaeozoic extension and, like the Russian basins, constituted a major sink for Triassic sedimentation (Roberts & Lippard 2005). The lateral extension of the basin is well constrained by the gravity data (Fig. 10.2a). The SVD of the new magnetic data highlights the positions of the shallow salt structures and also allows an estimation of the basin outline, whereas especially in the southern part of the Nordkapp Basin long-wavelength effects from the Norsel High conceal the real basin extension (Figs. 8.2 and 10.1a). The main regional orientation of the Nordkapp Basin, also expressed by the Måsøy and Thor Iversen fault complexes, is mostly

oriented N°100-110 to N°70-80 and coincides with local, low- to medium-wavelength, magnetic trends (Fig. 10.8a).

The Thor Iversen Fault Complex is a prolongation of the Troms-Finnmark and Måsøy fault complexes and represents a regional deformation zone in the Barents Sea. These principal fault trends were characterised by peak faulting activity at specific times, and many can be linked fairly confidently with known faults on the Finnmark mainland (Gabrielsen *et al.* 1992, Jensen & Sørensen 1992). The NE-SW offshore fault trend is known to have been active in Devonian-Carboniferous time exploiting the Caledonian structural heritage (Faleide *et al.* 1984, Gabrielsen *et al.* 1992, Bugge *et al.* 1995). Basin-bordering movements continued through the Permo-Triassic interval and appear to have extended into the Late Mesozoic. Many such NE-SW-trending faults can be traced onshore, in Finnmark (Gabrielsen 1984, Lippard & Roberts 1987). The existing faults in Finnmark, especially those in the western areas, were subjected to successive reactivations in the Permo-Triassic and notably in the Jurassic-Late Cretaceous (Roberts & Lippard 2005).

From the new dataset, some evidence was found for a NE-SW structural trend both north and south of the Thor Iversen Fault Complex, possibly indicating a prolongation of one of the regional trends which defines the Tiddlybanken Basin and West Kola Graben described by Ivanova (2001). A feature of some dispute is the narrow part of the Nordkapp Basin and its geotectonic significance. A strike-slip pattern along the NE-SW-striking lineament and the irregular and slightly rotated magnetic lineaments possibly suggest the presence of an almost N-S-trending shear zone, which might then be related to the reactivation and superposition of old Caledonian and Timanian patterns or a rifting event in the central Nordkapp Basin, partly decoupled from the southern basin (Gernigon *et al.* 2007b).

The Nordkapp Basin is bounded to the north by the Bjarmeland Platform and to the south by the Finnmark Platform, and is divided into northeastern and southwestern segments. Caledonian basement structures, detected in the new magnetic data, are disrupted in the vicinity of the basin, but at least in the western part of the survey area can be traced both north and south of the basin. The assumed sedimentary thickness of c. 10-16 km in the basin allows only an ambiguous interpretation of this feature. Either the thick pile of sedimentary rocks masks the magnetic basement signature or the basement was at least strongly deformed during the rifting process. In fact, from 2D modelling an involvement of the Caledonian basement in the rifting process is evident, with different stages recognisable from thinning (Fig. 11.8) to break up (Fig. 11.5).

Both the southern and the central parts of the Nordkapp Basin are characterised by two regional gravity lows (G-NL1 and G-NL2) surrounded by broad gravity highs (G-BH3, G-BH4, G-NH1, G-NH2, G-NH3 and G-FH4). The magnetics, however, do not reflect the presence of such a dominant sedimentary basin, but the western part of the central Nordkapp Basin does show a magnetic domain (M-NL1), flanked to the northeast and southeast by two magnetic highs (M-

BH2 and M-NH1), which both extend into the sedimentary basin. Even though the origin of these highs remains unclear, as pointed out earlier, we consider them as reflecting an old basement structure of probable Precambrian age. Before rifting was initiated, this was likely one NW-SE-striking unit perhaps associated with old Timanian trends. From the TDR of the new magnetic data, we deduce a difference in basement depth probably associated with a NW-SE-striking fault system at the eastern rim of the magnetic low and separating the wider western part from the narrower and shallower eastern part of the central Nordkapp Basin. Gernigon *et al.* (2007) explained the changing structural style of the Nordkapp Basin from west to east by an interaction between rift deformation affected by pre-existing oblique, deep features and/or pre-existing graben. We agree with this interpretation and see the observed NW-SE-trending lineament in the southwestern part of the central Nordkapp Basin in the same context and link it with the fault system observed in the Ottar Basin. The trend is sub-parallel to the Trollfjorden-Komagelva Fault Zone, which dates to Meso/Neoproterozoic or even Archaean times (Roberts *et al.* 1997) before being reactivated at several stages during the Timanian and Caledonian orogenies and the rifting phases in the Late Palaeozoic and later times.

The southern Nordkapp Basin is even less pronounced on the magnetic data. No distinct magnetic low is observed and the dominant magnetic high associated with the Norsel High (M-BH8) reaches far into the basin with a long-wavelength anomaly and covers the northeastern part of the southern Nordkapp Basin, concealing the basinal characteristics and large depth to basement depth in this area (Fig. 10.2). Although a relative high is observed in both the gravity and the magnetic data, the lateral extension of the magnetic anomaly far exceeds the one seen in the gravity map. The correlation in itself suggests an old, probably uplifted, basement block of high density and magnetisation. As discussed earlier, the different shapes of the anomalies and the much wider magnetic anomaly indicate the presence of additional high-magnetic to intermediate dense material, e.g. mafic rocks. It is likely that some mafic material intruded into the basement and the sedimentary succession during the various rifting phases and that volcanic rocks accumulated on top of the paleosurface. From 2D modelling, magma infiltration along detachment faults is also suggested (Ch. 11). Carboniferous dolerite dykes are, for example, exposed on Magerøya and Late Devonian dykes on the Varanger Peninsula (Lippard & Prestvik 1997, Robins 1998, Guise & Roberts 2002, Rice *et al.* 2004). Although the presence of volcanic material in the southern Nordkapp Basin has, to our knowledge, not been confirmed so far, we propose this model to explain the contradictory expressions of the gravity and magnetic data. Furthermore, there is definitely more evidence for the presence of high-magnetic material in the vicinity of the Nordkapp Basin. Two noticeable lineaments are crossing the southern Nordkapp Basin, trending NE-SW and NW-SE. The NE-SW-trending structures were discussed earlier as first-order lineaments, probably associated with the northern boundary of the Måsøy Fault Complex and a reactivation of old Caledonian faults during the opening of the Nordkapp Basin. The NW-SE-striking lineament runs through the central southern Nordkapp Basin and can be traced far into the Finnmark Platform. Because of its orientation it can be of Precambrian age similar to the lineaments observed farther north, north of the Norsel High and in the southeastern central Nordkapp Basin.

In contrast to the other magnetic patterns this NW-SE striking lineament shows an apparently sharper and symmetrical signal, which indicates the presence of dykes or fault-intruded high-magnetic material (Grauch *et al.* 2001, Grauch & Hudson 2007). In this particular case, we suggest that it is a fault intruded by mafic material. Based on Euler deconvolution, the depth to the source is rather shallow and definitely intra-sedimentary (up to ~3500 m). Unfortunately, none of the three seismic lines crosses this feature. Even so, depending on the dip angle and thickness of the intrusions, such bodies may be difficult to see on seismic sections. However, as shown before, volcanic rocks and mafic intrusions are rather common in the basement. For the southern Nordkapp Basin and parts of the Finnmark Platform, we suggest a discrete volcanic event, possibly associated with the rifting of the Nordkapp Basin and a likely uplift of the basement block of the Norsel High. Mafic material was most likely emplaced into the southern Nordkapp Basin mainly southeast of the Norsel High and intruded along reactivated Caledonian or older basement faults.

Shallow magnetic patterns in the Nordkapp Basin show both NE-SW- and NW-SE-striking lineaments, indicating the likely pre-existence of Precambrian and Caledonian faults. We have, however, observed a gradual decrease in the NE-SW-trending magnetic patterns within the Nordkapp Basin towards the east. Although the densely distributed salt diapirs within the basin might blur many of the fault patterns, this can be considered as an additional indication for the gradual thinning of the Caledonian nappes and thrust sheets towards the east.

10.1.8 The Ottar Basin

The Ottar Basin is situated between the Loppa High and the Mercurius High in the northwest and the Norsel High in the southeast. According to Breivik *et al.* (1995) the basin is c. 170 km long and 50-80 km wide with a predominant NE-SW trend. Two large salt domes are present within the basin, the Samson and the Norvarg domes. The domes were apparently created by non-penetrative movements of deeply buried, Upper Palaeozoic salt (Gabrielsen *et al.* 1990, Gudlaugsson *et al.* 1998). From the gravity and magnetic data they appear rather inconspicuous; two gravity lows are visible to the north and east of the Norsel High, separated by a NW-SE-oriented narrow bar with relatively higher gravity. For the magnetics, the signature of this basin is even smaller; two minima are visible, slightly displaced compared to the gravity anomalies. The southern one appears to be better developed. In comparison with the Nordkapp Basin the long-wavelength content in this area is rather high. No indications of salt diapirism have been observed. Magnetic or gravity patterns of shallower origin are almost absent and points to a different evolutionary history. From the magnetics, undisturbed Caledonian nappe related anomalies can be observed in the southern part of the basin. Fault-related structures are observed in the north around the Norvarg Dome and were discussed previously.

Surprisingly little is published on the Ottar Basin. Identified as late as 1988 by Jensen & Broks (1988), Breivik *et al.* (1995) subsequently carried out an intensive study on the deep-seated, immobilised salt in the basin and estimated the basin's depth. They provided evidence for a wider and deeper basin than had been reported from previous studies (Dengo & Røssland 1992, Jensen & Sørensen 1992) and concluded that the Ottar Basin is a much more important structure than previously thought, comparable in dimensions and depth to the Nordkapp Basin. From gravity modelling across the Norvarg Dome, Breivik *et al.* (1995) estimated a basin depth of about 9.5 km and an average salt thickness of 2.4 km. Across the Samson Dome, salt was observed below the near base Permian reflector and the salt thickness was estimated to 3.5 km (Breivik *et al.* 1995). Gudlaugsson *et al.* (1998), however, assumed an even greater salt thickness of 4-6 km and interpreted the Ottar Basin as a major, Late Palaeozoic, rift basin. Based on the new magnetic data we propose that the basin developed possibly during only one major rifting phase in the Late Palaeozoic. The absence of almost any magnetic pattern suggests that there was only a minimal reactivation, if any at all, in later times. Later rift phases might also have led to a mobilisation of the salt, similar and comparable to that in the Nordkapp Basin.

10.1.9 The Finnmark Platform - Kola Kanin Monocline

The Finnmark Platform formed a relatively stable and slowly subsiding block during the Late Carboniferous and Permian, influenced only by movements along NE-SW (Caledonian) and NW-SE (Timanian) trending structures (Gabrielsen *et al.* 1990, Alsgaard 1993, Gee & Pease, 2004, Rafaelsen *et al.* 2008). It is bounded to the northwest by the deep Harstad and Tromsø basins and to the north by the Hammerfest and Nordkapp basins. From the mid-Carboniferous and throughout the Permian, the platform formed a northerly dipping, distally steepening carbonate ramp with build-ups (Samuelsberg *et al.* 2003). In the new magnetic dataset the Finnmark Platform occupies the southern parts of the survey area.

In the south easternmost part of the new survey, a broad, NW-SE-elongated gravity low (G-FL4 and G-FL5) is observed. The minimum has an analogue in the magnetic data (M-FL2 and M-VL1), but a more distinct magnetic pattern is also visible and probably disturbs a response from a deep and old structure. It is situated to the north of the Varanger Peninsula and coincides with a northwestern prolongation of the Kola-Kanin Monocline (Fig. 10.3b). The NW-SE regional trends also coincide with well-known onshore Archaean and Proterozoic megastructures (Karpuz *et al.* 1995, Roberts *et al.* 1997) that are further discussed in the next chapter dealing specifically with onshore-offshore relationships. To the west, the gravity map is dominated by relative gravity highs (G-FH3 and G-FH3), in an area where the magnetics show a contradictory picture with local but significant lows (M-FL3 and M-FL4). A correlation with gravity is observed only for the magnetic high in the central part of the Finnmark Platform (M-FH2), at least in the western part. Except for the Kola-Kanin Monocline, where gravity and magnetics correlate, the identified gravity highs and lows appear to be of a more regional

character. The magnetics, however, seem to spot rather local and probably shallower features, except for the M-FH2. This structure is most likely basement-related and shows a clear linear trend associated with the development and eastward propagation of the Caledonian nappes.

The magnetic signature of the Finnmark Platform is complex and involves both shallow and deep magnetic sources. Due to the natural ambiguity of potential field data it is difficult to distinguish between all the factors especially because they interact. The subsidence patterns, bathymetry and shapes of the sedimentary basins are commonly controlled by the deep basement architecture of the platform and, similar to the Bjarmeland Platform, some correlation also exists between deep structures and subcropping units. Nevertheless, the deep-seated contributions are certainly most important for explaining the amplitude of the gravity and the magnetic total field. Short-wavelength features highlighted by filtering (high-pass or tilt derivative) may represent the lithological contrasts of shallow faults rooted or controlled by deeper crustal faults or shear zones (Figs. 10.6a & b).

Whereas the Caledonian trends dominate on the Bjarmeland Platform, we observe on the Finnmark Platform a similar influence of both the Caledonian and the earlier Timanian trends. The Timanian trend is clearly expressed in major and deep-seated fault structures such as the Austhavet and the Trollfjorden-Komagelva fault zones. The orientations of the Kola-Kanin Monocline and the Tiddybanken Basin are also parallel to the NW-SE trend. Second-order magnetic lineaments observed offshore and fault systems mapped onshore in northern Finnmark (e.g. Lippard & Roberts 1987) actually show both NW-SE and NE-SW trends, but the Timanian trend is definitely dominating and towards the east the NE-SW trends are almost no longer visible. Roberts & Siedlecka (2002) considered that the Timanide orogen, centred in the Russian southern Barents Sea, the Pechora Basin and the Timans, had a major influence on the basement configuration of the eastern Finnmark Platform, whereas the Caledonian and Inuitian orogenies were more active in the western and northern parts of the Barents Sea (Rønnevik *et al.* 1981).

On the other hand, the characteristic, curved and eastward-convex, magnetic signature of the Caledonian propagation is clearly visible on the Finnmark Platform and even farther to the east than on the Bjarmeland Platform. With the Måsøy and Thor Iversen fault complexes and the observed NE-SW-trending complex on the Finnmark Platform, another pattern from Caledonian times is observed. The entire impact of this fault complex zone, however, is not yet clear. Especially in the area south of the narrowest part of the Nordkapp Basin, with an apparent strike-slip component noted along the lineaments, the more chaotic magnetic pattern remains suspicious and unclear. Based on observed kinks in some of the lineaments to the south of the complex zone, we suspect the presence of an approximately 30 km wide and apparently N-S-oriented belt that may have acted as a transpression zone, perhaps limited to the sedimentary units and with no basement structures involved.

From the new magnetic data, the north-eastward propagation of the Caledonides shows a rather clear magnetic signature, obviously related to the different nappes or thrust sheets, which is curved and convex to the east in the offshore regions. We assume a similar nappe-like structure to that observed in the onshore regions of Finnmark with varying thicknesses of the allochthons. The boundary of these different nappes possibly associated with fault generation and/or block rotation, generates this characteristic magnetic signature. The significant high-magnetic amplitudes also suggest an involvement of the Precambrian basement in the Caledonian deformation at least in the northwestern part of the survey area. Analogues for such a deformation can be found on the mainland in West Finnmark (Olesen *et al.* 1990). The Precambrian rocks within the Alta-Kvænangen and Repparfjord-Komagfjord tectonic windows were for instance, partly deformed, thrust and rotated during the Caledonian nappe emplacement (Roberts 1985, Gayer *et al.* 1987).

The region in and around the Nordkapp Basin is heavily disturbed due to the rifting and basin development, but a correlation of the different lineaments to the south and north of the southern Nordkapp Basin can be made by amplitude analysis. A marked high-amplitude lineament in the central part of the survey area is trending NNW-SSE into the Norsel High anomaly, disappearing at the Nordkapp Basin and continuing farther south on the Finnmark Platform, north of the Nordkinn Peninsula. To the east, the amplitude of this pattern is fading out and on the Bjarmeland Platform north of the central Nordkapp Basin it is already absent. An explanation for this could be a reduced magnetic contrast between the different nappes to the east, probably combined with reduced folding and thrusting of the involved Precambrian basement and/or an increased thickness of the overlying sedimentary rocks, which are likely to conceal the magnetic signature deriving from the basement. In our opinion it is a bit of both: the folding and faulting of the basement is diminishing to the east, as can also be observed onshore on Varanger Peninsula for the Lower Allochthon for example (Siedlecki 1980, Gernigon *et al.* 2007b, Herrevold *et al.* 2009). To the north, the younger sedimentary succession is considered to thicken and this can explain the absence of the magnetic signature in this part of the survey area.

In the southernmost part of the survey area the new aeromagnetic data highlight new positive trends and structures. The southwestern Finnmark Platform, as shown by the new aeromagnetic data, is dominated by NW-SE and NE-SW-striking lineaments, which can partly be traced across the Austhavet Fault Zone. In the southeastern part of the platform, WNW-ESE-striking lineaments are observed northeast of the Varanger Peninsula (e.g. Fig. 10.6a). They coincide with discrete gravity changes in the Finnmark Platform and can be correlated with thrusts and folded structures onshore described in some detail in the following chapter. A prominent N°80-trending high-amplitude and elongated magnetic anomaly (M-FH1) is particularly noticeable here and clearly delimits two magnetic domains in the southern part of the Finnmark Platform and also coincides with discrete trends in the gravity signature.

The new magnetic data also refine the magnetic picture of the hinge zone located between the Finnmark Platform and the Kola-Kanin Monocline. North of the Varanger Peninsula, the deeper part of the Finnmark Platform is characterised by an underlying rift topography with fault blocks containing siliciclastic sedimentary rocks of Early Carboniferous age. These rocks were onlapped in the Mid Carboniferous in certain intervals by minor carbonate evaporites (Bugge *et al.* 1995). Exploration wells have been drilled on the Finnmark Platform, all reaching the Upper Palaeozoic (7120/12-4 on the western platform and 7229/11-1, 7128/4-1, 7128/6-1 and 7228/9-1 in the east, Larssen *et al.* 2005). The Palaeozoic sedimentary rocks are overlapped by Triassic and Cretaceous units, tilted to the north and truncated in the southern part of the platform (e.g. Bugge *et al.* 1995).

The Kola-Kanin Monocline represents a thick complex of Riphean to Vendian age, which extends into the southern part of the BAS-06 survey area. The regional gravity low could roughly represent the potential field expression of the West Varanger Graben, which is part of the Kola-Kanin Monocline. The thickness of the Riphean metasedimentary rocks may be as much as 10 km on the Kola Shelf but is probably less north of Varanger Peninsula. These formations underlie the Palaeozoic and Mesozoic sedimentary successions that pinch out on the southern flank of the monocline. A more detailed description of the eastern provinces and their interrelationships can be found in Gernigon *et al.* (2007b).

10.1.10 Onshore-offshore relationships

The recent datasets BASAR-09, BASAR-08 and BAS-06 partly overlap onto the northern onshore parts of the Finnmark and Troms region (Fig. 10.10). This overlap allows us to constrain and understand the meaning of the magnetic anomalies, which extend offshore (e.g. Gernigon *et al.* 2007b, Brønner *et al.* 2009). With the new compilation, a comprehensive and high-resolution magnetic dataset for the Finnmark Platform is available and can be linked with onshore observations.

The principal features of the bedrock geology of the Finnmark and Troms region are described on the NGU 1:500,000 bedrock geology map by Siedlecka & Roberts (1996) for the Finnmark and on 1:250,000 bedrock map sheets by Roberts (1973), Zwaan (1988), Grogan & Zwaan (1997) and Zwaan *et al.* (1998) for Troms (Fig. 2.1). The geology is described more fully in many of the published papers cited in chapter 2, section 2. The previous aeromagnetic magnetic compilation of the Finnmark Region (Olesen *et al.* 1990) has also been merged with the new aeromagnetic data to provide a better onshore coverage of the new survey (Fig. 10.10).

The new aeromagnetic data improved the resolution of the magnetic field in both the offshore and the onshore areas in northern Finnmark and also in the offshore areas of Finnmark and Troms. The higher resolution has revealed a large number of interesting onshore-offshore relationships which, for eastern and central Finnmark, have already been discussed in the BAS-

06 and BASAR-08 reports (Gernigon *et al.* 2007b, Brønner *et al.* 2009). The new magnetic compilation comprises also the new data from BASAR-09 and the lately released dataset of the HRAMS-97/98 survey. Both surveys are mostly limited to the offshore regions, but could improve the magnetic signature along the Finnmark Platform quite substantially and, together with the previous survey, provide a comprehensive overview of the structures along the entire North Norwegian coast. For the sake of completeness, the previous interpretation is summarised here, slightly updated and complemented by the new magnetic data and the observations to the west.

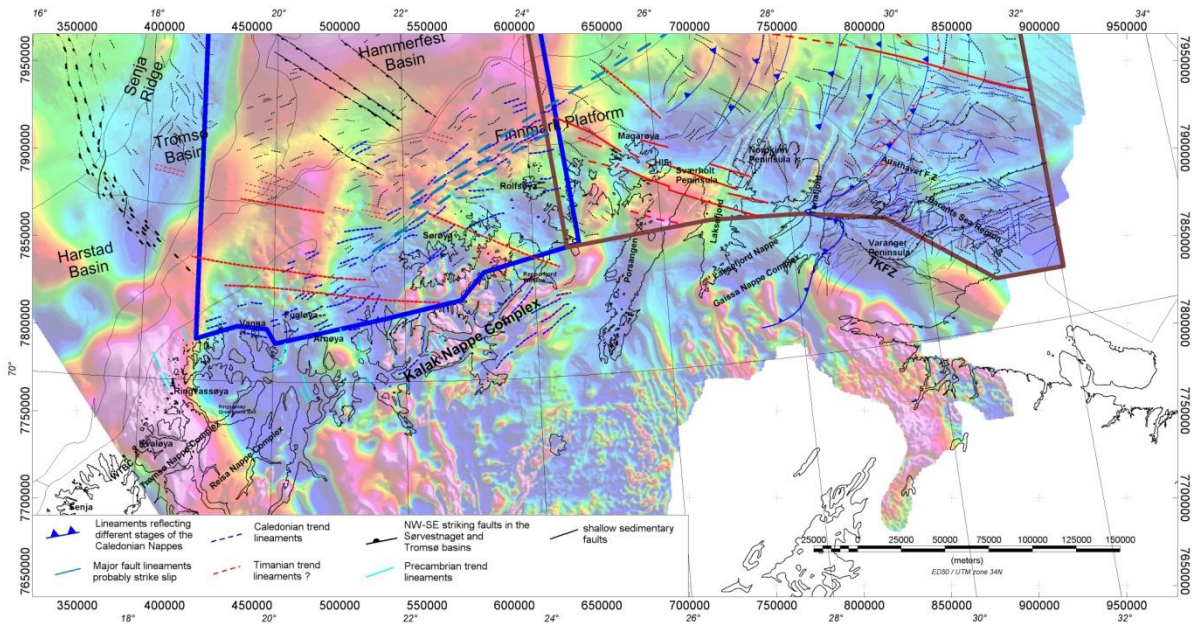


Figure 10.10 Onshore-offshore correlation utilising the TMI data from the new regional compilation with the main structural interpretations.

From the magnetic data, two principal trends are observed, striking NE-SW and NW-SE, intersecting approximately northwest of Magerøya. The NW-SE trend is most prominent in the eastern part of eastern Finnmark (Fig. 10.10) and runs parallel to the Trollfjorden-Komagelv Fault Zone (TKFZ). This trend obviously correlates with the dominant Timanide-related fault and fold patterns onshore northern Finnmark the Varanger Peninsula and on the Finnmark Platform (see above). Such NW-SE-trending faults are also present on Nordkinn Peninsula. These faults were active during Late Palaeozoic extension (Roberts & Lippard 2005), locally with coeval mafic dyke intrusions, which would explain the high and sharp magnetic signal along these faults. Offshore on the Finnmark Platform and in the southern Nordkapp Basin we observe additional NW-SE-striking features with a similar amplitude pattern, emphasising the Late Palaeozoic rifting as the major tectonic event in this area, coupled with mafic intrusions and possibly sills. Farther west, NW-SE-trending structures are fading out. Some lineaments with this orientation are visible offshore on the Finnmark Platform north and northwest of Sørøya and onshore on Sørøya and Kvaløya, but in contrast to the Varanger Peninsula there is

no observed correlation with the onshore geology. The Kalak Nappe Complex (KNC) conceals these structures, which clearly originated in the underlying Precambrian crystalline basement.

NNE-SSW- to NE-SW-trending faults represent the second group of faults observed in northern Finnmark (Lippard & Roberts 1987), Troms and offshore. The NE-SW offshore faults are known to have been active in Devonian-Carboniferous time (Gabrielsen 1984, Bugge *et al.* 1995) in this southwestern Barents Shelf domain, presumably reflecting the Caledonian structure (e.g. Faleide *et al.* 1984, Gabrielsen 1984), and are also locally well expressed in the surface geology (Fig. 2.1). The magnetic signature of these patterns is continuously observable in the offshore areas, but the geology onshore Norway does not reflect this trend.

On the Varanger Peninsula NE-SW -oriented lineaments are quite pronounced (Karpuz *et al.* 1993b) and can be traced far into the offshore areas on the Finnmark Platform. In the westernmost part of the peninsula the Tanahorn Nappe and the subjacent Gaissa Nappe Complex constitute a 'metamorphic front' of the Caledonide orogen, which is well expressed in both magnetics and geology. This structure can be followed into the Barents Sea and links perfectly with an eastward-bending structure which is part of a set of lineaments and most likely expresses different stages in the eastward propagation of the Caledonian nappes (see above). East of the base of the Tanahorn Nappe, the magnetic trends vary mainly from NW-SE close to Berlevåg to N°70-N°80 farther to the east, defining a distinct magnetic region within the Lower Allochthon. The main N°70 magnetic anomaly trend observed in this southern part of the Barents Sea Region correlates with the formations and thrusts observed between Kongsfjorden and Syltefjorden (Fig. 10.11). Strike slip components are assumed and offshore anomalies seem to be affected by minor dextral strike-slip offsets along the N°110-trending Austhavet Fault Zone.

Farther west, on the Nordkinn Peninsula, however, the magnetic signatures change significantly. Although NW-SE trending faults are still observed west and southwest of Nordkinn, NE-SW-striking, high-amplitude lineaments that flank the peninsula to the east and west become predominant and reflect the general strike of the strata in this wide area. This high magnetisation was observed already on the NGU-70 aeromagnetic datasets in the eastern part of the Nordkinn Peninsula (Åm 1975), and its origin was ascribed to a profusion of thinbeds and foresets composed almost exclusively of high-magnetic minerals (magnetite, hematite and ilmenite) in cross-bedded fluvial metasandstones (Siedlecka & Siedlecki 1970, Siedlecka & Roberts 1992, Siedlecka & Roberts 1996, Roberts 2007, Fig. 2.1). The distribution of this unit, shown on the geological map (Fig. 2.1) reveals a remarkably good correlation with the distribution of magnetic anomalies in the onshore domain, which can be traced offshore towards the northeast and across the Austhavet Fault Zone. The magnetic lineaments show a converging trend offshore, suggesting the presence of a major anticlinal fold, plunging towards north-northeast. The shape of the anomaly offshore and the north-northeast plunge of the main fold suggest that this part of the KNC offshore may be overrun by a younger thrust sheet just to the northwest (Fig. 10.11).

It generally appears that the low-magnetic KNC not only increasingly blurs the signal of the underlying Precambrian basement (Olesen et al. 1990), but also that the mapped contacts and faults are barely expressed in the magnetic data. On Magerøya and the Porsanger and Sværholt peninsulas, the magnetic anomalies are rather small. Susceptibility measurements on samples reveal a relatively uniform and low magnetic basement in this region with some local examples of highly induced magnetisation e.g. in the Honningsvåg Igneous Suite (HIS) (Torsvik *et al.* 1992). The Magerøy Nappe is the uppermost unit in the Caledonian tectonostratigraphy of Finnmark (Roberts & Andersen 1985), and was deformed by large-scale, north-plunging folds during the nappe emplacement in Silurian time. The metasedimentary rocks are intruded by the HIS, which has been modelled by Lønne & Sellevoll (1975) and Torsvik *et al.* (1992) to a depth of approximately 6 km.

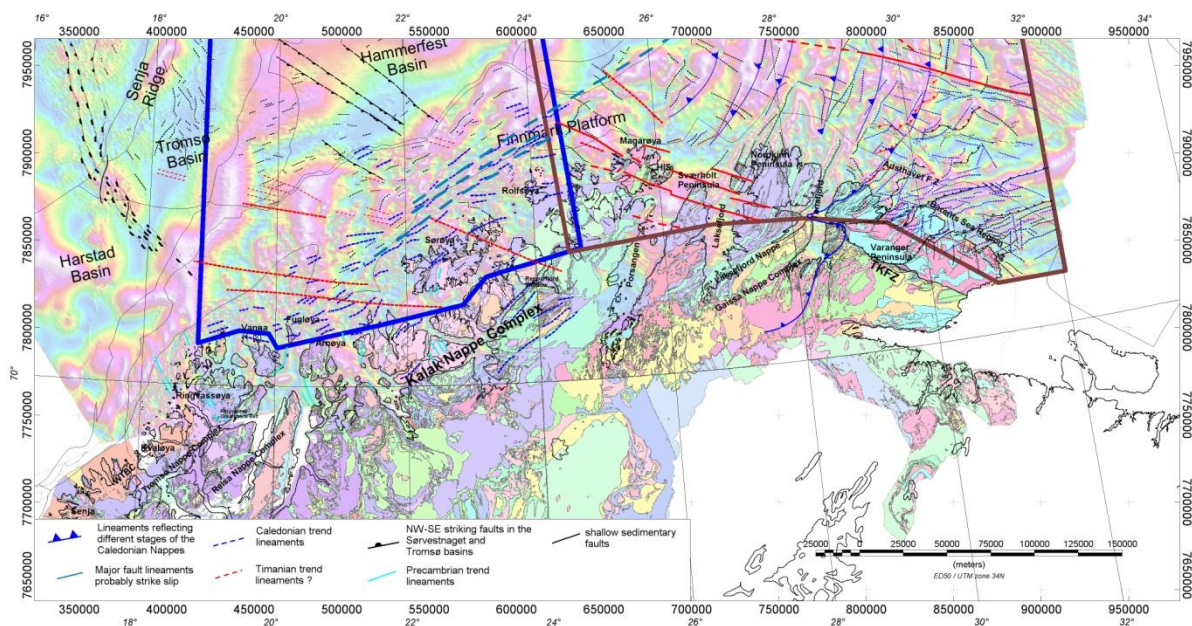


Figure 10.11 Onshore-offshore correlation: TILT derivative with main structural interpretations and onshore geology map (Siedlecka & Roberts, 1996).

The westernmost part of the KNC is almost free of NE-SW-striking lineaments, except for the Repparfjord-Komagfjord window, south of Kvaløya, which comprises Palaeoproterozoic rocks of the Raipas Supergroup, which were deformed and metamorphosed during the polyphase Svecofennian Orogeny at 1.85 Ga (Pharaoh *et al.* 1983). During the Caledonian Orogeny a reactivation of the underlying basement and thrust rotation occurred (Gayer et al. 1987) such that NE-SW-striking lineaments now predominate on both magnetic and geology maps.

The BASAR-09 survey unfortunately did not extend onshore into mainland Norway, but covered just the northernmost islands of Sørøya and Rolfsøya. The new dataset therefore only provides limited new information regarding an onshore-offshore correlation in western Finnmark. However, in the new magnetic compilation the BASAR-09 data were merged with

the existing data sets onshore Norway and the data were evaluated for onshore-offshore features.

In this area of western Finnmark almost no lineaments were observed onshore which could be traced into the offshore areas. Furthermore, the NE-SW trend, which is generally known to be the main trend of the Caledonide Orogen, is absent. As discussed before (Ch. 2, section 2), the Reisa and Kalak Nappe Complexes comprise low-magnetic bedrock units, which one could expect to produce rather small amplitudes along faults and contacts within the nappes. On the other hand, NE-SW-striking features are clearly observed in the offshore regions, where new data were acquired during the BASAR-09 survey. One could conclude that the magnetic data onshore Norway are of lower quality with too low a resolution to map these features. However, some areas like Sørøya, northern Kvaløya and the northern Porsanger Peninsula were covered with new aeromagnetic data and they are showing the same poor correlation between magnetics and geology and the missing NE-SW striking lineaments. One could perhaps conclude that the NE-SW-trending lineaments are related to a major strike-slip shear zone, running all the way from offshore Troms to south of the Nordkapp Basin, probably associated with the Måsøy and Thor Iversen Fault complexes (Barrère *et al.* 2009b). The inferred trend is comparable to that of the Møre-Trøndelag Fault Complex in central Norway, indicating a rather old and regional fault complex, which was exposed to several periods of reactivation. The structure is limited to the offshore areas and seems to be truncated in the south at the Bothnian-Senja shear zone.

If we summarise the structural interpretation of the new magnetic map for the southern Norwegian Barents Sea, we would conclude that there are very few or no magnetic signatures from the Uppermost, Upper and Middle Allochthons, in either the onshore or the offshore areas. Only in the Upper Allochthon in the eastern part of Magerøya and further eastwards to the metamorphic front, in the Middle and Lower Allochthons, a structural correlation can be observed.

The magnetic expression of faulting and thrusting is the combination of basement magnetisation and remagnetisation during tectonic processes (e.g. Grauch & Hudson 2007). For the Lower Allochthon, and to some extent also for the Middle Allochthon, high-magnetic Precambrian basement is involved and underwent a significant and probably deep-seated tectonic deformation, whereas the higher-grade Upper and Uppermost Allochthons apparently show more ductile characteristics on top of the underlying nappes, with much less deformation involving the underlying basement, and are consequently not discernible in the magnetic data.

The strike-slip feature on the Finnmark Platform offshore western Finnmark, however, is noticeable and must thus be considered as a deep-seated, crustal-scale thrust complex, possibly activated in Late Ordovician to Early Silurian times at an early stage of the Laurentia-Baltica collision. The origin of this structure, however, remains speculative. Based on the magnetic data, a relationship with the emplacement and/or evolution of the Loppa and Stappen highs is conceivable.

11 2D MODELLING ALONG SPECIFIC TRANSECTS

Laurent Gernigon

Both gravity and magnetic data are independent of seismic data and are sensitive to different physical parameters. Therefore, an integrated study can support the interpretation in exploration and regional investigation work and allow us to test further structural and geological models. The most recent gravity and magnetic NGU compilations already highlight the complexity of the study area and provide complementary and new information about structural trends, dyke intrusions, basin segmentation and crustal features that are often not clearly observable and detectable on seismics (Gernigon *et al.* 2007, Brønner *et al.* 2009). A joint interpretation that successfully combines seismic and potential field data will produce a synergy that would significantly improve the geological, regional and structural interpretation of potential prospects in the vicinity of the Bjørnøya Basin (BB), Loppa High (LH) and Stappen High (SH), now well covered by the new BASAR-09 survey.

Joint gravity and magnetic modelling will be carried out to validate our interpretation of basinal and crustal structures. Particularly the crustal nature of the BB, SH and LH remains unclear and is better assessed by forward modelling of the gravity and magnetic field combined with advanced inversion techniques. In the discussion, we also aim to test and describe the crustal and tectonic mechanisms that have controlled the joint development of the SH, LH and BB since the Caledonian Orogeny.

When dealing with the petroleum implication for the Western Barents Sea region, the top basement interpreted from magnetic and gravity depth estimates is often the best available approximation to the true crystalline (i.e., metamorphic/igneous) basement configuration. Basement depth (or equivalently, sedimentary thickness) and basement types are primary exploration risk parameters. Estimates of basement depth are directly applicable to basin modelling (e.g., source rock volume estimation) and thermal maturity applications (e.g., source rocks burial depth). Basement structure inferred from magnetic depth estimates provides insight into the evolution of more recent sedimentary features (e.g., sub/minibasin compartmentalisation, salt structure distribution/kinesis, localisation of reservoir-bearing structures, sand channels) (Gernigon *et al.* 2007c, Olesen *et al.* 2010). In areas where the inherited basement fabric/architecture has been affected (either continuously or episodically) the basin development and main faults are commonly of basement origin.

The movement and flow of fluids within a basin, such as hydrocarbon migration along lateral and vertical carrier beds, can be facilitated by such basement-involved sedimentary faults/fractures. Basin heat-flow patterns can also be moderated by fluid circulation along

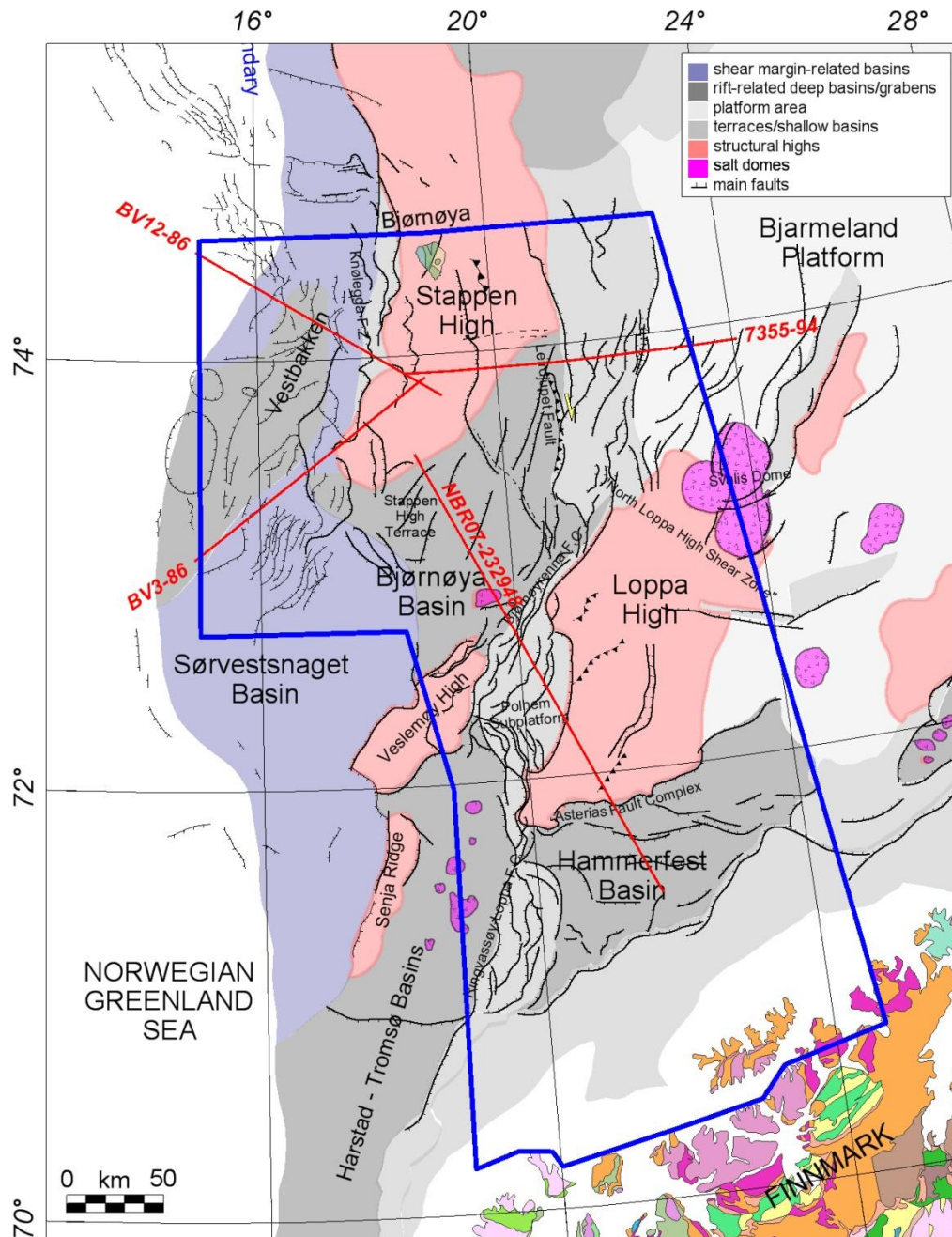


Figure 11.1 Outline of the main structural elements of the western Barents Sea (modified after Gabrielsen et al. 1990) and location of the four transects modelled and discussed in the present chapter. The map also shows some of the main geological units of western Finnmark from the geological map of the Arctic (Harrison et al. 2008) and highlights the main structural highs (in pink) in the western Barents Sea. The blue polygon represents the outline of the new BASAR-09 aeromagnetic survey.

basement-involved fault systems. Thus, the ability to estimate/interpret basement structures via magnetic depth estimates provides a more complete understanding of critical first-order basin exploration parameters.

This chapter presents the preliminary results established along four regional transects selected across the new BASAR-09 aeromagnetic survey.

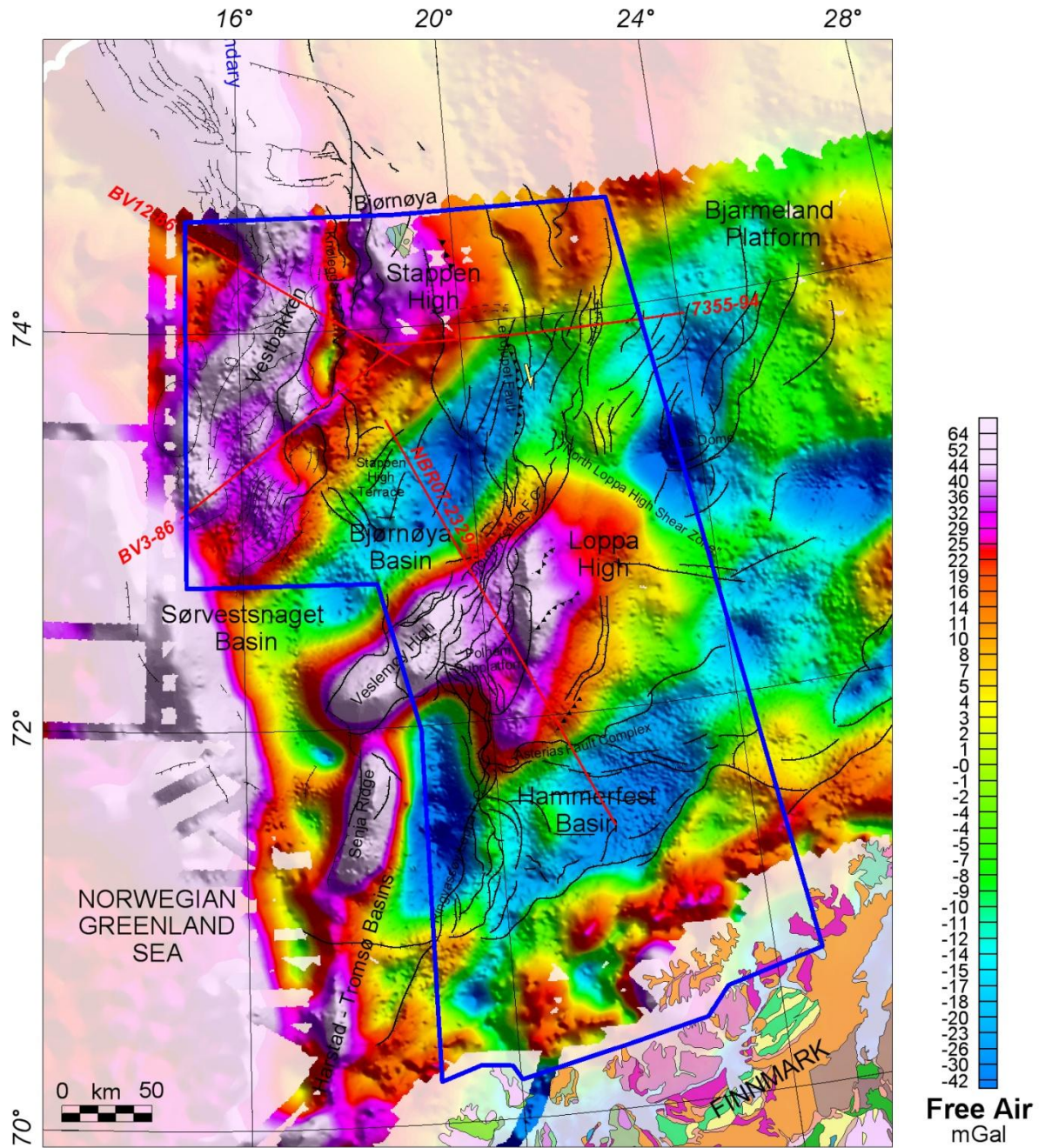


Figure 11.2 Free-air gravity map of the western Barents Sea and location of the regional transects. The map also shows the main onshore geological units. The Loppa and Stappen highs produce significant gravity positive anomalies. The Hammerfest, Tromsø and Bjørnøya basins are characterised by gravity lows.

11.1 Potential field modelling: methods and assumptions

11.1.1 Gravity and magnetic modelling

The interpretation and modelling processes described here were designed and carried out to quantitatively validate the interpretation of the NBR07-232948, BV03-86, BV12-86 and 7355-94-11 seismic lines located on figures 11.1, 11.2, 11.3, 11.4 and 11.5. Methods and workflow carried out during this study are summarised in figure 11.6.

In the study area, the basin geometry is generally well constrained by the reflection seismic data down to at least Permian depths, but the main unknowns remain the importance and distribution in depth of the pre-Permian (Palaeozoic) basins and low-grade metasedimentary rocks. More specifically and as further described below, poor seismic imaging (even on the more recent Fugro lines) does not always allow a proper understanding of the basin architecture northwest of the LH towards the SH.

Both gravity and magnetic anomalies (Figs. 11.2, 11.3) provide relevant indications about the nature and distribution of the main magnetic basement units. Combined with long-offset seismic lines, the anomalies provide an independent means of analysing the basin and basement architecture. Despite the large uncertainties about the basement depth in most of the study area, forward modelling allowed us to quantify and/or estimate its geometry to some degree. The quantitative interpretation of potential field data aims to estimate three types of information about sources of geological interest: 1) the depth to basement, 2) the dimensions of the basement terranes dimension, and 3) their relevant physical properties. Such an interpretation suffers from inherent ambiguity. It is impossible to obtain all three types of information simultaneously without other constraints. In many applications, we are often interested in depth rather than either dimension or physical property contrast.

11.1.2 Forward modelling

Using 2³/₄D forward modelling, we can better constrain the depth to basement, identify several characteristic features in the distinct petrophysical properties and better assess the crustal architecture along three regional transects. This technique has been used and also further described in the previous NGU reports already provided to the BASAR-08 partners (Brønner *et al.* 2009).

The 2³/₄D forward modelling has been carried out using the commercial software GM-SYS (Northwest Geophysical Associates Incorporation 2006). GM-SYS is an interactive gravity and magnetic modelling program applying a method of summing the effects of irregular polygons modified after Talwani (1973). The method also uses the divergence theorem (Blakely 1995) for the magnetic modelling. With the 2³/₄D approach, structures (bodies) of

varying and limited extent, both laterally and perpendicularly to the line and in front of and behind the plane of the profile, may be defined and their effects included in the calculated anomaly.

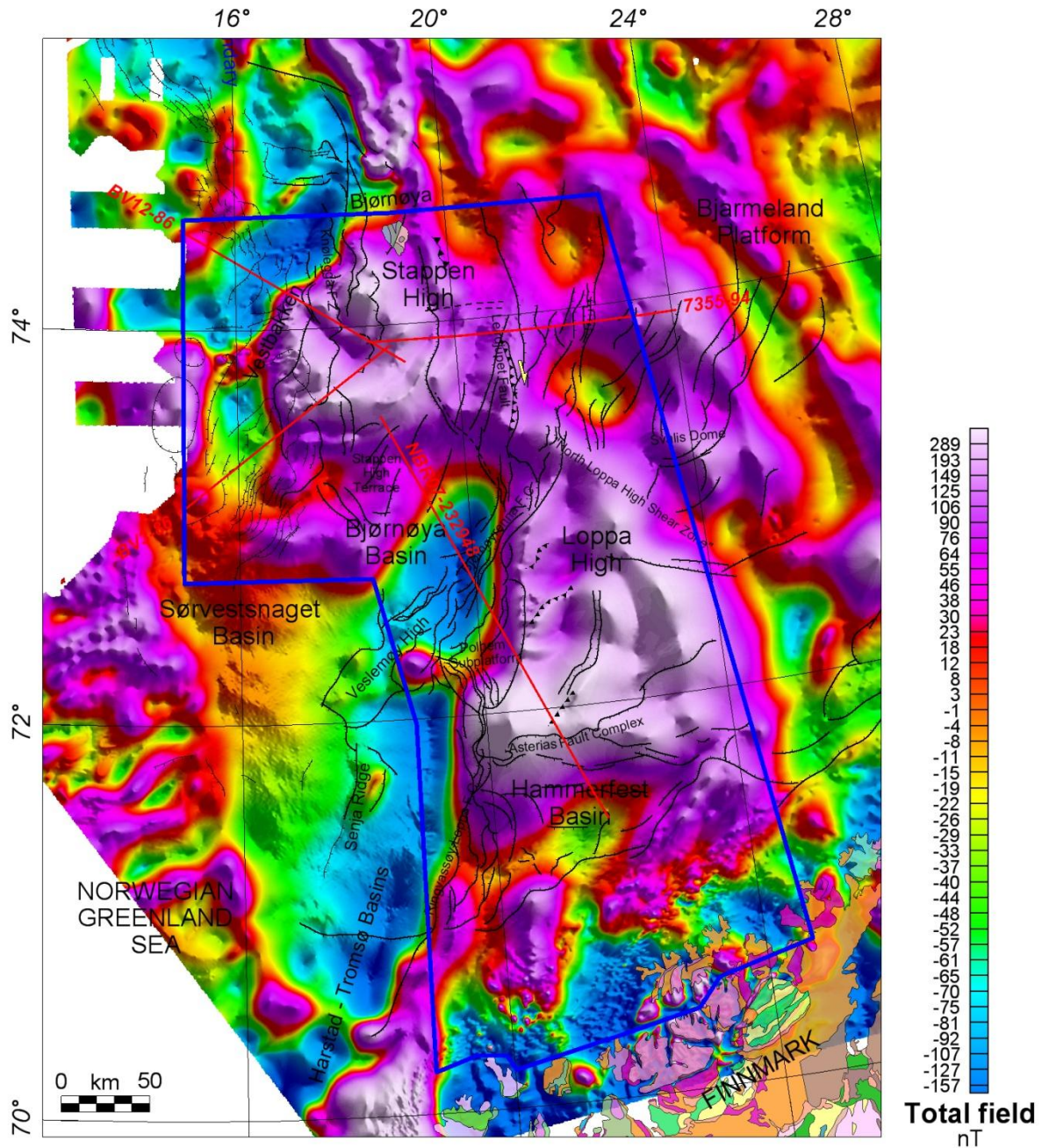


Figure 11.3 Location of the regional transects on the magnetic total field anomaly map of the southwestern Barents Sea. Note the prominent positive and regional anomalies associated with the Loppa and the Stappen highs.

The shallow geometry of the models is based on the interpretation of major seismic reflectors interpreted on the seismic sections provided by Det norske oljeselskap ASA (Fig. 11.1). The line drawing interpretation has been carried out at NGU.

Our modelling procedure (Fig. 11.6) includes a direct interaction with the seismic data and the magnetic and gravity field. The SEG-Y files have first been depth-converted for this specific project and the depth-converted SEG-Y files have been imported as background and guide in GM-SYS. The few available wells have been used to constrain the shallower levels and provided velocity information used to refine the velocity model. Check-shot values (provided by K. Hogstad) were used to refine locally the initial velocity model, by dynamic readjustment of the velocity grid using the Themis-EasydepthTM software (Beicip-Franlab 2002).

The modelled layer geometries in the top 5-10 km below the sea floor are relatively well constrained by the seismic interpretation. Wherever possible, features interpreted on the seismic data have been used to constrain the geometries of the basins and various geobodies (e.g. main depocenter, faults, salt diapirs, etc.) were included in the modelling, where indicated.

Along the different transects, the middle crust boundary and the Moho have only been modelled in order to fit the overall gross shapes of the potential fields and to be consistent with the limited crustal information including, for example, the IKU transects (Gudlaugsson *et al.* 1987) and recent regional compilations (Ritzmann *et al.* 2007). To constrain the initial Moho depth, we used a recent Moho compilation of the European plate (Grad *et al.* 2009) which provides an updated version of the Barents50 model (Ritzmann *et al.* 2007). In the southern part of the survey, we also obtained deep velocity information from the OBS modelling published by Mjelde *et al.* (2002).

The models were constructed in different steps including: 1) the definition of the 2D initial crustal geometry, 2) the lateral and perpendicular extension of the main seismic horizons to infinity in order to reduce the edge effects when necessary; 3) the definition of the appropriate density and susceptibilities values, 4) indirect information from Euler and Werner deconvolution tested by 5) the forward modelling.

For every sedimentary interval of velocities we attributed a density using appropriate velocity-density functions (Nafe and Drake 1957, Gardner *et al.* 1984, Christensen and Mooney 1995, Birch 1996, Godfrey *et al.* 1997). The average density for each polygon can then be calculated from the interval velocities measured and/or expected in the deep part of the basins. Top basement and Moho usually coincide with the main density contrasts in the lithosphere. Furthermore, petrophysical constraints were adopted from the recent onshore-offshore compilation of Barrère (2009).

Density, magnetic susceptibility and remanence values from onshore samples measured at NGU (Troms and Finnmark regions, Olesen *et al.* 1990) were chosen as starting values in the models. Average density values were applied to all layers. The densities of the

sedimentary layers are based on a review of the available well data (Tsikalas 1992, Gernigon *et al.* 2007). Tables published by Breivik *et al.* (1995, 1998) and Ritzmann *et al.*

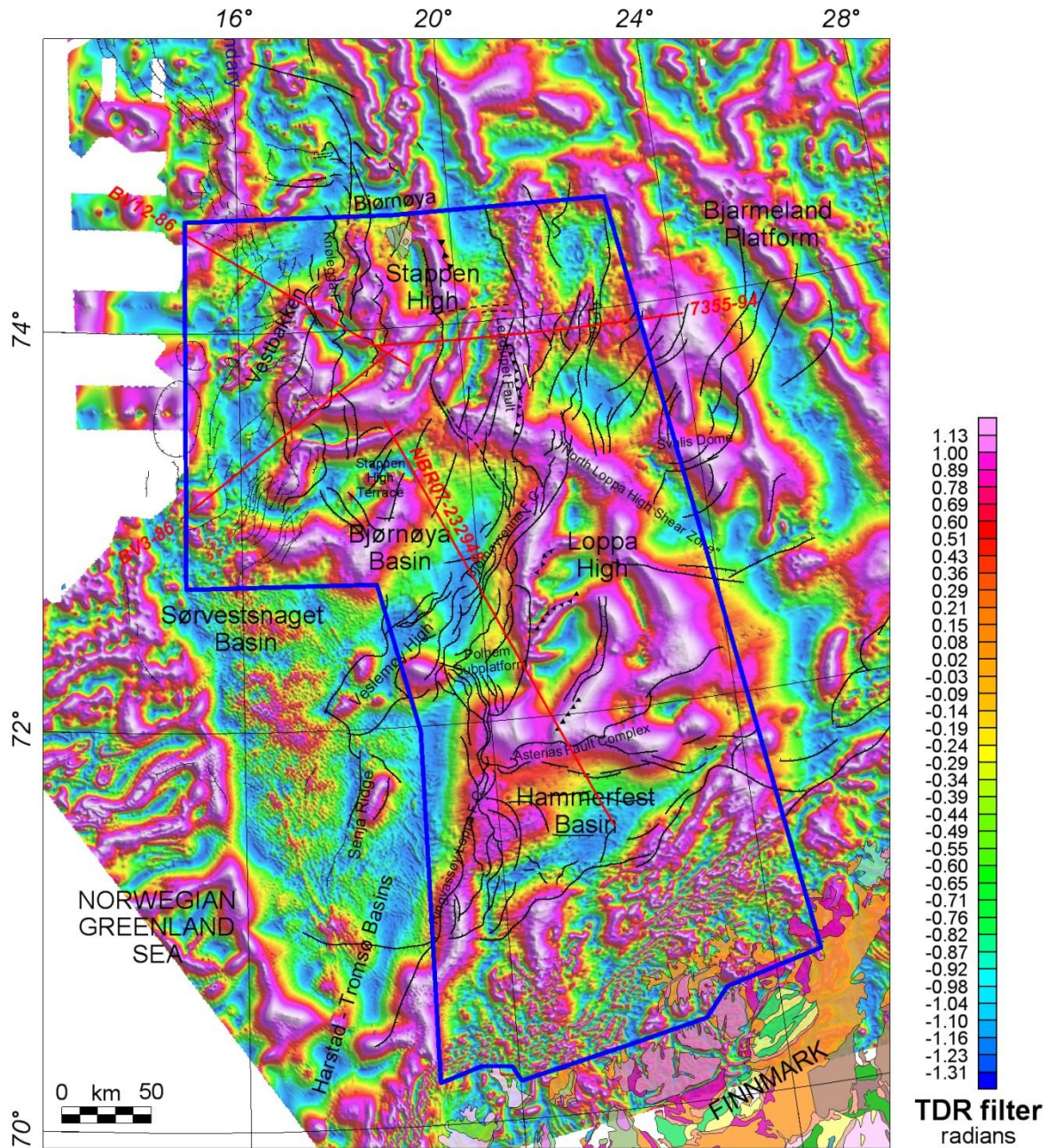


Figure 11.4 Tilt derivative filter (TDR) of the magnetic total field. The TDR enhances the subtle magnetic anomalies and maximizes the geometrical contrast of the internal basin structures. To remove noise and levelling still existing on the old compilation (BASAR-09 not included), a Butterworth filter has been applied on the total magnetic field before TDR and deconvolution calculation. The TDR has the property of being positive over a source and negative elsewhere. The TDR tends to enhance mapping of the subtle magnetic anomalies and maximizes the geometrical contrast of the internal basin structure. The TDR compared with other edge detection measures (e.g. the horizontal gradient, the second vertical derivative and the analytic signal) have some advantage of responding well to both shallow and deep sources. Using synthetic models, Verduzco *et al.* (2004) showed that the TDR has its zero values close to the edges of the body for RTP corrected fields.

(2007) based on velocity–density relationships for the deepest sedimentary units obtained from the seismic refraction and reflection/gravity studies have also been considered. In our model we set an average density of 2750 kg/m³ for the upper crust, 2950–3100 kg/m³ for the lower crust and 3300 kg/m³ for the upper mantle. Sediment densities vary from 2100 to 2650 kg/m³. These values and density contrasts are consistent with the regional models carried out in the previous projects. The petrophysically attributed geometrical models were subsequently iteratively modified using forward modelling and inversion techniques and adjusted to the observed gravity and magnetic fields.

The body responses were modelled in their correct x, y and z locations not projected into a plane. The calculations do not take into account the spherical and curvature effect of the Earth over the distance of the baseline. Induced errors due to this assumption, based on comparison of similar modelling and spherical 3D models by Wienecke *et al.* (2007), are of the order of 10%, which is considered as insignificant for our modelling.

11.1.3 Magnetic modelling

Interpretation and modelling of magnetic data are usually more complex and tricky as compared with gravity data. The magnetic susceptibilities of the different rock types can differ by 2 to 3 orders of magnitude, in contrast to gravity data where crustal densities differ only by 30%. Our model considers reasonable geological assumptions but the reader should be aware that magnetic modelling always has to apply simplifications due to uncertainties, the lack of direct measurements and method limitations. Particularly the part of remanence versus induced magnetisation is not well constrained. The combined interpretation of seismic, gravity and magnetic data and a relative understanding of the tectonic setting generally reduce these uncertainties and ambiguities. At this stage, only relative and average variations of the rock susceptibilities can be proposed.

Magnetic modelling helped to split and identify the crust into blocks of contrasting magnetic properties. Onshore-offshore relationships (Fig. 10.13) also help us to understand the meaning of the main gravity and magnetic provinces. For modelling, magnetic induction (J_i) is assumed to be the principal method of generating magnetic anomalies in continental crust; in these bodies the dimensionless apparent Königsberger ratio (Q), the ratio of the remanent magnetisation to the induced magnetisation, is set to zero. Some inferred igneous bodies and terrains could have non-zero Q values, implying a local contribution from magnetic remanence (J_r) to fit the observed magnetic anomalies.

In the absence of detailed magnetic measurements on drillcores from the Barents Sea basement, the magnetic properties of the crust along the BASAR-09 survey remain the least-constrained part of our validation process. Magnetic data are normalised to the current magnetic field, but this field was frequently reversed in the Earth's geological past, resulting in strong negative magnetisations in the dataset. The true values of Q might be significantly

different to those modelled if there is a high angle between real remanent vectors and the current-inducing field vector.

Inclination and declination have been aligned to the present-day geomagnetic field observed in the central part of the transect (average inclination $I=79.4^\circ$, average declination $D=7.4^\circ$). The induced magnetisation (H) is proportional to the strength of the present-day induced, geomagnetic field (B) ($B=53646$ nT). Aligning the induced magnetisation and the remanence magnetisation corresponds to adding their respective vectors. This simplification tends to give maximum magnetisation values and we consider the direction of the remanent field to be the same as for the induced field. This is usually the case for felsic to intermediate crystalline rocks. The ratio of remanent magnetisation (J_r) to induced magnetisation (J_i) is expressed by the Königsberger ratio (Q-ratio) (Olesen *et al.*, 1991).

The remanent magnetisation of the Archaean to Palaeoproterozoic and Caledonian rocks is related to the abundance of magnetic minerals within the rocks and the thermo-mechanical history and geomagnetic field when the rocks formed. In order to compute the Q-ratio, both magnetic susceptibility and remanence were considered for each unit. The Q-ratio was estimated for each block and geologically interpreted with respect to published values. From the values published by Olesen *et al.* (1990), Barrère *et al.* (2009), a mean remanence of 0.2-0.3 A/m for the older Archaean to Palaeoproterozoic rocks and mafic complexes and a remanence value of 0.0001 to 0.01 A/m for the Caledonian rocks were originally selected (Barrère *et al.* 2009), tested, adjusted or rejected when necessary. The Curie temperature for magnetite is 580° C, and therefore we limit the extension of potential magnetic sources to the basement and lower crustal blocks. Mantle rocks below the Moho are assumed to be quasi non-magnetic.

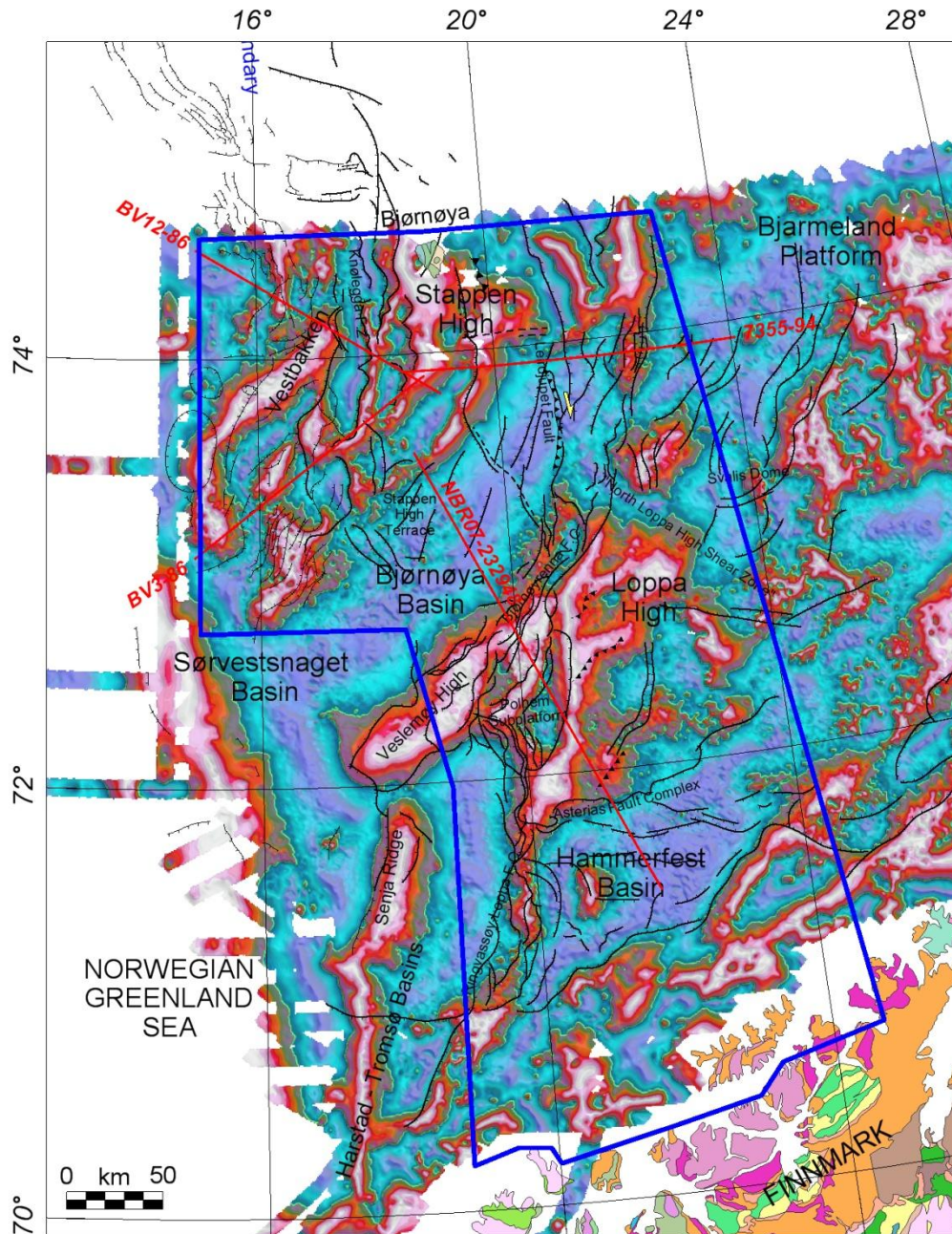


Figure 11.5 Blend image of the Tilt derivative (TDR) and TDX filters of the free-air gravity field. The TDR enhances the subtle magnetic anomalies and maximises the geometrical contrast of the internal basin structures. The TDX enhances the edge of each of the anomalies (Cooper and Cowan, 2006). To remove noise still existing on the old compilation, a Butterworth low-pass filter has been applied on the total magnetic field before the tilt derivative filtering. This composite map highlights the main basement structures, basins and structural trends of the study area.

11.1.4 Quantitative approach: Werner and Euler deconvolution

Different methods have been developed to estimate the depth of the magnetic sources by simple inversion and an overview was presented in chapter 9. These methods consider simplified source geometries (dimensions) and are independent of the susceptibility contrast. The depths estimated by such methods can be used as quantitative solutions in some ideal situations if the anomaly is well isolated and the noise insignificant or well removed. For 2D modelling, the estimated depths provided a good starting point for a genuine structural interpretation (e.g., the interactive modelling). Two methods have been used in the project, 1) the extended Euler deconvolution and 2) the Werner deconvolution. The methods are usually simple to carry out but require a level of expertise to properly adjust the main parameter and refine the main solutions. The intelligent use of these two extreme types of solutions can lead to a close approximation both in terms of depth estimation and its ability to reveal the geometry of the different magnetic bodies. Indeed, with some experience we can attain a very good interpretation directly using Werner's depth, horizontal location, dip angle, and magnetic susceptibility contrast. Clusters or linear alignments of Werner and Euler solutions usually indicate, respectively, tops and edges of different magnetic units or a rough indication of the main magnetic source.

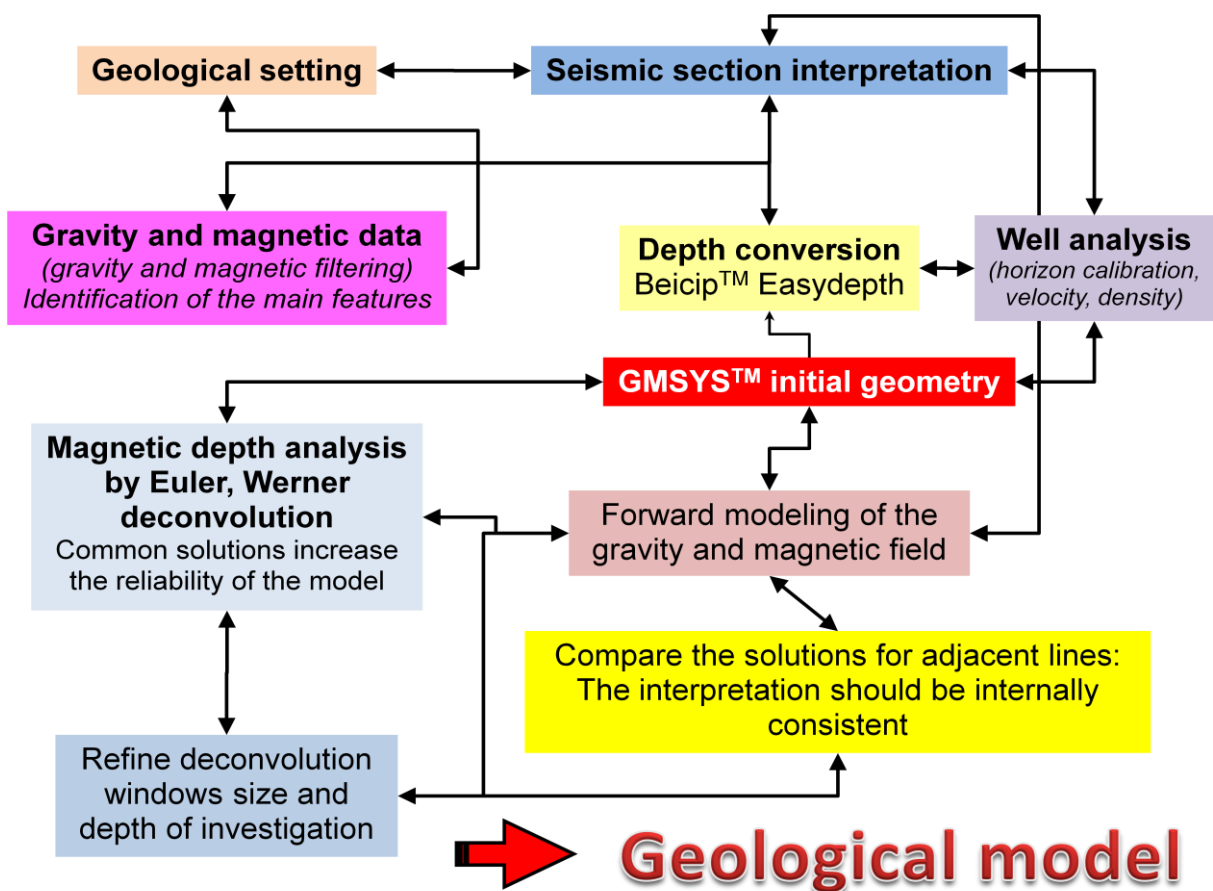


Figure 11.6 Workflow and integrated interpretation of the potential field modelling.

11.2 Implementation and modelling results

11.2.1 Transect 1: Section NBR07-232948

General structure and seismic observations

The first transect along NBR07-232948 runs NNW-SSE from the central part of the Hammerfest Basin to the eastern flank of the SH (Figs. 11.1 & 11.7). This ~260 km long transect crosses over the southern part of the LH, the Polhem Subplatform and the BB. This section is the only best seismic profile we could use for this specific BASAR-09 multiclient project. Compared to the other profiles, the NBR07-232948 provides a much better dataset help to constrain and identify the different crustal units and structures expected in the vicinity of the LH and SH areas. Apart from the sea bottom, the main regional horizons include notably the 1) base Quaternary, 2) base Upper Cretaceous 3) near base Cretaceous, 4) base of Upper Jurassic, 5) Intra-Middle Triassic, 6) near top Lower Triassic, 7) intra Early Triassic, 8) near top Permian and 9) near top basement reflectors (Devonian-Carboniferous ?). Wells 7121/1-1R and 7121/5-3 along the NBR07-232948 section have been used for local calibration.

Hammerfest Basin

Southeast of the NBR07-232948, the Hammerfest Basin (Figs. 11.1 & 11.7) is a relatively shallow Mesozoic basin, 50-75 km wide, located between the Finnmark Platform and the LH (Berglund *et al.* 1986). The structure of the basin is mostly dominated by extension and shows a clear graben-type feature. A component of strike-slip deformation has been suggested in the Late Jurassic-Early Cretaceous (Gabrielsen and Færseth 1989). The basin is separated from the Finnmark Platform to the south-southeast by the Troms-Finnmark Fault Complex and borders the LH along the Asterias Fault Complex to the north. The Asterias Fault Complex has an east-west trend, and is a zone of normal faulting and local transpression which dies out into the eastern flexure as it begins to trend in a north-northeast direction. The western limitation of the Hammersfest Basin is defined by the southern segment of the Ringvasøy-Loppa Fault Complex and its eastern border is marked by a progressive flexure towards the Bjarmeland Platform (Gabrielsen *et al.* 1990). The Hammerfest Basin includes both deep-seated, high-angle faults along the basin margin and a normal fault detached in the Permian-Carboniferous strata. As earlier suggested by Gabrielsen and Færseth (1989), the extension of the Trollfjorden-Komagelva Fault Zone trend could explain the subdivision of the Hammerfest Basin. The central fault system is composed of different segments with E-W, ENE-WSW and WNW-ESE-trending faults that formed the Hammerfest Basin fault system named (informally) by Gabrielsen (1984).

The origin of the Hammerfest Basin can be traced back to the time of post-Caledonian orogenic collapse (Gudlaugsson *et al.* 1998). It has been affected by extension in the Carboniferous (Berglund *et al.* 1986) and from the Triassic to Early Jurassic. The basin was probably a distinct depocentre already in late Scythian time (Gabrielsen *et al.* 1990). The main rifting episode initiated in the Mid Jurassic and continued during a period of major tectonic subsidence (Sag phase) in the Early Cretaceous.

Loppa High and Polhem Subplatform

Further north, the LH is structurally complex and is defined at the base Cretaceous level. Deep-seated block faulting coincides with the LH's diamond-shaped outline, a feature which is also suggested by the gravity and the magnetic data (Figs. 11.2, 11.3).

The seismic profile crossing the western boundary of the LH shows clear evidence of syn-tectonic sedimentation in response to down-to-the-west normal faulting towards the BB (Fig. 11.7). The faulting occurred mostly in the Mesozoic (Jurassic-Cretaceous), whilst due to difficulties in establishing reliable stratigraphic correlations, earlier movements are documented only from the Permian to the Early Triassic. An angular unconformity at the crest of the LH was either partly caused by a footwall uplift and erosion in response to tectonic 'unroofing' in the Carboniferous rifting phase (Gudlaugsson *et al.* 1998) or could have been initiated earlier in Devonian time during the inferred post-orogenic collapse (e.g. Barrère *et al.* 2009). The NBR07-232948 section suggests the presence of pre-Permian sub-basins on the footwall of the main LH that could coincide with Carboniferous and/or older sediments. So far a distinction between Carboniferous and older sediments has not been possible during the interpretation. The tectonic regime associated with these sub-basins is also unclear and not necessarily associated with extension.

Bordering the LH to the west are notably the Bjørnøyrenna and Ringvassøy-Loppa Fault Complexes (Gabrielsen *et al.* 1990). Some of these faults detached near the base Permian possibly above small salt layers, also identified on the southern flank of the LH in the NBR07-232948 section. Compared to the southeastern flank of the LH, this second generation of steeper faults affects much deeper formations (Carboniferous) on the Polhem Platform. Smaller scale faults that are generally located within the highs and basins, affect them on a minor scale and mostly represent reactivation and compaction features. The faults creating the sub-platform were active during many phases. Gabrielsen (1984) considered that they initiated in the Early Permian and that many of the listric faults were formed in the Late Jurassic to Early Cretaceous and were later reactivated. The Polhem Subplatform originated as part of a paleo-LH but was downfaulted relative to the crest of the main crustal block on the LH.

The stratigraphic framework for the LH consists of multiple sub-units that are linked to tectonic events and changes in accommodation space. The LH has been clearly affected by several phases of uplift/subsidence, and subsequent tilting and erosion characterise the

geological evolution of this high. Recent re-assessment of the Upper Palaeozoic stratigraphy (Larssen *et al.* 2005) interprets the LH as a Mid Carboniferous rift (topography) filled and draped successively by Upper Palaeozoic siliciclastic deposits, evaporites and carbonates. On the eastern flank of the LH, faulting and block tilting on the NBR07-232948 section are documented from the Late Permian to the Early Triassic, and gradual onlaps of the Early and Mid Triassic sequences are observed before an unclear phase of rapid subsidence occurred in the Late Triassic (Larssen *et al.* 2005). The paleo-LH remained a positive structural feature throughout Early to Mid Triassic times, possibly acting as a sediment barrier to prograding systems from the south and east (Smelror *et al.*, 2009). This is notably suggested by the thinning of the Permo-Triassic sequences observed in the southeastern part of the section.

The main phase of Late Permian faulting to the west of the LH is most likely related to the regional extension in the North Atlantic region between East Greenland and Mid Norway. The relatively thick Upper Permian successions, observed west of the high, were likely sourced from the paleo-LH and potentially also from the paleo-SH or NE Greenland Platform, which were closely related before rifting and thinning of the BB.

During Triassic time, multiple phases of smaller scaled uplifts occurred where the paleo-LH was the main local source area for small scale systems prograding from the west to the east, with a marked change around late Mid Triassic time to dominantly subsidence (Smelror *et al.* 2009). Early-Mid Triassic fault activity also coincides with a phase of minor uplift, associated with footwall uplift accommodated by the Bjørnøyrenna and Ringvassøy-Loppa Fault Complexes and more specifically by the major detachment observed east of the Polhem Platform clearly imaged on the NBR07-232948 section (Fig. 11.7). This detachment formed between the Bjørnøyrenna and Ringvassøy-Loppa Fault Complexes and appears to be a major crustal feature, which is also suggested by the modelling (see next chapter).

Accommodation space east of the paleo-LH was filled in during Anisian-Early Ladinian time, and westward progradation of sediments continued on top of the high and westwards up to the Late Triassic. According to recent interpretations of Bjørkesett *et al.* (2010), minor systems could also have prograded from the west and a change could have occurred from Early Carnian time, when the paleo-LH became the main depocenter. This is not clearly observed in our sections at the present stage.

Between the Polhem Subplatform and LH, we observed a major contrast between the continuous reflections of the sedimentary layers of the Polhem Subplatform and the irregular low reflective seismic facies interpreted as crystalline basement. This contrast can be followed obliquely beneath the Polhem Subplatform towards the bottom of the BB.

Bjørnøya Basin

One of the difficulties encountered in the present study was the poor seismic imaging of the deep part of the Bjørnøya Basin. Local chaotic facies, salt and several multiples have not allowed us to constrain properly either the geometry of the basin or the precise ages of the deeper horizons, which are still speculative in our interpretation. Tentatively, we have proposed a rough indication of the base Cretaceous unconformity along the NBR07-232948 transect but with large uncertainties. Triassic, Permian and Carboniferous sedimentary sequences most likely exist underneath the Cretaceous strata, but cannot be identified with certainty. In the BB, the section NBR07-232948 illustrates a central salt diapir (Carboniferous?) which affects and drags the sedimentary strata at least from the Triassic(?) to Tertiary age. Active salt tectonics occurred during this period and associated faults are locally observed on seismics.

Mid-Late Cretaceous time marks the tectonic and/or thermal sagging of the BB. Even though minor faulting has affected the basin (mostly on the flanks), the tectonic processes leading to such a deep Cretaceous Basin are relatively unclear. Was it controlled only by post-rift thermal subsidence? A key solution to this problem can be found in the Fingerdjupet Subbasin farther north, not properly investigated at this stage, but definitively a potential key area. The Fingerdjupet Subbasin formed in the Early Cretaceous as a shallow part of the growing BB and was affected by a major extensional episode during Late Jurassic Mid Cretaceous times and possibly into the Late Cretaceous. Before Mid Triassic time, the basin was closely associated with the paleo-SH and paleo-LH to the west. It contains mainly a thick Late Permian section (Gabrielsen *et al.* 1990). The Leirdjupet Fault Complex clearly marks the limit of the subbasin and seems to be associated with a clear NW-SE magnetic anomaly also observed north of the LH and interpreted as a major, deep-seated, Caledonian shear zone (named here the North LH Shear Zone, NLHSZ), reactivated during the Palaeozoic and Mesozoic. The thick Cretaceous sequences found in the BB thin slightly towards the SH and disappear by erosion due to the significant Tertiary which is uplift particularly pronounced towards the SH. Compressional features have also been revealed by the NBR07-232948 seismic line and probably represent an inversion of deeper, southeast-dipping, low-angle Cretaceous faults. This phase of compressional tectonics was probably underestimated in previous studies, but significant compressional features observed on both sides of the sag confirms the importance of a compressive phase initiated in latest Cretaceous time. To some extent the LH represents an incipient piggy-back basin, that developed between the LH and the SH in its latest stage of evolution.

Stappen High

Northwest of the BB, the SH is also a pronounced structural high in the Western Barents Sea (Figs. 11.1, 11.7). The SH is limited to the west by the Knølegga Fault Complex and to the east by the Sørkapp Basin. The SH trend probably extends towards the Sørkapp Basin and up to Svalbard. The southern part of the SH is strongly affected by NNE-SSW trending

faults which also extend towards a similar gravity lineament observed in the central part of the BB.

At the level of the SH, a first look at the seismic section 7355-94, modelled later, suggested that a major detachment dipping to the northwest could be observed along the northern flank of the SH, most likely controlling the southern Sørkapp Basin. This contrasts significantly with the opposite SW- to W-dipping detachment fault complex that probably controls the BB (e.g. the Bjørnøya Fault Complex). It seems that between the SH and the LH, a complex accommodation zone developed between the major detachments. This accommodation has probably controlled the development of the BB towards the north and its complex transition with the Fingerdjupet Subbasin at the level of the North LH Shear Zone.

Like the LH, the SH has undergone a complex but poorly understood tectonic history consisting of phases of faulting, tilting, uplift and subsidence that resulted in several condensed successions of Palaeozoic and Triassic sedimentary rocks (Worsley *et al.* 2001). Even with the present-day seismics, the imaging is not good enough to fully constrain the structure of the SH.

To the northwest of the BB, the island Bjørnøya constitutes the emerged part of the SH and represents a Late Upper Palaeozoic to Triassic window into the Barents Shelf (Mørk *et al.* 1990, Braathen *et al.* 1999, Worsley *et al.* 2001, Worsley 2008) which provides direct geological information about the SH.

The pre-Devonian 'economic basement' on Bjørnøya comprises a Precambrian to Lower Palaeozoic metasedimentary succession generally referred to as equivalent to the 'Hecla Hoek' on Svalbard (Worsley *et al.* 2001). Recent contributions agree that Bjørnøya and the SH has been affected by Caledonian deformation (Braathen 1999; Ritzmann and Faleide 2007). However, uncertainties remain about the origin and position of the SH basement before the Caledonian Orogeny. Some assume that Bjørnøya and possibly the SH were part of Laurentia before the closure of the Iapetus Ocean. Smith (2000) suggested that Bjørnøya was an integral part of the Franklinian Basin (eastern North Greenland) during Early Palaeozoic deposition and was attached to eastern North Greenland until the time of Early Tertiary rifting. A corollary of this interpretation of the Phanerozoic location of Bjørnøya is that any Caledonian strike-slip, orogen-parallel displacements and suture(s) must have been located outboard of the combined Bjørnøya-Greenland terranes. Recently, Ritzmann and Faleide (2007) proposed a Baltica-Laurentia suture at the level of the Bjørnøya Fault Complex between the LH and the SH. However, their models also consider the Lofoten Islands as part of Laurentia, a hypothesis which contradicts significant magnetic and geological evidence that the Lofoten Islands are obviously part of Baltica (Olesen *et al.* 1997, Barrère *et al.* 2009).

The Upper Devonian sedimentary rocks reported on Bjørnøya are conglomerates and shales which are part of the Billefjorden Group overlying the metamorphic basement (Larssen *et al.* 2005). Southeast of the SH, rifting in the BB is thought to have initiated in the Late Palaeozoic. More precisely, a Late Devonian to Early Carboniferous tectonic event, involving coupled strike-slip movements and normal faulting, probably initiated the formation of the BB half-graben between the LH and the SH (Gudlaugsson *et al.* 1998). Carboniferous and Permian fault movements have also been reported from Bjørnøya (Braathen *et al.* 1999).

During the Early Cretaceous, the SH developed into a shallow marine environment (Worsley 2008) and could have emerged in Valanginian-Bareman time (Smelror *et al.* 2009). Concomitantly, a major subsidence led to an extreme deepening of the BB controlling the deposition of a thick Cretaceous succession southeast of the SH (Faleide *et al.* 1993, Worsley *et al.* 2001). The Late Cretaceous to Palaeocene rift phase between Norway and Greenland was progressively dominated by strike-slip movements and deformation within the De Geer Zone leading to the formation of pull-apart basins between SH and the Northeast Greenland margin (Faleide *et al.* 1993).

The continental strike-slip system, active from the Palaeocene to the Eocene, was followed by a passive sheared margin development, leading to the onset of breakup in Early Oligocene time. The breakup development of a sheared margin located south and west of the SH is younger, locally magmatic (e.g. the Vestbakken volcanic province) and not yet totally understood.

Lower Tertiary deposits are virtually absent on the SH but marine slope to basinal successions are preserved along its western margin. Most of the study area has been eroded during the Late Tertiary uplift, which partly explains the present observation of the Upper Triassic section sub-cropping the Quaternary (Løseth *et al.* 1992, Richardsen *et al.* 1993, Sigmond 2002).

Correlation with the magnetic and gravity data

During this work, potential field techniques have been used as complementary tools for the interpretation of the seismic lines. Relevant filtering has been carried out in order to enhance the main structural changes and magmatic features observed along the section. A detailed documentation of the conventional techniques used in the report is beyond the scope of this project and we simply refer to the previous chapters for a more comprehensive and detailed description of the different filtering techniques.

The various magnetic and gravity attribute maps, interpreted in the previous chapter, describe the features and patterns of the basement blocks relative to their surroundings (e.g.

Figs. 10.8, 9.9 and 9.10). We used a conservative term 'structural contrasts' for the extended linear features observed in the maps, although many of these features could still be associated with significant basement blocks. The structural pattern of the basement as revealed from combined gravity and magnetic interpretations, is characterised by a hierarchy of structural elements involving 1) large structural zones, 2) tectonic domains and 3) sub-domains and internal magnetic lineaments. For each domain, there also appear additional extended features that overprint some of these structures and are potentially related to deposition of basin sediments and salt tectonics.

The section NBR07-232948 is particularly characterised by prominent gravity and magnetic highs at the level of the LH, which can be easily correlated with the different seismic units and structures when appropriate filtering is selected. Like in the other section, TDR and other relevant high-pass filtering have been plotted along the seismic section (Fig. 11.7).

A noticeable gravity high (0-40 mGal) is observed from the Asterias Fault Complex to the BB and a prominent magnetic total field amplitude (up to 330 nT) from the Polhem Subplatform to the Asterias Fault Complex. The maximum magnetic amplitude observed on the LH is located slightly to the west where it probably coincides with a basement spur at the intersection between the Asterias Fault Complex and the Ringvassøy-Loppa Fault Complex in the southwestern part of the LH. On the TDR map, we clearly see that the regional anomalies at this level coincide with the intersection of two main magnetic trends: 1) NW-SE, possibly associated with the trend of the Asterias Fault Complex, and possibly itself controlled by a deeper shear zone sub-parallel to the Trollfjorden-Komagelva Fault Zone, and 2) NE-SW to NNE-SSW trends which are dominant over most of the LH and observed up the NW-SE-trending North LH Shear Zone. Surprisingly, the western part of the Polhem Subplatform is still characterised by a pronounced free-air anomaly (15-30 mGal) up to the salt diapir observed at x-axis km 84-85 (Fig. 5.1). We also point out that numerous, NE-SW, magnetic TDR trends characterise the LH. On seismics they represent the transition between pre-Permian perched sub-basins expected on the LH. Some could be associated with a Carboniferous rift (Larssen *et al.* 2005) but we also believe that they could reflect locally blind Caledonian thrusts, possibly reactivated during Late Palaeozoic time.

Farther west, the transect is marked by a gradual decline in the free air up to -30 mGal along the southern flank of the SH (Fig. 11.7). On the contrary, the magnetic amplitude decreases slowly from the nearby Asterias Fault Complex towards the central salt dome (-297 nT) and then increases towards the SH (65 nT). Both gravity and magnetic signals decrease at the level of the Hammerfest Basin (-154 nT and -27 mGal). Using filters, sub-gravity and magnetic units can be identified and local changes in the signal usually fit well with the main structural domains observed along the seismic transect (Fig. 11.7).

In the western part of the BB, an amplitude change of the magnetic signal is observed around km 80-90. It almost fits with the edge of the deeply buried terrace observed on seismics. It also coincides with the deep transitional structural domain between the flank of

the SH and the deepest Cretaceous depocentre (as observed today). This intermediate structure (called the 'Stappen High terrace' in the present report) (Figs. 11.1, 11.7) lies on the southern flank of the SH and is not clearly observed on the free air anomaly map (Fig. 11.2), but is suggested by the total magnetic field (Figs. 11.3, 11.7) to belong to the main SH, positive magnetic high domain to the north (Fig. 11.3).

Modelling results and deep structures

Along the transect, the unit that includes the LH and the Polhem Subplatform represents a distinct crustal unit with a deep Moho (> 30 km) compared to the surrounding terranes where modelling proposes a new Moho estimation at a shallower level both in the Hammerfest Basin (~ 25 km) and beneath the BB (~ 20 - 25 km) (Figs. 11.7). Uncertainties still exist in this model but assuming reasonable densities for the crust and the sediments, higher densities (up to 3.1-3.3) are required underneath the main Cretaceous and Palaeozoic basins to fit the observed gravity signature. In both areas, our initial modelling could not totally fit with the previous Moho depth proposed by the Barents50 compilation (Ritzmann *et al.* 2007) and a much shallower Moho in the BB and deeper Moho in the LH appears more reasonable with local differences of ± 5 km. After different tests, our Moho estimation is expected to have uncertainties of only ± 2 km. In both cases a thinner crust is to be expected on either side of the LH. Compared to the LH where the crystalline crust is almost 30 km thick, the normal crust beneath the BB is less than 10 km thick suggesting a drastic thinning of the lithosphere.

The top basement has been modelled assuming a relative contrast between the deep Palaeozoic or Mesozoic sediments and the crystalline rocks (Fig. 11.7). Our basement definition is expected to be equal or deeper compared to the petroleum "economic basement" that usually also includes the pre-Devonian formations. Our result has been compared with the previous NGU 3D compilation of the top basement (Skilbrei 1993).

Using Euler and Werner deconvolution techniques (Ku and Sharp 1983), we first ran the multi-windows routine along the transect to estimate roughly the main magnetic contrasts located at depths up to 15 km (Fig. 11.7, tables 11.1, 11.2). Without any seismic input, this result already highlighted the main crustal highs and basins with two positive anomalies at the SH and LH where 'the susceptibility contrast' is higher.

The basement block identified on the LH has been modelled in the present study as a trapezoidal-shaped body (Fig. 11.7). The shallow basement modelled by gravity (top of the 2750 kg/m³ unit) and magnetics was set at ~ 2 km depth on the main high, where the shallower Werner solutions concentrate. It coincides with the main, prominent, NNE-SSW trend which we observe at the edge of the gravity filter and TDR. On top of this main high, the TDR filter suggests a local perturbation of the main NNE-SSW trend by local NW-SE

and NW-SE trends which are interpreted as basement faults (these do not represent levelling errors). We also propose a mid-lower crust with a density of 2950 kg/m^3 required to fit the main gravity high. On seismics, the mid-lower crust coincides with strong amplitude reflections observed along the NBR07-232948 line and could be associated with deep-seated Precambrian terranes affected by the Caledonian deformation (Barrère 2009).

The forward modelling of basement has been compared with the results of the Werner and Euler deconvolution and a good correlation has been obtained, notably on top of the LH where refined solutions suggest a top basement between 1.9 and 2.8 km in the vicinity of the main spur. These solutions are located close to the main sediment/basement contact expected on seismics at the level of the Asterias Fault Complex, but are relatively shallower. Both Euler and Werner clusters are also observed between 7 and 10 km at the edge of the SH and coincide with the basement expected from the forward modelling (Fig. 11.7). Shallower sources between 1.5 and 3 km have also been observed but were too shallow to fit properly with our top basement from GM-SYS modelling. They also coincide with seismic facies that still suggest the presence of sedimentary strata. Other cluster solutions have been observed but definitively at shallower and sedimentary levels: they fit locally with the position and structures observed at the 'near Base Cretaceous' level. The Werner solutions are also sensitive to the magnetic contrast between the salt (diagenetic) and sediments as suggested by a cluster located at ~ 2 km close to the central salt dome (Fig. 11.7).

The LH forms a triangular shape on the 2D section, cutting the basement spur that is defined on the southwestern edge of the LH. Two detachments and/or shear zones (D1, D2) have been identified on both sides. West of the LH, the D1 controlled the development of the Polhem Subplatform collapsing towards the BB. It fits a density contrast between the crystalline crust (2750 kg/m^3) and the deep Palaeozoic basin expected beneath the level of the Permian (2650 kg/m^3). The D2 shear zone controlled the development of an intermediate terrace between the LH and the Asterias Fault Complex and shows evidence of reactivation and local inversion. A third detachment (D3) is also suspected to exist near 200 km and coincides with a cluster of Werner solutions. To explain the main magnetic high observed at this level, we also considered a higher susceptibility contrast between D2 and D3 (0.07 and 0.08 SI compared to 0.02-0.03 SI), which was also suggested by the deconvolution of the magnetic signal. Euler and Werner solutions suggest a mid to lower crustal origin for the sources, but forward modelling also proposes an upper crustal magnetic unit at crustal level. Both D1 and D2 are associated with the formation of deep Palaeozoic basins expected between the Permian formations and the top basement. A small Palaeozoic graben is suspected to exist between D2 and D3. The D3 shear zone and the Asterias Fault Complex can eventually be associated with a 'pop-up' structure possibly related to Late Palaeozoic (Permian transpression?) movements proposed at the level of well 7121/1-1. Similar, observed NE-SW, magnetic TDR trends (Fig. 11.4) could therefore represent similar tranpressive or compressive features on the LH. This observation partly

fits the recent interpretation of Novoa & Svåná (2009), proposed for the internal geometry of growth sediments deposited on the flanks of the LH, who suggested that the structure may have resulted from a phase of compression during Permian and Early-Mid Triassic time, rather than pure extension. However, we point out that the nature of Carboniferous-Permian tectonics on top of the LH is still unclear. The deep normal faults (rift related) that have commonly been suggested for the LH (Larssen *et al.* 2005) could just as well represent blind thrusts. Nevertheless, we believe that these features are due to local tectonics and do not necessarily reflect a major regional compressive stress regime as proposed by Novoa & Svåná (2009), but are probably the consequence of local readjustments on top of the Loppa High. This needs to be investigated in greater detail in the future.

The modelled top basement is lying at a maximum depth of ~8 km in the southeastern terrace. The top basement also deepens to 9-11 km underneath the Polhem Subplatform and is expected at a maximum depth of 15 km in the central part of the BB, assuming that the deeper sediments have been poorly compacted (salt layers?). In the southeastern terrace, the shape of the TDR filter fits well with the basement highs and lows and a sudden jump coincides with a possible basement fault at depth. The NE-SW-trending low TDR anomalies coincide with the southwestern end of a narrow NE-SW elongated Palaeozoic graben (sub-Permian) observed east of the main basement high which itself represents the top of the hanging-wall controlled by the D1 detachment (Figs. 11.4, 11.7).

We note that the main detachment D1 affects the basement and does not necessarily coincide with the trend of the Bjørnøyrenna Fault Complex as strictly defined by Gabrielsen (1990). The Bjørnøyrenna Fault Complex is mostly defined at the Mesozoic level and, for us, does not represent the main crustal feature. Even though more structural investigation is required, we tentatively propose that the Bjørnøyrenna Fault Complex could be the result of a flexural rotation/rolling-hinge mechanism (Axen and Bartley 1997) associated with the uplift of the LH and subsequent progressive westward migration of the faulting. In that case, the D1 shear zone could represent a primary breakaway and the Bjørnøyrenna Fault Complex a second breakaway associated with a rolling-hinge.

In its shallow part, the detachment separates the sedimentary reflectors of the Polhem Subplatform and the irregular and poorly reflective crustal facies in the crystalline basement. At 12 km depth, the detachment D1 crosscuts the basement rocks of the Polhem Subplatform, separating two crustal blocks at depth. As a consequence, the detachment dip could change from an angle of 30° to 10°. In other words, we interpret D1 as a major listric 'ramp and flat' detachment fault developing west of the LH. The apparent throw along the detachment is estimated between 15 and 20 km. A major antithetic fault zone is also proposed around 100 km (Fig. 11.7) but the precise significance of this feature is not yet understood and needs to be correlated with adjacent long offset lines at some stage.

Beneath the BB, pre-Cretaceous structures and the nature of the crust still remain relatively unclear on seismics due to the great depths and poor imaging. A layered seismic pattern, however, is observed underneath the near 'base Cretaceous unconformity' at depth greater than 10 km. The deepest part of the basin coincides with 'en echelon' anomalies observed on the TDR map of the free-air gravity (Fig. 11.2, 11.5), which suggests a segmentation of the BB in sub-synclines and intermediate transfer ridges. According to the depth of the pre-Cretaceous sedimentary rocks, they have most likely been affected by metamorphism (low greenschist-facies). In previous studies (Barrère *et al.* 2009), we have already suggested the presence of high-density material in the deeper part of the Polhem Subplatform, but the vintage seismic data could not pinpoint the exact location and shape of this high-density unit. Alternative models involving an extremely high upper-crustal density and/or a very high lower crustal density and/or a very shallow Moho are still possible. In our model, the Moho was modelled relatively shallow depth (20-25 km) below the deeper part of the BB.

Along the profile, between kilometres 70 and 120 km, the crust is extremely thin and was modelled using relatively high density values (3100 kg/m^3). Compared to Barrère's model, we consider the presence of a relatively dense lower crust underneath the Polhem Subplatform similar to the lower crust observed farther south. Our lower crustal body, with higher density, is located a little more to the northwest compared to the previous interpretation. A relatively low susceptibility of 0.01 SI is proposed for this lower crustal body which does not significantly affect the magnetic signal. The interpretation of this body is unclear but since large-scale volcanism is not really recognised in the Bjørnøya area, we disregard a magmatic underplating interpretation and rather favour a high-density, pre-existing lower crust in the granulite/eclogite facies and/or alternatively a possible serpentinisation of the uppermost mantle if we consider the drastic thinning of the basin.

On either side of the BB, sediments and metasedimentary rocks (density $< 2700 \text{ kg/m}^3$) are also proposed. A maximum thickness of 6 km is proposed in the central part of the basin with ± 2 km of uncertainties if we consider a reasonable density variation in the deepest part of the basin.

To the northwest, the transect constrains only the flank of the SH (Fig. 11.7). Strictly speaking, we are close to the SH but still in the BB. In this area, the basement is expected to shallow progressively to a depth of less than 10 km. Between x-axis km 0-50 a continental sub-platform is interpreted with a top basement located at a depth of 11-12 km. At this level, the Moho is deepening towards the north-northwest and is close to 27 km at 0 km. Both Mesozoic and Palaeozoic sediments are expected underneath the Cretaceous monocline, but clear structures and limits are impossible to resolve on the seismics. Considering a conjugate system, the southeastern flank of the SH could be the equivalent of the Polhem Subplatform and may contain Permian to Jurassic formations. Close to x-axis km 50 km (Fig. 11.7), on the section, modelling, gravity and signal change suggest a contact, possibly a southeast-dipping border fault or detachment (D4) which is also modestly indicated on the

seismics. This contact fits with the eastern edge of a prominent NE-SE tilt derivative magnetic anomaly, which can be correlated with a gravity change. It can be associated with shallower reactivation and inversion observed in the Cretaceous and Mesozoic sections that were eroded on the western side of the transect. Close to 10-20 km, a major basement shift is also observed and shows a clear concentration of Werner solutions. It is interpreted as a major crustal fault (D5) with a top basement on the hanging-wall located at 5-7 km (Fig. 11.7).

Depth of investigation	0-25 km
Windows lengths	10-30 km
Windows expansion increment	500 m
Windows expansion shift	500 m
Residual cut-off	95%
X cut off	5%

Table 11.1 Parameters used for the Werner deconvolution along profile NBR07-232958.

Depth of investigation	0-30 km
Windows length (fix)	20 km
Maximum % error	5%
Structural index	0.5

Table 11.2 Parameters used for the Euler deconvolution along profile NBR07-232958.

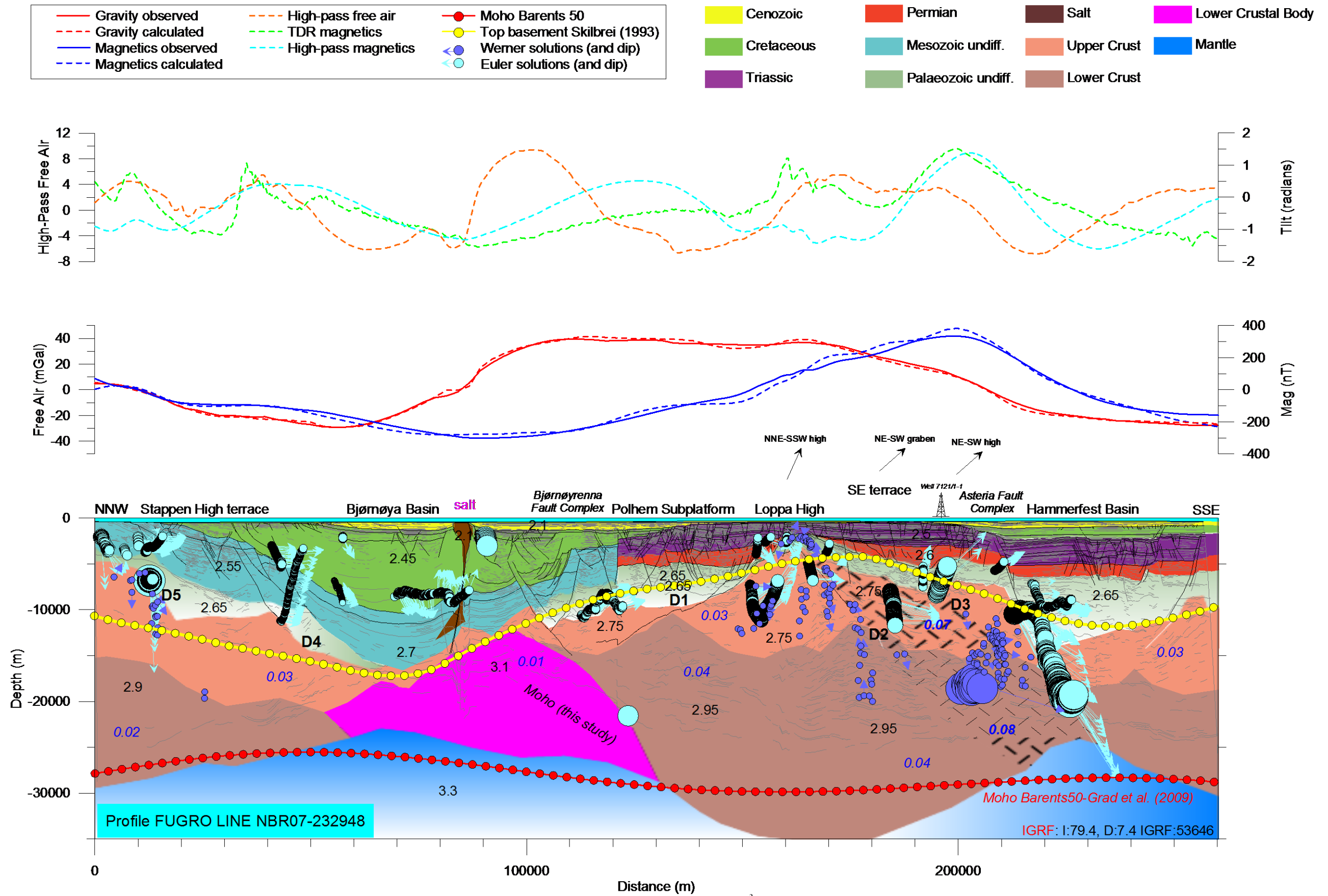


Figure 11.7 Forward modelling results along seismic line NBR07-232958. Each polygon is characterised by a density value in $g.cm^{-3}$ (black numbers) and susceptibility in SI (blue italic numbers).

11.2.2 Transect 2: Section 7355-94

General structure and seismic observations

The section 7355-94 (Fig. 11.1) represents one of the old regional lines available to all BASAR-09 partners. The profile extends almost E-W from the Bjarmeland Platform up to the SH area, 50 km south of Bjørnøya. The line is of relatively good quality but calibration is lacking in most of the area (Fig. 11.8). Near-base Cretaceous, near-top Permian and intra-Triassic markers can be recognised. One particular aspect is the thickness of the Cretaceous basin which changes drastically from several kilometres at the level of the BB to less than 1 km along our section, located north of the so-called 'North Loppa High Shear Zone', a feature highlighted both by the gravity and the magnetic filters (Figs. 11.4, 11.5) and introduced in the previous NGU reports. This already suggests a major crustal and rheological change between the Bjarmeland Platform and the BB area.

Along the transect, the Triassic sequences are well developed in the Bjarmeland Platform and clearly thin towards the SH, where the Triassic and younger sediments are locally eroded. Beneath the Permian, we were able to identify some markers on the original SEG Y file. In our interpretation, they could suggest the presence of deeper Palaeozoic basins mostly developed in the western part of the section (Devonian-Carboniferous). A major fault complex seems to have controlled the development of the Palaeozoic basin interpreted here, with a major detachment expected on the western flank of the SH. This early detachment has been reactivated during the Mesozoic and controlled the minor faults which affect the Triassic-Cretaceous basins, though with a higher angle. At the level of the SH, seismic data suggest the presence of pre-Triassic terraces and narrow grabens, also tested by modelling.

Correlation with the magnetic and gravity data

The gravity signal along the transect varies from -18 mGal to the east in the Bjarmeland Platform to 31 mGal in the central part of the SH (Fig. 11.8). Taken as a whole, the gravity increases from east to west and already points out two main crustal domains on both sides of a crustal contact expected approximately at x-axis km 88 in the central part of the transect where the main NE-dipping Palaeozoic detachment is expected to occur. This detachment possibly represents an old, reactivated, Caledonian thrust and is expected to extend to the south close to the North Loppa High Shear Zone and the Leirdjupet Fault which show an opposite polarity. We believe that the Leirdjupet Fault is a major Mesozoic fault, formed during the BB development and rooted at depth on top of the pre-existing low-angle detachment. Using filtering techniques such as the TDR combined with TDX, sub-structural elements can be identified and correlated with the seismic observations (Fig. 11.8).

The total magnetic field along the profiles varies between 60 nT and 272 nT on the SH. The main magnetic low (x-axis km 120) coincides with the local gravity high at the same level as a hanging-wall ramp anticline suggested by our seismic interpretation at BCU level. At depth, this magnetic low domain could coincide with the location of the main Palaeozoic basin in the hangingwall proposed underneath the Trias.

The main magnetic anomaly is located in the SH area (x-axis km 0-40) and seems to be bounded to the east by a major fault highlighted by the TDR and other filters at x-axis km 37. To the east, a high magnetic anomaly is also observed between x-axis km 140-177. It does not fit with any changes in the Mesozoic basin (an almost uniform Triassic sequence) and most likely reflects a basement feature not clearly observed on seismics.

Modelling results and deep structures

Using joint gravity and magnetic forward modelling, we obtained a relatively good approximation of the magnetic basement (Fig. 11.8). The shallowest basement is modelled in the SH area. Werner solutions already suggested that the magnetic sources are mostly localised in the upper crust. Clusters at ~2.5 km depth (Fig.11.8; tables 11.3, 11.4) focusing between x-axis km 37 and x-axis km 55 that indicate the shallowest basement is to be expected at that level. Between x-axis km 0 and x-axis km 50, where the prominent magnetic anomaly is observed, the magnetic basement refined by forward modelling is estimated around 3-5 km depth. This anomaly has been modelled using susceptibilities of 0.025-0.03 SI in the uppermost crystalline basement. This contrasts with the slightly lower values (0.01-0.015 SI) recorded in the central part of the transect, to the east of the main fault that is proposed at x-axis km 37.

The top basement is deepening to the east, and defines an intermediate terrace at around 4.5 to 7 km depth between x-axis km 50 and x-axis km 90. East of x-axis km 90 where the major NE-dipping detachment is likely to occur the basement surface is deepening up to 10 km. Werner solutions have been obtained at the edge of the crustal hanging-wall suggested by our model. The deepest Palaeozoic basin controlled by the detachment is assumed to exist there. Conceptually, it may represent a deep Devonian(?)–Carboniferous depocentre associated with the collapse and reactivation of old, NE-dipping, Caledonian nappes (see later discussion). In that context, the SH may represent a major crustal footwall active during the Palaeozoic. The shallow basement modelled to the east can then represent the tilted part of the crustal hanging-wall.

Assuming this model, the magnetic low is explained by the presence of a thick Palaeozoic–Mesozoic section overlying a thin crust. As suggested in the previous reports, the presence of unmobilised salt could eventually decrease the average density and therefore increase the Palaeozoic thickness by a few km at this level. This is a possible alternative because the

Svalis Dome is not so far away (Fig.11.1), but there is no obvious evidence for salt on the seismic provided. We also consider a different density for the lower crust on either side of the crustal detachment expected at x-axis km 90. The upper crust density is set to 2750 kg/m³ for the upper crustal bodies.

The Moho depth deduced from our 2D modelling is relatively consistent with the previous Barents 50 Moho estimation of Ritzmann *et al.* (2007). It varies between 35 km underneath the SH to 29 km depth beneath the thickest Palaeozoic basin expected in the central part of the 7355-94 section. This estimation considers a density of 2650 kg/m³ for the pre-Permian bodies.

Depth of investigation	0-25 km
Windows length	10-90 km
Windows expansion increment	500 m
Windows expansion shift	500 m
Residual cut-off	75%
X cut off	5%

Table 11.3 Parameters used for the Werner deconvolution along profile 7355-94.

Depth of investigation	0-20 km
Windows length (fix)	50 km
Maximum % error	5%
Structural index	0.5

Table 11.4 Parameters used for the Euler deconvolution along profile 7355-94.

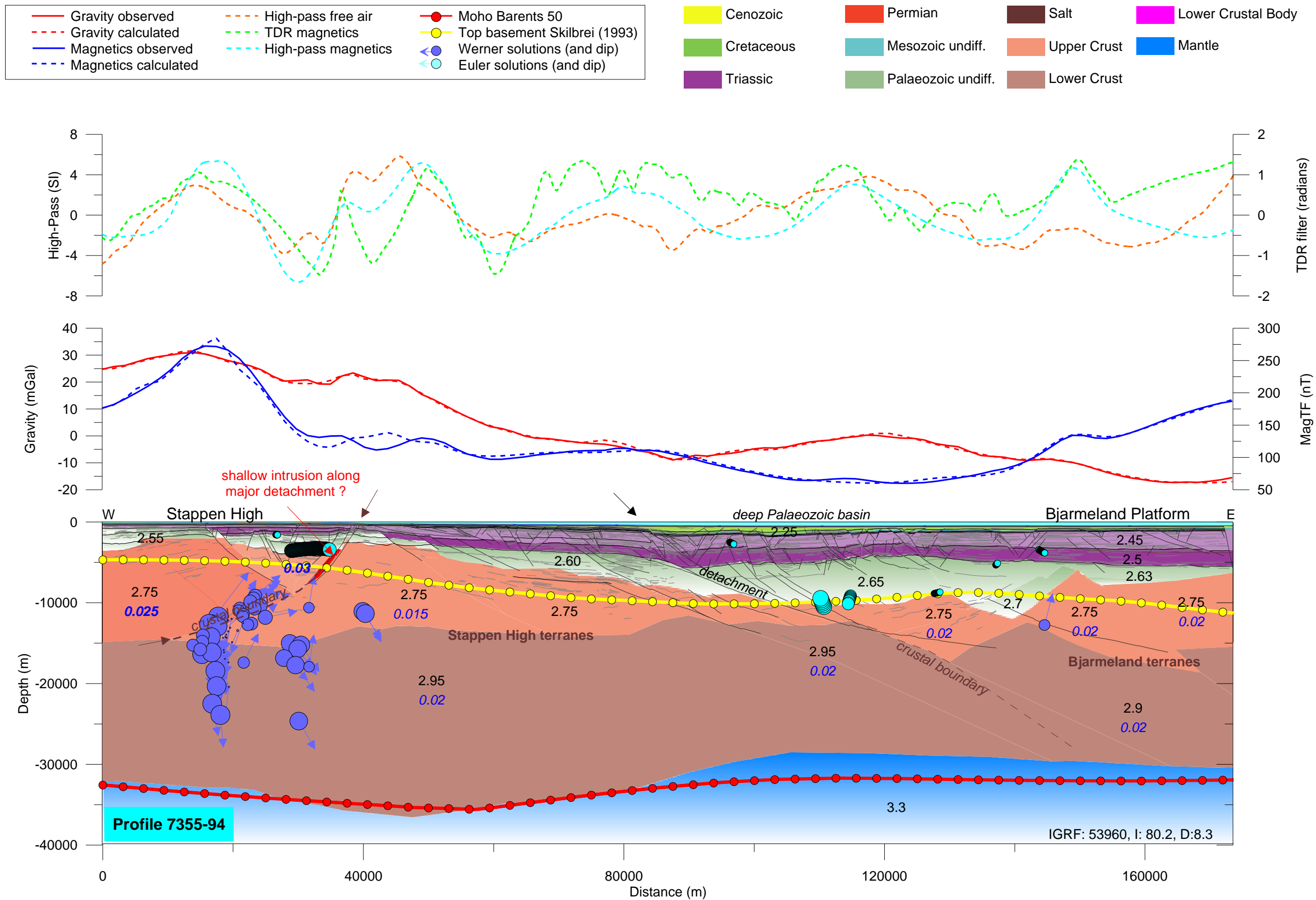


Figure 11.8 Forward modelling results along seismic line 7355-94. Each polygon is characterised by a density value in g.cm⁻³ (black numbers) and susceptibility in SI (blue italic numbers)

11.3 Transect 3: Section BV12-86

General structure and seismic observations

The section BV12-86 is part of the 1986 NPD Bjørnøya West Survey and also represents one of the few regional lines available to all BASAR-09 partners (Fig. 11.1). The line is of relatively good quality but does not allow a good interpretation of the deep structures due to poor imaging near the SH and the presence of volcanic rocks in the Vestbakken volcanic province (Fig. 11.9). Direct calibration is also lacking in most of the area. The line is NW-SE oriented and covers the southern part of the SH and a large part of the Vestbakken volcanic province, officially defined west of the Knølegga Fault Zone (Gabrielsen *et al.* 1990). The Vestbakken volcanic province is located at a rifted margin segment southwest of Bjørnøya, linking the Senja and Hornsund sheared margin segments to the south and north, respectively.

The quality of this line is particularly poor at the level of the SH where limited stratigraphic control and the presence of numerous multiples constitute major limitations for a detailed analysis of the specific stratigraphic section and its deep structures. Nevertheless, the BV12-86 section images well the Cenozoic sequences that developed to the west during the formation of the Eocene sheared margin and after the onset of spreading in the northern part of the Norwegian-Greenland Sea sometime in the Latest Eocene-Early Oligocene (Faleide *et al.* 1988, Engen *et al.* 2008).

We refer to Jepsen (1998) for the most recent interpretation and a more detailed description of these successions, which is beyond the scope of this report. To summarize, the Cenozoic sedimentary wedge to the west can be roughly divided into a lower faulted part and an upper undeformed (or poorly faulted) section. The lower faulted part is probably the consequence of a releasing bend that gave rise to a narrow basin/shear margin formation. The observed structures are mainly extensional, but transpressional structures are to be seen locally. The lowermost unit of the Cenozoic section is characterised by faulted structures locally affected by lava flows and sill intrusions that have given rise to the strong and discontinuous reflections mostly observed west of the Knølegga Fault Zone. This magmatic feature represents part of the volcanic province interpreted mostly as Early Eocene by Faleide *et al.* (1988). Prominent volcanoes as well as sill intrusions are also observed at the outer margin (Faleide *et al.* 1988). Repeated tectonic activity in a pull-apart setting within the Vestbakken volcanic province denotes that the Cenozoic evolution of the NE Norwegian-Greenland Sea was complex, and as many as eight tectonic and three volcanic events have been identified (Jepsen 1998). Along the BV12-86 section, truncation of the underlying strata is observed on top of the faulted blocks. West of the Knølegga Fault Zone, the deepest sedimentary section is clearly syn-rift and was tilted to the west and downfaulted up to 1 to 1.5 s TWT. The deeper unit, overlying the intrusions (and/or lava flows) consists of low- to

intermediate- amplitude reflectors that gradually change to higher amplitude and more continuous reflectors towards the east. This section most likely corresponds to the Eocene unit 'R' introduced by Richardsen *et al.* (1991). The existence of deeper sedimentary units cannot easily be confirmed on the seismic line Bv12-86 alone and has been tested by modelling.

To the east, the Knølegga Fault Zone is characterised by a clear and major west-dipping border fault on the western flank of the SH. The transition to the main Vestbakken volcanic province, however, is not so abrupt and rather defines a ~15 km deep intermediate terrace where synformal features can be recognised on seismics (Fig. 11.9). To the east, structures on the SH cannot be clearly observed due to the presence of numerous multiples. Some reflections can be observed locally but with large uncertainties due to multiples and poor processing.

Correlation with the magnetic and gravity data

The main structural elements observed on seismics has a clear gravity signature. The free air gravity amplitude varies from 10 mgal to 53 mGal at the level of the Vestbakken volcanic province and is around 25 mGal at the level of the SH. The most pronounced anomaly is observed between x-axis km 25 and 98, west of the Knølegga Fault Zone and consists of two sub-anomalies highlighted by the high-pass filtering of the gravity field (Fig. 11.9). At x-axis km 50, the gravity anomaly could reflect the presence of a deeper intermediate high that separates Mesozoic(?) sub-basins but without an associated magnetic signal.

An apparent gravity low (14 mGal) coincides with the Knølegga Fault Zone (x-axis km 98), a feature also suggested by the tilt derivative filter of the gravity which better highlights specific trends and sub-units. The Knølegga Fault Zone represents a N-S anomaly which is slightly different compared to the N45 trending anomaly observed on either side. On the eastern part of the section, the main N45 tilt anomaly extends up to Bjørnøya where the expected 'Hecla Hoek' is exposed. On the western side, the section covers the northern end of the N45 anomaly.

Along the transect, the total magnetic field varies between -130 nT in the area of the Vestbakken volcanic province area to 230 nT in the easternmost part of the profile, including the SH and the narrow graben associated with the Knølegga Fault Zone, which rather form a fault complex. Basically, the highest magnetic amplitude represents the shallower level observed in the surrounding area of the SH, and the lower amplitude almost fits with the thickest sedimentary section observed on seismics to the west. The lowest magnetic signature (x-axis km 55) corresponds to a graben affected by the Tertiary magmatism and increases to the west up to 45 nT where a clear NE-SW anomaly can be observed.

The TDR filtering of the magnetic field also reveals the complexity of the system and some of the trend fits with the structure already revealed by the gravity filtering at the level of the SH and Vestbakken volcanic province.

Modelling results and deep structures

The BV12-96 profile represents almost a western prolongation of the 7355-94 profile, previously described. Consequently, we adopted the same density and susceptibility values and basement geometries for better correlation and homogeneity of the modelling, one of the biggest challenges at the regional scale of the entire Barents Sea (see 3D modelling chapter).

Assuming susceptibilities of 0.025 SI for the upper basement in the SH area (Fig. 11.9), we modelled the top of the crystalline magnetic basement from 2 km to a maximum of 6 km, to the east of the Knølegga Fault Zone. Assuming a rough regional comparison with the geology of Bjørnøya, non-magnetic sediments and Palaeozoic formations (Devonian-Carboniferous) are expected to lie on top of the magnetic crystalline basement but this cannot be differentiated on seismic and the contact between the undifferentiated Palaeozoic and the crystalline basement is mostly based on the magnetic modelling of the SH. Like the previous profile 7355-94, we assumed susceptibilities of 0.025-0.03 SI for the upper crust on the SH. Our magnetic top-basement estimation fits with the joint gravity modelling and the previous result along the 7355-94 profile. Local discrepancies exist when compared with the previous estimation of Skilbrei (1993), but the average estimation of 4 km is almost similar. In the western part of the transect, we obtained locally reliable Euler solutions near the SH (Fig. 11.9, table 11.5, 11.6).

To the west, the magnetic basement deepens to ~ 6 km near the Knølegga Fault Zone and up to 7 or possibly 10 km maximum in the Vestbakken volcanic province. We note that this area is influenced by magmatism, which is likely to influence our estimates. West of the Knølegga Fault Zone, we obtain clear and reliable clusters of Euler solutions which coincide well with the sill complexes observed on seismics. This shows that the sill/lava complex contributes to the total magnetic signal observed along the modelled profile. However, the contribution of the sill complex versus deeper basement sources is not yet well understood.

Our proposed magnetic model fits with the density modelling result and the previous estimation of Skilbrei *et al.* (1993). Eldholm *et al.* (1987) and Faleide *et al.* (1988) have proposed that the Vestbakken volcanic province could be underlain by oceanic crust but the new magnetic dataset does not suggest the typical striped oceanic pattern. The continent ocean transition is located much more to the west outside our new survey area. We propose that the Vestbakken volcanic province is lying above continental and/or transitional crust. Between x-axis km 30 and x-axis km 80, we expected around 3-5 km of sediments (density

of $2500 \text{ kg}\cdot\text{m}^{-3}$) underneath the sill complex (or lava flows) observed on seismics. This interpretation agrees with the early assumption of Richardsen *et al.* (1991) which suggested the presence of a deeper basin beneath the volcanic rocks. This may also suggest that Paleocene and/or older sediments may exist beneath the Tertiary lava flows. The low density proposed for the pre-sill sediments ($2500\text{-}2550 \text{ kg}\cdot\text{m}^{-3}$) could mostly reflect Mesozoic-Paleocene sediments (referred to for simplification as Mesozoic on the Fig. 11.9) but cannot, a priori, support the presence of old Palaeozoic units with higher densities ($>2600 \text{ kg}\cdot\text{m}^{-3}$). Between x-axis km 40 and 65, we interpreted and modelled an intra-basin high to fit the local gravity high signature observed at that level. The density used to fit the signal is slightly higher than in the surrounding basins (density of $2500 \text{ kg}\cdot\text{m}^{-3}$).

According to the model, we do not consider the Knølegga Fault Zone to represent a simple upper crustal fault zone but rather to mark the beginning of a major crustal transition zone (20 km broad) where the upper crust defined on the SH plateau (density of $2750 \text{ kg}\cdot\text{m}^{-3}$) laterally disappears and is replaced by higher density material in the western part of the section. High-density basement ($> 2900 \text{ kg}\cdot\text{m}^{-3}$) is also necessary just underneath the basin to fit the gravity signature observed in the area of the Vestbakken volcanic province (LCB-1 on Fig. 11.9). Conventional susceptibility values deduced from the previous studies and the onshore-offshore correlation cannot explain alone the magnetic signal at that level and indicates that the lower crust in the western part of the BV-12-86 profile is different from the crust modelled in the SH. Using an average susceptibility of 0.02 SI but also a remanence of 1.5 A/m, the high-density basement could explain the observed low-magnetic signature. The sudden drop of the magnetic field clearly fits the proposed crustal change in the central part of the transect.

Accepting the tectonic evolution proposed for the BB, the Knølegga Fault Zone may represent a prolongation of the Ringvassøy-Loppa Fault Complex, before drastic crustal thinning of the crust between the SH and the LH (Gernigon *et al.* in prep). Even if further studies are required to confirm this idea, the high-density terranes modelled west of the Knølegga Fault Zone could possibly represent some form of similarity with the crust observed within the Vestlemøy High and the Senja Ridge.

In the westernmost part of the transect, high density basement is expected at minimum depths of 5.5 to 7 km (Fig. 11.9). The top basement modelled locally fits with strong amplitude, dome-shaped reflections observed on seismics. The domal shaped feature at x-axis km 18 fits with the N-S-trending magnetic anomaly highlighted by the TDR filter (Fig. 11.4). At this level, we expect high-density material beneath the sag-basin (LCB2). Such a high-density material could represent infiltrated mantle and/or intruded lower continental crust. Real oceanic crust is expected 60-100 km to the west but the COB is still a subject of uncertainties due to poor magnetic coverage in this area.

Taking into consideration the basin geometry and the magnetic modelling, our Moho estimation is a bit different compared to the recent compilation of Ritzmann *et al.* (2007) and Grad *et al.* (2009). It fits underneath the SH and in the westernmost part of the transect but at the level of the Vestbakken volcanic province we modelled a shallower Moho (8 to 10 km shallower compared to the previous authors). This was a prerequisite to fit the prominent, observed gravity high.

Depth of investigation	0-25 km
Windows lengths	10-50 km
Windows expansion increment	500 m
Windows expansion shift	500 m
Residual cut-off	100%
X cut off	5%

Table 11.5 Parameters used for the Werner deconvolution along profile BV12-86.

Depth of investigation	0-20 km
Windows length (fix)	20 km
Maximum % error	5%
Structural index	0.5

Table 11.6 Parameters used for the Euler deconvolution along profile BV12-86.

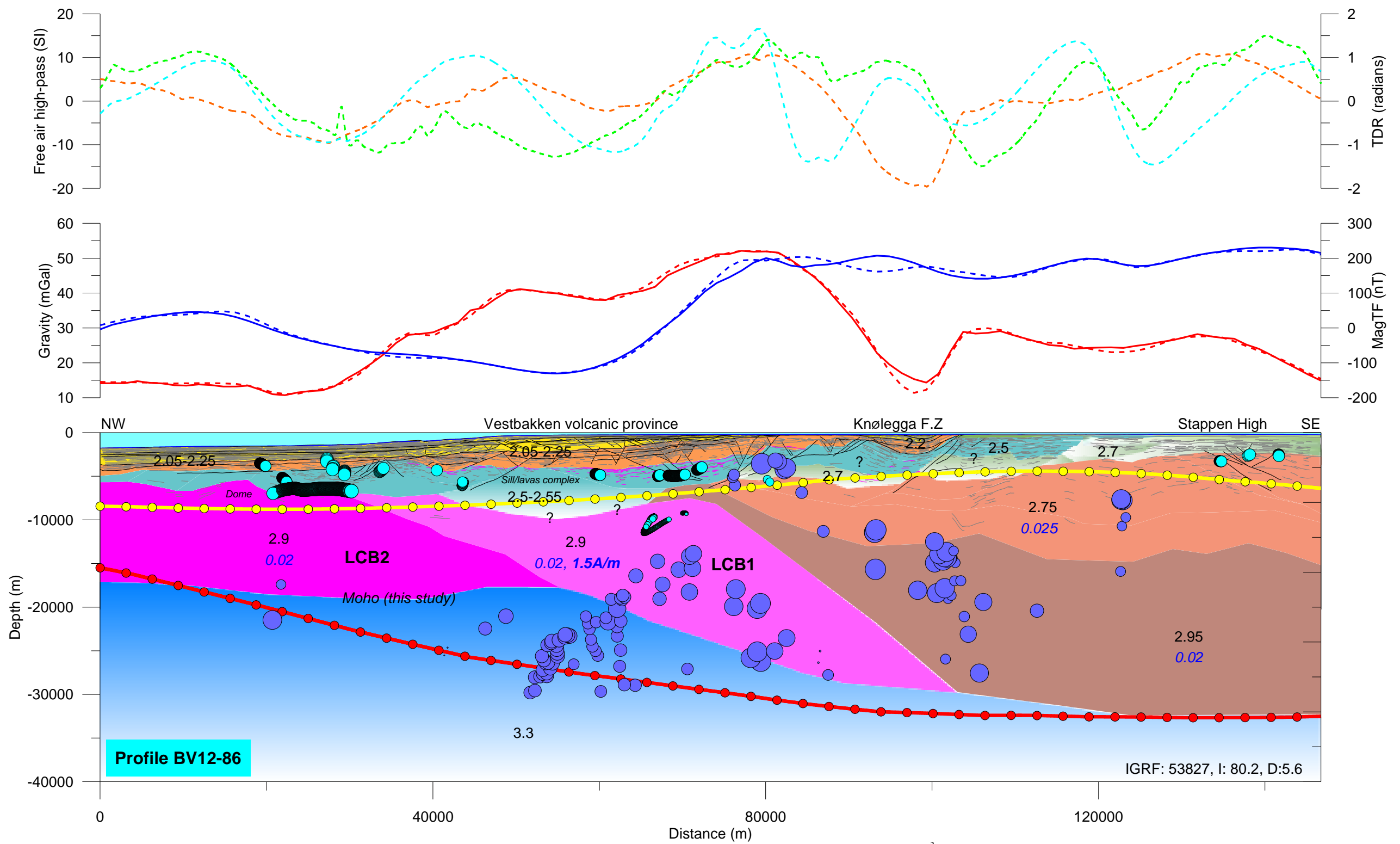
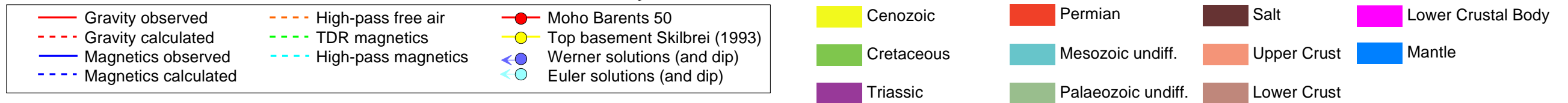


Figure 11.9 Forward modelling results along seismic line BV12-86. Each polygon is characterised by a density value in $g \cdot cm^{-3}$ (black numbers) and a susceptibility in SI (blue italic numbers).

11.3.1 Transect 3: Section BV3-86

General structure and seismic observations

The section BV3-86 represents the southern prolongation of profile 7355-94 and is almost perpendicular to the BV12-86 profile (Fig. 11.1). The profile is NE-SW-oriented and extends from the SH to a transition zone between the Sørvestnaget Basin and the Vestbakken volcanic province, previously described. This section shows a structure relatively similar to the BV12-86 and also illustrates the transition between the shallow SH and the transtensional basins that formed to the west of the Knølegga Fault Zone (Fig. 11.10). The seismic quality was relatively good but limited to the uppermost part of the basin. Compared to the Fugro line, only limited observations are available for the mid- to lower-crustal parts.

Correlation with the magnetic and gravity data

The gravity free-air anomalies vary between 17 mGal near the SH to 47 mGal in the outer part of the Vestbakken volcanic province (Fig. 11.10). The highest gravity high represents the prolongation of the major anomaly also described in the central part of the BV12-86 section but is located in a more distal position of the BV03-86 profile. This NW-SE anomaly can easily be tracked on the filtered gravity map where we see that the anomaly is slightly oblique to the regional magnetic domain. The anomaly is N-S oriented in the south near the BV03-86 section, swings into a NW-SE-trend towards the BV12-86 and stops at the level of the Knølegga Fault Zone, a major crustal boundary.

The main structural boundary observed on seismics at x-axis km 75 coincides with a clear magnetic boundary with a low-magnetic domain to the southwest and a high-magnetic region to the northeast. This boundary does not coincide with the southern prolongation of the Knølegga Fault Zone, located around x-axis km 120. The new BASAR-09 data shows the presence of high-frequency anomalies at this location. They are most likely a consequence of the sill/lava complex observed on seismic.

Clear identification and modelling of the structures are difficult in the northern part of the BV03-86 section, where most of the magnetic anomalies appear to be sub-parallel or slightly oblique to the seismic section. There, we are mostly oblique to the main faults and the upper crustal structures which are suggested by the magnetic anomalies.

Modelling results and deep structures

Assuming susceptibilities of 0.025 SI for the upper basement in the SH area, we modelled the top of the crystalline magnetic basement between 2 km and a maximum of 6 km, north of the Knølegga Fault Zone. This is obviously coherent with the result of the BV12-96 modelling. Non-magnetic sediments and Palaeozoic formations (Devonian-Carboniferous) are also expected to lie on top of the magnetic crystalline basement but cannot be differentiated on seismics and like BV03-86 the contact between the undifferentiated Palaeozoic and the crystalline basement is mostly based on the magnetic modelling on the SH. Our magnetic top-basement estimation fits with the joint gravity modelling and the previous result along the adjacent 7355-94 and BV2-86 profiles. Local discrepancies exist when compared with the previous estimation of Skilbrei (1993), but the average estimation of 4 km is almost similar in the SH and the Vestbakken volcanic province. Difference of up to 5 km of is observed at the level of the Knølegga Fault Zone but our transect at that level is locally influenced by edge effects, which could explain the discrepancy in our 2D model.

In the northern part of the transect, higher susceptibilities (0.04 SI) have been required near the Knølegga Fault Zone and a crustal contact and/or intrusion are expected there in order to explain the prominent magnetic high observed at x-axis km 105. We also obtained reliable Werner and Euler solutions (Table 11.7, 11.8) in the upper crust, suggesting that the magnetic sources are located at around 5-10 km depth in the vicinity of specific highly magnetic basement deduced indirectly by the forward modelling approach (Fig. 11.10). We point out that this specific location represents a junction of different magnetic trends (N10 and N85) observed on the magnetic TDR. This may indicate the presence of a major crustal contact, not distinguishable on seismics.

To the west, the magnetic basement deepens to ~ 6 km near the Knølegga Fault Zone and up to 6-8 km in the Vestbakken volcanic province. West of the Knølegga Fault Zone, we obtain a clear and reliable cluster of Euler solutions on top of the sill complex observed on seismics. This shows that the sill/lava complex could explain part of the total magnetic signal observed along the modelled profile. Compared to the BV12-86, the crust underlying the Vestbakken volcanic province also has high density ($2950 \text{ kg}\cdot\text{m}^{-3}$) but shows a lower susceptibility (0.015 SI) and no remanence. Our proposed magnetic model fits with the density modelling result and the previous estimation of Skilbrei *et al.* (1993). We expected around 3-5 km of sediments (density of $2500 \text{ kg}\cdot\text{m}^{-3}$) underneath the sill complex (or lava flows) observed on seismics.

Between x-axis km 5 and 40, we interpreted and modelled a high-density/high-magnetic crustal body to fit the observed potential field signatures. The density used to fit the signal was $2950 \text{ kg}\cdot\text{m}^{-3}$, the susceptibility 0.03 SI and the remanence 1 A/m. Such a high-density material could represent infiltrated mantle and/or intruded lower continental crust as has also been proposed in the outer part of the previous BV12-86 section.

Taking into consideration the basin geometry and the magnetic modelling, our Moho estimation along BV03-86 is slightly different compared to the recent compilation of Ritzmann *et al.* (2007) and Grad *et al.* (2009). It fits below the SH and in the northern part of the transect but below the Vestbakken volcanic province we modelled a shallower Moho (almost 10 km shallower compared to the previous authors). This was a requisite to fit the prominent gravity high. However, we recognise an uncertainty of ± 3 km.

Depth of investigation	0-25 km
Windows length	10-50 km
Windows expansion increment	500 m
Windows expansion shift	500 m
Residual cut-off	100%
X cut off	5%

Table 11.7 Parameters used for the Werner deconvolution along profile BV3-86.

Depth of investigation	0-20 km
Windows length (fix)	30 km
Maximum % error	5%
Structural index	0.5

Table 11.8 Parameters used for the Euler deconvolution along profile BV12-86.

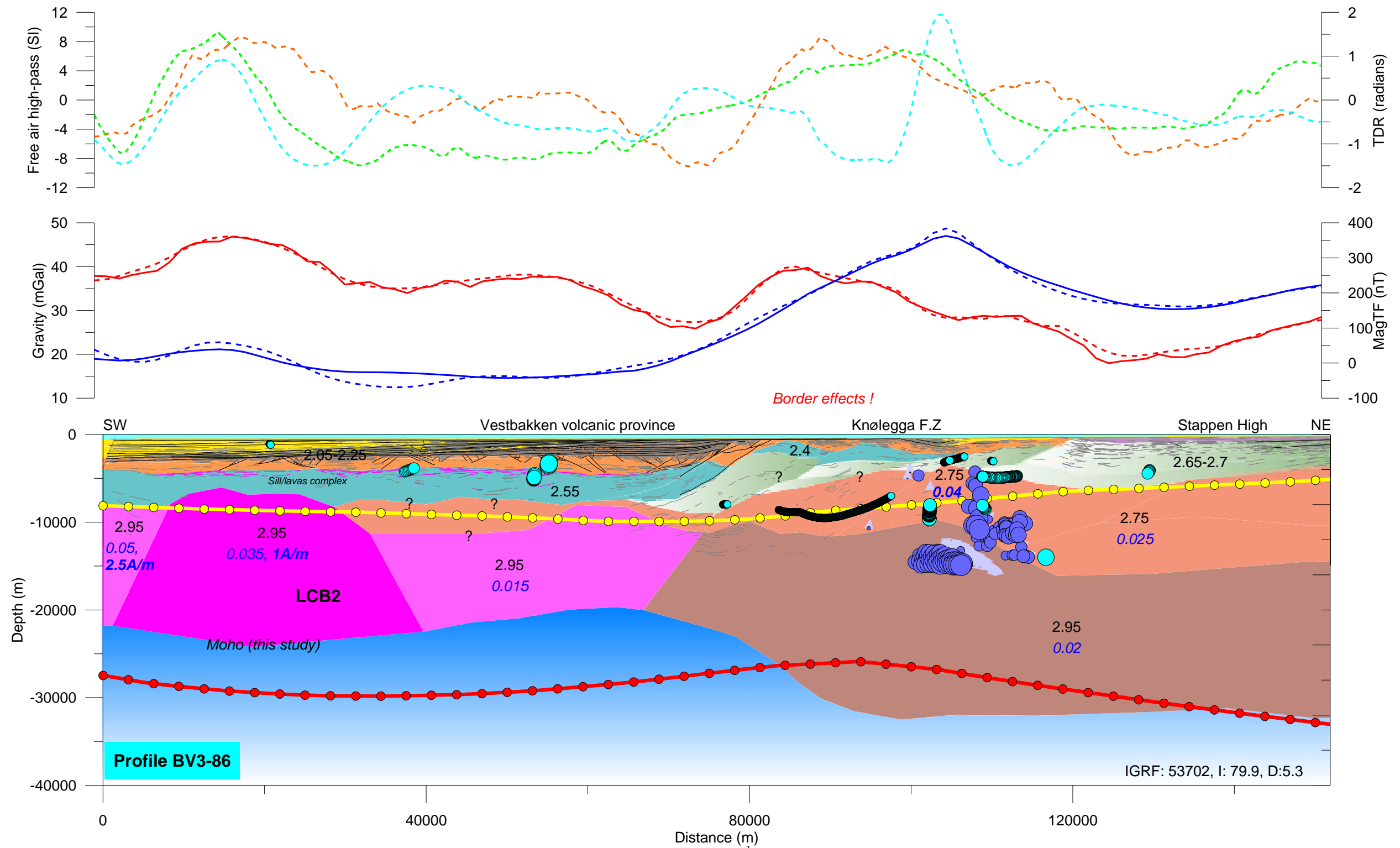
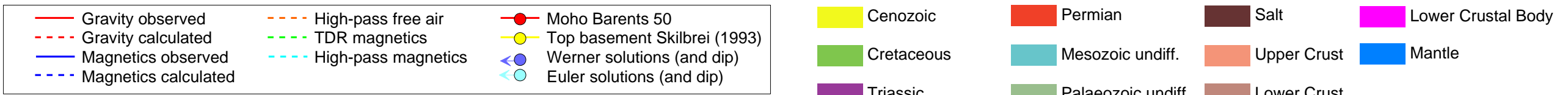


Figure 11.10 Forward modelling results along seismic line BV03-86. Each polygon is characterised by a density value in $g.cm^{-3}$ (black numbers) and a susceptibility in SI (blue italic numbers).

11.4 Implication of the modelling, ongoing understanding and challenging models to test

11.4.1 Crustal structure and implications for the stretching model

Several studies have recognised that, undeniably, the western Barents Sea basement structures are inherited from the Caledonian orogen (Gabrielsen *et al.* 1990, Gudlaugsson *et al.*, 1998; Ritzmann *et al.* 2007). Gernigon *et al.* (2006) and Barrère *et al.* (2009) proposed a recent reinterpretation of the ancient Caledonian suture and deformation zones affecting the southwestern Barents Shelf. They also interpret the variety of rift orientations in the southwestern Barents Sea (NNE-SSW, NNW-SSE) as evidence of a mechanical anisotropy inherited from the ancient Barentsian Caledonian accreted terranes. Such an anisotropy and compositional upper-crustal layering have most likely controlled the upper-crustal deformation since the Scandian post-orogenic collapse (Fig. 11.11). The modelling described in this chapter reveals information on the tectonic scenario that has progressively been developed since the commencement of the new Barents Sea aeromagnetic projects (Gernigon *et al.* 2007, Brønner *et al.* 2009).

Compared to previous crustal models (e.g. Ritzman *et al.* 2007, Barrère *et al.* 2009), we consider that a much shallower Moho exists between the SH and the LH. The BB displays a lateral variation in the basin structure between two massive blocks (e.g. SH and LH) with most likely thick and mafic lower crusts affected by upper brittle faulting but poorly affected by major crustal thinning as compared to surroundings. Extension most likely focused around the main blocks already during the Palaeozoic with the major deformation clearly which was observed at the edge of these 'rigid' blocks. This led to the formation of the main border fault complex observed and modelled at the edge of the LH (e.g. the W-dipping Bjørnøyrenna Fault Complex on profile NBR07-232958) and in the northern part of the SH (the NE-dipping detachment modelled on section 7335-94).

During Jurassic to Early (mid?) Cretaceous time the BB acted as a flexural sag triggered by an extreme thinning of the continental crust and locally accommodated by these detachments. The very rapid thinning of the lowermost sedimentary layer (Late Jurassic-Cretaceous sequences) towards the basin centre appears to have occurred sympathetically with later increased amounts of crustal thinning. This can be explained if extensional deformation was gradually focused towards the basin centre in response to intra-crustal simple-shear deformation, as the syn-rift sediments were being deposited. This interpretation agrees with classic stretching models that involve a footwall flank uplift following the extra thinning of the lower crust and/or lithospheric mantle that has been proposed between the SH and the LH. The literature reports an uplift of the LH linked to a fault zone oriented N-S and active along the western margin from Late Permian to Early

Triassic time (Gabrielsen 1984, Gabrielsen *et al.* 1990). Following our model, we interpret this uplift as originating from an earlier hanging-wall denudation of the LH controlled by deep-crustal detachments.

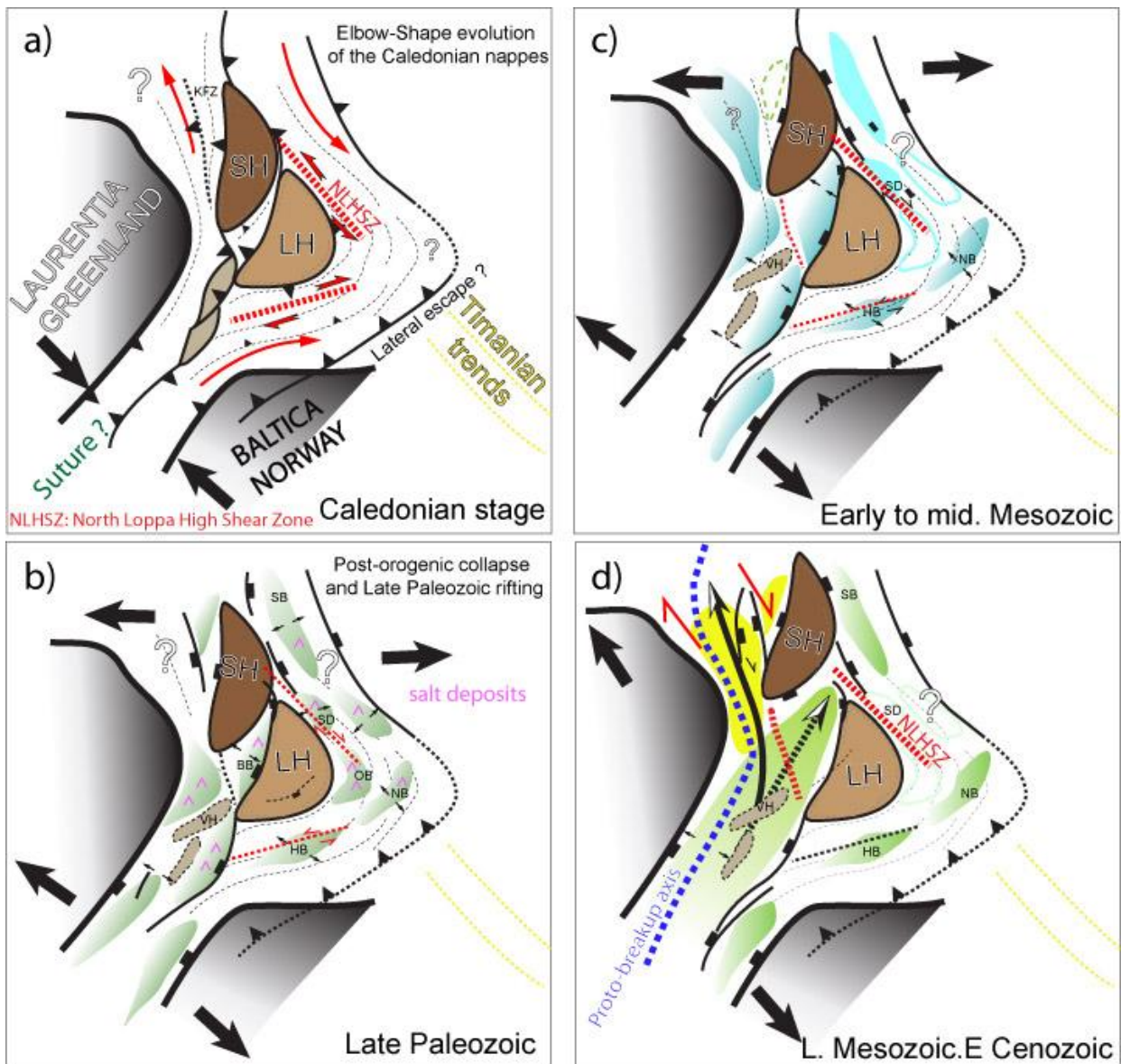


Figure 11.11 Conceptual models of the geodynamic evolution of the study area. Abbreviation: BB: BB; HB: Hammerfest Basin; KFC: Knølegga Fault Zone; LH: Loppa High; NB: Nordkapp Basin; NLHSZ: North Loppa High Shear Zone; OB: Ottar Basin SB: Sørkapp Basin; SD: Svalis Dome; SH: Stappen High; VH: Vestlemøy High. Gernigon *et al.* (manuscript in preparation).

The high-density, lower-crustal body expected beneath the BB (see section NBR07-232958) is difficult to reconcile with magmatic underplating. There is no evidence for the significant quantities of intruded or extruded magma in the vicinity of the BB. We proposed the presence of serpentinitised upper mantle underneath the BB with pre-existing high-grade metamorphic lower crust to explain the high density ($> 3000 \text{ kg}\cdot\text{m}^{-3}$) required beneath the BB to fit the observed signal. The propagation of low-angle detachment surfaces, possibly

inherited from the Caledonian post-orogenic collapse, into sub-crustal mantle, could ultimately localise mantle exhumation and increase the mantle serpentinisation.

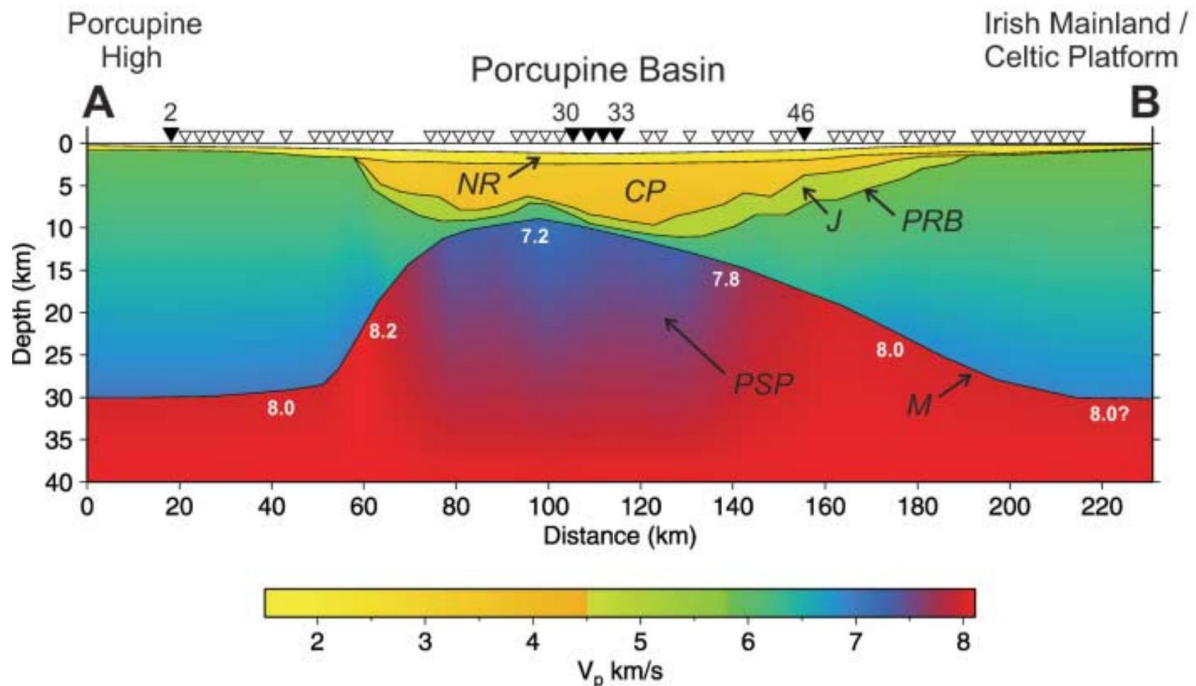


Figure 11.12 Model for the crustal and sedimentary structure across the Porcupine Basin after O'Reilly *et al.* 2006). In shape and structure, this Irish basin could represent a good crustal analogue of the Bjørnøya Basin. Vertical exaggeration is 1:1.5. Triangles show the positions of OBSs used in this study. NR, Neogene to Recent post-rift sequence; CP, Cretaceous to Palaeogene post-rift sequence; J: predominantly Jurassic synrift sediment sequence; PRB: pre-rift basement; M: Moho; PSP: partially serpentinised mantle peridotite. Low velocities in the subcrustal mantle (V_p c. 7.2–7.8 $\text{km}\cdot\text{s}^{-1}$) are interpreted as evidence for partially serpentinised peridotites. Numbers are seismic P-wave velocities ($\text{km}\cdot\text{s}^{-1}$) in the subcrustal region of the model, added for clarity.

We expect a prominently rotated faulted structure in the deep part of the BB. Consequently, the interpretation of the deep block should be reinterpreted carefully since it won't necessarily display classic tilted block features bounded by high-angle faults. It could involve much more complex systems of low-angle detachments subsequently cut by steeper faults during the thinning process. The quality of the data and the depth of such a block do not allow us to constrain accurately the geometry in this report (this should require a complete 2D-3D regional mapping of the deep BB), but Reston (2007 & 2009) has clearly illustrated the difficulty in interpreting such highly extended features and their petroleum implications. The Porcupine Basin (Fig. 11.12) also shows similar features and is also relatively similar in size and shape (O'Reilly *et al.* 2006). Well constrained by wells and seismics, it could be a good basin analogue of the BB, developed by thinning propagation between the SH and the LH (Gernigon *et al.*, in prep.).

11.4.2 Deep structures, sutures and modelling results: still open questions

Our working hypotheses are initially based on the potential field analysis of the BASAR-09 survey (completing the previous surveys BAS-06 and BASAR-08) and suggest that both the SH and the LH represent very old basement terranes amalgamated and closely connected by the end of the Caledonian orogeny. Onshore-offshore investigations and the regional magnetic signature suggest that the LH basement may partly represent the northern prolongation of the old, highly magnetic, Precambrian terranes possibly linked with the Transcandinavian Igneous Belt province (1.8 Ga in age) observed onshore (Barrère *et al.* 2009). Consequently LH could have been part of the stable Baltica before the closure of Iapetus and the onset of the main Scandian phases of the Caledonian Orogeny (Fig. 11.11).

The gravity and magnetic signature of the SH appears to be similar to that of the LH but its origin before the Caledonian Orogeny could have been different. Uncertainties remain about the origin and position of the SH basement before the Caledonian Orogeny. Some assume that Bjørnøya and possibly the SH were part of Laurentia before the closure of the Iapetus Ocean (Smith 2000). In that case, this interpretation of the Phanerozoic location of Bjørnøya is that any Caledonian strike-slip, orogen-parallel displacements and suture(s) must have been located outboard of the combined Bjørnøya-Greenland craton. Accordingly, the suture should be expected to be present beneath the BB, possibly at the level of the high-density lower crust (high-density migmatites/peridotites/eclogite melange?). Alternatively, terranes observed on Bjørnøya could have been thrust above deeper Precambrian Baltican basement and in that case, the suture would be expected west of the SH, most likely at the level of the breakup axis since uppermost mantle heterogeneity has a tendency to localise the lithospheric deformation and the rift/margin development (Yamasaki and Gernigon, 2009).

Even though the old basement configuration is still controversial and not yet fully understood, both the SH and the LH appear in our modelling as distinct and thick crustal blocks, at least since Devonian time. The SH and LH were close together at that time but a major crustal contact (crustal shear zone, major thrust) probably separated the two crustal terranes. The west-dipping detachment observed on the western flank of the LH could therefore represent a reactivated thrust that formed between the SH and the LH during the Caledonian deformation. In that case, the SH could represent, initially, a major crustal hanging-wall as proposed by Moretti *et al.* (1988).

Most fundamentally, the SH and the LH are interpreted to represent continental rigid blocks that behaved as 'buffer' during the Caledonian Orogeny and subsequent Palaeozoic-Mesozoic rifting episodes (Gernigon *et al.*, in prep). These blocks most likely controlled the elbow-shaped configuration of the Caledonian nappes as earlier suggested by Gernigon *et al.* (2007) and further developed and described in Barrère *et al.* (2009) and Brønner *et al.* (2009). After the Caledonian Orogeny, we believe that the original rigid blocks probably

acted as continental ribbons and locking zones during the subsequent Palaeozoic and Mesozoic rift history and consequently influenced both the Palaeozoic and the Late Mesozoic basin development and the entire paleogeographic evolution of the area (Fig. 11.11).

The new and most challenging hypothesis considers that some of the Palaeozoic basins in most of the Bjarmeland Platform could have also developed along NW-SE regional trends up to the northern SH (Fig. 11.11). Should we be able to develop this tectonic model further, it could totally change the classic paleogeographic hypothesis which favours the development of NE-SW-trending Palaeozoic basins in most of the western Barents Sea (e.g. Gudlaugsson *et al.* 1988, Faleide *et al.* 2008). We conclude that the trends of the Late Palaeozoic basins, most likely influenced by the reactivation of Caledonian structures, are not necessarily sub-parallel to the NE-SW trending Mesozoic axes as has often been suggested in the literature.

The few seismic lines at our disposal suggest that a major detachment fault dipping to the northwest can be observed along the northern flank of the SH, most likely controlling the southern Sørkapp Basin. Collapse of the Caledonian nappes and reactivation of the main thrusts could explain the NE-dipping polarity of the main detachment inferred to exist between the SH and the Bjarmeland Platform (see section 7355-94). However, it contrasts significantly with the opposite, SW- to W-dipping, detachment fault complex that probably controls the BB. It would seem that between the SH and the LH a complex accommodation zone developed between the major detachments. This accommodation zone has been highlighted by a NNW-SSE magnetic trend on the old NGU compilation and seems to have controlled the Mesozoic basin development and deposition towards the north. The NW-SE trend of the accommodation zone has most likely had a significant influence on later tectonic development of the LH and SH, and the BB system could coincide with a major shear zone that was active during Caledonian time (informally named North Loppa High Shear Zone, NLHSZ).

As part of the system, the BB represents a hyper-extended basin that developed between the SH and the LH from Devonian to Late Mesozoic time. This basin is probably more segmented, as suggested by the observed gravity and magnetic trends and magnitudes, but in general seems to have propagated from south to north with time. We believe that when the BB reached the NLSZ level, it failed to extend farther north and probably influenced the regional stress regime which triggered a complete reorganisation of the rifting, migrating to the west to initiate the sheared margin south and west of the SH (Fig. 11.11). Basically, without the presence of this old crustal accommodation zone, the breakup between the western Barents Sea and Greenland would have occurred east of the SH and not to the west as finally observed. We believe that the NLHSZ probably stopped the propagation of the BB, and has been interpreted as a thinning propagator (Gernigon *et al.*, in prep.). Without the influence of this major inherited (Caledonian) feature, the Tertiary breakup could have

occurred in the central part of the present day Bjørnøya Basin. The disappearance of the Mesozoic propagator was therefore associated with a lateral shift of the deformation towards the west, leading to the development of the sheared margin and sedimentary basin to the west and south of the SH and described by sections BV3-86 and BV12-86. The age and nature of these western basins, now partly hidden by volcanic rocks are unknown, but according our tectonic model they should have started to be active precisely during the declining activity of the stage of thinning system proposed for the BB.

The late phase of rifting was concentrated south and west of the SH, and even though it has not yet been investigated in detail, the Knølegga Fault Zone and its related features probably controlled part of the late oblique margin setting. In our tectonic model we propose that the Knølegga Fault Zone could have been closely related to the Ringvassøy-Loppa Fault Complex before the drastic thinning of the crust and opening of the BB (Fig. 11.11). It could also explain the unclear transition zone between the BB and the Sørvestsnaget Basin and would also fit with our idea of a fan-shaped evolution of the Caledonian nappes (Fig. 11.11).

11.5 Conclusions – Limitations - Perspectives

- Forward modelling combined with the Euler and Werner deconvolution technique has been carried along selected regional transects (NBR07-232958, 7355-94, BV03-86 and BV12-86). We depth-converted and interpreted the sections and carried out both gravity and magnetic forward modelling constrained by the Euler and Werner deconvolution results.
- The modelling provides a refined interpretation of the top basement and Moho estimates. We show notably a major thinning of the BB compared to the surrounding LH and SH, which are only mildly affected by the crustal thinning.
- The models tend to agree with the previous geodynamic scenario of rigid and ‘buffer’ blocks proposed for the LH and the SH. In this context, the BB is interpreted as a hyper-extended basin propagating to the north. This thinning propagator ends at the level of the North Loppa High Shear Zone, a complex NW-SE-trending shear system associated with the Caledonian nappes, initially stacked against the rigid blocks of the LH and SH (Gernigon *et al.*, in prep.).
- Limitations in the present report mostly related to the quality of the seismics, which does not allow us to fully understand the deep structures everywhere. The use of extra NBR Fugro lines is definitively a prerequisite for investigating the deep structures. Extra transects should contribute to a better understanding of the SH-LH system. The deep geometry of the Bjørnøya Basin needs to be better constrained. The significance of the perched sub-Permian basins that are clearly highlighted by

the new magnetic field in the LH area is also unclear and the inferred presence of old NE-SW thrusts(?) also needs to be investigated in more detail.

- The lack of long-offset data in the Vestbakken area is also restrictive and does not allow us to identify the deep, sub-basalt basin suggested by the potential field modelling. Access to better seismics would be conducive to a better understanding of this complex transtensional system.
- More fundamentally, the complexity of the structural development of the western Barents Sea is a matter for further investigation. In the present report, we have mostly focused on the LH, BB and SH, which are the most prominent structures within the BASAR-09 area, but many adjacent structures remain untested by modelling (e.g. Svalis Dome, Vestlemøy High, Tromsø, Harstad and Hammerfest basins,).
- We also propose to obtain specific susceptibility measurement on Bjørnøya. Susceptibility values of the different rock units already sampled in this 'basement windows' of the Barents Sea could provide relevant information and should contribute a refinement of the modelling.

12 3D MODELLING

Marco Brønner

12.1 Introduction

A number of crustal models for the Barents Sea has been published in recent years (Ritzmann *et al.* 2007, Marelló & Ebbing 2009, Barrère 2009) with the aim improving the depth-to-basement map and to better understand the structural setting and evolution of the Barents Sea.

Whilst the BARENTS50 model (Ritzmann *et al.* 2007) covers the entire Barents Sea and was mainly designed for seismological uses and in a rather low resolution (50 km), Barrère (2009) concentrated on the SW Barents Sea with a much higher resolution of c. 10 km. She modified the top basement of Skilbrei (1991, 1995), making use of a significantly improved seismic coverage (e.g. Breivik *et al.* 2005) and with an improved aeromagnetic and gravity database (e.g. Olesen *et al.* 2009). Marelló & Ebbing (2009) updated and improved the BARENTS50 model by potential field modelling and a higher resolution of 25 km, considering various constraints from seismic, wells and petrophysics.

Barrère *et al.* (2009) also presented a characterisation of the basement lithology, by evaluating the petrophysical data from onshore Norway and some offshore wells. The structure of the western Barents Sea shelf has a complex history imprinted in the basement structure and lithologies. Based on these results and in combination with an interpretation of magnetic lineaments, Barrère *et al.* (2009) provided a subdivision of the western Barents Sea into different basement blocks.

In the BASAR-08 project (Brønner *et al.* 2009) we discussed the 3D model of Barrère (2009) with respect to the new BASAR-08 data and presented an updated magnetic crustal characterisation for the survey area. With the acquisition of the BASAR-09 data and the release of the HRAM-97/98 survey, we obtained a new high-resolution aeromagnetic compilation for the entire southern Norwegian Barents Sea. 2D modelling along selected seismic lines, structural interpretation and onshore-offshore correlations carried out with the magnetic data from all the projects BAS-06, BASAR-08 and -09 have allowed us to gain new insights into the structural settings and tectonic evolution of the Barents Sea. The new constraints and new concepts, which evolved from the new magnetic data, are beneficial for a further update and improvement of the existing 3D models.

12.2 Modelling Concept

The SW Barents Sea margin has been studied by 3D modelling integrating a wealth of geophysical data: seismic profiles, commercial and scientific drilling on the shelf and mainland Norway, petrophysical sampling and a dense coverage of gravity and aeromagnetic

data. Magnetic depth estimates provide a good starting point for a genuine structural interpretation (e.g. an interactive modelling or a constrained inversion). Skilbrei *et al.* (1991) and Mørk *et al.* (2002) showed that the susceptibilities of the basement can range between 0.005 and 0.035 SI, whereas the susceptibilities of the overlying sedimentary rocks are only in the order of 0.0003 SI, some one to two orders of magnitude lower. The range of susceptibilities for the basement is depending on composition and varies from 0.005 to 0.01 SI for Caledonian basement, 0.01 to 0.035 SI for Precambrian basement, to even higher values for mafic-intruded basement (e.g. Barrère *et al.* 2009). Therefore, magnetic data are extremely useful for estimating the depth to top basement.

For the 3D modelling the IGMAS software (Götze and Lahmeyer, 1988) has been used. Within IGMAS the geometry is defined along parallel, vertical cross-sections (white solid lines, Fig. 12.1). The distance between the vertical sections can be defined arbitrarily, depending on the complexity of the modelled structures. The geometry is automatically triangulated between the sections to polyhedrons that define the 3D geometry. Densities and magnetisations (Q-value and susceptibility) are subsequently defined for every polyhedron. The gravity and magnetic fields are then calculated and the resulting field compared with the observed potential field.

Magnetisation of crustal rocks is mainly related to the magnetite content in the bedrock, e.g. sedimentary rocks can be considered non-magnetic relative to basement rocks. The Curie temperature of magnetite is 580°C and at this temperature rocks lose their ability to remain magnetised. Assuming a normal thermal gradient, the Curie temperature is located in the deep crust (e.g. Ebbing *et al.* 2009). Therefore, we can limit the extension of magnetic sources to the crust. Magnetic field calculations require the definition of an external magnetic field. We define the normal inducing magnetic field with a field-strength of 53,300 nT, an inclination of 79° and a declination of 4.3°. We can also use the true magnetic field over the study area, which improves the results slightly, but increases substantially the computation time. Therefore, we use a constant magnetic field and the remanent magnetisation is modelled parallel to the induced magnetic field.

To establish a 3D model, information about the geometry and density/magnetisation of the crustal rocks is needed. These parameters are described in the following section.

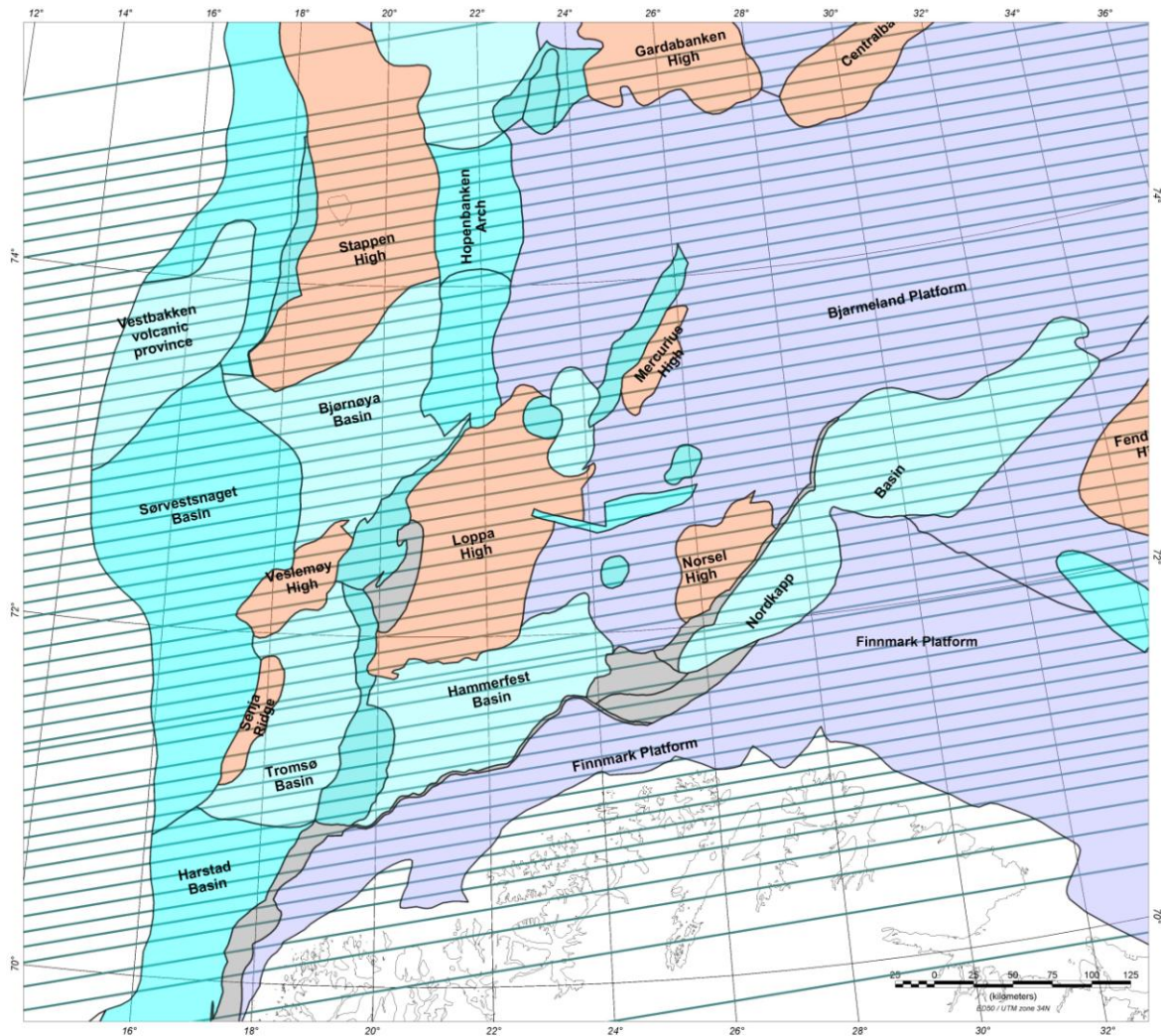


Figure 12.1 Structural map and outline of the 3D model. Lines indicate the vertical planes defining the 3D model.

12.3 Data

The gravity anomaly map (Fig. 12.2) is a combination of free-air gravity for the offshore parts and Bouguer gravity onshore Norway and Bjørnøya (Olesen *et al.* 2010). Full Bouguer correction for the onshore areas was carried out using a topographic grid with a resolution of 50 m and reduction densities of 2670 kg/m³.

Magnetic data (Fig. 12.3) derived from the new aeromagnetic compilation for the Norwegian Barents Sea (Ch. 5). The dataset is compiled from reprocessed aeromagnetic surveys and line spacing ranges from 0.5 to 2.5 km over mainland Norway and from 1 to 5 km over the continental shelf.

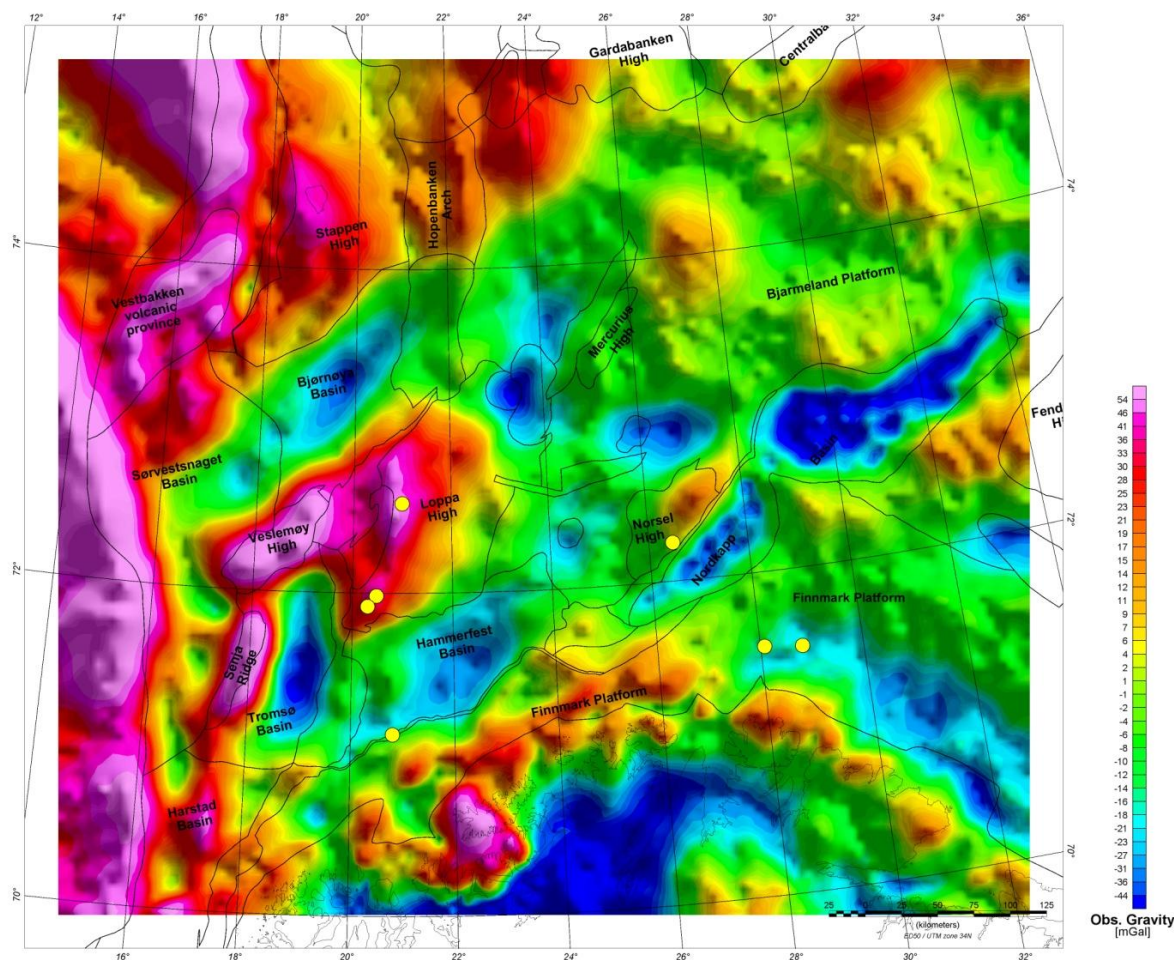


Figure 12.2 Gravity compilation used for 3D modelling. For gravity data a compilation of free-air gravity in the offshore parts and Bouguer gravity with reduction density of 2670 kg/m^3 onshore Norway and Bjørnøya was applied. Outline of the 3D model.

12.3.1 Petrophysical data

Densities of the sedimentary layers are based on well data (Tsikalas, 1992) and tables published by Ritzmann *et al.* (2007) based on velocity-density relationships of sedimentary units obtained from the seismic refraction and reflection/gravity studies. Bedrock densities are based on direct onshore sampling and laboratory measurements (Olesen *et al.* 1990, Galitchanina *et al.* 1995).

Deep-crustal densities are based on published values from refraction models (Breivik *et al.* 1998, 2002, 2003, 2005, Mjelde *et al.* 2002) inferred from velocity-density relationships and gravity modelling (Gernigon *et al.* 2007, Brønner *et al.* 2009). The density errors from the velocity-density relations are in the order of $\pm 50 \text{ kg/m}^3$ and $\pm 100 \text{ kg/m}^3$ for the upper- and deep-crustal layers, respectively.

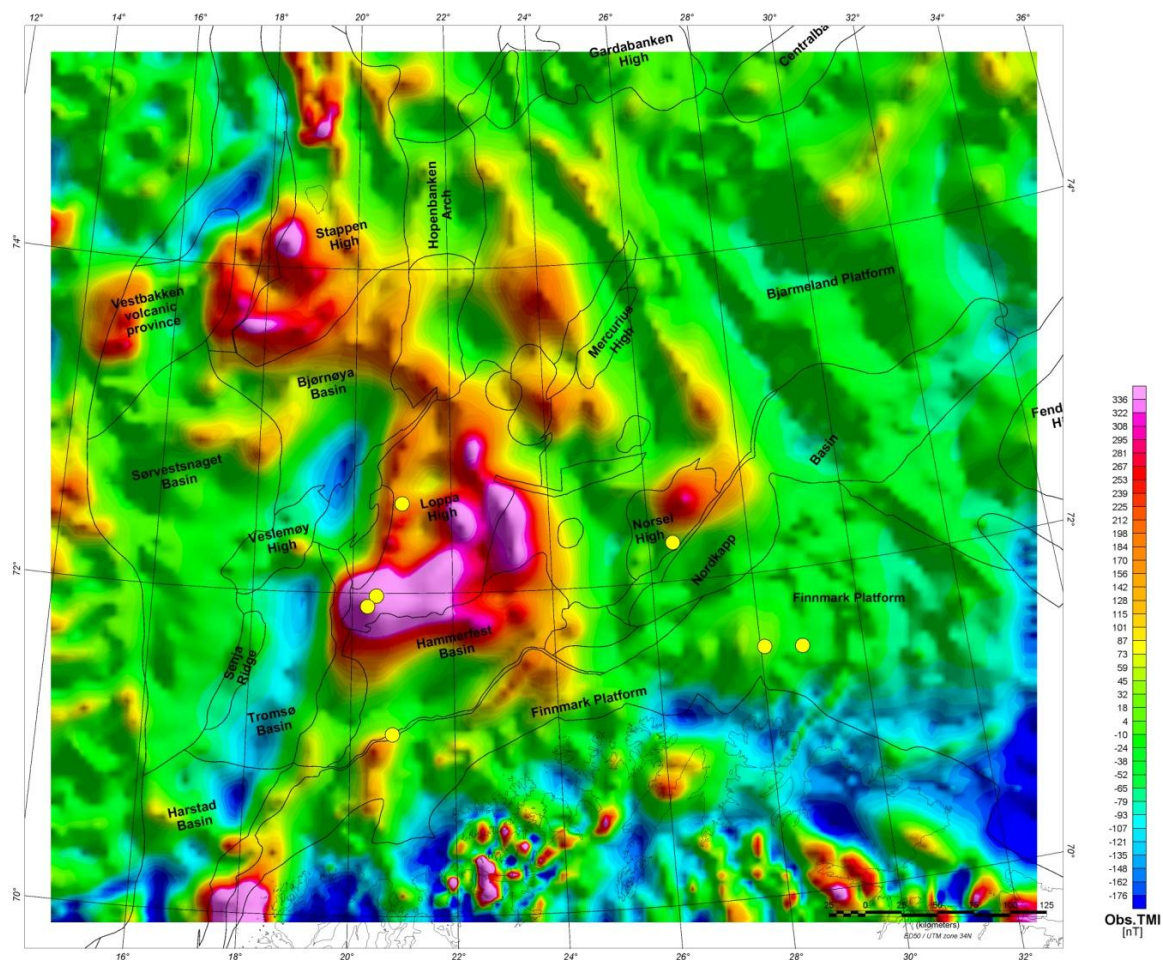


Figure 12.3 Aeromagnetic compilation used for 3D modelling. Outline of the 3D model.

For the magnetic field, the magnetic susceptibility and remanence from the magnetic modelling along the deep IKU lines A, B and C by Barrère *et al.* (2009) were used as initial parameters. Those values were derived from onshore and offshore samples from the Troms and Finnmark regions (Olesen *et al.* 1990; Slagstad *et al.* 2008). Q-ratios (the relationship between remanent and induced magnetisation) were adapted according to the petrophysical data and modified during the modelling. We set a homogeneous and low Q-ratio for the lower crust and mantle of $Q=0.4$ and a magnetic susceptibility of $2000 \cdot 10^{-5}$ (SI). Sedimentary rocks are set to 30×10^{-5} (SI) as they are very low-magnetic in comparison to the basement rocks.

An overview of the model parameters is given in table 12.1.

12.3.2 Geometric constraints from seismics

To constrain the sedimentary layers we used two industrial, depth-converted, seismic horizons: base Cretaceous and top Permian. These horizons were produced by depth-conversion of seismic horizons using regional velocity laws calibrated by well data. The sedimentary rocks are thus subdivided into four sedimentary units: Cenozoic/Cretaceous,

Jurassic/Triassic and Palaeozoic. Seven wells (yellow circles, Fig. 12.2) reach the top basement in the southwestern Barents Sea region; they were used to calibrate the modelled top basement and check the reliability of the depth-converted seismic horizons.

For the initial model we used the western part of the regional model by Marello & Ebbing (2009) and updated and refined it tentatively from 25 km to 10 km resolution. Their model is, in turn, an updated and refined version of the BARENTS50 model, which is a seismic-velocity model of the crust in the Barents Sea with a lateral resolution of 50 km. The BARENTS50 model is based on 2D wide-angle reflection and refraction lines, passive seismological stations and, to a limited extent, potential field data (Ritzmann *et al.* 2007). Marello & Ebbing (2009) added additional and reinterpreted data to better constrain the model, and used combined gravity and magnetic forward modelling and intensive and comprehensive analysis of the potential field data to evaluate and consider the different basement structures in the Barents Sea, which resulted in a more detailed and more reliable 3D model.

For the the initial crustal structure the IKU deep-seismic reflection profiles and the seismic refraction data (Mjelde *et al.* 2002, Breivik *et al.* 2002, 2003, 2005) were used to constrain it.

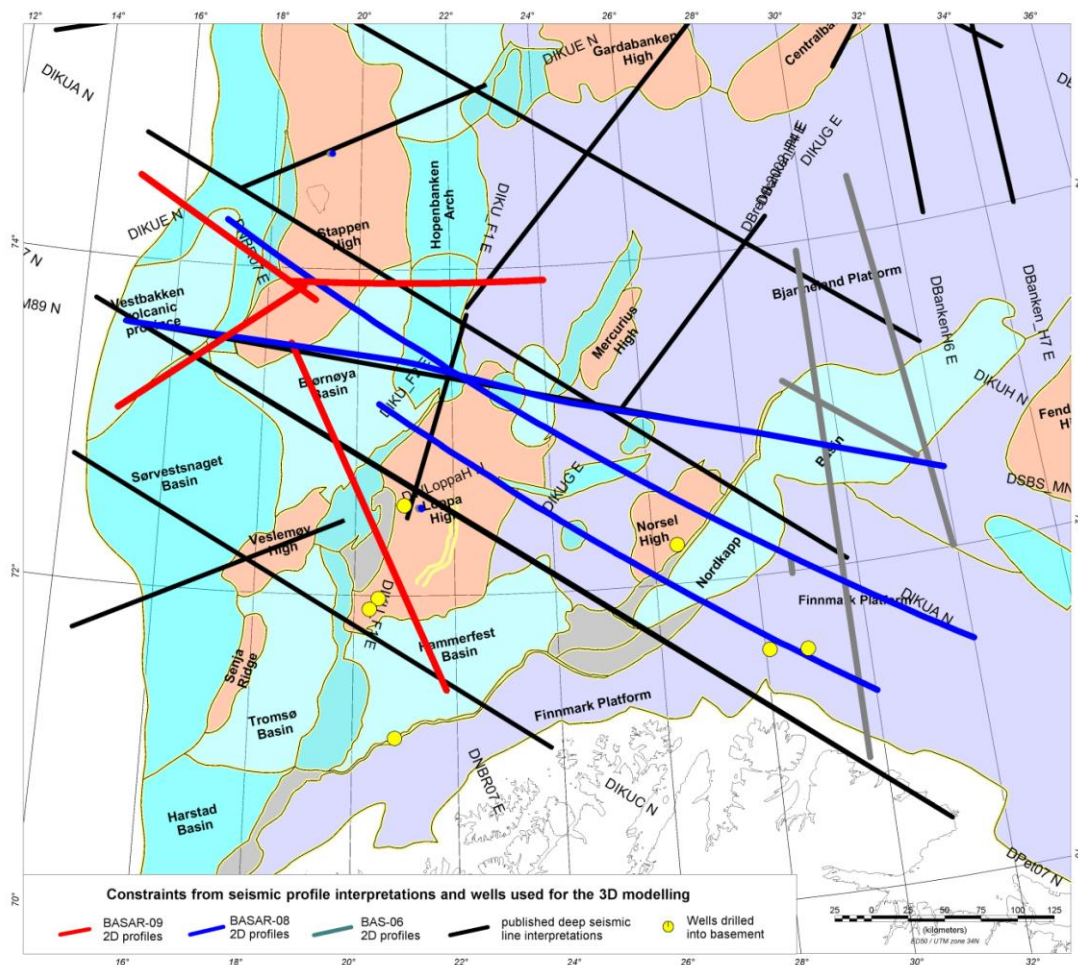


Figure 12.4 Presentation of the additional data from wells, deep seismic profiling and 2D grav/mag modelling along seismic lines, used to constrain the model geometry.

2D interpretation along selected seismic lines from the different recent projects BAS-06, BASAR-08 and -09 were used to refine the model and to test different scenarios. A recent OBS profile (PETROBAR, Clark *et al.* 2009) has also been used. This profile is running along profile IKU-B, but is extended in the northwest and southeast, and includes stations located onshore Norway.

12.3.3 Model parameters

The different crustal units applied in the model are presented in table 12.1. The original petrophysical parameters, derived from samples and logs onshore Norway and from wells, were adjusted to average values for each model unit to fit the observed potential fields. The corresponding number is used to identify each unit in the presented 2D slices from the 3D model (Figs. 12.7-12.10)

Stratigraphy	Unit	Density (kg/m ³)	Q-ratio	Susceptibility (10 ⁻⁵ SI)	No.
Sediment	Water	1040	0	0	1
	Cenozoic- Cretaceous	2350	0	30	2
	Jurassic- Triassic	2460	0	30	3
	Palaeozoic	2640	0	30	4
	Deep Palaeozoic	2750	0	30	5
Upper crust	Caledonian basement	2750	0.5	500	6
	Precambrian basement	2750	0.5	2300- 3000	7
	Loppa High basement	2770	0.6	4000	8
	Stappen High basement	2760	0.5	3000	9
	COT basement	2750	0.8	2300	9a
	Volcanic rocks	2750 - 2770	2	3500- 4000	10
Oceanic crust		2950	1	1000	10a
Lower crust	Lower crust	2940	0.4	400	11
	LCB	3000	1.5	3500	12
	Mantle	3260	0.4	0	13

Table 12.1 Modelling parameters: different crustal units are defined by a combination of petrophysical values obtained by density and magnetic modelling.

12.4 Modelling

One of the major outcomes of the BASAR-08 project was the impact of the overlying low-magnetic Caledonian basement for the observed magnetic field in the southwestern Barents Sea. Onshore-offshore correlations could link the fronts of Caledonian nappes and thrust sheets observed onshore Norway with curved eastward-convex lineaments in the magnetic field, which were consequently interpreted as the expression of different stages of the eastward propagation of the Caledonian thrust sheets (Brønner *et al.* 2009). The 3D models by Barrère (2009) and Marellò & Ebbing (2009) interpreted the magnetic field variations as being due to different basement types and deduced from this complex evolution scenarios for the Barents Sea, which in general are most likely correct. However, based on the new dataset we extended the model geometry and conclude that at least some of the magnetic variations are the result of two different basement types with variable thickness, lying on top of each other, similar to what we observe onshore Norway.

Furthermore, the comparison of the main gravity and magnetic anomalies (Fig. 10.3) clearly shows significant differences and indicates a superposition of different lithological units (Ch. 10, Ch.11). 2D modelling suggested different scenarios, such as thin layers of volcanic rocks on top of the basement and/or serpentinised lower crustal bodies as an explanation, which we wanted to test and extrapolate in a 3D model.

For the modelling, the additional constraints and interpretations were added to the initial model and geometries were subsequently adjusted, starting from the deeper model upwards. Contradictory geometries from overlapping or crossing profiles were modified to fit the potential field data and will be discussed for some examples. The major part of the model was subsequently refined from 25 km to 10 km resolution (Fig. 12.1).

We would like to point out that the resolution along the seismic and interpreted 2D profiles is, of course, much higher and it was not the goal of the 3D model to fit them perfectly but to test trends and scenarios, indicated from the 2D lines, and to extrapolate structures into 3D. The current stage of the model is far from final, but reflects the present stage of knowledge to the extent of the given resolution. Refinement within smaller areas and across local structures is definitely possible but was not a part of the scope of this work and remains as one of our future tasks.

12.4.1 Model correlation

The general patterns of the observed and the modelled gravity and magnetic anomalies (Figs. 12.5a & 12.6a) are comparable. The long- and most of the intermediate-wavelength anomalies for both gravity and magnetics are well explained, and remaining misfits are mainly due to the limited resolution of the 3D model and geo-structures like salt domes, which were not applied to the model.

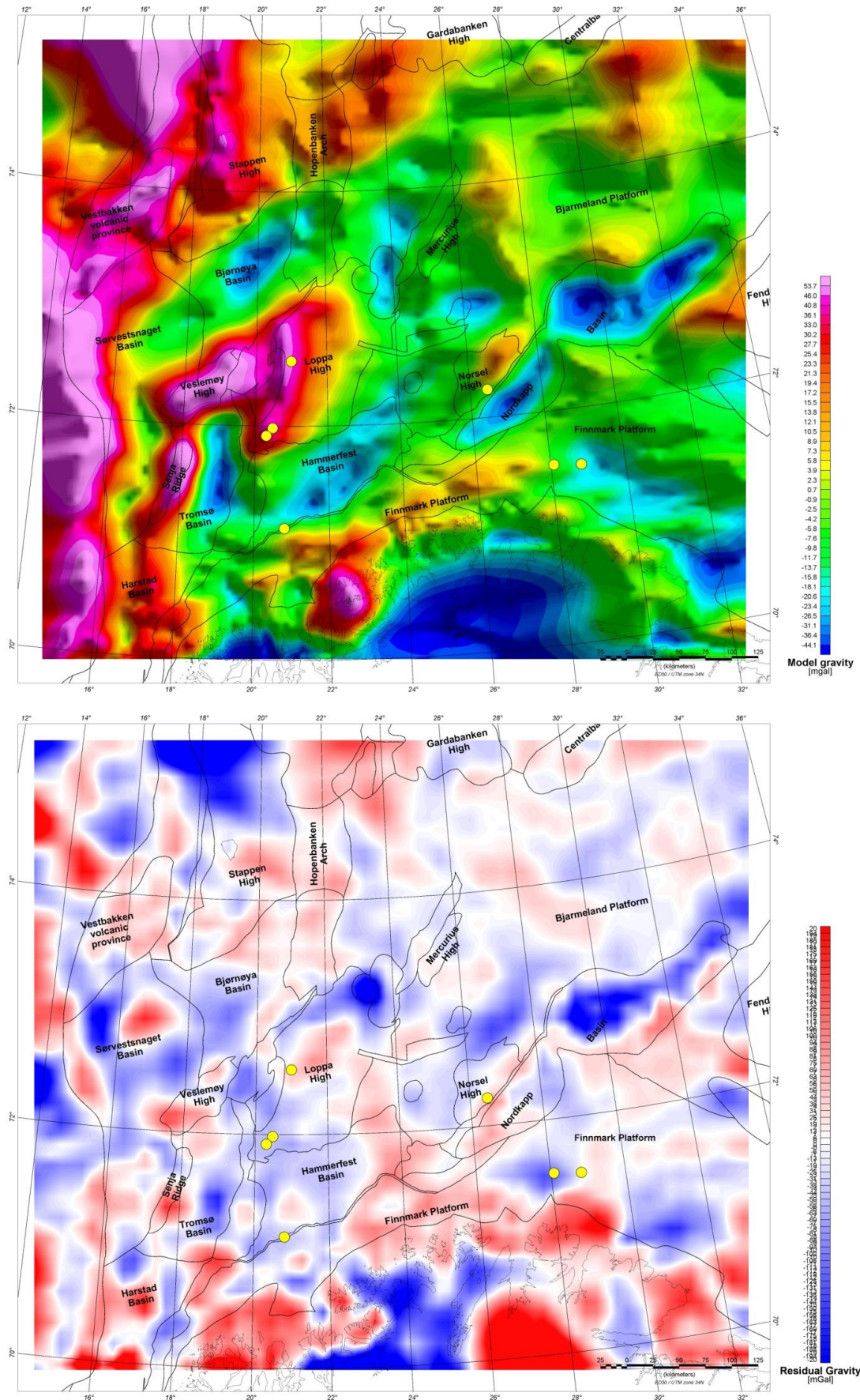


Figure 12.5 a) Calculated gravity from the 3D model and b) difference field with the observed gravity. The standard deviation is c. 8 mGal, which can to a large extent be explained by local mismatches like salt structures(Nordkapp Basin, Svalis Dome), which were not included in the 3D model.

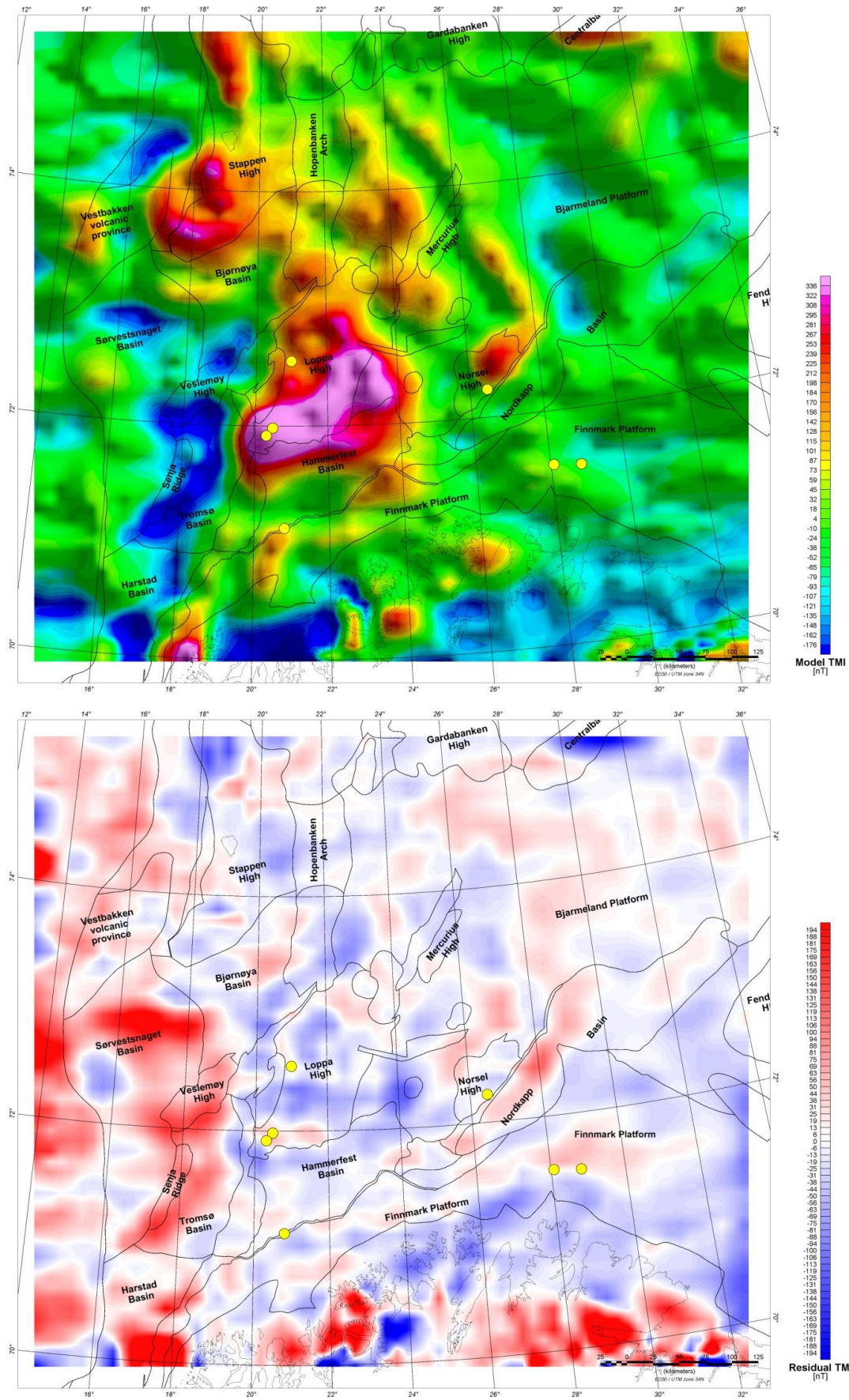


Figure 12.6 a) Calculated TMI from the 3D model and b) difference field with the observed TMI. The standard deviation is c. 70 nT, which can to a large extent be explained by local mismatches along the COT, where constraints were only sparsely available, and low model resolution onshore Norway.

The final differences between the measured and modelled gravity anomalies have a standard deviation of c. 8 mGal (Fig. 12.5b). The biggest mismatches are observed in the Nordkapp Basin and at the Svalis Dome due to the missing salt structures in the model. Furthermore, noticeable mass deficiencies and surpluses do still exist at the northern and southern ends of the model, where the model resolution decreases to 20 km and smaller wavelengths were not adjusted.

For the magnetics the adjustment is also very good. The standard deviation for the model is about 70 nT and remaining mismatches are mainly concentrated in the western part of the model in the area of the COT (Fig. 12.6b). Here, additional constraining information was sparsely distributed and adjustments within this area were thus given lower priority. In the south, onshore Norway, the short-wavelength anomalies have been negligibly adjusted due to the reduced model resolution.

12.4.2 Modelling results

The 3D model is shown and discussed along some representative 2D profiles as well as on the basis of the depth-to-basement map and Moho depth from modelling. The positions of the presented 2D profiles are shown in figure 12.8. The numbers in the profiles correspond to the numbers for every unit in table 12.1.

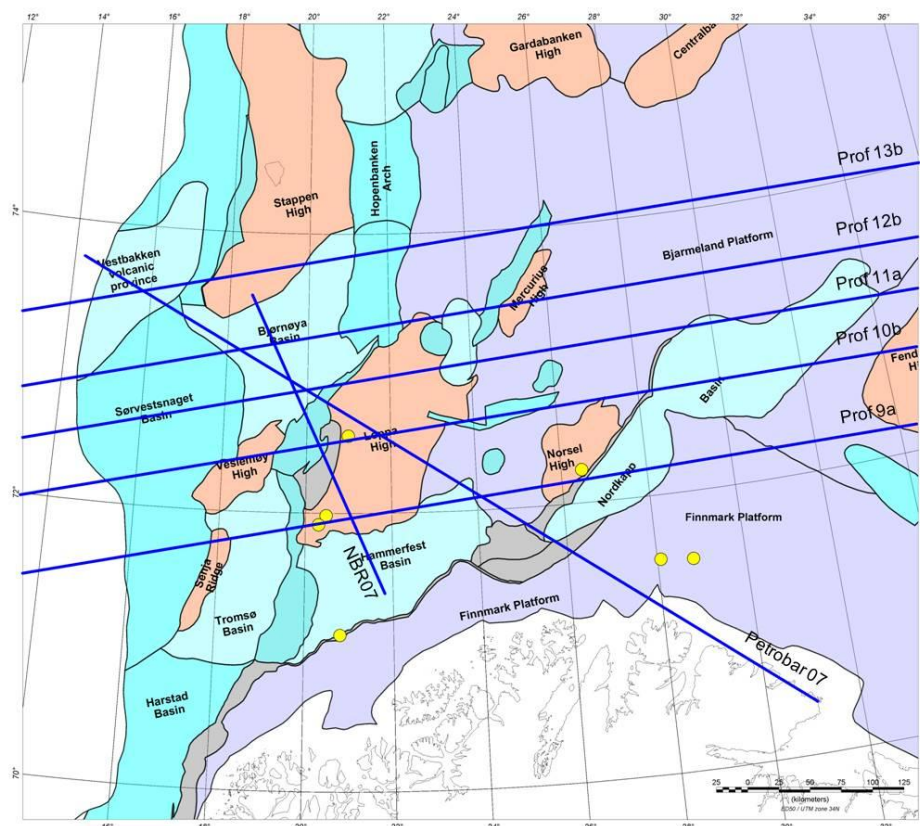


Figure 12.7 Structural map of the southwestern Barents Sea (Gabrielsen et al. 1990) with the positions of the presented 2D profiles from the 3D model.

Profile 9a (Fig. 12.8a) runs from the southern part of the Sørvestsnaget Basin across the Senja Ridge, the Tromsø Basin and the Loppa High. It covers the northeasternmost part of the Hammerfest Basin and the southwesternmost edge of the Norsel High, before it crosses the southern Nordkapp Basin and the northern part of the Finnmark Platform.

The Senja Ridge separates the two deep (more than 10 km) basins Sørvestsnaget and Tromsø and is noticeable from gravity by its very steep and narrow amplitude, whilst the structure has no expression in the magnetics. The depth-to-basement was observed from seismics at more than 5 km depth with mostly Cenozoic to Mesozoic sediments on top (Faleide *et al.* 2003, Breivik *et al.* 1998), which gave a basement density for the ridge similar to lower continental crust to explain the high amplitude.

The Loppa High is well expressed on this line on both gravity and magnetic data, which indicates a basement block with significant higher density and magnetisation than the surrounding basement. The magnetic signal shows an amplitude of more than 800 nT at the western flank of the Loppa High. Wells were drilled into the basement here (Ch. 9) and observed dolerite, which was measured to have significant high magnetisation (Slagstad *et al.* 2008) and explains the amplitude.

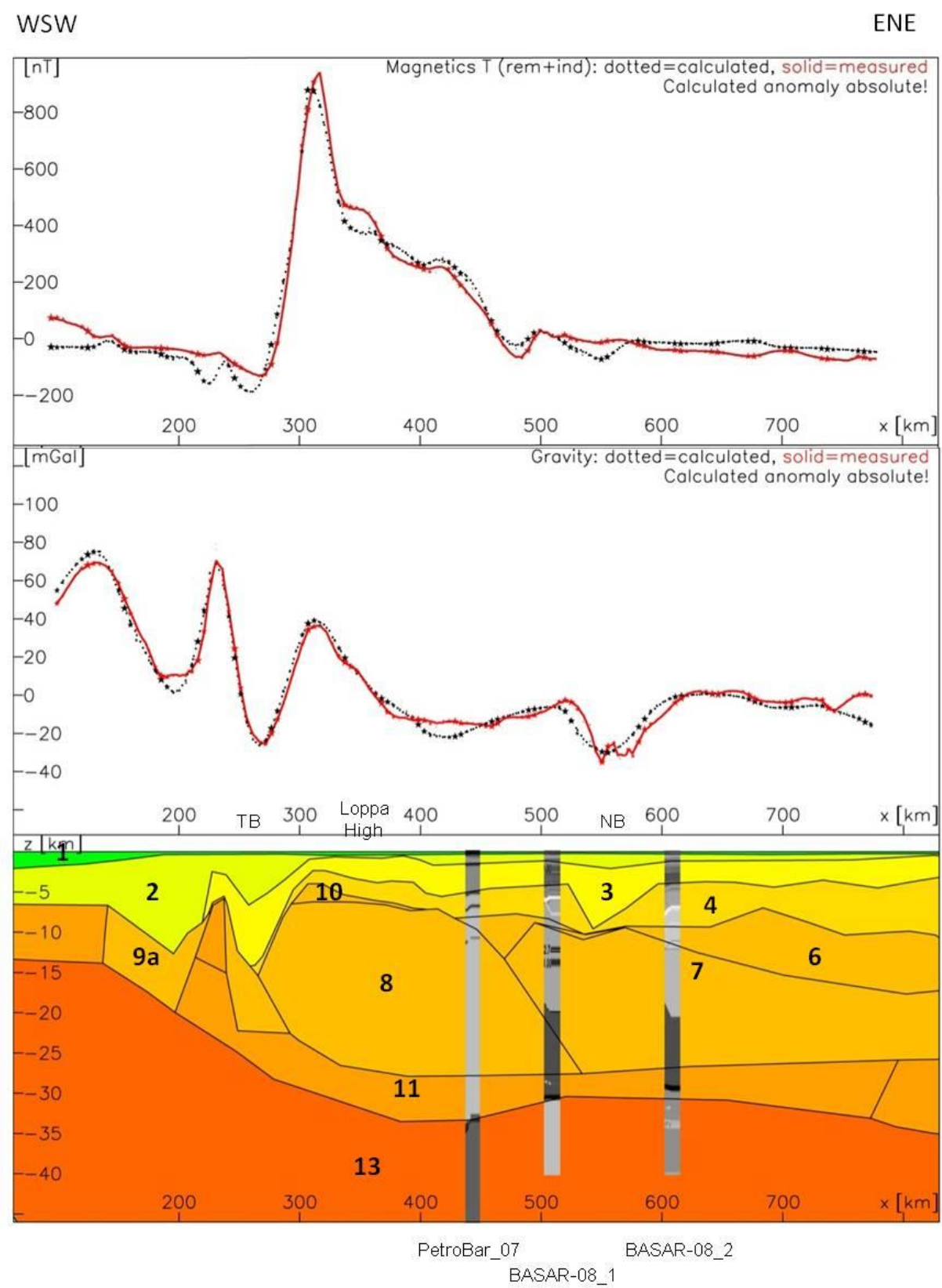
East of this block in between the Loppa and Norsel highs a magnetic low is observed, which correlates with the Ottar Basin. The Ottar Basin is assumed to be a Late Palaeozoic rift basin (Breivik *et al.* 1995), probably consisting of highly compacted sediments which might explain the absence of any expression for the basin in the Bouguer gravity. It reflects very well a problem we face during modelling to distinguish between low-magnetic, Caledonian basements and deep-seated, highly compacted sediments; both have similar densities and the magnetic signal of the slightly higher Caledonian basement is too small to distinguish from other more shallow origins. We know from well logs that certain sedimentary successions can show a similar density as basement at depths of c. 8-10 km and deeper.

The Norsel High and the adjacent Nordkapp Basin show a different basement structure than the Loppa High with lower density and magnetisation. An interpreted Caledonian basement on top of Precambrian basement was used in conjunction with constraining information to explain the discrepancies between observed gravity and magnetic field (Ch. 10) and revealed the Nordkapp Basin to be framed by Caledonian Nappes, which is even more obvious on profile 10b (Fig. 12.8b).

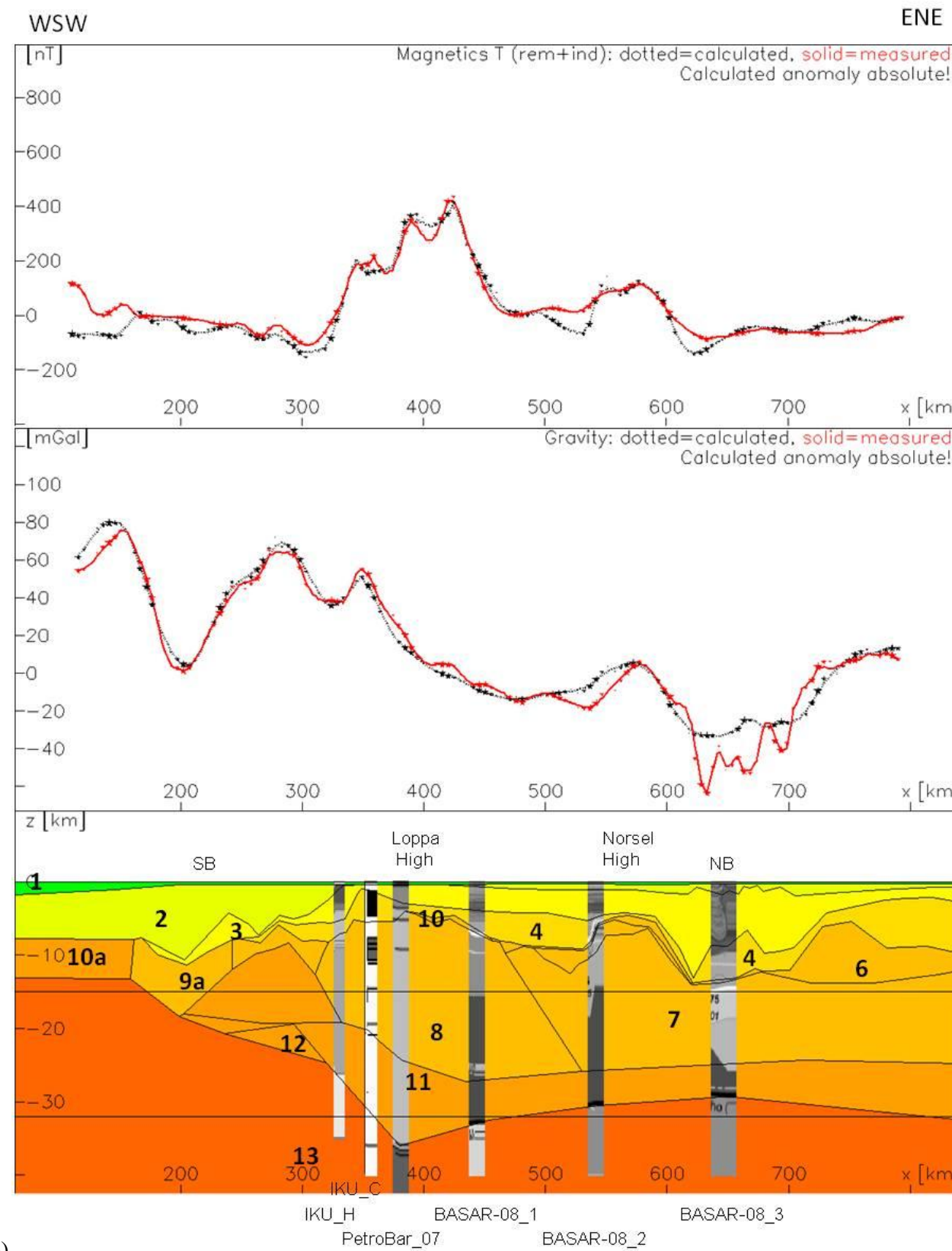
This profile (10b) shows a cross-section from the Sørvestsnaget Basin over the Veslemøy and Loppa highs to the Bjarmeland Platform and the central Nordkapp Basin. The Veslemøy High shows a similar feature as the Senja High in the potential field data and thus is considered as a similar structure.

The Moho depth beneath the Loppa High is derived from the results from the OBS line Petrobar07 (Clark *et al.* 2009), increasing to c. 35 km, which fits well with the gravity data. The magnetic high at the Loppa High confirms again the different basement structure of this block in comparison to its surroundings.

On the Bjarmeland Platform the profile crosses the tail like structure observed from the magnetics (Brønner *et al.* 2009), which obviously appears as a kind of compressional front in the basement and marks the western boundary of the Nordkapp Basin, while the eastern flank is composed of thickened Caledonian basement.

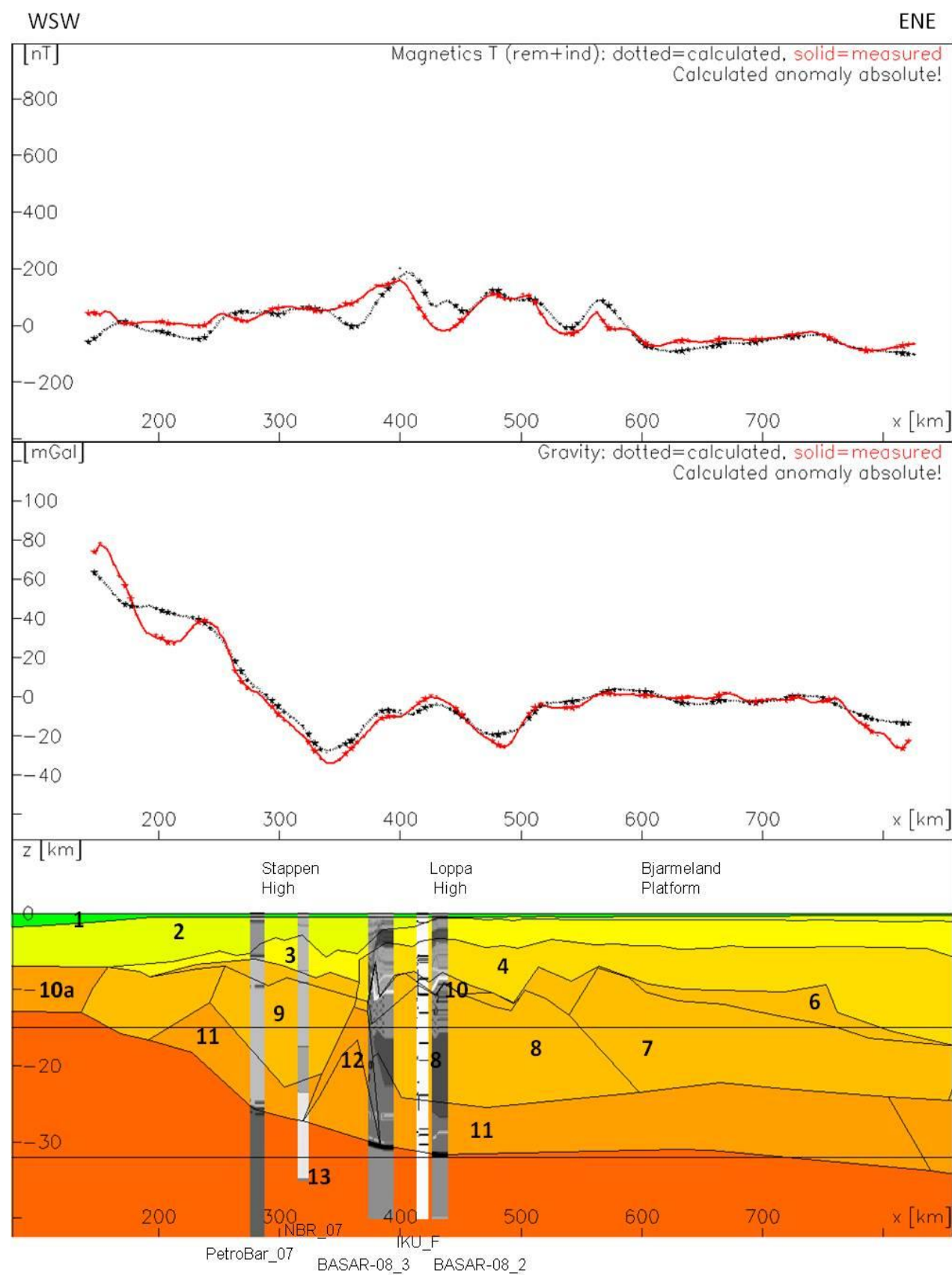
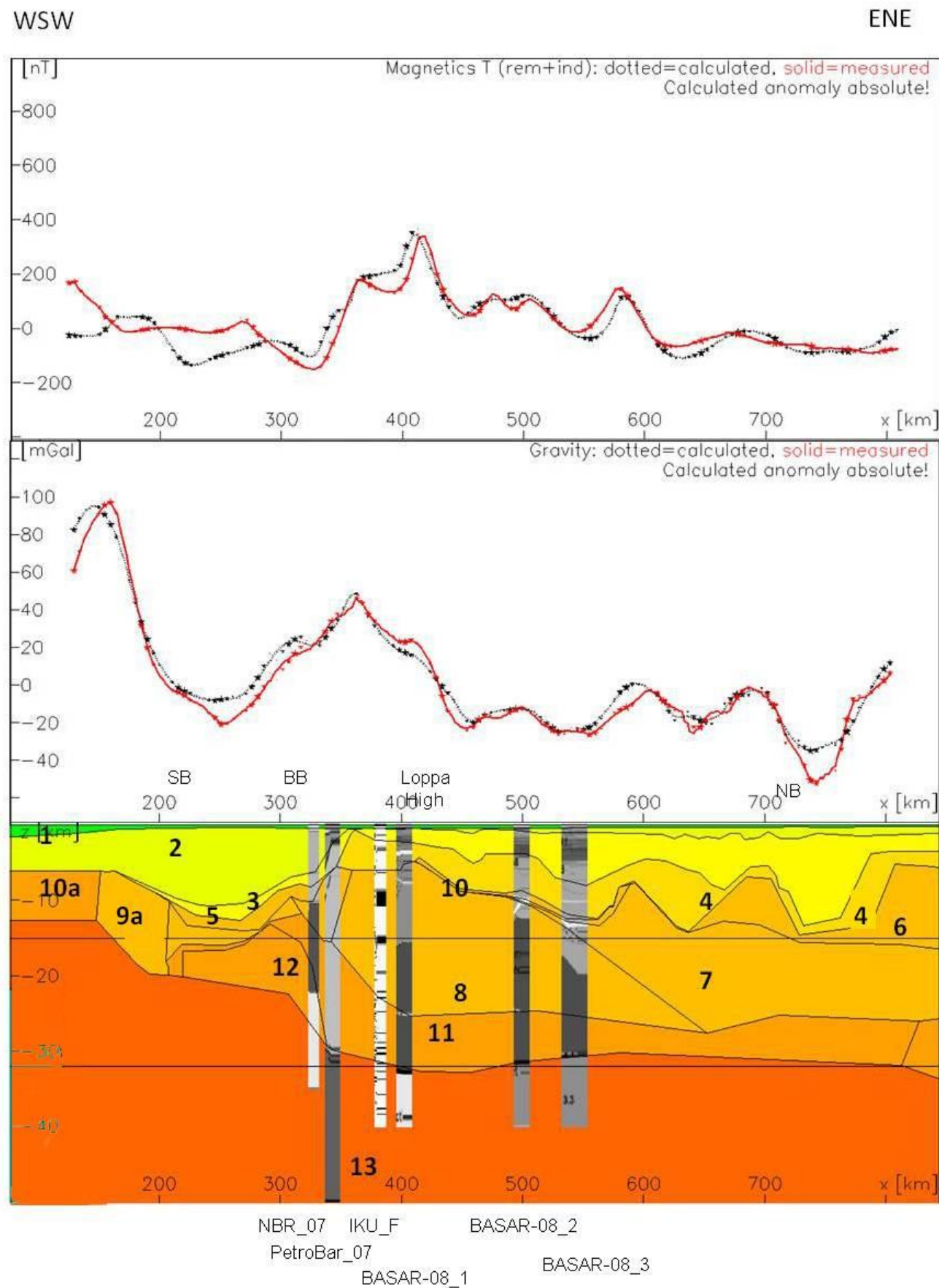


a)



b)

Figure 12.8 ENE-WSW oriented cross-sections from the 3D model: a) Profile 9a and b) 10b with magnetic and gravity correlation between observed and calculated field. The model geometry from the 3D model with addressed units and parameters (See Table 12.1) is shown.



a)

b)

Figure 12.9 ENE-WSW oriented cross-sections from the 3D model: a) Profile 11a and b) 12b with magnetic and gravity correlation between observed and calculated field. The model geometry from the 3D model with addressed units and parameters (See Table 12.1) is shown.

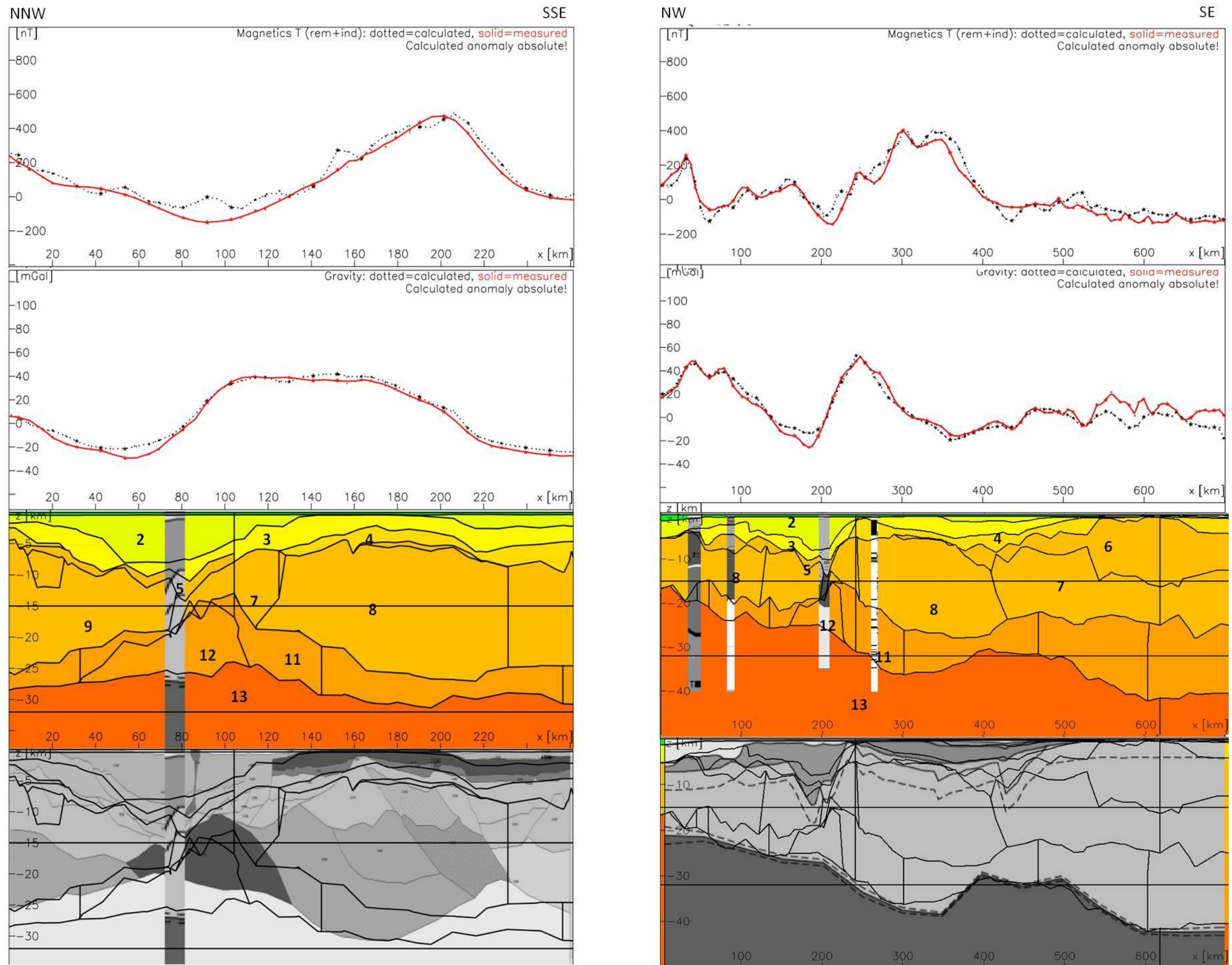


Figure 12.10 NW-SE oriented cross-sections from the 3D model: a) NBR07-232948 b) Petrobar_07 with magnetic and gravity correlation between observed and calculated field. The model geometry from the 3D model with addressed units and parameters (see Table 12.1) is shown, and a comparison between the 3D model results and the ones from the 2D interpretation.

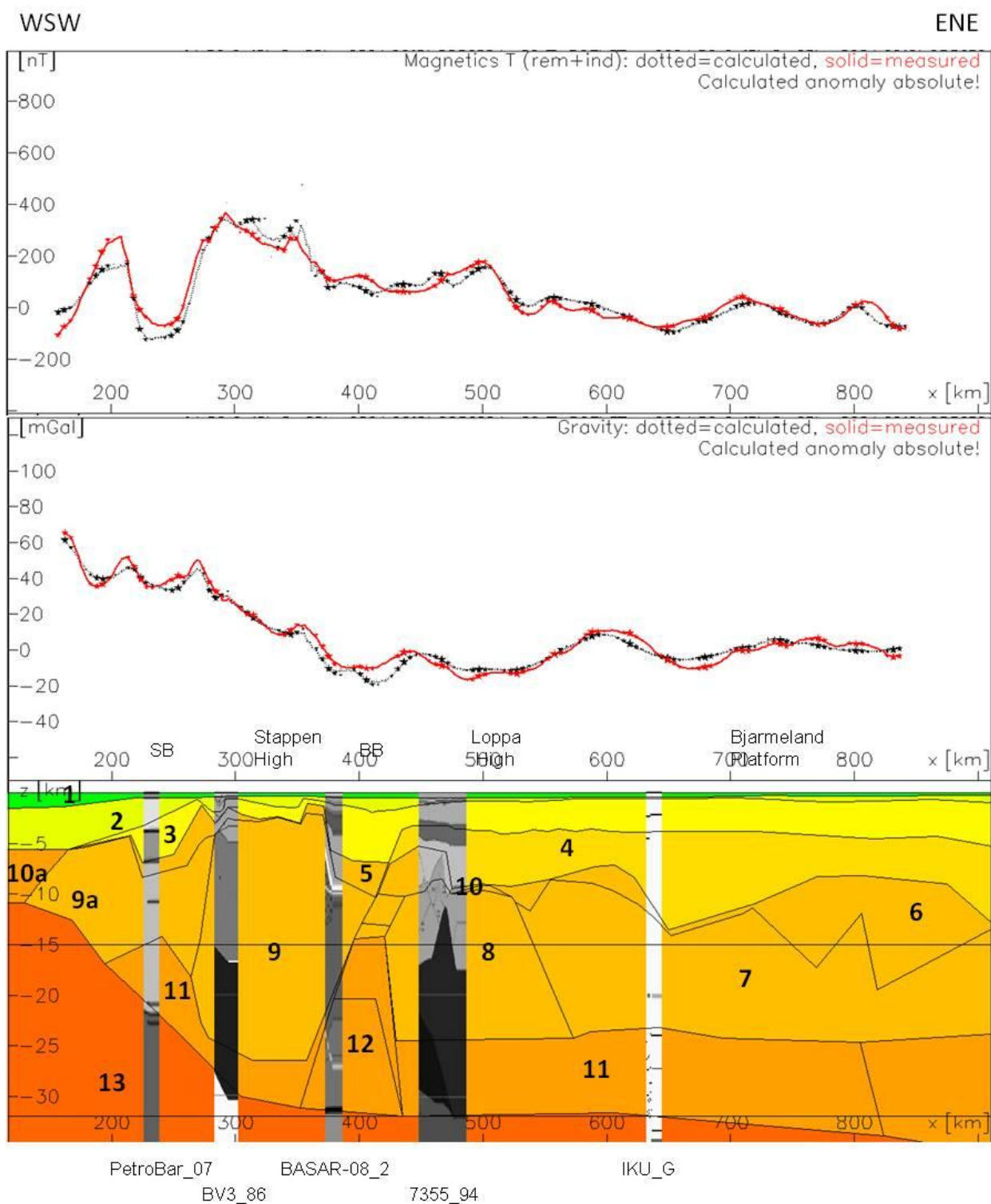


Figure 12.11 ENE-WSW oriented cross-section from the 3D model: Profile 13b with magnetic and gravity correlation between observed and calculated field. The model geometry from the 3D model with addressed units and parameters (See Table 12.1) is shown.

Interestingly, Moho depth is in the order of 30-32.5 km below the Bjarmeland Platform and northwards and shows a gradual decrease from north to south.

Farther to the north, the presented profile 11a (Fig. 12.9a) runs across the Sørvestsnaget Basin, Bjørnøya Basin, Loppa High and the Bjarmeland Platform to the northeastern part of the Nordkapp Basin.

The boundary between the Sørvestsnaget Basin and the Bjørnøya Basin is barely expressed on the gravity data, but on the magnetics the Bjørnøya Basin appears as a noticeable minimum. Clark *et al.* (2009) identified the Moho at the western flank of the Bjørnøya Basin at about 30 km, whilst our interpretation of a NBR line to the west (Ch. 10) sees the Moho already much shallower at 22 km. From 3D modelling such a large increase seems to be difficult to accept but the trend is reliable, although crustal thinning and an increase in the thickness of the sediments are contradictory to an increase in the magnetic signal over the Sørvestsnaget Basin. We therefore incorporated a LCB in the model as proposed by Barrère *et al.* (2009) and in the 2D modelling (Ch. 11). The LCB is of high density and high magnetisation which would appear to contradict the results from the 2D modelling. From the 3D model, however, we observe the need for an increase in the magnetisation towards the north, which either indicates a significant northward thickening of the LCB or an increase in magnetisation in that direction. However, as a simplification we decided to implement in the 3D model a LCB with higher magnetisation, which results in a different geometry to that of the 2D modelling (Fig. 12.11a) but confirms the need and supports the scenario for a LCB along the axis of the Bjørnøya Basin.

The northernmost part of the Nordkapp Basin overlies Caledonian basement, inferred to comprise several thrust sheets and thus comparable to what we observe onshore northern Norway.

Profile 12b (Fig. 12.9b) crosses south of the Stappen High and the northern edge of the Loppa High with the Bjørnøya Basin in between. It also crosses the Mercurius High and the Bjarmeland Platform.

The Mercurius High is rather inconspicuous from both the gravity and the magnetics. The Bjarmeland Platform shows rather small variations in both datasets and reveals the interaction of the two overlying Caledonian and Precambrian basement types, which are sufficient to explain both gravity and magnetics perfectly.

The Stappen and Loppa highs are observed from seismics to have similar top basement depths, but the signature in the observed potential field data is different and the Stappen High appears much smaller in amplitude, which indicates different basement structures for these two prominent highs (see Ch.11). This is even more obvious in profile 13b (Fig. 12.11), where the Stappen High is rather shallow and is still not particularly well expressed, either in the gravity

or magnetic data. The Loppa High basement shows a noticeable higher density and magnetisation.

The Bjørnøya Basin in between the two highs is observed from seismics to have thick sedimentary successions of more than 10 km, which at the eastern flank in particular is in contradiction to the observed gravity and magnetic field. We have already discussed the need for a high-density LCB, but from the 3D modelling, a high-density high-magnetic body is indicated along the profiles 12a and 13b to explain the observed fields, which could be explained by a significant crustal thinning, serpentinization of the uppermost mantle and intrusions penetrating the crust. The interpreted seismic sections Figs 12.10a & b are unfortunately not ideally located to confirm this indication, but such an interpretation appears to be rather self-evident to us since alternative magnetic sources such as sill intrusions in the sediments have hitherto not been reported from the Bjørnøya Basin.

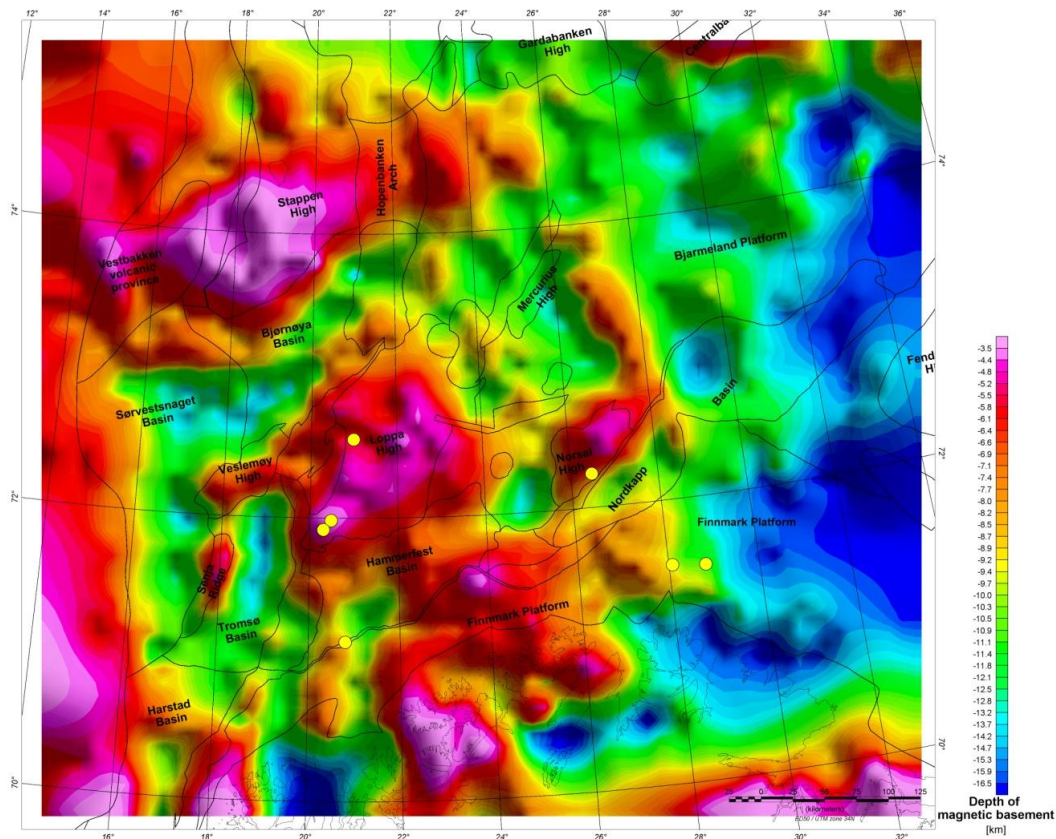
The correlation between the two seismic lines and the 3D model is fairly good. The Petrobar_07 profile fits very well, while the NBR line shows some differences in particular in the Moho geometry. Based on the 2D interpretation the Moho is shallower underneath both the Bjørnøya and the Hammerfest Basin. For the Hammerfest Basin, from 3D modelling, a bulging Moho is not indicated along the line, but is slightly displaced to the west (Fig. 12.13), a feature which might be caused by possible side effects in the 2D modelling. The need for a LCB beneath the Bjørnøya Basin is also obvious from 3D modelling and has been discussed earlier. The discrepancies in the Moho configuration are most likely a combination of the different model resolutions and 3D effects. The general concept, however, is supported by the 3D model.

12.4.3 Depth to top basement

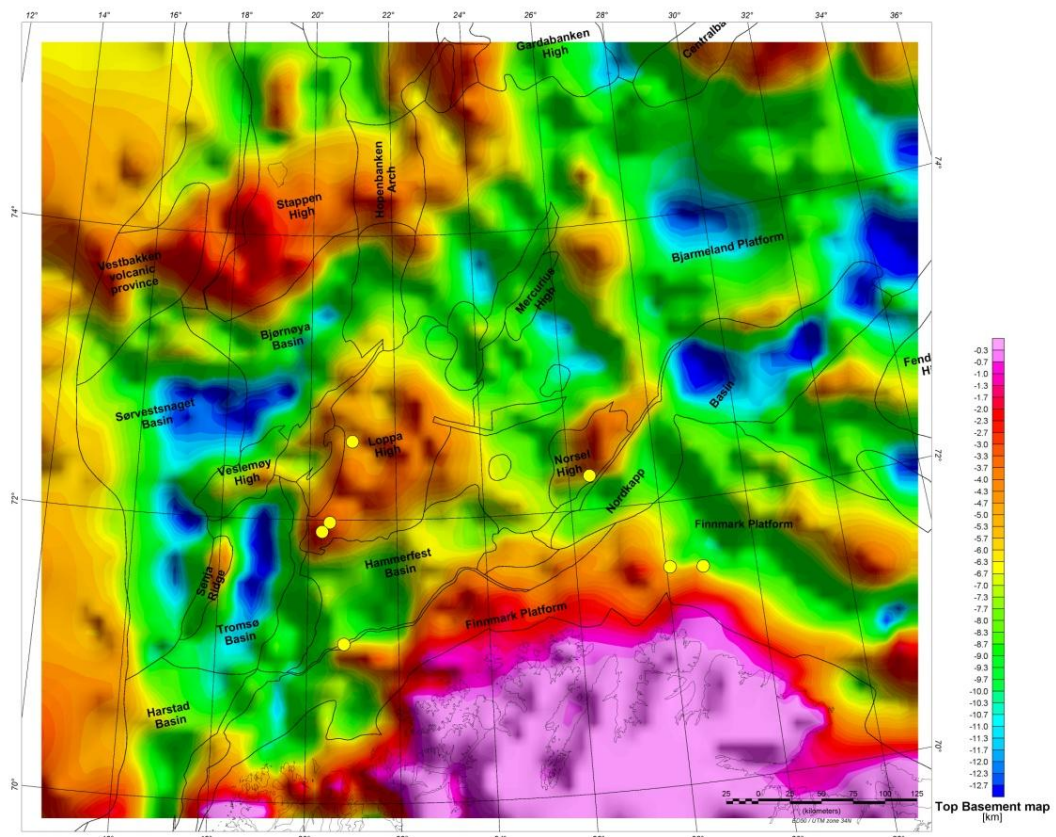
In the presented model we differentiated between the top of the magnetic source and the low-magnetic Caledonian basement to define the top basement more accurately (Figs. 12.12a & b). We will refer to the different top basements as '*top basement*' (Fig. 12.12b) and '*top magnetic basement*' (Fig. 12.12a).

Over large parts of the shelf, the top basement is located at depths between 4 and 10 km. The shallowest basement (< 2 km) is mapped at the Stappen High, southwest of Bjørnøya. The pre-Devonian 'economic basement' on Bjørnøya represents Precambrian to Lower Palaeozoic metasedimentary rocks (Worsley *et al.* 2001) and was not considered as basement in this model.

Three wells were drilled into the Loppa High basement (Tab. 9.2), whereof the northernmost one reached basement already in a depth of c. 1500 m. We could not get additional information about the lithology or petrophysical parameters of the drilled basement, but from modelling we can exclude the general high-magnetic 'Loppa High basement' type in such a shallow position.



a)



b)

Figure 12.12 a) Depth-to-magnetic basement as defined in the 3D model with different basement units (see in Table 12.1): b) Top basement map including Caledonian nappes as defined in the 3D model.

The drilled basement in well 7220/6-1 must be low-magnetic and either a kind of '*economical basement*' or low-magnetic Caledonian basement as it was discussed for the structural interpretation (Ch. 10).

The deepest top basement is observed in the basins at c. 14 km, more specifically in the Sørvestsnaget, Bjørnøya, Tromsø and central Nordkapp basins. The Hammerfest and southern Nordkapp basins, however, are comparatively shallow with 10 km and 11 km depths for the top basement, respectively.

Comparing both basement structures, the major differences are observed east of the Norsel High. There the top magnetic basement is dipping eastwards down to c. 17-18 km depth, whilst the top basement is on average at 10 km depth. The thickness of the low-magnetic Caledonian basement is apparently increasing towards the east to up to 8 km, which is comparable with the estimated thickness of the nappes onshore Mid Norway (Olesen *et al.* 2007).

This result is disputable though, because of the interference of the Timanian orogeny from the east and a possible change in the composition of the basement in the eastern Barents Sea.

The NW-SE striking Timanian trend is predominant in the eastern Finnmark Platform, on the easternmost Varanger Peninsula and in the southeastern Barents Sea (Brønner *et al.* 2009, Gernigon *et al.* 2007), but from petrophysical observations onshore there is no direct evidence for any significant change in the character of the Precambrian basement and the observed Timanian trends could just reflect the tectonisation and fault activation that occurred during this Late Neoproterozoic collisional event.

From 3D modelling the distribution of Caledonian basement shows a relevant thickness onshore northern Norway, the Finnmark Platform and offshore in the eastern half of the model area. Although a clear identification and differentiation between Caledonian basement and compacted sediments is difficult at greater depths, (>8-10 km, see above), for the western half of the model area, north of the Finnmark Platform, Caledonian basement seems to be inferior and probably thin or absent in large areas west of the Norsel High. The basins here are embedded in magnetic, most likely older Precambrian basement. Basement depth from seismics and the magnetisations resulting from 3D modelling lend support to this conclusion.

East of the Norsel High in the central Nordkapp Basin, however, the basin flanks are formed of low-magnetic Caledonian basement and reflect the occurrence of the Caledonian nappes in this area.

Former studies presented different interpretations of the basement domains, based on the petrophysical characteristics they found from potential field interpretation and modelling (Barrère 2009, Marellò *et al.* 2010). With our modelling approach presented here, we could

show that the superpositional effect of different basement types lying on top of each other is an alternative to explain the observed magnetic field variations, and also reflects better the geometries we observe onshore. Disregarding local variations within the basement, the Barents Sea continental shelf basement is probably more homogeneous than expected and the field variations are a product of the superposition of Caledonian and Precambrian basement. Exceptions are Loppa High as a high-magnetic high-density basement block and the westernmost part of the model area at the COT, which probably has a different composition due to the alteration of the crust and the interaction with the mantle during the extension and break-up processes.

Furthermore, the Loppa High has been shown to be a solid basement block with a significantly higher density and magnetisation, whilst the Stappen High is different and it thus remains unclear whether it represents a different basement type or an intermingling of the 'Loppa basement type' with the surrounding 'Precambrian Barents Sea basement'. From 3D modelling, however, we observe a general basement type which, concerning its petrophysical parameters, reflects an average Precambrian basement as observed onshore northern Norway and is sufficient to explain the gravity and magnetic observations for the greater part of the study area, overlain by a significant thickness of low-magnetic Caledonian basement in the eastern part of the model.

12.4.4 Depth to the crust-mantle boundary (Moho)

The Moho (Fig. 12.13) is, in general, associated with a density contrast of 350 kg/m^3 between the lower crust and the upper mantle. Only across the lower crustal body (LCB) is this contrast slightly smaller. The resulting Moho geometry is adjusted to the constraining 2D profiles and reflects the Moho of Grad *et al.* (2009) in the remaining parts where we have no further constraints. The Moho undulates over the continental shelf between depths of c. 20 and 35 km and shows a general deepening in E- direction. Beneath onshore northern Norway the Moho is observed at larger depth of more than 40 km.

In the region of the Sørvestsnaget and Tromsø basins the Moho depth is rather constant at c. 20 km. The Hammerfest and Nordkapp basins are characterised by a bulging of the Moho, whilst the Loppa High shows a local Moho low with a depth of c. 35 km. For the Bjørnøya Basin, the Moho is of intermediate depth, gently dipping towards northeast from c. 20 km to 31 km, but the indication of a lower crustal body (LCB) with high density (Fig. 12.11) reveals significant crustal thinning and most likely an intensive interaction between crust and upper mantle along the basin axis. This is in agreement with the results of Clark *et al.* (2009) (Fig. 12.10b) who interpreted a much shallower Moho than had earlier been assumed west of the Loppa High.

The Stappen High, however, shows a local E-W striking deep in the Moho, whereas the rest of the Stappen High has a similar Moho depth as its surroundings and does not have the same imprint as the Loppa High (see above).

On the Bjarmeland and Finnmark platforms, the Moho is at a depth of c. 30 km and is dipping towards the east. The configuration mainly derived from Grad *et al.* (2009) and is in good correlation with the observed gravity data.

12.5 Conclusions

The 3D model displays a wealth of new and interesting information. Here we have limited ourselves to the ones which appear to be most important in the context of the scope of this project.

- The 3D model could test and confirm the different scenarios proposed from the 2D modelling.
- The LCB underneath the Bjørnøya Basin extends along the basin axis and reflects the amount of extension and crustal thinning that the basin was exposed to during its evolution.
- Thin layers of high-magnetic magmatic rock are locally detected on top of the Loppa and Norsel highs, as indicated by the observed magnetic field and observed on the Loppa High in two wells.
- The superposition of low-magnetic Caledonian and high-magnetic Precambrian basement on the Barents Sea shelf has a significant impact on the observed magnetic field variations and can distort and falsify a characterisation of the underlying basement
- The Loppa High has been identified as a large basement block of a different basement type than its surroundings. The nature of Stappen High, however, remains unclear; either it is another basement type on its own or it may represent an intermingling of different basement types.
- The Moho map reveals a thickening of the crust at the Loppa and Stappen highs and crustal thinning beneath the large basins.

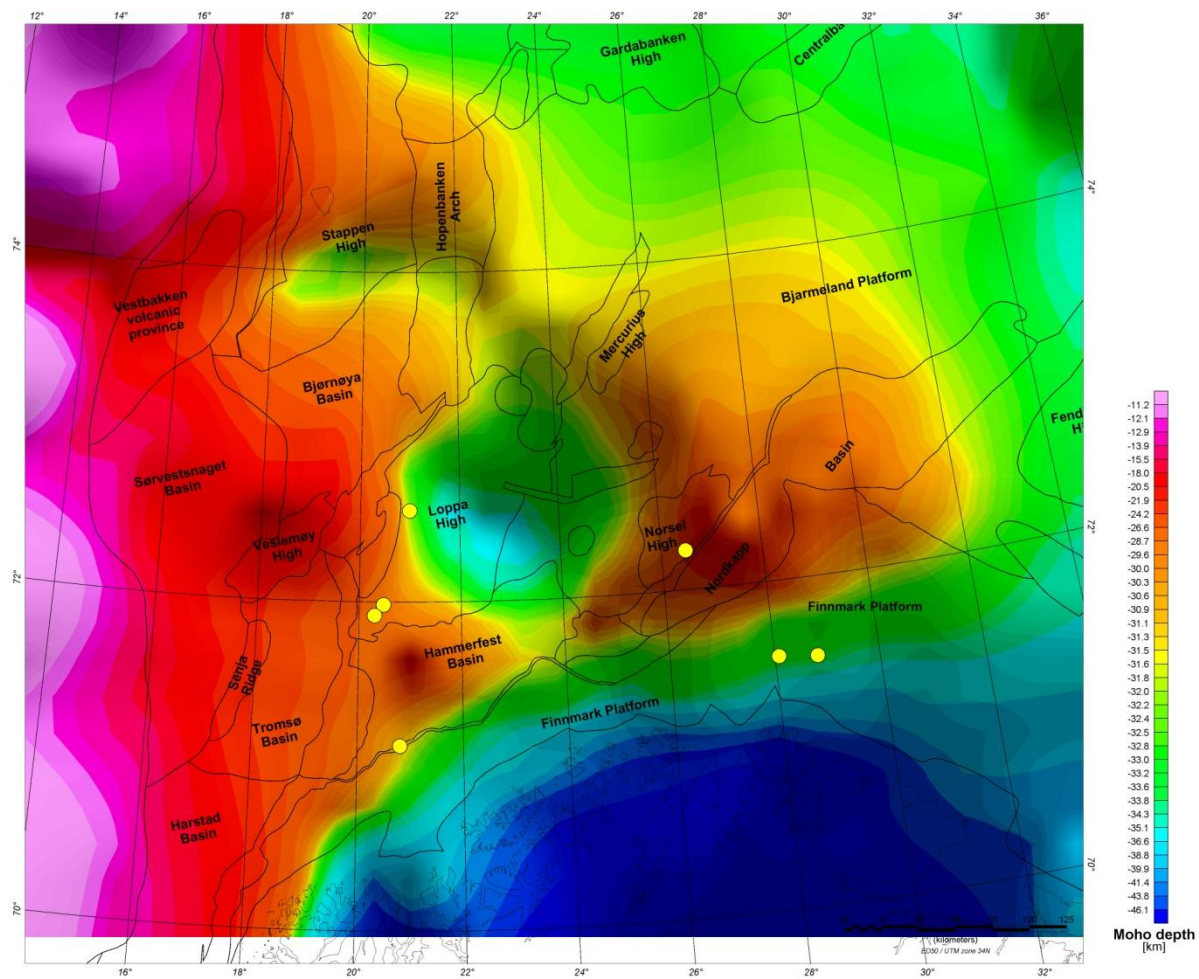


Figure 12.13 Depth to Moho from the 3D model.

13 2D THERMAL MODELLING

Christophe Pascal & Laurent Gernigon

13.1 Introduction

This chapter presents the results of the thermal modelling. Instead of conducting 3D modelling over the surveyed area of the Barents Shelf and consequently loosing the resolution needed to address the fine structure of the sedimentary basins, we preferred to focus on detailed 2D modelling of the NBR-232948 profile that has been interpreted in the previous chapters. The purpose of the modelling is to explore the influence of the complicated crustal structure along the NBR-232948 profile on the static thermal field.

13.2 Modelling approach

The computations were carried out using the commercial software FLAC3D 4.00 (www.itascacg.com/flac3d). FLAC3D is a modelling code designed to calculate large deformations and involves different types of rheologies but can also be used for steady-state or transient thermal computations. The code utilises an explicit finite difference formulation. In the present case, we used FLAC3D to solve the three-dimensional form of the steady-state heat equation:

$$q = -k \cdot \frac{\partial T}{\partial z} \quad (1)$$

where q is heat flow, k thermal conductivity, T temperature and z depth (positive downwards). More detailed mathematical aspects can be found in e.g. Haenel *et al.* (1988).

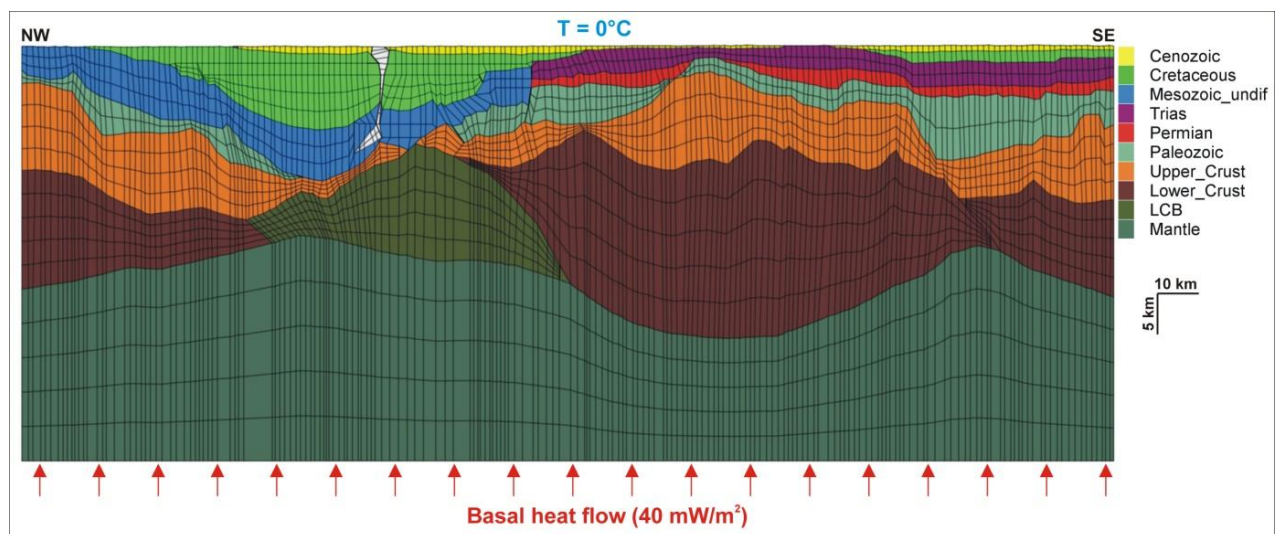


Figure 13.1 Modelling setup used in the present study. Surface temperatures and basal heat flow are applied and each rock unit has its own thermal properties (i.e. heat generation and thermal conductivity, Table 12.1). Note the salt pillow shown in white inside the Bjørnøya Basin.

Because FLAC3D is a full 3D code, our ‘2D’ model was built as a vertical thin plate with uniform geometries and properties along the Z axis. We built the geometry of the ‘2D’ thermal model according to the results of the crustal modelling presented in Chapter 11 (Fig. 11.7). The dimensions of the model and the rock units introduced in it are shown in Figure 12.1. The model involves ~8900 grid points and ~4200 zones with, in general, an irregular brick shape, allowing for a satisfactory accuracy.

Equation (1) is solved considering the presence of internal sources of heat (i.e. heat generation by decay of radioactive elements in rocks) and considering the set of boundary conditions given in Figure 13.1. Temperatures are fixed at the top edge of the model and set equal to 0°C. This temperature does not obligatorily correspond to present-day, sea-bottom temperatures but represents an approximation of the average temperature prevailing during latest Cenozoic times, deep underground temperatures being presumably in equilibrium with the long-term average surface temperature. A basal heat flow of 40 mW/m² was estimated by us using a trial-and-error approach, calibrated by measured temperatures in exploration wells. Heat generation rates (Table 13.1) were inferred according to lithological composition (Rybach 1988).

	Thermal conductivity (W/K.m)	Heat generation (μ W/m ³)
Salt	2.0 to 6.0	0.01
Cenozoic	1.5	1.5
Cretaceous	1.8	1.5
Mesozoic undiff.	2.0	1.5
Triassic	2.0	1.5
Permian	2.0	1.5
Palaeozoic	2.5	1.5
Upper crust	2.5	2.0
Lower crust	3.0	0.2
LCB	3.5	0.01
Mantle	3.5	0.01

Table 13.1 Thermal parameters used in the modelling.

Thermal conductivity values (Tab. 13.1) were also selected according to the lithology of the rocks penetrated in exploration wells (Clauser & Huengens 1995). Most sediments in the Barents Sea are shales and claystones bearing low thermal conductivity values (Smelror *et al.* 2009). It is noteworthy that an increase in thermal conductivity following compaction is simulated by means of setting higher values to the deepest or later exhumed sediments. We also set up the thermal conductivity values considering their decrease with temperature. Because rock salt is usually devoid of porosity, we only considered the effect of temperature when setting up thermal conductivity values for the salt pillow modelled in the Bjørnøya Basin (Fig. 13.1). Consequently, we assumed a gradual decrease in thermal conductivity from 6 W/K.m at the top of the salt dome, to 2 W/K.m at the root of the salt pillow. Standard values were used for the basement and the mantle with the exception of the Lower Crustal Body (LCB), which

most probably represents a mixture of ultramafic rocks whose thermal properties are assumed to be close to those traditionally attributed to mantle rocks.

13.3 Results

As a rule of thumb, model results need to be interpreted in terms of combinations of the blanketing efficiency of the cover rocks with distribution of internal sources of heat. The first-order control on lithosphere geotherms is exerted by variations in the thickness of the crust, which is on average less conductive than the mantle (Tab. 13.1), and explains the ‘wavy’ shape of the mantle isotherms (Fig. 13.2a). In detail, the depression of the modelled isotherms below the Bjørnøya Basin is further enhanced by (1) the high thermal conductivity (i.e. no thermal insulation of the underlying mantle) and very low heat generation attributed to the Lower Crustal Body (LCB), and (2) the extreme attenuation of the upper crust (i.e. the most heat-generating unit of the model).

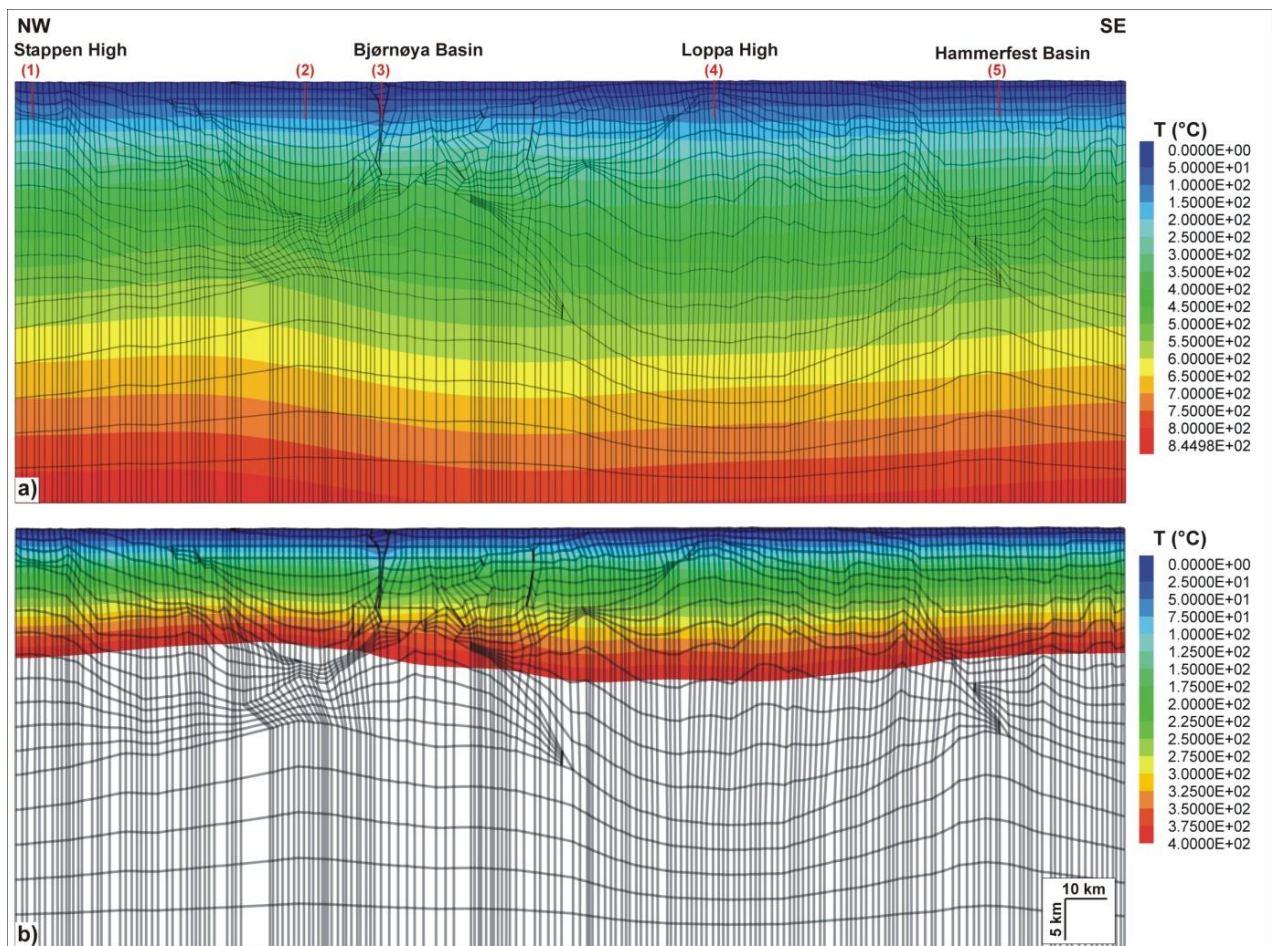


Figure 13.2 Modelled isotherms up to a) $\sim 850^{\circ}\text{C}$ and b) 400°C . Red vertical profiles depict locations where modelled temperatures were extracted for comparison with temperature data from exploration wells (see Fig. 12.3).

The blanketing effect of the thick pile of mainly Cretaceous shales in the Bjørnøya Basin is particularly pronounced in its northwestern part and highlighted by a significant rise in temperatures at depth (Fig. 13.2b). This effect is counteracted to the southeast by the reduction in size of the upper crust and the sediments and increase in thickness of the LCB, which is equivalent to reducing the abundance of heat-generating elements and decreasing the average thermal conductivity. Again, the blanketing effect of the thick sedimentary cover is well illustrated for the Hammerfest Basin. On average thermal conductivity of the sediments is higher for this basin than for the Bjørnøya Basin (Tab. 13.1) and, consequently, thermal blanketing less efficient. However, the thicker upper crust below the Hammerfest Basin results in a higher heat input as compared to the Bjørnøya Basin. The relatively high thermal conductivities on the Loppa High result in lower geothermal gradients with respect to the surroundings (Fig. 13.2b).

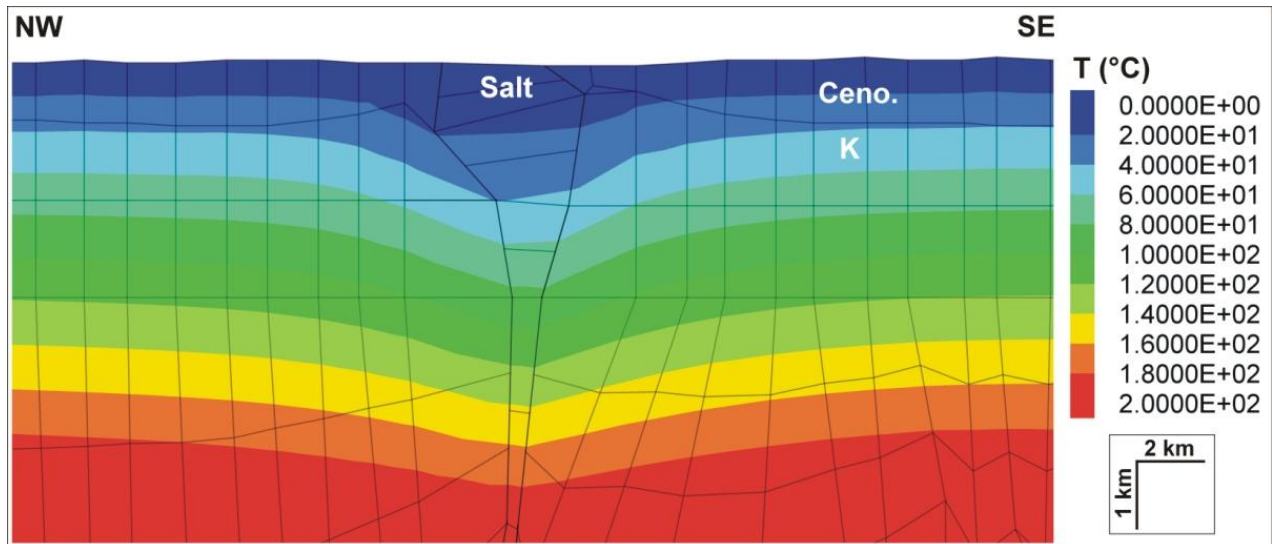


Figure 13.3 Snapshot of modelled temperature (see Fig. 12.2) showing the significant depression of the isotherms caused by the salt dome.

The most significant reduction in geothermal gradients is produced by the salt pillow in the Bjørnøya Basin (Figs.13.2 & 13.4). The very high thermal conductivity of salt as compared to the host rocks and to some extent its very low heat generation (Tab. 13.1) are responsible for the comparatively low temperatures that are modelled. The reduction in temperatures reaches up to $\sim 30^{\circ}\text{C}$ at 2 km depth but the effect is gradually damped farther down because of the assumed decrease in salt conductivity with temperature. The traditional view that salt domes produce positive thermal anomalies (e.g. Yu *et al.* 1992) does not hold in the present case, because our studied salt dome reaches the sea floor. As such, the dome can be viewed as an efficient path evacuating underground heat to the surface where it dissipates.

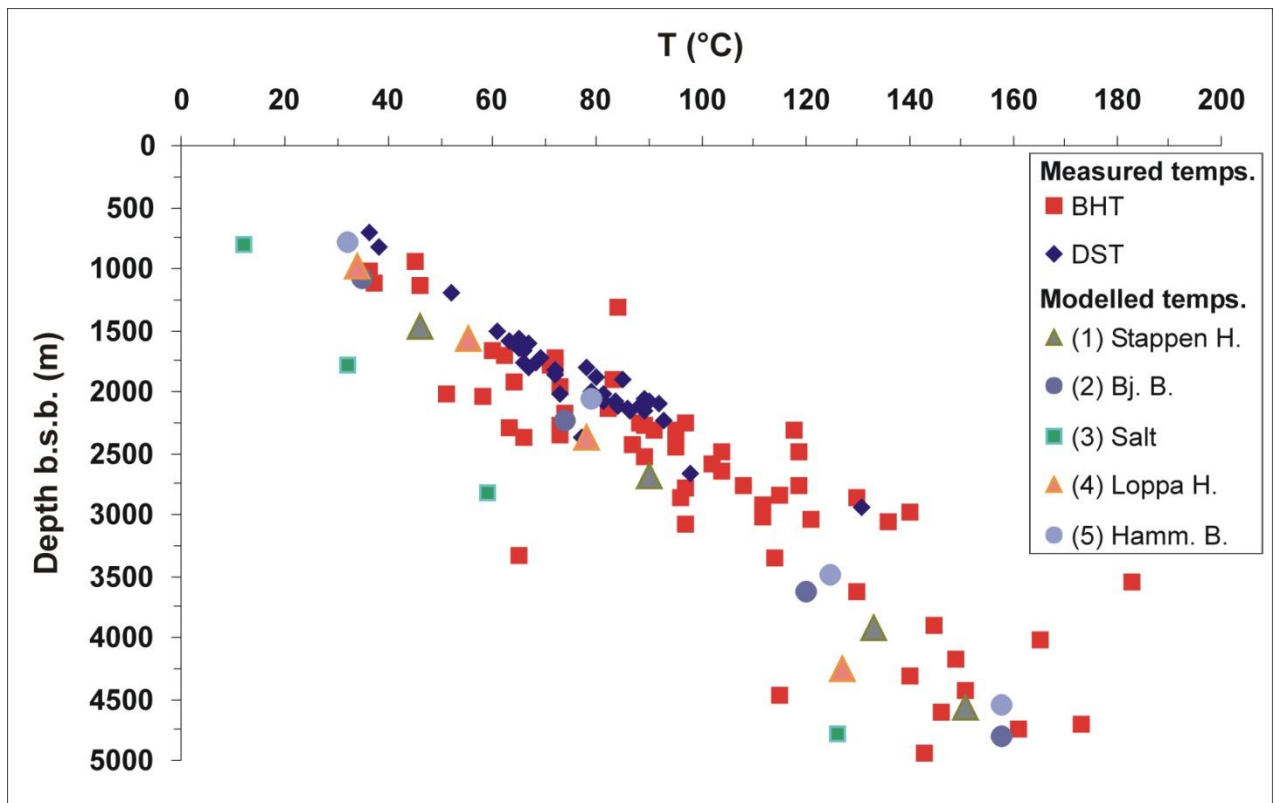


Figure 13.4 Comparison between modelled and measured temperatures in exploration wells (data source: Norsk Oljedirektoratet). Numbers refer to the sampling locations inside the numerical model (see Fig. 1.2). BHT = bottom-hole temperature, DST = drill-stem test.

Figure 13.4 shows modelled temperatures sampled at different depths and for five selected profiles (see location in Fig. 13.2) together with 95 temperatures measured in exploration wells in the western Barents Shelf and made available by the Norwegian Petroleum Directorate (see details in Pascal *et al.* 2009). DST temperatures are usually considered to be more reliable than BH temperatures (e.g. Goutorbe *et al.* 2007). However, in the present case DST temperatures are limited to the upper 3 km where they appear to be in somewhat reasonable agreement with BHT measured at equivalent depth levels. Down to ~2.5 km depth, DST and BH temperatures result in geothermal gradients of 38°C/km and 34°C/km, respectively. Interestingly, BHT data suggest a reduction in geothermal gradient down to 22°C/km and below 2.5 km, consistent with the hypothesis that thermal conductivities increase with depth and also with our modelling results.

A reasonable fit between data and modelled temperatures is obtained, in particular for the Hammerfest Basin profile where the highest temperatures and an average gradient of 33°C/km are also modelled (Fig. 13.4). The modelling results suggest slightly lower temperatures for the Bjørnøya Basin and the Stappen High but with similar geothermal gradients. The modelling suggests lower thermal gradients for the Loppa High (i.e. 28°C/km on average). As stated above, temperatures and geothermal gradients in the salt dome (and below) are considerably

reduced, in particular at shallow depths (i.e. 20 C/km between 1 and 2 km depth) and increase significantly at deeper levels (i.e. 34°C/km between 3 and 5 km depth).

13.4 Conclusions

Any thermal modelling study at the crustal scale is always hampered by a deficiency or lack of control points especially at great depths. Nevertheless, modelling a crustal section constrained by a wealth of geophysical and geological data permits us to draw first-order conclusions awaiting for further refinements in the future.

The major conclusions of our modelling exercise for the NBR-232948 profile are:

- thermal gradients of $\sim 33^\circ$ C/km are predicted at shallow depths (i.e. down to 2.5 km depth) for most of the modelled profile, in reasonable agreement with gradients determined from BHT data at equivalent depths but 15 % lower than those determined from DST temperatures;
- gradients at the Loppa High (i.e. $\sim 28^\circ$ C/km) appear to be lower than the regional average;
- the presence of a thick LCB below the southeastern half of the Bjørnøya Basin results in reduced heat input and no thermal blanketing of the mantle and, consequently, lower temperatures with respect to the northwestern half of the basin;
- the presence of a salt pillow piercing the sea floor of the Bjørnøya Basin implies a dramatic cooling (i.e. by $\sim 30^\circ$ C at 2 km depth) of the sediments in the close vicinity of the pillow with respect to sediments occurring farther away.

14 CONCLUSIONS AND PERSPECTIVES

14.1 Main results

- The new high-resolution aeromagnetic survey BASAR-09 yielded a consistent and high-quality aeromagnetic data set, identifying new and additional structures of short to intermediate wavelength. The data are of excellent quality and provide a new and more accurate magnetic picture for our geological understanding of the southern Norwegian Barents Sea.
- Various filters and derivatives were applied to enhance different magnetic features and to support the structural interpretation. A number of different lineaments were observed and correlated with both Caledonian and Timanian structures, providing a better image of the interaction of these two major events and the ancient development of the Barents Sea continental shelf.
- Additional fault structures and probable dykes were observed in the offshore domains, reactivated during the different rifting phases in the Barents Sea, providing new insights into the importance of rifting for the entire region.
- The Stappen and Loppa highs are the predominant magnetic features within the BASAR-09 survey area, and are linked to each other by a deep-seated narrow and elongated magnetic anomaly.
- With the acquisition of the new aeromagnetic survey BASAR-09 and the release of the high-resolution survey HRAMS-97/98, a new aeromagnetic map for the western Barents Sea has been compiled, reflecting a very comprehensive and in high-quality magnetic setting of the area.
- Onshore-offshore comparisons revealed a rather poor correlation between surface geology and magnetic signature. The Upper and Uppermost Allochthon of the Caledonides are evidently magnetically transparent and have little bearing on the magnetic signal.
- 2D grav/mag modelling along four regional seismic transects facilitates interpretation of the main structural elements highlighted by the BASAR-09 survey. The resulting models show the capability of integrated modelling for gaining additional information on sedimentary basins, intra-sedimentary geo-bodies and crustal geometries, but also reveal the weakness of the method when not giving sufficient consideration to 3D effects. This might partly explain the remaining discrepancies between calculated and

observed data and/or significant differences in the 2D and 3D modelling results.

- The Stappen and Loppa highs appear to be of a distinct and thick crustal terrane type obviously containing magnetic material. They may possibly have formed a ribbon microcontinent during the Palaeozoic and Mesozoic rifting episodes. The Loppa High is interpreted as a major continental rigid block that behaved as a ‘buffer’ region during Palaeozoic and subsequent Mesozoic rifting episodes and possibly earlier during the Caledonian orogeny.
- 3D modelling could test and confirm the general concepts proposed by the 2D modelling. The LCB underneath the Bjørnøya Basin is extending along the basin axis.
- Variations of the magnetic field, especially in the eastern half of the model could be explained by the superposition of two different basement types lying on top of each other, rather than with different basement domains.
- Heat flow modelling of one regional profile obtained a good fit between data and modelled temperatures and indicated a lower heat flow gradient for the Loppa High and lower temperatures in the Bjørnøya Basin due to the presence of the LCB.

14.2 Proposition for further work

The interpretation work of the high-quality aeromagnetic data set in combination with gravity is limited due to the ambiguity of the methods. Geometrical constraints are crucial and can only be achieved by a joint interpretation with seismic data. The structural interpretation of the data set proved the capabilities of potential field data to get a comprehensive overview of the structural and tectonic setting of an area. 2D and 3D modelling are beneficial to prove or disprove different scenarios, but they have to be constrained by additional seismic data.

To better understand the origin of e.g. Stappen High and Loppa High and the difference in the basement setting between the western and eastern part of the study area and to evolve a more detailed evolution theory for the Barents Sea, more information from seismic is necessary.

With more constraining information on hand the existing 3D model can easily be refined and updated for the entire or a smaller area of interest to get more detailed information about a specific structure.

Since the Norwegian-Russian dispute in the Barents Sea is settled, we propose a new aeromagnetic survey in the Norwegian part of this area to complete the high-resolution aeromagnetic mapping for the Barents Sea.

Furthermore, the comparison of the HRAMS-97/98 with the BASAR-09 data reveals the higher resolution using a denser line spacing of 1000 m in the Barents Sea. For a better interpretation of intrasedimentary structures and for a more accurate onshore-offshore correlation we recommend to infill and densify the line spacing.

15 ACKNOWLEDGEMENTS

Det norske oljeselskap, Eni Norge, NGU, NPD, and Statoil financed the BASAR-09 survey. We express our thanks to these companies. We further wish to thank in particular Kai Hogstad, Hans Konrad Johnsen, Peter Midbøe, Morten Sand and Snorre Olaussen for giving valuable advice and assistance during the survey planning and interpretation.

We also want to thank David Roberts for the last minute corrections.



16 REFERENCES

- Alsgaard, P. 1993: Eastern Barents Sea late Palaeozoic setting and potential source rocks. *In* Vorren, T.O., Bergsager, E., Dahl-Stamnes, Ø.A., Holter, E., Johansen, B., Lie, E., Lund, T.B. (eds) Arctic Geology and Petroleum Potential. *Norwegian Petroleum Society, Special Publication 2, Elsevier, Amsterdam*, 405-418.
- Åm, K., 1975: Aeromagnetic basement complex mapping north of latitude 62 N, Norway, *Norges geologiske undersøkelse* 316, 351-374.
- Andréasson, P.G., Gee, D.G., Whitehouse, M.J. & Schöberg, H. 2003: Subduction-flip during Iapetus Ocean closure and Baltica-Laurentia collision, Scandinavian Caledonides. *Terra Nova* 15, No.6, 362–369.
- Andresen, A. 1980: The age of the Precambrian basement in western Troms, Norway. *Geol. För. Stockh. Förh.* 101, 1291-298.
- Andresen, A., Fareth, E., Bergh, S., Kristensen, S.E. & Krogh, E., 1985: Review of Caledonian lithotectonic units in Troms, North Norway. *In: D.G. Gee & B.A. Sturt (Eds.). The Caledonide Orogen-Scandinavia and Related Areas, John Wiley and Sons, London*, 569-578.
- Arkani, H.J. 1988: Differential reduction to the pole of regional magnetic anomalies: *Geophysics*, 53, 1592-1600.
- Arkani H.J. 2007: Differential reduction to the pole: Revisited. *Geophysics* 72(1), L13-L20.
- Armitage, P.E.B. & Bergh, S.G. 2005: Structural development of the Mjelde-Skorelvvatn Zone on Kvaløya: a metasupracrustal shear belt in the Precambrian West Troms Basement Complex, North Norway. *Norwegian Journal of Geology*, 85, 105-119
- Bain, J. & Weyand, J. A. 1993: Complex salt features resolved by integrating seismic, gravity and magnetics. *EAGE/EAPG Annual Meeting, Expanded abstracts*.
- Bain, J., Weyand, J. & Weber, M. 1994: Resolving Complex Salt Features Using Gravity and Magnetics. *Fugro-LCT Technical Papers*.
- Bainbridge, G., Musselman, C., Whitehead, N. & McDonald, N. 2002: Euler 3D Deconvolution (v5.1.5). Processing, analysis and visualization system for 3D inversion of potential field. Tutorial and User guide. *Geosoft Manual*. 66 pp.
- Barbosa, V.C.F., Silva, J.B.C. & Medeiros, W.E. 1999: Stability analysis and improvement of structural index estimation in Euler deconvolution. *Geophysics* 64(1), 48-60.
- Barbosa, V.C.F., Silva, J.B.C. & Medeiros, W.E. 2000: Making Euler deconvolution applicable to small ground magnetic surveys. *Journal of Applied Geophysics* 43(1), 55-68.
- Barrère, C. 2009: Integrated geophysical modelling and tectonic evolution of the western Barents Sea, Philosophiae doctor, Norwegian University of Science and Technology (NTNU), Trondheim. 185p.
- Barrère, C., Ebbing, J. & Gernigon, L. 2009. Offshore prolongation of Caledonian structure and basement characterisation in the western Barents Sea from geophysical modelling, *Tectonophysics*, 18 p.
- Beicip-Franlab 2002: Tutorial - EasyDepth 2.0. The Basin Modeling line. *Beicip-Franlab*, 28 pp.

- Bergh, S.G., Eig, K, Kløvjan, O.S., Henningsen, T., Olesen, O. & Hansen, J.A.: The Lofoten-Vesterålen continental margin: a multiphase Mesozoic-Palaeogene rifted shelf as shown by offshore-onshore brittle fault-fracture analysis. *Norwegian Journal of Geology, Vol. 87*, 29-58. Trondheim 2007. ISSN 029-196X.
- Bergh, S.G. & Andresen, A., 1985. Tectonometamorphic Evolution of the Allochthonous Caledonian Rocks between Malangen and Balsfjord, Troms, North Norway. *Norges geologiske undersøkelse Bulletin. 401*, 1-34.
- Berglund, T.L., Augustson, J.H., Færseth, R.B. & Ramberg-Moe, H. 1986 The evolution of the Hammersfest Basin. In Spencer, A. M. (eds.) *Habitat of Hydrocarbons on the Norwegian Continental Margin*. Norwegian Petroleum Society (Graham and Trotman), 319-338
- Birch, F. 1996: Compressibility, elastic constants. In Clark, S. P. (eds.) *Handbook of physical constants*. Geological Society of America, Memoir 97, 97-174
- Binns, R. & Gayer, R. 1980: Silurian or Upper Ordovician fossils at Guolasjav'ri, Troms, Norway. *Nature* 284, 53-55.
- Binns, R.E., Chroston, P.N. & Matthews, D.W. 1981: Low-grade sediments on Precambrian gneiss on Vanna, Troms, Northern Norway. *Norges geologiske undersøkelse Bulletin* 359, 61-70.
- Binns, R.E. 1985: Rapport om berggrunnsgeologiske undersøkelser på Helgøy 1:250 000 kartblad, Troms, sommeren 1985. p441-447
- Bjørkesett, S., Glørstad-Clark, E., Clark, S.A. & Faleide, J.I. Year: Late Permian Triassic geological evolution of the paleo-Loppa High, SW Barents Sea. In Nakrem, H. A., Olaus Harstad, A. & Haukdal, G. (eds.) *29th Nordic Geological Winter Meeting*. Geological Society of Norway Radisson Blu Scandinavia Hotel, Oslo, 22
- Bhattacharyya, B. 1966: Continuous spectrum of the total-magnetic field anomaly due to a rectangular prismatic body. *Geophysics* 31, 97-121.
- Blakely, R. 1995: Potential Theory in Gravity and Magnetic Applications. *Cambridge University Press*, 461p.
- Blakely, R.J. & Simpson, R.W. 1986: Approximating edges of source bodies from magnetic or gravity anomalies. *Geophysics* 51, 1494-1498.
- Blakely, R.J., Wells, R.E., Yelin, T.S., Madin, I.P. & Beeson, M.H. 1995: Tectonic Setting of the Portland-Vancouver Area, Oregon and Washington - Constraints from Low-Altitude Aeromagnetic Data. *Geological Society of America Bulletin* 107(9), 1051-1062.
- Braathen, A., Maher, H.D., Haabet, T.E., Kristensen, S.E., Tørudbakken, B.O. & Worsley, D. 1999: Caledonian thrusting on Bjørnøya: implications for Palaeozoic and Mesozoic tectonism of the western Barents Shelf. *Norsk Geologisk Tidsskrift* 79(1), 57-68.
- Breivik, A.J., Gudlaugsson, S. T. & Faleide, J. I. 1995: Ottar Basin, SW Barents Sea; a major upper Palaeozoic rift basin containing large volumes of deeply buried salt. *Basin Research* 7, 299-312.
- Breivik, A.J., Mjelde, R., Grogan, P., Shimamura, H., Murai, Y. & Nishimura, Y. 2005: Caledonide development offshore-onshore Svalbard based on ocean bottom

- seismometer, conventional seismic, and potential field data. *Tectonophysics* 401, 79-117.
- Breivik, A.J., Faleide, J.I. & Gudlaugsson, S.T. 1998: South-western Barents Sea margin: late Mesozoic sedimentary basins and crustal extension, *Tectonophysics*, 293, 21-44.
- Breivik, A.J., Mjelde, R., Grogan, P., Shimamura, H., Murai, Y. & Nishimura, Y. 2003: Crustal structure and transform margin development south of Svalbard based on ocean bottom seismometer data, *Tectonophysics* 369, 37-70.
- Breivik, A.J., Mjelde, R., Grogan, P., Shimamura, H., Murai, Y., Nishimura, Y. & Kuwano, A. 2002: A possible Caledonide arm through the Barents Sea imaged by OBS data, *Tectonophysics* 355, 67-97.
- Brekke, H., Sjulstad, H.I., Magnus, C. & Williams, R.W. 2001: Sedimentary environments offshore Norway - an overview. In Martinsen, O. J. & Dreyer, T. (eds.) *Sedimentary Environments Offshore Norway-Palaeozoic to Recent*. Norsk Petroleums Forening, Special Publication 10, 1-15
- Brønner, M., Gernigon, L., Ebbing, J., Olesen, O., Roberts, D., Barrère, C. & Koziel, J. 2009: Barents Sea Aeromagnetic Remapping BASAR-08: Acquisition, processing and interpretation. NGU report 2009.020, Geological Survey of Norway (NGU) Trondheim, 150 p.
- Brocher, T. M. 2005: Compressional and Shear Wave Velocity Versus Depth in the San Francisco Bay Area, California. Rules for USGS Bay Area Velocity Model 05.0.0. *U.S.G.S open-File Report* 05-1317, 1-58.
- Brueckner, H.K. 1971: The age of the Torset granite, Langøy, Northern Norway. *Norsk Geologisk Tidsskrift* 51, 85-87.
- Bugge, T. & Fanavoll, S. 1995: The Svalis Dome, Barents Sea a geological playground for shallow stratigraphic drilling. *First Break* 13, 237-251.
- Bugge, T., Elvebakk G., Fanavoll, S., Mangerud, G., Smelror, M., Weiss, H. M., Gjelberg J., Kristensen, S. E. & Nilsen, K. 2002: Shallow stratigraphic drilling applied in hydrocarbon exploration of the Nordkapp Basin, Barents Sea. *Marine and Petroleum Geology* 19, 13-37.
- Bugge, T., Mangerud, G., Elvebakk, G., Mork, A., Nilsson, I., Fanavoll, S. & Vigran, J. O. 1995: The upper Palaeozoic succession on the Finnmark Platform, Barents Sea. *Norsk Geologisk Tidsskrift* 75, 3-30.
- Bugge, T., Mangerud, G., Elvebakk, G., Mork, A., Nilsson, I., Fanavoll, S. & Vigran, J. O. 1995: The upper Palaeozoic succession on the Finnmark Platform, Barents Sea. *Norsk Geologisk Tidsskrift* 75, 3-30.
- Burg, J.P. 1975: Maximum Entropy Spectral Analysis, *PhD thesis, Stanford University*, 123 pp.
- Christensen, N.I. & Mooney, W.D. 1995: Seismic velocity structure and composition of the continental crust: A global view. *Journal of Geophysical Research - Solid Earth* 100, 9761-9788.
- Chroston, P. N. 1986: Gravity anomalies on Varangerhalvøya, Finnmark. *Norges Geologiske Undersøkelse Bulletin* 404, 45-56.

- Clark, D. 1997: Magnetic petrophysics and magnetic petrology aids to geological interpretation of magnetic surveys. *AGSO Journal of Australian Geology and Geophysics* 17, 83-103.
- Clark, S. A., Faleide, J. I., Ritzmann, O. and Mjelde, R. 2009: Multi-stage rift evolution of the SW Barents Sea from wide-angle seismic velocity modeling. [EGU2009-12559](#).
- Clauser, C. & Huenges, E. 1995: Thermal conductivity of rocks and minerals. In: Ahrens, T. J. (ed.) *Rock Physics and Phase Relations - a Handbook of Physical Constants*, AGU Reference Shelf, Vol. 3, pp. 105-126, American Geophysical Union, Washington.
- Cochran, J.R. & Karner, G.D. 2007: Constraints on the deformation and rupturing of continental lithosphere of the Red Sea: the transition from rifting to drifting. In Karner, G. D., Manatschal, G. & Pinheiro, L. M. (eds.) *Imaging, Mapping and Modelling Continental Lithosphere Extension and Breakup*. Geological Society, London, Special Publications 282, 265-289
- Cooper, G.R.J. & Cowan, D.R. 2006: Enhancing potential field data using filters based on the local phase. *Computers & Geosciences* 32(10), 1585-1591.
- Corfu, F., Armitage, P.E.B., Kullerud, K. & Bergh, S.G. 2003: Preliminary U-Pb geochronology in the West Troms Basement Complex, North Norway: Archaean and Palaeoproterozoic events and younger overprints. *Norges geologiske undersøkelse Bulletin* 441, 61-72
- Corfu, F., Torsvik, T.H., Andersen, T.B., Ashwal, L.D., Ramsay, D.M. & Roberts, R.J. 2006: Early Silurian mafic-ultramafic and granitic plutonism in contemporaneous flysch, Magerøy, northern Norway: U-Pb ages and regional significance, *Journal of the Geological Society London* 163, 291-301.
- Dallmeyer, R. D. 1992: $^{40}\text{Ar}/^{39}\text{Ar}$ mineral ages within the Western Gneiss Terrane, Troms, Norway: evidence for polyphase Proterozoic tectonothermal activity (Svecokarilian and Sveconorwegian). *Precambrian Research* 57, 195-206.
- Dallmeyer, R. D. & Andresen, A., 1992. Polyphase tectonothermal evolution of exotic Caledonian nappes in Troms, Norway: Evidence from $^{40}\text{Ar}/^{39}\text{Ar}$ mineral ages. *Lithos*. 29, 19-42.
- Dengo, C. & Røssland, K. 1992: Extensional tectonic history of the western Barents Sea. In Larsen, R.M. (ed), *Structural and tectonic modelling and its application to petroleum geology: Norwegian Petroleum Society Special Publication*, 91-107.
- Dobrin, M. & Savit, C. 1988: *Introduction to geophysical prospecting. 4th edition*. McGraw-Hill, 867 pp.
- Doré, A. 1995: Barents Sea geology, petroleum resources and commercial potential. *Arctic* 48, 207-221.
- Doré, A. G., Lundin, E. R., Fichler, C. & Olesen, O. 1997: Patterns of basement structure and reactivation along the NE Atlantic margin. The role of basement reactivation in continental deformation. *Journal of the Geological Society, London* 154, p. 85-92.
- Doré, A.G. 1991: The Structural Foundation and Evolution of Mesozoic Seaways between Europe and the Arctic. *Palaeogeography Palaeoclimatology Palaeoecology* 87(1-4), 441-492.

- Drinkwater, N.J., Pickering, K.T. & Siedlecka, A. 1996: Deep-water fault-controlled sedimentation, Arctic Norway and Russia: Response to Late Proterozoic rifting and the opening of the Iapetus Ocean. *Journal of the Geological Society* 153, 427-436.
- Ebbing, J., Gernigon, L., Pascal, C., Olesen, O. and Osmundsen, P.T. 2009: A discussion of structural and thermal control of magnetic anomalies on the mid-Norwegian margin. *Geophysical Prospecting*, 57, 665–681.
- Eldholm, O., Faleide, J.I. & Myhre, A.M. 1987: Continent-Ocean Transition at the Western Barents Sea Svalbard Continental-Margin. *Geology* 15(12), 1118-1122.
- Engen, O., Faleide, J.I. & Dyreng, T.K. 2008: Opening of the Fram Strait gateway: A review of plate tectonic constraints. *Tectonophysics* 450(1-4), 51-69.
- Faleide, J. I., Gudlaugsson, S. T. & Jacquart, G. 1984: Evolution of the western Barents Sea. *Marine and Petroleum Geology* 1, 123-150.
- Faleide, J.I., Myhre, A.M. & Eldholm, O. 1988: Early Tertiary volcanism at the western Barents Sea margin. In Morton, M. & Parson, L.M. (eds.) *Early Tertiary volcanism and the opening of the NE Atlantic. Geological Society Special Publications* 39, 135-146.
- Faleide, J. I., Solheim, A., Fiedler, A., Hjelstuen, B. O., Andersen, E. S. & Vanneste, K. 1996: Late Cenozoic evolution of the western Barents Sea-Svalbard continental margin. Impact of glaciations on basin evolution; data and models from the Norwegian margin and adjacent areas. *Global and Planetary Change* 12, 53-74.
- Faleide, J. I., Vågnes, E. & Gudlaugsson, S. T. 1993: Late Mesozoic-Cenozoic evolution of the southwestern Barents Sea in a regional rift-shear tectonic setting. *Marine and Petroleum Geology* 10, 186-214.
- Faleide, J.I., Gudlaugsson, S.T., Johansen, B., Myhre, A.M., Eldholm, O. & Norway, N.P.O.L.N. 1984: Free-air gravity anomaly maps of the Greenland Sea and the Barents Sea; Geo-scientific investigations in the Barents and Greenland Norwegian Seas. *Skrifter Norsk Polarinstitut* 180, 63-67.
- Faleide, J.I., Tsikalas, F., Breivik, A.J., Mjelde, R., Ritzmann, O., Engen, Ø., Wilson, J. & Eldholm, O. 2008: Structure and evolution of the continental margin off Norway and the Barents Sea. *Episodes* 31(1), 82-01.
- Fichler, C., Rueslåtten, H., Gram, C., Ingebrigtsen, A. & Olesen, O. 2007: Salt interpretation with special focus on magnetic data, Nordkapp Basin, Barents Sea. Expanded Abstract EGM 2007 International Workshop Innovation in EM, Grav and Mag Methods. a new Perspective for Exploration. Capri, Italy, 16-18 April 2007 .
- Fichler, C., Rundovde, E., Johansen, S. & Sæther, B. M. 1997: Barents Sea tectonic structures visualized by ERS1 satellite gravity with indications of an offshore Baikalian trend. *First Break* 15, 355-363.
- Flanagan G., Davis S., Campbell, C. & Doughtie, J. 1988: Integration of high sensitivity aeromagnetics and seismic to define salt and sediment structures in the Gulf of Mexico. *58th Annual International Meeting, Society of Exploration Geophysics, Expanded Abstracts*, 582-585.
- Florio, G., Fedi, M. & Pasteka, R. 2006: On the application of Euler deconvolution to the analytic signal. *Geophysics* 71(6), L87-L93.

- Furnes H. & Pedersen R.B., 1995: The Lyngen magmatic complex: Geology and geochemistry. *Geonytt*, v.22, p. 30
- Gabrielsen R., Færseth, R., Jensen, L., Kalheim, J. & Riis, F. 1990: Structural elements of the Norwegian Continental Shelf. Part 1. The Barents Sea region. *Norwegian Petroleum Directorate Bulletin* 6, 0-33.
- Gabrielsen, R. & Færseth, R. 1989: The inner shelf of North Cape, Norway, and its implications for the Barents Shelf-Finnmark Caledonide boundary. *Norsk Geologisk Tidsskrift* 69, 57-62.
- Gabrielsen, R. 1984: Long-lived fault zones and their influence on the tectonic development of the southwestern Barents Sea. *Journal of the Geological Society, London* 141, 651-662.
- Gabrielsen, R. H., Klovjan, O. S., Rasmussen, A. & Stolan, T. 1992: Interaction between halokinesis and faulting; structuring of the margins of the Nordkapp Basin, Barents Sea region, In Larsen, R.M. *et al.* (eds.) Structural and tectonic modelling and its application to petroleum geology; proceedings. *Norwegian Petroleum Society (NPF) Special Publication 1*, 121-131.
- Galitchanina, L.D., Glaznev, V.N., Mitrofanov, F.P. & Olesen, O. 1995: Surface density characteristics of the Baltic Shield and adjacent territories, *Norwegian Journal of Geology, Special Publications.*, 349-354.
- Gardner G., Gardner, L. & Gregory, A. 1974: Formation velocity and density-the diagnostic basics for stratigraphic traps. *Geophysics* 39, 770-780.
- Gayer, R.A., Hayes, S.J. & Rice, A.H.N. 1985: The structural development of the Kalak Nappe Complex of eastern and central Porsangerhalvøy, Finnmark, Norway. *Norges geologiske undersøkelse Bulletin* 400, 67-87.
- Gayer, R.A., Rice, A.H.N., Roberts, D., Townsend, C. & Welbon, A. 1987: Restoration of the Caledonian Baltoscandian margin from balanced cross-sections: the problem of excess continental crust. *Transactions of the Royal Society of Edinburgh: Earth Sciences* 78, 197-217.
- Gee, D. G. & Pease, V. 2004: The Neoproterozoic Timanide orogen of eastern Baltica; introduction. The Neoproterozoic Timanide Orogen of eastern Baltica. *Memoirs of the Geological Society of London* 30, 1-3.
- Gee, D. G. & Teben'kov, A. 2004: Svalbard; a fragment of the Laurentian margin; The Neoproterozoic Timanide Orogen of eastern Baltica. *Memoirs of the Geological Society of London* 30, 191-206.
- Gee, D. G., Bogolepova, K. & Lorenz, H., 2006: The Timanide, Caledonide and Uralide orogens in the Eurasian high Arctic, and relationships to the palaeo-continent Laurentia, Baltica and Siberia. In Gee, D.G & Stephenson, R.A. (eds.) European Lithosphere Dynamics. *Geological Society, London, Memoirs* 32, 507-520.
- Gee, D.G., Fossen, H., Henriksen, N. & Higgins, A.K. 2008: From the early Palaeozoic platforms of Baltica and Laurentia to the Caledonide orogen of Scandinavia and Greenland. *Episodes* 31(1), 44-51.
- Geosoft, 2004: Oasis montaj v 6.0 Mapping and processing system, The core software platform for working with large volume spatial data. Quick start tutorials. *Geosoft Incorporated*, 258 pp.

- Geosoft, 2005a: Oasis montaj MAGMAP Filtering. 2D frequency domain processing of potential Field Data tutorial. *Geosoft Incorporated*, 66 pp.
- Geosoft, 2005b: Montaj Geophysics Levelling System, Processing and Enhancing Geophysical Data Extension for Oasis montja v6.2. Tutorial and user guide. *Geosoft Incorporated*, 68 pp.
- Gernigon, L., Marelllo, L., Mogaard, J.O., Werner, S.C. & Skilbrei, J.R. 2007a: Barents Sea Aeromagnetic Survey BAS - 06: Acquisition-processing report and preliminary interpretation. NGU Report 2007.035, Geological Survey of Norway, Trondheim, 142 pp.
- Gernigon, L., Olesen, O. & Continental-Shelf-Geophysics-team 2007b: Challenging the Established Truths. *Geoexplor* 4, 40-44.
- Gibson, R. I. & Millegan, P. 1998: Geologic applications of gravity and magnetics; case histories. *AAPG Studies in Geology 43 and SEG Geophysical Reference Series 8*, 175 p.
- Gjelsvik, T. 1998: Nye aspekter ved forhold mellom den baikalske og den kaledonske deformasjonen og dets betydning for deformasjonshistorien i Barentshav-regionen, basert på strukturgeologisk kartlegging, Varanger-halvøyen, Finnmark, Nord-Norge. *Unpublished Cand. Scient. thesis, University of Bergen*, 112 pp.
- Godfrey, N.J., Beaudoin, B.C. & Klemperer, S.L. 1997: Ophiolitic basement to the Great Valley forearc basin, California, from seismic and gravity data: Implications for crustal growth at the North American continental margin. *Geological Society of America Bulletin* 109(12), 1536-1562.
- Götze, H.J. & Lahmeyer, B. 1988: Application of 3-Dimensional Interactive Modeling in Gravity and Magnetics, *Geophysics*, 53, 1096-1108.
- Goutorbe, B., Lucazeau, F. & Bonneville, A. 2007: Comparison of several BHT correction methods: a case study on an Australian data set, *Geophysical Journal International*, 170, 913-922.
- Grad, M., Tiira, T. & ESC-Working-Group 2009: The Moho depth map of the European Plate. *Geophysical Journal International* 176(1), 279-292.
- Grauch, V. J. S. & Hudson, M., R. 2007: Guides to understanding the aeromagnetic expression of faults in sedimentary basins: Lessons learned from the central Rio Grande rift, New Mexico. *Geosphere*, 3, 6, 596–623, doi: 10.1130/GES00128.1
- Grauch, V.J.S., Hudson, M.R. & Minor, S.A. 2001: Aeromagnetic expression of faults that offset basin fill, Albuquerque Basin, New Mexico. *Geophysics* 66(3), 707-720.
- Grauch, V.J.S., Cordell, L. 1987: Limitations on determining density or magnetic boundaries from the horizontal gradient of gravity or pseudogravity data. *Geophysics* 52, 118– 121.
- Grogan, P., Nyberg, K., Fotland, B., Myklebust, R., Dahlgren, S. & Riis, F. 1998: Cretaceous Magmatism South and East of Svalbard. Evidence from Seismic Reflection and Magnetic Data. *Polarforschung* 68, 25-34.
- Grogan, P.W. & Zwaan, K.B. 1997: Geologisk kart over Norge, berggrunnskart HELGØY M 1:250.000 Norges geologiske undersøkelse

- Gudlaugsson, S.T., Faleide, J. I., Johansen, S. E. & Breivik, A. J. 1994: Late Palaeozoic structural development of the southwestern Barents Sea. Structure and Tectonic History of the Western Barents Sea (S. T. Gudlaugsson), *Dr. Philos. thesis*, University of Oslo.
- Gudlaugsson, S.T., Faleide, J., Johansen, S. & Breivik, A. 1998: Late Palaeozoic structural development of the southwestern Barents Sea. *Marine and Petroleum Geology* 15, 73-102.
- Guise, P.G. & Roberts, D. 2002: Devonian ages from $^{40}\text{Ar}/^{39}\text{Ar}$ dating of plagioclase in dolerite dykes, eastern Varanger Peninsula, North Norway. *Norges Geologiske Undersøkelse Bulletin* 440, 27-37.
- Gunn, P.J. 1997: Application of aeromagnetic surveys to sedimentary basin studies, *Journal of Australian Geology & Geophysics* 17, 133-144.
- Haenel, R., Rybach, L. & Stegena, L. 1988: *Handbook of Terrestrial Heat-Flow Determination*. Dordrecht, Kluwer Academic Publishers.
- Hathaway, D.H., Wilson, R.M. & Reichmann, E.J. 1999: A synthesis of solar cycle prediction techniques. *Journal of Geophysical Research-Space Physics* 104(A10), 22375-22388.
- Harrison, J.C., St-Onge, M.R., Petrov, O., Strelnikov, S., Lopatin, B., Wilson, F., Tella, S., Paul, D.K., Lynds, T., Shokalsky, S., Huits, C., Bergman, S., Jepsen, H.F. & Solli, A. 2008: Geological map of the Arctic; Open file 5816. Geological Survey of Canada.
- Hartman, R.R., Tesky, D.J. & Friedberg, J.L. 1971: A system for rapid digital aeromagnetic interpretation. *Geophysics* 36, 891-918.
- Herrevold, T., Gabrielsen, R.H. & Roberts, D., 2009: The southeastern part of the Trollfjorden-Komagelva Fault Zone, Varanger Peninsula, Finnmark, North Norway. *Norwegian Journal of Geology*, 89, 305-325
- Hospers, J. & Ediriweera, K.K. 1991: Depth and configuration of the crystalline basement in the Viking Graben area, Northern North Sea. *Journal of the Geological Society, London* 148, 261-265.
- Hrouda, F., Smid, J. & Schulmann, K. 2001: Anisotropy of magnetic susceptibility and its carriers in salt domes of the SW Zagros Mts., Iran. *American Geophysical Union, Fall Meeting* 2001, abstract #GP41A-0247.
- Hsu, S.-K. 2002: Imaging magnetic sources using Euler's equation. *Geophysical Prospecting* 50, 15-25.
- Hsu, S. K., Sibuet, J. C. & Shyu, C. T. 1996: High-resolution detection of geologic boundaries from potential-field anomalies: An enhanced analytical signal technique. *Geophysics* 61, 373-386.
- Hsu, S. K., Sibuet, J. C. & Shyu, C. T. 1996: High-resolution detection of geologic boundaries from potential-field anomalies: An enhanced analytical signal technique. *Geophysics* 61, 373-386.
- Hudec, M.R., Jackson, M.P.A. & Schultz-Ela, D.D. 2009: The paradox of minibasin subsidence into salt: Clues to the evolution of crustal basins. *Geological Society of America Bulletin* 121(1-2), 201-221.
- Ivanova, N. M. 2001: The geological structure and petroleum potential of the Kola-Kanin Monocline, Russian Barents Sea. *Petroleum Geoscience* 7, 343-350.

- Ivanova, N. M., Sakoulina, T. S. & Roslov, Y. V. 2006: Deep seismic investigation across the Barents-Kara region and Novozemelskiy fold belt (Arctic shelf). Seismic probing of continents and their margins. *Tectonophysics* 420, 123-140.
- Jackson, M. P. & Talbot, C. J. 1986: External shapes, strain rates, and dynamics of salt structures. *Geological Society of America Bulletin* 97, 305-323.
- Jain, S. 1976: An automatic method of direct interpretation of magnetic profiles. *Geophysics* 41(3), 531-541.
- Jakobsson, M., Cherkis, N.Z., Woodward, J., Macnab, R. & Coakley, B. 2000: New grid of Arctic bathymetry aids scientists and mapmakers, *Eos, Transactions, American Geophysical Union* 81, 89-96.
- Jebsen, C. 1998: Kenozoic utvikling av Vestbakkvulkanittprovinsen på den vestlige Barentshavsmarginen, Cand. Scient, Univsersitetet i Oslo, Oslo.
- Jensen L.M. & Broks T.M. 1988: Late Movements on the Trollfjord-Komagelv Fault Zone and rifting in the Nordkapp Basin, Abstract 6th annual TGS meeting, Institut for Geologi, UiO, Intern Skriftserie, 54, 24-25
- Jensen, L. N. & Sørensen, K. 1992: Tectonic framework and halokinesis of the Nordkapp Basin, Barents Sea. Structural and tectonic modeling and its application to petroleum geology; proceedings. *Norwegian Petroleum Society (NPF) Special Publication 1*, 109-120.
- Johansen, S., Ostisty, B., Birkeland, Ø., Fedorovski, Y., Martirosjan, V., Christensen, O., Cheredeev, S., Ignatenko, E.A. & Margulis, L. 1993: Hydrocarbon potential in the Barents Sea region. play distribution and potential. In Vorren, T.O., Bergsager, E., Dahl-Stammes, Ø.A., Holter, E., Johansen, B., Lie, E., Lund, T.B. (eds.). Arctic Geology and Petroleum Potential. *Norwegian Petroleum Society, Special Publication 2*, Elsevier, Amsterdam, 273-320.
- Juhojuntti, N., Juhlin, C. & Dyrelius, D. 2001: Crustal reflectivity underneath the Central Scandinavian Caledonides. *Tectonophysics* 334(3-4), 191-210.
- Karner, D., Studinger, M. & Bell, R.E. 2005: Gravity anomalies of sedimentary basins and their mechanical implications: Application to the Ross Sea basins, West Antarctica. *Earth and Planetary Science Letters* 235(3-4), 577-596.
- Karpuz, M. R., Roberts, D., Moralev, V. & Terekhov, E. 1993a: Regional lineament framework of eastern Finnmark, Norway, western Kola Peninsula, Russia, and southern Barents Sea.; Proceedings of the Ninth thematic conference on Geologic remote sensing; exploration, environment, and engineering. *Proceedings of the Thematic Conference on Remote Sensing for Exploration Geology* 9, 733-750.
- Karpuz, M.R., Roberts, D., Olesen, O., Gabrielsen, R.H. & Herrevold, T. 1993b: Application of multiple data sets to structural studies on Varanger Peninsula, Northern Norway. *International Journal of Remote Sensing* 14, 7979-1003.
- Karpuz, M. R., Roberts, D., Moralev, V. M. & Terekhov, E. 1995: Regional lineaments of eastern Finnmark, Norway, and the western Kola Peninsula, Russia. Geology of the eastern Finnmark-western Kola Peninsula region; proceedings of the International

- Barents symposium on "Geology and minerals in the Barents region". *Norges geologiske undersøkelse Special Publication 7*, 121-135.
- Keating, P. 1998: Weighted Euler deconvolution of gravity data. *Geophysics 63*, 1595-1603.
- Keating, P. & Pilkington, M. 2004: Euler deconvolution of the analytic signal and its application to magnetic interpretation. *Geophysical Prospecting 52*(3), 165-182.
- Kirkland, C.L., Daly, J.S. & Whitehouse, M.J. 2005: Early Silurian magmatism and the Scandian evolution of the Kalak nappe complex, Finnmark, Arctic Norway. *Journal of the Geological Society, London 162*, 985-1003.
- Koyi, H., Talbot, C. J. & Torudbakken, B. O. 1993: Salt diapirs of the Southwest Nordkapp Basin; analogue modelling. New insights into salt tectonics; collection of invited papers reflecting the recent developments in the field of salt tectonics. *Tectonophysics 228*, 167-187.
- Krogh, E. J., Andresen, A., Bryhni, I., Broks, T. M. & Kristensen, S. E., 1990. Eclogites and polyphase P-T cycling in the Caledonian Uppermost Allochthon in Troms, northern Norway. *Journal of Metamorphic Geology. 8*, 289-309.
- Ku, C.C. & Sharp, J.A. 1983: Werner deconvolution for automated magnetic interpretation and its refinement using Marquardt's inverse modeling. *Geophysics 48*(6), 754-774.
- Kullerud, K., Corfu, F., Bergh, S., Davidsen, B. & Ravna, E.K. 2006a: U-Pb constraints on the Archaean and Early Proterozoic evolution of the West Troms Basement Complex, North Norway. *Bulletin of Geological Society of Finland 1*, 79.
- Kullerud K., Skjerlie K.P., Corfu F. & de la Rosa J. 2006b: The 2.40 Ga Ringvassøy mafic dykes, West Troms Basement Complex, Norway: the concluding act of early Paleoproterozoic continental breakup. *Precambrian Research 150*, 183-200.
- Lahti, I & Karinen, T, 2010: Tilt derivative multiscale edges of magnetic data. *The Leading Edge, Vol. 29,1*, 24-29
- Larssen, G. B., Elvebakk, G., Henriksen, L., Kristensen, S. E., Nilsson, I., Samuelsberg, T., Svånå, T., Stemmerik, L. & Worsley, D. 2005: Upper Palaeozoic lithostratigraphy of the southern part of the Norwegian Barents Sea. *Norge Geologiske Undersøkelse Bulletin 444*, 3-443.
- Lauritsen, T., Blomstrand, L.B., Olesen, O. & Mørk, A. 2007: OSRAM II-Origin of sediment-Related AeroMagnetic II. Magnetic Susceptibility Measurements on Shallow Stratigraphic Cores from Finnmark Platform, Nordkapp Basin and Svalis Dome. *Geological Survey of Norway (NGU) Report 2007.028*. 99 pp.
- Levell, B.K. & Roberts, D. 1977: A re-investigation of the geology of north-west Varanger Peninsula, east Finnmark, north Norway. *Norges Geologiske Undersøkelse Bulletin 334*, 83-90.
- Lindahl, I., Stevens, B. P. J. & Zwaan, K. B., 2005. The geology of the Váddás area, Troms. A key to our understanding of the Upper Allochthon in the Caledonides of northern Norway. *Norges geologiske undersøkelse Bulletin. 445*, 5-43.
- Lippard, S. & Roberts, D. 1987: Faults systems in Caledonian Finnmark and the southern Barents Sea. *Norges Geologiske Undersøkelse Bulletin 410*, p. 55-64.

- Lippard, S. 1987: Tectonic Development of the SW Barents Sea with Special Reference to the Strategic Blocks. *Norsk Geologisk Tidsskrift* 67(4), 435-435.
- Lønne, W. & Sellevoll, M.A. 1975: A reconnaissance gravity survey of Magerøy, Finnmark, Northern Norway. *Norges geologiske undersøkelse* 319, 1-15.
- Løseth, H., Lippard, S.J. & Sættem, J. 1992: Cenozoic uplift and erosion of the Barents Sea-evidence from the Svalis Dome area. In: Vorren, T.O. Bergsaker, E., Dahl-Stammes, Ø.A., Holter, E., Jonhansen, B., Lie, E. & Lund, T.B. (eds.) *Arctic geology and petroleum potential. Norwegian Petroleum Society, Special Publications* 2, 643-664.
- Løvaås, L., Mogaard, J., Olesen, O., Koziel, J. & Lynum, R. 2006: Southern Nordkapp Basin Aeromagnetic Survey 2006 (SNAS-06). Data acquisition and processing report. *Geological Survey of Norway (NGU) Report 2006.089*. 51 pp.
- Ludwig, W., Nafe, J. & Drake, C. 1970: Seismic refraction. In Maxwell, A.E. (ed) *The Sea*, Volume 4. *Wiley-interscience, New York*, 53-84.
- Luyendyk, A.P.J. 1997: Processing of airborne magnetic data. *AGSO Journal of Australian Geology and Geophysics* 17(2), 31-38.
- Maher, H. D. J. 2001: Manifestations of Cretaceous High Arctic large igneous province in Svalbard. *Journal of Geology* 109, 91-104.
- Marello, L. & Ebbing, J., 2009: 3D geophysical model of the Barents Sea and characterization of crustal properties. *AAPG-3PARCTIC, Moscow September (Poster)*.
- Marello, L. & Ebbing, J., Gernigon, L., 2010: Magnetic basement study in the Barents Sea from inversion and forward modelling, *Tectonophysics*, 493, 153-171
- Mari, J.-L., Glangeaud, F. & Coppens, F. 2001: Traitement du signal pour géologues et géophysiciens-Techniques de base, 2. *Editions Technip*, 268 pp.
- Marson, I. & Klingele, E. E. 1993: Advantages of using the vertical gradient of gravity for 3-D interpretation. *Geophysics* 58, 1588-1595.
- Martinec, Z. 1994: The density contrast at the Mohorovičić discontinuity. *Geophysical Journal International* 177, 539-544.
- Mathisen, O. 1976: A method for Bouguer reduction with rapid calculation of terrain corrections *Geographical Survey of Norway geodetic publications* 18, 40 p.
- Matton, G., Jébrak M., & Lee, J.K.W., 2005. Resolving the Richat enigma: Doming and hydrothermal karstification above an alkaline complex. *Geology* 33 (8): 665–668.
- Mauring, E. & Kihle, A. 2006: Leveling aerogeophysical data using a moving differential median filter. *Geophysics* 71(1), L5-L11.
- Mauring, E., Beard, L.P., Kihle, O. & Smethurst, M.A. 2002: A comparison of aeromagnetic levelling techniques with an introduction to median levelling. *Geophysical Prospecting* 50(1), 43-54.
- McDonald, A. J., Fletcher, C. J., Carruthers, R. M., Wilson, D. & Evans, R. B. 1992: Interpretation of regional gravity and magnetic surveys of Wales, using shaded relief and Euler deconvolution techniques. *Geological Magazine* 5, 532-531.
- Melezhik, V.A., Zwaan, K.B., Motuza, G., Roberts, D., Solli, A., Fallick, A.E., Gorokhov, I.M. & Kusnetsov, A.B. 2003: New insights into the geology of high-grade Caledonian

- marbles based on isotope chemostratigraphy. *Norwegian Journal of Geology* 83, 209-242.
- Melezhik et al. 2007 *Geological Magazine* 145, 161-172.
- Millegan, P.S. 1998: High-resolution aeromagnetic surveying. R.I. Gibson and P.S. Millegan (eds.) *Geologic applications of gravity and magnetics: Case histories*. Society of Exploration Geophysicists and American Association of Petroleum Geologists, 18-19.
- Miller, H.G. & Singh, V. 1994: Potential-Field Tilt - a New Concept for Location of Potential-Field Sources. *Journal of Applied Geophysics* 32(2-3), 213-217.
- Mjelde, R., Breivik, A.J., Elstad, H., Ryseth, A.E., Skilbrei, J.R., Opsal, J.G., Shimamura, H., Murai, Y. & Nishimura, Y. 2002: Geological development of the Sorvestsnaget Basin, SW Barents Sea, from ocean bottom seismic, surface seismic and gravity data, *Norwegian Journal of Geology*, 82, 183-202.
- Moretti, I., Colletta, B. & Vially, R. 1988: Theoretical-Model of Block Rotation Along Circular Faults. *Tectonophysics* 153(1-4), 313-320.
- Motuz G., Motuz V., Beliatsky B. & Savva E. 2001: The Ringvassøya Greenstone Belt (Tromsø, North Norway): implications for a Mesoarchean subduction zone. EUROPROBE time-slice symposium "Archaean and Proterozoic Plate Tectonics: Geological and Geophysical Records", St. Petersburg, Russia, October 1-November 3, 43-44.
- Mørk, A., Vigran, J.O. & Hochuli, P.A. 1990: Geology and palynology of the Triassic succession of Bjørnøya. *Polar Research* 8, 141-163.
- Mørk M.B.E., McEnroe S.A. and Olesen O. 2002. Magnetic susceptibility of Mesozoic and Cenozoic sediments off Mid Norway and the role of siderite: implications for interpretation of high-resolution aeromagnetic anomalies. *Marine and Petroleum Geology* 19, 1115-1126.
- Mudge, S. 1991: New developments in resolving detail in aeromagnetic data. *Exploration Geophysics* 22, 277-284.
- Murphy, C. 2007. Interpreting FTG Gravity Data using Horizontal Tensor Components. Extended Abstract EGM 2007 International Workshop. Innovation in EM, Grav and Mag Methods: a new Perspective for Exploration, Capri, Italy, April 15-18.
- Mushayandevu, M.F., Lesur, V., Reid, A.B. & Fairhead, J.D. 2004: Grid Euler deconvolution with constraints for 2D structures. *Geophysics* 69(2), 489-496.
- Musset, A. E. & Khan, M. A. 2000: Looking into the Earth. *Cambridge University Press*, 470p.
- Nabighian, M. N. 1972: The Analytic Signal of Two-Dimensional Magnetic Bodies with Polynomial Cross-Sections; Its Properties and Use for Automated Anomaly Interpretation. *Geophysics* 37, 505-517.
- Nabighian, M. N. 1974: Additional comments on the analytic signal of two-dimensional magnetic bodies with polygonal cross-section. *Geophysics* 39, 85-92.
- Nabighian, M. N. 1984: Toward a three-dimensional automatic interpretation of potential field data via generalized Hilbert transforms; fundamental relations. *Geophysics* 49, 780-786.

- Nafe, J. E. & Drake C. 1957: Variation with depth in shallow and deep water marine sediments of porosity, density and the velocities of compressional and shear waves. *Geophysics* 22, 523-552.
- Naidu, P. S. & Mathew, M. P. 1998: Analysis of geophysical potential fields. a digital signal processing approach. In Berkout, A.J. (ed). *Advances in Exploration Geophysics series, Elsevier, Amsterdam* 5, 0-295.
- Nettleton, L. L. 1976: Gravity and Magnetics in Oil prospecting. *McGraw-Hill, New York*, 462 pp.
- Nilsen, K.T., Vendeville B. C., Johansen J. T. & A. 1994: An example of salt tectonics controlled by regional tectonics; the Nordkapp Basin, Norway. AAPG annual convention. *Annual Meeting Abstracts - American Association of Petroleum Geologists and Society of Economic Pale*, 1994, 225.
- Nilsen, K.T., Vendeville, B.C. & Johansen, J.T. 1995: Influence of regional tectonics on halokinesis in the Nordkapp Basin, Barents Sea, In Jackson, M.P., Roberts, D.G. and Snelson, S. (eds), Salt tectonics: a global perspective. *AAPG Memoir* 65, 413-436.
- Northwest Geophysical Associates Incorporation 2006: *GM-SYS Gravity and Magnetic Modeling software. Users Guide v 4.10*. 110 pp.
- Novoa, E. & Svåná, T. 2009: The Loppa High: Compression Or Extension Feature during the Permian and Triassic? In *AAPG Search and Discover Article #90096©2009 AAPG 3-P Arctic Conference and Exhibition, Moscow, Russia*.
- Nyland, B., Jensen, L.N., Skagen, J., Skarpnes, O. & Vorren, T.O. 1992: Tertiary uplift and erosion in the Barents Sea: magnitude, timing and consequences. In Larsen, R.M., Brekke, H., Larsen, B.T. and Tallerås, E. (eds.). Structural and tectonic modeling and its application to petroleum geology. *Norwegian Petroleum Society Special Publication 1*, Elsevier, Amsterdam, 153-162.
- O'Reilly, B.M., Hauser, F., Ravaut, C., Shannon, P.M. & Readman, P.W. 2006: Crustal thinning, mantle exhumation and serpentinitization in the Porcupine Basin, offshore Ireland: evidence from wide-angle seismic data. *Journal of the Geological Society* 163, 775-787.
- Olesen, O., Brønner, M., Ebbing, J., Gellein, J., Gernigon, L., Koziel, J., Lauritsen, T., Mykelbust, R., Pascal, C., Sand, M., Solheim, A. & Usov, S. 2010: New aeromagnetic and gravity compilations from Norway and adjacent areas - methods and applications. In Vinning, B. A. & Pickering, S. C. (eds.) *Petroleum Geology: From mature basins to new frontiers. Proceedings of the 7th Petroleum Geology Conference*. Geological Society of London 559-586
- Olesen O., Gernigon L., Ebbing, J., Mogaard, J., Pascal, C. and Wienecke, S.: 2006: Interpretation of aeromagnetic data along the Jan Mayen Fracture Zone, JAS-05. *Geological Survey of Norway (NGU) report 2006.018*. 162 pp.
- Olesen, O., Balling, N., Barrère, C., Breiner, N., Davidsen, B., Ebbing, J., Elvebakk, H., Gernigon, L., Koziel, J., Lutro, O., Midttømme, K., Nordgulen, Ø., Olsen, L., Osmundsen, P.T., Pascal, C., Ramstad, R.K., Rønning, J.S., Skilbrei, J.R., Slagstad, T.,

- Wissing, B., 2007: KONTIKI Final Report, CONTInental Crust and Heat Generation In 3D, *NGU report 2007.042*, pp. 438
- Olesen, O., Gernigon, L., Hauge, J., Kihle, O., Koziel, J., Lauritsen, T., Myklebust, R., Skilbrei, J.R. & Usov, S. 2009: Magnetic anomaly map, Norway and adjacent areas. 1: 3 million. *Geological Survey of Norway, Trondheim*.
- Olesen, O., Håbrekke, H., Kihle, O. & Smethurst, M. 1992: Finnmark fylkke, aeromagnetisk anomalikart, M. 1:500.000. *Norges geologiske undersøkelse (NGU)*.
- Olesen, O., Roberts, D., Henkel, H., Lile, B.L. & Torsvik, T.H. 1990: Aeromagnetic and gravimetric interpretation of regional structural features in the Caledonides of West Finnmark and North Troms, northern Norway. *Norges geologiske undersøkelse Bulletin 419*, 1-24.
- Olesen, O., Torsvik, T.H., Tveten, E., Zwaan, K.B., Løseth, H., & Henningsen, T. 1997: Basement structure of the continent margin in the Lofoten-Lopphavet area, northern Norway: constraints from potential field data, on-land structural mapping and paleomagnetic data. *Norsk Geologisk Tidsskrift 77*, 15-30.
- Osmundsen, P.T., Sommaruga, A., Skilbrei, J.R. & Olesen, O. 2002: Deep structure of the Mid Norway rifted margin, *Norwegian Journal of Geology*, 82, 205-224.
- Pascal, C., Litvinova, T. and Negrov, O.B. 2009: Chapter 2: Heat flow of the Barents Sea. In Smelror, M., *et al.* (eds.) *ATLAS: Geological History of the Barents Sea*, Norges geologiske undersøkelse (Geological Survey of Norway, NGU), 30-31.
- Pharaoh, Tim C.; Ramsey, Donald; Jansen, Øystein: 1983: Stratigraphy and structure of the northern part of the Repparfjord - Komagfjord window, Finnmark, Northern Norway. ;Norges geologiske undersøkelse;TIDSSKRIFTARTIKKEL;NGU; No.377;1-45 sider
- Pilkington, M., Jansa, J. F. & Grieve, R. A. F. 1995: Geophysical studies of the Montagnais impact crater, Canada. *Meteoritics 30*, 446-450.
- Pilkington, M., Miles, W. F., Ross, G. M. & Roest, W. R. 2000: Potential-field signatures of buried Precambrian basement in the Western Canada Sedimentary Basin: The Lithoprobe-Alberta basement transect-Le transect Lithoprobe du socle Albertain. *Canadian Journal of Earth Sciences – Revue Canadienne des Sciences de la Terre 37*, 1453-1471.
- Popowski, T., Connard, G. & French, R., 2006. *GMSYS-3D: 3D Gravity and Magnetic Modeling for OasisMontaj - User Guide*. Northwest Geophysical Associates, Corvallis, Oregon, 32 pp.
- Press, W.H., Teukolsky, S.A., Vetterling, W.T. & Flannery, B.P. 2002: Numerical Recipes in C++. The art of Scientific Computing Second Edition. Cambridge University Press. 972 pp
- Prieto, C. 1993: Gulf of Mexico-understanding the magnetic response due to salt intrusion. International Geophysical Corporation Footnote Series.
- Rafaelsen, B., Elvebakk, G., Andreassen, K., Stemmerik, L., Colpaert, A., Samuelsen, T.J., 2008: From detached to attached carbonate buildup complexes — 3D seismic data from the upper Palaeozoic, Finnmark Platform, southwestern Barents Sea. *Sedimentary Geology*, 206, 17-32.

- Ramberg, I.B., Bryhni, I., Nøttvedt, A. And Rangnes, K. (eds.) 2008, The Making of a Land – Geology og Norway. Trondheim, Norsk Geologisk Forening, 6xxp.
- Ramberg, I.B. and Smithson, S.B. 1975.: Geophysical Interpretation of Crustal Structure along the South-eastern Coast of Norway and Skagerrak. *GSA Bulletin*, 86(6), 769-774
- Ramsay, D.M., Sturt, B.A., Jansen, Ø., Andersen, T.B. & Sinha-Roy, S. 1985: The tectonostratigraphy of western Porsangerhalvøya, Finnmark, north Norway. In *Gee, D.G. & Sturt, B.A. (eds) The Caledonide Orogen – Scandinavia and related areas*. John Wiley & Sons Ltd., Chichester, 611-619.
- Ravat, D. 1996: Analysis of the Euler method and its applicability in environmental magnetic investigations. *Journal of Environmental and Engineering Geophysics 1*, 229-238.
- Ravat, D., Wang, B., Wildermuth, E. & Taylor, P. T. 2002: Gradients in the interpretation of satellite-altitude magnetic data; an example from central Africa. Earth's gravity and magnetic fields from space. *Journal of Geodynamics 33*, 131-142.
- Reid, A., Allsop, J., Granser, H., Millet, A. & Somerton, I. 1990: Magnetic interpretation in three dimensions using Euler deconvolution. *Geophysics 55*, 80-91.
- Reitan, P.H. 1963: The geology of the Komagfjord tectonic window of the Raipas suite, Finnmark, Norway. Norges geologiske undersøkelse; TIDSSKRIFTARTIKKEL;NGU; No.221;1-71 + kar sider
- Reston, T.J. 2007: Extension discrepancy at North Atlantic nonvolcanic rifted margins: Depth-dependent stretching or unrecognized faulting? *Geology 35*(4), 367-370.
- Reston, T.J. 2009: The extension discrepancy and syn-rift subsidence deficit at rifted margins. *Petroleum Geoscience 15*(3), 217-237.
- Rice, A. H.N., Gayer, R. A., Robinson, D. & Bevins, R. E. 1989a: Strike-slip restoration of the Barents Sea Caledonides terrane, Finnmark, North Norway. *Tectonics 8*, 247-264.
- Rice, A.H.N., Bevins, R.E., Robinson, D. & Bevins, R.E. 1989b: Evolution of low-grade metamorphic zones in the Caledonides of Finnmark, N. Norway. In Gayer, R.A. (ed.) *The Caledonian geology of Scandinavia*. Graham & Trotman, London, 177-191.
- Rice, A.H.N. 1994: Stratigraphic overlap of the Late Proterozoic Vadsø and Barents Sea Groups and correlation across the Trollfjorden-Komagelva Fault Zone, Finnmark, North Norway. *Norsk Geologisk Tidsskrift 74*, 48-57.
- Rice, A.H.N. 2001: Field evidence for thrusting of the basement rocks coring tectonic windows in the Scandinavian Caledonides: an insight from the Kunes Nappe, Finnmark, Norway. *Norsk Geologisk Tidsskrift 81*, 321-328.
- Rice, A.H.N., Frank, W. 2003: The early Caledonian (Finnmarkian) event reassessed in Finnmark: $^{40}\text{Ar}/^{39}\text{Ar}$ cleavage age data from NW Varangerhalvøya, N. Norway. *Tectonophysics 374* (3-4), 219–236.
- Rice, A.H.N., Ntaflos, T., Gayer, R.A. & Beckinsale, R.D. 2004: Metadolerite geochronology and dolerite geochemistry from East Finnmark, northern Scandinavian Caledonides. *Geological Magazine 141*, 301-318.
- Richardsen, G., Henriksen, E. & Vorren, T.O. 1991: Evolution of the Cenozoic sedimentary wedge during rifting and sea-floor spreading west of the Stappen High, Western Barents Sea. *Marine Geology 101*(1-4), 11-30.

- Richardson, G., Vorren, T.O. & Tørudbakken, B.O. 1993: Post-Early Cretaceous Uplift and Erosion in the Southern Barents Sea - a Discussion based on analysis of seismic Interval velocities. *Norsk Geologisk Tidsskrift* 73(1), 3-20.
- Riis, F. 1992: Dating and measuring of erosion, uplift and subsidence in Norway and the Norwegian shelf in glacial periods. *Norsk Geologisk Tidsskrift*, 72, 325–331.
- Ritzmann, O., Hinz, K., Jokat, W., Reichert, C., Coffin, M. F., Duncan, R. A., Erzinger, J., Hinz, K. & Talwani, M. 1997: Crustal structure of the East Antarctic passive margin at 6 degrees E.; *Abstracts of the International Lithosphere program workshop on Volcanic margins*. p. 34-35.
- Ritzmann, O., Maercklin, N., Faleide, J.I., Bungum, H., Mooney, W.D. & Detweiler, S.T. 2007: A three-dimensional geophysical model of the crust in the Barents Sea region: Model construction and basement characterization, *Geophysical Journal International*, 170, 417-435.
- Roberts, D. 1972: Tectonic Deformation in the Barents Sea Region of Varanger Peninsula, Finnmark. *Norges Geologiske Undersøkelse* 282, 1-39.
- Roberts, D. 1981: Geologisk kart over Norge, berggrunnskart NORDKAPP 1:250.000. *Norges geologiske undersøkelse (NGU), Trondheim*.
- Roberts, D. 1985: The Caledonian fold belt in Finnmark: a synopsis. *Norske geologiske undersøkelse Bulletin* 403, 161-177.
- Roberts, D. 1995: Principal features of the structural geology of Rybachi and Sredni Peninsulas, and some comparisons with Varanger Peninsula. *Norges geologiske undersøkelse Special Publication* 7, 247-258.
- Roberts, D. 1996: Caledonian and Baikalian tectonic structures on Varanger Peninsula, Finnmark, and coastal areas of Kola Peninsula, NW Russia. *Norges geologiske undersøkelse Bulletin* 431, 59-65.
- Roberts, D., Olesen, O. & Karpuz, K.R. 1997: Seismo- and neotectonics in Finnmark, Kola Peninsula and the southern Barents Sea. Part 1: Geological and neotectonic framework. *Tectonophysics* 270, 1-13.
- Roberts, D. 2003: The Scandinavian Caledonides; event chronology, palaeogeographic settings and likely modern analogues; *Tectonophysics* 365, 283-299.
- Roberts, D. 2007: Palaeocurrent data from the Kalak Nappe Complex, northern Norway: a key element in models of terrane affiliation. *Norwegian Journal of Geology* 87, 319-328.
- Roberts, D. 2009: Berggrunnskart Berlevåg 2336 1, M 1:50 000, revidert foreløpig utgave. *Norges geologiske undersøkelse*.
- Roberts, D. & Andersen, T.B. 1985: Nordkapp. Beskrivelse til det berggrunnsgeologiske kartbladet M 1:250 000. *Norges Geologiske Undersøkelse Skrifter* 61, 1-49.
- Roberts, D. & Gee, D.G. 1985: An introduction to the structure of the Scandinavian Caledonides. In Gee, D.G. & Sturt, B.A. (eds.) *The Caledonide orogen – Scandinavia and related areas*. John Wiley & Sons, Chichester, 55-68.
- Roberts, D., Mitchell, J.G. & Andersen, T.B. 1991: A post-Caledonian dolerite dyke from Magerøya, North Norway: age and geochemistry. *Norsk Geologisk Tidsskrift* 71, 289-294.

- Roberts, D. & Siedlecka, A. 2002: Timanian orogenic deformation along the northeastern margin of Baltica, Northwest Russia and Northeast Norway, and Avalonian-Cadomian connections. *Tectonophysics* 352(1-2), 169-184.
- Roberts, D. & Olovyanishnikov, V. 2004: Structural and tectonic development of the Timanide orogen. *Geological Society London Memoirs* 30, 47-57.
- Roberts, D. & Lippard, S. 2005: Inferred Mesozoic faulting in Finnmark. Current status and offshore links. *Norges Geologiske Undersøkelse Bulletin* 443, 55-60.
- Roberts D., Nordgulen, O. and Melezhik, V. 2007: The Uppermost Allochthon in the Scandinavian Caledonides: From a Laurentian ancestry through Taconian orogeny to Scandian crustal growth on Baltica *Geological Society of America Memoirs*, 2007, 200, p. 357-377
- Roberts, R.J., Torsvik, T.H., Andersen, T.B. & Rehnstrom, E.F. 2003: The Early Carboniferous Mageroy dykes, northern Norway: palaeomagnetism and palaeogeography. *Geological Magazine* 140(4), 443-451.
- Roberts, R.J., Corfu, F., Torsvik, T.H., Ashwal, L.D. & Ramsay, D.M. 2006: Short-lived mafic magmatism at 560-570 Ma in the northern Norwegian Caledonides: U-Pb zircon ages from the Seiland Igneous Province, *Geological Magazine* 143, 887-903.
- Roberts, R.J., Corfu, F., Torsvik, T.H., Hetherington, C.J. and Ashwal L.D., 2010: Age of alkaline rocks in the Seiland Igneous Province, Northern Norway, *Journal of the Geological Society*, 167 71-81.
- Robins, B., 1996: The Seiland Igneous Province, North Norway: field trip IGCP project, *NGU Report 96.127*, 33 pp.
- Robins, B. 1998: The mode of emplacement of the Honningsvåg Intrusive Suite, Magerøya, northern Norway, *Geological Magazine* 135, 231-244.
- Roest, W. R., Verhoef, J. & Pilkington, M. 1992: Magnetic interpretation using the 3-D analytic signal. *Geophysics* 57, 116-125.
- Rønnevik, H. C., Illing, L. V. & Hobson, G. D. 1981: Geology of the Barents Sea. In Illing, L.V. and Hobson, G.D. (eds.), Petroleum geology of the continental shelf of North-West Europe. *Proceedings of the second conference*, 395-406.
- Rønnevik, H.C. & Jacobsen, H.P. 1984. Structural highs and basins in the western Barents Sea, Spence A.M. (ed.), Petroleum Geology of the north European margin. *Norsk Petroleum Forening, London*, Graham and Trotman, 19-32.
- Rybach, L. 1988: Determination of heat production rate. In R., Haenel, L. Rybach & L. Stegena (eds.) *Handbook of Terrestrial Heat-Flow Determination*. Dordrecht, Kluwer Academic Publishers, 125-142.
- Saad, A. 1993: Interactive integrated interpretation of gravity, magnetic and seismic data-tools and examples. *Offshore Technology Conference abstract*, OTC#7079
- Samuelsberg, T.J., Elvebakk, G. & Stemmerik, L. 2003: Late Palaeozoic evolution of the Finnmark Platform, southern Norwegian Barents Sea. *Norsk Geologisk Tidsskrift* 83, 351-362.

- Siedlecka, A. & Roberts, D. 1992: The bedrock geology of Varanger Peninsula, Finmark, North Norway; an excursion guide. *Norges geologiske undersøkelse Special Publication 5*, 1-45.
- Siedlecka, A. & Roberts, D. 1996: Finnmark Fylke. Berggrunnsgeologi M 1:500 000. *Norges Geologiske Undersøkelse (NGU), Trondheim.*
- Siedlecka, A. & Siedlecki, S. 1967: Some new aspects of the geology of the Varanger Peninsula (northern Norway). *Norges geologiske undersøkelse Bulletin 247*, 288-306.
- Siedlecka, A. & Siedlecki, S. 1970: Rekognosering av den magnetiske anomali på østsiden av Nordkylhalvøya. *Unpublished NGU report.*
- Siedlecka, A. 1975: Late Precambrian stratigraphy and structure of the northeastern margin of the Fennoscandian Shield. *Norges geologiske undersøkelse 316*, 313-348.
- Siedlecka, A. 1987: Development of the Upper Proterozoic Sedimentary Basins of Varanger Peninsula, North Norway. *Norsk Geologisk Tidsskrift 67(4)*, 437-437.
- Siedlecka, A. 1984: SYLTEFJORD. Foreløpig berggrunnsgeologisk kart 2436, 1:50.000. *Norges geologiske undersøkelse (NGU), Trondheim.*
- Siedlecki, S. 1980: Geologisk kart over Norge, berggrunnskart VADSØ-M. 1. 250.000. *Norges geologiske undersøkelse (NGU), Trondheim.*
- Sigmond, E.M.O. 2002: Geological map, land and sea areas of northern Europe, 1:4 million. *Geological Survey of Norway Trondheim.*
- Sigmond, E.M.O., Gustavson, M. & Roberts, D. 1984: Berggrunnskart over Norge – M 1:1 million. *Norges geologiske undersøkelse, Trondheim.*
- Silva, I.A.B.C. & Barbosa, V.C.F. 2003: 3D Euler deconvolution: Theoretical basis for automatically selecting good solutions. *Geophysics 68(6)*, 1962-1968.
- Simonov, A. G., M. & Yakovlev, Y. 1998: The Riphean oil of the Rybachiy Peninsula. Myth or key to a major direction for oil and gas prospecting within the Barents Sea (in Russian). *Bulletin of Murmansk's State technical University*, 1.
- Skilbrei, J.R. 1993: An evaluation of magnetic top basement depth determinations from the southwestern Barents Sea. *Doktor ingeniøravhandling 1993:68*. Norges tekniske høgskole, Trondheim.
- Skilbrei, J.R., Kihle, O., Olesen, O., Gellein, J., Sindre, A., Solheim, D. & Nyland, B. 2000: Gravity anomaly map of Norway and adjacent ocean areas, scale 1:3 Million: *Geological Survey of Norway (NGU), Trondheim.*
- Skilbrei, J.R. 1991: Interpretation of Depth to the Magnetic Basement in the Northern Barents Sea (South of Svalbard). *Tectonophysics 200(1-3)*, 127-141.
- Skilbrei, J.R. 1992: Preliminary interpretation of aeromagnetic data from Spitsbergen, Svalbard Archipelago (76°-79°N): Implications for structure of the basement. *Marine Geology 106*, 53-68.
- Skilbrei, J.R. 1993: Interpretation of geophysical data from the northwestern Barents Sea and Spitzbergen, Universitetet i Trondheim Norges Tekniske Høgskole.
- Skilbrei, J.R., Habrekke, H., Christoffersen, T. & Myklebust, R.A. 1990: Aeromagnetic surveying at high latitudes, a case history from the northern Barents Sea. *First Break 8*, 2, 46-50.

- Skilbrei, J.R., Kihle, O., Olesen, O., Gellein, J., Sindre, A., Solheim, D. & Nyland, B. 2000: Gravity map of Norway and adjacent ocean areas, scale 1:3 Million. *Geological survey of Norway (NGU)*.
- Skilbrei, J.R., Olesen, O., Osmundsen, P.T., Kihle, O., Aaro, S. & Fjellanger E. 2002: A study of basement structures and onshore-offshore correlations in Central Norway. *Norwegian Journal of Geology*, 82, 263-279.
- Skilbrei, J.R., Olesen, O., Osmundsen, P.T., Kihle, O., Aaro, S. & Fjellanger, E. 1992: A study of basement structures and onshore-offshore correlations in Central Norway. *Norwegian Journal of Geology* 82(4), 263-279.
- Skilbrei, J.R., Skyseth, T. & Olesen, O. 1991: Petrophysical Data and Opaque Mineralogy of High-Grade and Retrogressed Lithologies - Implications for the Interpretation of Aeromagnetic Anomalies in Northern Vestranden, Central Norway. *Tectonophysics* 192(1-2), 21-31.
- Skilbrei, J.R. 1995: Aspects of the geology of the southwestern Barents Sea from aeromagnetic data. *Norges geologiske undersøkelse Bulletin* 427, 64-67.
- Slagstad, T., Melezhik, V. A., Kirkland, C. L., Zwaan, K. B., Roberts, D., Gorokhov, I. M. & Fallick, A. E. 2006: Carbonate isotope chemostratigraphy suggests revisions to the geological history of the West Finnmark Caledonides, North Norway. *Journal of the Geological Society of London* 163, 277-289.
- Slagstad, T., Barrère, C., Davidsen, B. & Ramstad, R.K., 2008. Petrophysical and thermal properties of pre-Devonian basement rocks on the Norwegian continental margin, *Norges geologiske undersøkelse Bulletin* 448, 1-6.
- Smelror, M., Petrov, O., Larssen, G.B. & Werner, S.C. 2009: *ATLAS: Geological History of the Barents Sea*. Norges geologiske undersøkelse (Geological Survey of Norway, NGU), 135 pp.
- Smith, M.P. 2000: Cambro-Ordovician stratigraphy of Bjornoya and North Greenland: constraints on tectonic models for the Arctic Caledonides and the Tertiary opening of the Greenland Sea. *Journal of the Geological Society* 157, 459-470.
- Spector, A. & Grant, F. S. 1970: Statistical models for interpreting aeromagnetic data. *Geophysics*, 35, 293-302.
- Stavrev, P. & Reid, A. 2007: Degrees of homogeneity of potential fields and structural indices of Euler deconvolution. *Geophysics* 72(1), L1-L12.
- Stemmerik, L. & Worsley, D. 1989: Late Palaeozoic sequence correlations, North Greenland, Svalbard and the Barents Shelf. In Collison, J.D. (ed.), *Correlation in hydrocarbon exploration. Norwegian Petroleum Society, Graham and Trotman, London*, 99-111.
- Stemmerik, L. & Worsley, D. 1989: Late Palaeozoic sequence correlations, North Greenland, Svalbard and the Barents Shelf. In Collison, J.D. (ed.), *Correlation in hydrocarbon exploration. Norwegian Petroleum Society, Graham and Trotman, London*, 99-111.
- Stephens, M.B. & Gee, D., 1985: A tectonic model for the evolution of the eugeoclinal terranes in the central Scandinavian Caledonides. D. Gee & B.A. Sturt (eds.), *The Caledonide Orogen—Scandinavia and Related Areas*. Wiley, Chichester, 953-970.

- Sundvoll, B. & Roberts, D. 2003: A likely Early Ordovician age for the regional penetrative cleavage in the Gaissa Nappe Complex, northern Norway. *Norges Geologiske Undersøkelse Bulletin* 441, 51-59.
- Talwani, M. 1973. Computer Usage in the Computation of Gravity Anomalies. *Methods in Computational Physics* 13, 343-389.
- Taylor, P.N. & Pickering, K.T. 1981: Rb–Sr isotopic age determination on the late Precambrian Kongsfjord Formation, and the timing of compressional deformation in the Barents Sea Group, East Finnmark. *Norges Geologiske Undersøkelse Bulletin* 278, 81-92.
- Thompson, D.T. 1982: EULDPH: A new technique for making computer-assisted depth estimates from magnetic data. *Geophysics* 47, 31-37.
- Thurston, J.B. & Brown, R.J. 1994: Automated Source-Edge Location with a New Variable Pass-Band Horizontal-Gradient Operator. *Geophysics* 59(4), 546-554.
- Torsvik, T.H., Olesen, O., Trench, A., Andersen, T.B., Walderhaug, H.J. & Smethurst, M.A. 1992: Geophysical Investigation of the Honningsvåg Igneous Complex, Scandinavian Caledonides. *Journal of the Geological Society* 149, 373-381.
- Torsvik, T.H. & Cocks, L.R.M. 2005: Norway in space and time: A Centennial cavalcade. *Norwegian Journal of Geology*, 85, 73-86.
- Tsikalas, F. 1992: A study of seismic velocity, density and porosity in Barents Sea wells (N. Norway). *Unpublished Master Thesis*, University of Oslo, Norway, 169 pp.
- Tveten, E. & Zwaan, K. B. 1993: Geology of the coast-region from Lofoten to Loppa, with special emphasis on faults, joints and related structures. *Norges geologiske undersøkelse Report* 93.083.
- Vendeville, B. & Jackson, M. P. 1992. The rise of diapirs during thin-skinned extension. *Marine and Petroleum Geology* 9, 331-353.
- Verduzco, B., Fairhead, J.D., Green, C.M. & MacKenzie, C. 2004: The meter reader-New insights into magnetic derivatives for structural mapping. *The Leading Edge* 23, 116-119.
- Werner, S. 1953: Interpretation of magnetic anomalies of sheet-like bodies. *Sveriges Geologiska Arsbok*, 43, 6, 130 pp.
- Wienecke, S., Ebbing, J. & Gernigon, L. 2007: 3D gravity modelling, isostasy and elastic thickness calculation in the Barents Sea, Geological Survey of Norway-NGU Report 2007.022, 1-56
- Winograd, S. 1978: On Computing the Discrete Fourier Transform. *Mathematics of Computation* 32(141), 175-199.
- Worsley, D. 2006: The post-Caledonian geological development of Svalbard and the Barents Sea. The Boreal Triassic conference, Longyearbyen, Svalbard, NGF *extended Abstract and Proceedings*.
- Worsley, D., Agdestein, T., Gjelberg, J.G., Kirkemo, K., Mork, A., Nilsson, I., Olaussen, S., Steel, R.J. & Stemmerik, L. 2001: The geological evolution of Bjørnøya, Arctic Norway: implications for the Barents Shelf. *Norsk Geologisk Tidsskrift* 81(3), 195-234.
- Yu, Z., Lerche, I. & Lowrie, A. 1992: Thermal impact of salt: simulation of thermal anomalies in the Gulf of Mexico, 138, 181-192.

- Zozulya, D., Kullerud, K., Ravna, E. K., Corfu, F. & Savchenko, Y.: Geology, age and geochemical constraints on the origin of the Late Archaean Mikkelvik alkaline stock, West Troms Basement Complex in Northern Norway. *Norwegian Journal of Geology*, vol. 89, pp 327-340, Trondheim 2009, ISSN 029-196X.
- Zwaan, K.B. & Roberts, D. 1978: Tectonostratigraphic succession and development of the Finnmarkian Nappe Sequence, North Norway. *Nor.geol. unders.* 343, 53-71.
- Zwaan, B. K. & van Roermund, H. L. M. 1990: A rift-related mafic dyke swarm in the Corrovarre Nappe of the Caledonian Middle Allochthon, Troms, North Norway, and its tectonometamorphic evolution. *Norges geologiske undersøkelse Bulletin 419*, 25-44.
- Zwaan, K. B., Fareth, E. & Grogan, P.W. 1998: Geologisk kart over Norge, berggrunnskart NORDREISA, M 1:250.000. Norges geologiske undersøkelse.
- Zwaan, K.B., 1988: geologisk kart over Norge, berggrunnskart TROMSØ, M 1:250.000. *Norges geologiske undersøkelse, Trondheim*.
- Zwaan, K.B. 1995: Geology of the West Troms Basement Complex, northern Norway, with emphasis on the Senja Shear Belt: a preliminary account. I: Current research and development at NGU. *Norges geologiske undersøkelse Bulletin 427*, 33-36.

17 LIST OF FIGURES AND TABLES:

Figure 1.1 3D cartoon and examples of the application of modern NGU aeromagnetic surveys to basin or geodynamic studies. The cartoon illustrates structures and geological units that can cause observable magnetic responses (Gernigon et al. 2007a).

Figure 1.2 Geographic location of the BASAR-09 survey area and outline of the previous aeromagnetic surveys in and surrounding the Barents Sea (Olesen et al. 2006, 2010, Gernigon et al. 2007b). Alta and Tromsø airports were used during the survey acquisition.

Figure 1.3 Location of the BASAR-09 survey area (and outline of BAS-06 and BASAR-08). The main structural elements of the western Barents Sea are from NPD (Gabrielsen et al. 1990).

Figure 2.1 Finnmark and Troms geology from a 1:500,000 map (Siedlecka & Roberts 1996) and several 1:250,000 maps (Roberts 1973, Zwaan 1988, Grogan & Zwaan 1997, Zwaan et al. 1998). The main structural elements of the southern Finnmark Platform are shown with survey outlines (blue- BASAR-09, brown-BASAR08/BAS-06) and locations of the geological sections in this report (black) (Gabrielsen et al. 1990).

Figure 2.2 Regional palaeotectonics and main orogens and rift zones of the Barents Sea area. Reconstruction at end-Permian time (modified after Gudlaugsson et al. 1998).

Figure 3.1 Piper Chieftain from Fly Taxi Nord with the towed Scintrex Caesium Vapour MEP 410 high-sensitivity magnetometer (still in the docking cradle).

Figure 3.2 Flight pattern (red lines and blue tie-lines) of the BASAR-09 survey.

Figure 3.3 Sensor altitude (plane radar altitude – 70 m). In the offshore regions the sensor height was in a range of approximately 220 -250 m. Over onshore Finnmark the ground clearance was generally higher on account of the steep coastal topography and changing weather conditions.

Figure 3.4 Observations and prediction models of sunspot numbers from the US National Oceanic and Atmospheric Administration (NOAA)(<http://www.swpc.noaa.gov/SolarCycle>). Monthly averages (updated monthly) of the sunspot numbers show that the number of sunspots visible on the sun waxes and wanes with an approximate 11-year mega cycle. The BASAR-09 survey was carried out during a period of extremely low solar activity, which presented excellent conditions for the aeromagnetic acquisition.

Figure 3.5 Diagram of the monthly mean values of the horizontal intensity of the geomagnetic field (H) observed at the Tromsø Observatory from 1987 to 2010. This graph illustrates the good correlation between the periodic and semi-periodic evolution of the field and sunspot activity. A similar variation between the polynomial average of H and its running average illustrates the average good magnetic conditions for aeromagnetic surveying during the period May-October 2009. Geomagnetic data derive from Tromsø Geophysical Observatory (<http://www.tgo.uit.no/aix>).

Figure 3.6 Profiles with locally intermediate quality due to strong diurnal variations (i.e. diurnal variation between 10 and 30 nT per 10 minutes) were evaluated for re-flying. The total length of intermediate-quality data is 2700 km (i.e. 3.5 % of the total survey). The red

lines mark the profiles which were decided to be reflowed.

Figure 4.1 BASAR-09 TMI RAW magnetic profile data (without levelling) gridded by means of the minimum curvature algorithm (grid cell size at 400 x 400 m). Note that the artefacts are mostly parallel to the line profiles due to diurnals. Projection UTM 36, WGS 84.

Figure 4.2 The IGRF-2009 (formally 2005) model within the BASAR-09 survey area.

Figure 4.3 BASAR-09 IGRF-corrected total magnetic field of the TMI RAW data.

Figure 4.4 a) Statistical tie levelling of the magnetic profiles and b) additional basemag corrected tie-lines (Sørøya (red rectangular) and Bjørnøya (green) basestation corrected). Gridding of the tie profiles used the minimum curvature algorithm (grid resolution: 400 x 400 m).

Figure 4.5 Full levelling of the magnetic data. Gridding of the profiles used the minimum curvature algorithm (grid resolution: 400 x 400 m).

Figure 4.6 a) TMI field after micro-levelling and b) magnetic residual after micro-levelling by decorrugation and subtraction of the total field obtained by statistical levelling (400 x 400 m grid cell spacing).

Figure 4.7 a) BASAR-09 total magnetic field from both tie-lines and in-lines after micro-levelling. Results from the FFT decorrugation technique of Geosoft. The 400 x 400 m grid was produced using the minimum curvature gridding algorithm. b) Vintage NGU-69, NGU-70 and BAMS-85 data (Olesen et al. 2010).

Figure 5.1 Updated regional compilation with BASAR-09 and previous BASAR-08, BAS-06, HRAMS-97/98, BSA-87 SPA-88, NGU-69 and -70 and mainland data (Åm 1975, Skilbrei et al. 1990, Skilbrei 1991, 1992, 1993, Olesen et al. 2006, 2010, Brønner et al. 2009).

Figure 5.2 Regional compilation using vintage NGU data (Åm 1975, Skilbrei et al. 1990, Skilbrei, 1991, 1992, 1993, Olesen et al. 2006, 2010).

Figure 6.1 Bouguer gravity of the southern Barents Sea (reduction density 2.67 g/cm³).

Figure 7.1 Gridded anomaly map of the total magnetic field reduced to the pole (Incl: 72.58°; Decl: 20.28°). The RTP transformation was carried out using a 2D-FFT filtering along the microlevelled grid (400 x 400 m). The RTP correction transforms the anomaly into the one that would be observed with vertical magnetisation and with a vertical Earth's field, i.e. the anomaly that would be observed if the sources were located at the Earth's magnetic north pole. As a result, reduction to the pole removes asymmetries caused by the non-vertical inducing field and places the anomalies more directly over their causative bodies, thus facilitating the interpretation of the magnetic dataset. For the Barents Sea latitude these changes are relatively small.

Figure 7.2 a) High-pass filtering (30 km) of the magnetic total field. This filter underlines the distribution of the short wavelengths. B) Low-pass filtered data (30 km) showing the corresponding residual field. Grid cell size is 400 x 400 m.

Figure 7.3 Upward continuations of the magnetic total field to a) 5 km and b) 20 km, respectively. Upward continuation uses wavelength filtering to simulate the appearance of potential-field maps as if the data had been recorded at a higher altitude. Large-scale regional anomalies and the main crustal patterns are revealed by this process.

Figure 8.1 First vertical derivative obtained by convolution along the magnetic total field,

reduced to the pole and gridded with a cell size of 400 m using minimum curvature. The vertical derivative of an anomaly is related to the depth and geometry of the causative body. The gradient operator attenuates broad, more regional anomalies and enhances local, more subtle, magnetic responses and, as such, is sensitive to shallow magnetic source bodies and contacts.

Figure 8.2 Second vertical derivative (SVD) obtained by convolution along the magnetic total field reduced to the pole. The data were low-pass filtered with a) 2 km and b) 5 km cut-off to suppress high-frequency noise and to highlight contact features of different wavelengths.

Figure 8.3 Horizontal gradient magnitude (HGM) of the BASAR-09 dataset, reduced to the pole. After the reduction-to-pole correction, a magnetic body is spatially more directly associated with the related magnetic response. The horizontal gradient magnitude of the anomaly slope is then located near or over the body edge; i.e., the horizontal gradient operator, in map form, produces maximum ridges over edges of magnetic basement blocks and faults or other magnetic bodies. In addition, the horizontal gradient highlights linear and round-shaped features, related to magnetic contacts, in the dataset.

Figure 8.4 Analytic signal of the magnetic total field grid, reduced to the pole (400 x 400 m cell size, normalised colour distribution).

Figure 8.5 Tilt derivative of the magnetic total field. The tilt derivative (TDR) is an alternative method for deriving the maximum gradient anomalies associated with magnetic contacts.

Figure 9.1 Result from the located Euler deconvolution data. Solutions derived by using a structural index of 0.

Figure 9.2 Result from the located Euler deconvolution data. Solutions derived by using a structural index of 0.5

Figure 9.3 Result from the located Euler deconvolution data. Solutions derived by using a structural index of 1.

Figure 10.1 a) Magnetic total field (left) and b) outline of the main anomalies (right). Black and yellow lines underline the main structural features of the area (Gabrielsen et al. 1990).

Figure 10.2 a) Bouguer map and b) interpretation of the main anomaly highs and lows. Black and yellow lines underline the main structural features of the area (Gabrielsen et al. 1990).

Figure 10.3 Interpretation of the main anomaly highs and lows from Bouguer (filled) and TMI (outlines) maps. Black and yellow lines underline the main structural features of the area (Gabrielsen et al. 1990). Grey lines represent the faults mapped at base Cretaceous level (Gabrielsen et al. 1990).

Figure 10.4 Structural interpretation of the Hammerfest Basin and 20 km high-pass filtering of the TMI data.

Figure 10.5 Structural interpretation of the Tromsø Basin with the TMI data.

Figure 10.6 a) TMI grid with complete structural interpretation, b) Structural elements with complete structural interpretation. Blue curved lines are observed lineaments from the magnetic map and are most likely associated with Caledonian nappes, dark blue lines are major faults. Red lines show fault-related lineaments probably associated with high-magnetic material such as dykes (see text). Black and yellow lines underline the main

structural features of the area (Gabrielsen et al. 1990). Grey lines represent the faults mapped at base Cretaceous level (Gabrielsen et al. 1990), black and blue dotted lines represent second-order lineaments with a more shallow origin, based on magnetic interpretation.

Figure 10.7 a) TILT derivative from TMI grid with principal possibly intruded faults, b) 30 km high-pass filter from TMI with complete structural interpretation and c) the complete structural interpretation. Blue curved lines are observed lineaments from the magnetic map and are most likely associated with Caledonian nappes, dark blue lines are major faults. Red lines show fault-related lineaments probably associated with high-magnetic material such as dykes (see text). Black and yellow lines underline the main structural features of the area (Gabrielsen et al. 1990). Grey lines represent the faults mapped at base Cretaceous level (Gabrielsen et al. 1990), black and blue dashed lines represent second-order lineaments with a more shallow origin based on magnetic interpretation.

Figure 10.8 a) 30 km high-pass filtering of the Bouguer gravity with complete structural interpretation from the new magnetic data b) TILT derivative multiscale edge detection to (Lahti & Karinen 2010) determine the tilt of the main magnetic basement highs. Blue curved lines are observed lineaments from the magnetic map and are most likely associated with Caledonian nappes, dark blue lines represent major faults. Red lines show fault-related lineaments probably associated with high-magnetic material such as dykes (see text). Black and yellow lines underline the main structural features of the area (Gabrielsen et al. 1990). Grey lines represent the faults mapped at base Cretaceous level (Gabrielsen et al. 1990), black (BASAR-08) and blue (BAS-06) dashed lines represent second-order lineaments with a more shallow origin, based on magnetic interpretation.

Figure 10.9 Comparison between (a) the new and (b) the vintage magnetic data for the Nordkapp Basin. The BASAR-08 data (left) have a significantly higher resolution, showing various features such as salt structures and faults in much more detail.

Figure 10.10 Onshore-offshore correlation utilising the TMI data from the new regional compilation with the main structural interpretations.

Figure 10.11 Onshore-offshore correlation: TILT derivative with main structural interpretations and onshore geology map (Siedlecka & Roberts, 1996).

Figure 11.1 Outline of the main structural elements of the western Barents Sea (modified after Gabrielsen et al. 1990) and location of the four transects modelled and discussed in the present chapter. The map also shows some of the main geological units of western Finnmark from the geological map of the Arctic (Harrison et al. 2008) and highlights the main structural highs (in pink) in the western Barents Sea. The blue polygon represents the outline of the new BASAR-09 aeromagnetic survey.

Figure 11.2 Free-air gravity map of the western Barents Sea and location of the regional transects. The map also shows the main onshore geological units. The Loppa and Stappen highs produce significant gravity positive anomalies. The Hammerfest, Tromsø and Bjørnøya basins are characterised by gravity lows.

Figure 11.3 Location of the regional transects on the magnetic total field anomaly map of the southwestern Barents Sea. Note the prominent positive and regional anomalies associated

with the Loppa and the Stappen highs.

Figure 11.4 Tilt derivative filter (TDR) of the magnetic total field. The TDR enhances the subtle magnetic anomalies and maximizes the geometrical contrast of the internal basin structures. To remove noise and levelling still existing on the old compilation (BASAR-09 not included), a Butterworth filter has been applied on the total magnetic field before TDR and deconvolution calculation. The TDR has the property of being positive over a source and negative elsewhere. The TDR tends to enhance mapping of the subtle magnetic anomalies and maximizes the geometrical contrast of the internal basin structure. The TDR compared with other edge detection measures (e.g. the horizontal gradient, the second vertical derivative and the analytic signal) have some advantage of responding well to both shallow and deep sources. Using synthetic models, Verduzco et al. (2004) showed that the TDR has its zero values close to the edges of the body for RTP corrected fields.

Figure 11.5 Blend image of the Tilt derivative (TDR) and TDX filters of the free-air gravity field. The TDR enhances the subtle magnetic anomalies and maximises the geometrical contrast of the internal basin structures. The TDX enhances the edge of each of the anomalies (Cooper and Cowan, 2006). To remove noise still existing on the old compilation, a Butterworth low-pass filter has been applied on the total magnetic field before the tilt derivative filtering. This composite map highlights the main basement structures, basins and structural trends of the study area.

Figure 11.6 Workflow and integrated interpretation of the potential field modelling.

Figure 11.7 Forward modelling results along seismic line NBR07-232958. Each polygon is characterised by a density value in g.cm^{-3} (black numbers) and susceptibility in SI (blue italic numbers).

Figure 11.8 Forward modelling results along seismic line 7355-94. Each polygon is characterised by a density value in g.cm^{-3} (black numbers) and susceptibility in SI (blue italic numbers)

Figure 11.9 Forward modelling results along seismic line BV12-86. Each polygon is characterised by a density value in g.cm^{-3} (black numbers) and a susceptibility in SI (blue italic numbers).

Figure 11.10 Forward modelling results along seismic line BV03-86. Each polygon is characterised by a density value in g.cm^{-3} (black numbers) and a susceptibility in SI (blue italic numbers).

Figure 11.11 Conceptual models of the geodynamic evolution of the study area. Abbreviation: BB: BB; HB: Hammerfest Basin; KFC: Knølegga Fault Zone; LH: Loppa High; NB: Nordkapp Basin; NLHSZ: North Loppa High Shear Zone; OB: Ottar Basin SB: Sørkapp Basin; SD: Svalis Dome; SH: Stappen High; VH: Vestlemøy High. Gernigon et al. (manuscript in preparation).

Figure 11.12 Model for the crustal and sedimentary structure across the Porcupine Basin after O'Reilly et al. 2006). In shape and structure, this Irish basin could represent a good crustal analogue of the Bjørnøya Basin. Vertical exaggeration is 1:1.5. Triangles show the positions of OBSs used in this study. NR, Neogene to Recent post-rift sequence; CP, Cretaceous to Palaeogene post-rift sequence; J: predominantly Jurassic synrift sediment

sequence; PRB: pre-rift basement; M: Moho; PSP: partially serpentinised mantle peridotite. Low velocities in the subcrustal mantle (V_p c. 7.2–7.8 km.s⁻¹) are interpreted as evidence for partially serpentinised peridotites. Numbers are seismic P-wave velocities (km.s⁻¹) in the subcrustal region of the model, added for clarity.

Figure 12.1 Structural map and outline of the 3D model. Lines indicate the vertical planes defining the 3D model.

Figure 12.2 Gravity compilation used for 3D modelling. For gravity data a compilation of free-air gravity in the offshore parts and Bouguer gravity with reduction density of 2670 kg/ m³ onshore Norway and Bjørnøya was applied. Outline of the 3D model.

Figure 12.3 Aeromagnetic compilation used for 3D modelling. Outline of the 3D model.

Figure 12.4 Presentation of the additional data from wells, deep seismic profiling and 2D grav/mag modelling along seismic lines, used to constrain the model geometry.

Figure 12.5 a) Calculated gravity from the 3D model and b) difference field with the observed gravity. The standard deviation is c. 8 mGal, which can to a large extent be explained by local mismatches like salt structures(Nordkapp Basin, Svalis Dome), which were not included in the 3D model.

Figure 12.6 a) Calculated TMI from the 3D model and b) difference field with the observed TMI. The standard deviation is c. 70 nT, which can to a large extent be explained by local mismatches along the COT, where constraints were only sparsely available, and low model resolution onshore Norway.

Figure 12.7 Structural map of the southwestern Barents Sea (Gabrielsen et al. 1990) with the positions of the presented 2D profiles from the 3D model.

Figure 12.8 ENE-WSW oriented cross-sections from the 3D model: a) Profile 9a and b) 10b with magnetic and gravity correlation between observed and calculated field. The model geometry from the 3D model with addressed units and parameters (See Table 12.1) is shown.

Figure 12.9 ENE-WSW oriented cross-sections from the 3D model: a) Profile 11a and b) 12b with magnetic and gravity correlation between observed and calculated field. The model geometry from the 3D model with addressed units and parameters (See Table 12.1) is shown.

Figure 12.10 NW-SE oriented cross-sections from the 3D model: a) NBR07-232948 b) Petrobar_07 with magnetic and gravity correlation between observed and calculated field. The model geometry from the 3D model with addressed units and parameters (see Table 12.1) is shown, and a comparison between the 3D model results and the ones from the 2D interpretation.

Figure 12.11 ENE-WSW oriented cross-section from the 3D model: Profile 13b with magnetic and gravity correlation between observed and calculated field. The model geometry from the 3D model with addressed units and parameters (See Table 12.1) is shown.

Figure 12.12 a) Depth-to-magnetic basement as defined in the 3D model with different basement units (see in Table 12.1): b) Top basement map including Caledonian nappes as defined in the 3D model.

Figure 12.13 Depth to Moho from the 3D model.

Figure 13.1 Modelling setup used in the present study. Surface temperatures and basal heat flow are applied and each rock unit has its own thermal properties (i.e. heat generation and thermal conductivity, Table 12.1). Note the salt pillow shown in white inside the Bjørnøya Basin.

Figure 13.2 Modelled isotherms up to a) ~850°C and b) 400°C. Red vertical profiles depict locations where modelled temperatures were extracted for comparison with temperature data from exploration wells (see Fig. 12.3).

Figure 13.3 Snapshot of modelled temperature (see Fig. 12.2) showing the significant depression of the isotherms caused by the salt dome.

Figure 13.4 Comparison between modelled and measured temperatures in exploration wells (data source: Norsk Oljedirektoratet). Numbers refer to the sampling locations inside the numerical model (see Fig. 1.2). BHT = bottom-hole temperature, DST = drill-stem test.

Table 3.1 Coordinates of the BASAR-09 survey area.

Table 3.2 Main characteristics of the BASAR-09 survey.

Table 3.3 Results from data QC and the re-fly programme of BASAR-09.

Table 4.1 Overview of tie-line corrections with lowpass filtered records from base-magnetometers in Sørøya and Bjørnøya. If no correlation was found, only statistical levelling was applied.

Table 9.1 Summary of the structural indices for simple geometric models from magnetic or gravity anomalies (Reid et al. 1990, Marson & Klingele 1993, Bainbridge et al. 2002).

Table 9.2 Wells, with drilled basement, were used to constrain the Euler deconvolution results.

Table 11.1 Parameters used for the Werner deconvolution along profile NBR07-232958.

Table 11.2 Parameters used for the Euler deconvolution along profile NBR07-232958.

Table 11.3 Parameters used for the Werner deconvolution along profile 7355-94.

Table 11.4 Parameters used for the Euler deconvolution along profile 7355-94.

Table 11.5 Parameters used for the Werner deconvolution along profile BV12-86.

Table 11.6 Parameters used for the Euler deconvolution along profile BV12-86.

Table 11.7 Parameters used for the Werner deconvolution along profile BV3-86.

Table 11.8 Parameters used for the Euler deconvolution along profile BV12-86.

Table 12.1 Modelling parameters: different crustal units are defined by a combination of petrophysical values obtained by density and magnetic modelling.

Table 13.1 Thermal parameters used in the modelling.

18 APPENDIX 1 CD CONTENT

18.1 Folders

Report

Presentations

Data

Figures & Maps

18.1.1 Report

NGU BASAR-09 report in PDF format

18.1.2 Presentations

Presentations showed to our partners in MS PowerPoint format (.ppt)

18.1.3 Data

- Profile

Profile data *BASAR09_Mag_proc.** Geosoft database and ASCII file

Name	Format	Description
1 UMTE	10.0	UTM coordinates WGS84 UTM36N
2 UTMN	10.0	UTM coordinates WGS84 UTM36N
3 LATITUDE	24.2	geographical coordinates
4 LONGITUDE	16.2	geographical coordinates
5 ALT_gps	10.2	GPS altitude
6 ALT_R_ft	10.2	Radar altitude in feet
7 ALT_R_m_corr	14.2	corrected Radar altitude in metre
8 ALT_R_m_sensor	20.2	corrected Sensor altitude in metre
9 DATE	12.2	Date
10 GPSTIME	18.2	Gpstime
11 Mag_raw	12.2	uncorrected recorded magnetic field
12 Mag_raw_NOSPK	14.2	Spike corrected recorded magnetic field
13 BMAG_B	12.2	Basemagentometre Bjørnøya
14 BMAG_B_FILT20K	12.2	Basemagentometre Bjørnøya 20 km low-pass filtered
15 BMAG_S	12.2	Basemagentometre Sørøya
16 BMAG_S_FILT20k	12.2	Basemagentometre Sørøya 20 km low-pass filtered
17 IGRF	12.2	IGRF field
18 MAG_anom	18.2	IGRF corrected magnetic field
19 Mag_anom_tlev	23.2	Tie-line leveled magnetic field
20 MAG_lev_line_rev1	41.2	levelled magnetic data, in-lines
21 Mag_mic_Final	15.2	final TMI, microlevelled all lines, tie-lines and in-lines
22 Mag_mic_Final_rtp	10.2	final TMI reduced to pole
23 Mag_mic_Final_rtp_h30k	10.2	30 km high-pass filter of final TMIRTP
24 Mag_mic_line_rev1	36.2	microlevelled in-lines
25 MAG_tlev_stat	23.2	statistical tie-line levelling
26 MAG_tmic_rev1	20.1	microlevelled tie-lines
27 Dec	10.1	Declination
28 Inc	10.2	Inclination
29 NSAT	10.0	number of satellites

- Grids

Gridded data in UTM 36N, WGS84 & UTM 34N, ED50 for the compilation

Geosoft grid files

XYZ files

└ Filtering

 Various filtering of TMI data

└ Processing

- shp-files

18.1.4 Figures & Maps

Selected report figures in JPG and GeoTif format

Selected maps in PDF format

- Total magnetic field
- Total magnetic field
- 30 km high-pass filter from TMI field
- TILT derivative from TMI field
- Analytic signal from TMI field